Vol. 178 No. 1, December 1, 1985 ISSN 0003-2670
Fourier-Transform Mass Spectrometry: Fundamental Aspects and Analytical Applications

ANALYTICA CHIMICA ACTA

International journal devoted to all branches of analytical chemistry

ELSEVIER

ANALYTICA CHIMICA ACTA

International journal devoted to all branches of analytical chemistry
Revue internationale consacrée à tous les domaines de la chimie analytique
Internationale Zeitschrift für alle Gebiete der analytischen Chemie

PUBLICATION SCHEDULE FOR 1985

	J	F	M	A	M	J	J	A	S	O	N	D
Analytica Chimica Acta	167	168	169	170/1 170/2	171	172	173	174	175	176	177	178 178

Scope. *Analytica Chimica Acta* publishes original papers, short communications, and reviews dealing with ev aspect of modern chemical analysis both fundamental and applied.

Submission of Papers. Manuscripts (three copies) should be submitted as designated below for rapid and effici handling:

Papers from the Americas to: Professor Harry L. Pardue, Department of Chemistry, Purdue University, West Lafaye IN 47907, U.S.A.

Papers from all other countries to: Dr. A. M. G. Macdonald, Department of Chemistry, The University, P.O. Box 3 Birmingham B15 2TT, England. Papers dealing particularly with computer techniques to: Professor J. T. Cle Universität Bern, Pharmazeutisches Institut, Baltzerstrasse 5, CH-3012 Bern, Switzerland.

Submission of an article is understood to imply that the article is original and unpublished and is not being conside for publication elsewhere. Upon acceptance of an article by the journal, authors will be asked to transfer the copyri of the article to the publisher. This transfer will ensure the widest possible dissemination of information.

Information for Authors. Papers in English, French and German are published. There are no page charg Manuscripts should conform in layout and style to the papers published in this Volume. Authors should cons Vol. 170 for detailed information. Reprints of this information are available from the Editors or from: Elsevier Edito Services Ltd., Mayfield House, 256 Banbury Road, Oxford OX2 7DH (Great Britain).

Reprints. Fifty reprints will be supplied free of charge. Additional reprints (minimum 100) can be ordered. An or form containing price quotations will be sent to the authors together with the proofs of their article.

Advertisements. Advertisement rates are available from the publisher.

Subscriptions. Subscriptions should be sent to: Elsevier Science Publishers B.V., Journals Department, P.O. E 211, 1000 AE Amsterdam, The Netherlands. Tel: 5803 911, Telex: 18582.

Publication. *Analytica Chimica Acta* appears in 12 volumes in 1985. The subscription for 1985 (Vols. 167–178) Dfl. 2400.00 plus Dfl. 264.00 (p.p.h.) (total approx. US $986.70). All earlier volumes (Vols. 1–166) except Vols. and 28 are available at Dfl. 231.00 (US $85.56), plus Dfl. 15.00 (US $5.56) p.p.h., per volume.

Our p.p.h. (postage, packing and handling) charge includes surface delivery of all issues, except to subscribers in t U.S.A., Canada, Japan, Australia, New Zealand, P.R. China, India, Israel, South Africa, Malaysia, Singapore, Sou Korea, Taiwan, Pakistan, Hong Kong and Brazil who receive all issues by air delivery (S.A.L. — Surface Air Lifted) no extra cost. For the rest of the world, airmail and S.A.L. charges are available upon request.

Claims for issues not received should be made within three months of publication of the issues. If not they cannot honoured free of charge.

For further information, or a free sample copy of this or any other Elsevier Science Publishers journal, readers in t U.S.A. and Canada can contact the following address: Elsevier Science Publishing Co. Inc., Journal Informati Center, 52 Vanderbilt Avenue, New York, NY 10017, U.S.A., Tel: (212) 916-1250.

ANALYTICA CHIMICA ACTA
VOL. 178 (1985)


RESPECT COPYRIGHT
BERNE
CONVENTION
100 YEARS
1886-1986
ENCOURAGE CREATIVITY

ANALYTICA CHIMICA ACTA

International journal devoted to all branches of analytical chemistry

ELSEVIER Amsterdam–Oxford–New York–Tokyo

Anal. Chim. Acta, Vol. 178 (1985)

0003-2670/85/$03.

Printed in The Netherlands

Fourier-Transform Mass Spectrometry: Fundamental Aspects and Analytical Applications

Analytica Chimica Acta, 178 (1985) 1—15
Elsevier Science Publishers B.V., Amsterdam — Printed in The Netherlands

FUNDAMENTAL ASPECTS AND APPLICATIONS OF FOURIER-TRANSFORM ION-CYCLOTRON RESONANCE SPECTROMETRY

MELVIN B. COMISAROW

Department of Chemistry, University of British Columbia, Vancouver, British Columbia V6T 1Y6 (Canada)

(Received 22nd July 1985)

SUMMARY

The operating principles, features, advantages, applications and potential of Fourier-transform ion-cyclotron resonance (F.t./i.c.r. or F.t.m.s.) mass spectrometry are discussed. It is shown that F.t./i.c.r. technology creates a high-performance mass spectrometer with high speed, high sensitivity, ultrahigh mass resolution, very wide mass range and unparalleled versatility.

The subject matter of this paper is derived from an earlier form of a particular type of mass spectrometry called ion-cyclotron resonance (i.c.r.) mass spectrometry [1, 2]. The application, a decade ago, of Fourier multiplex concepts [3, 4] to i.c.r. mass spectrometry created a new technique called Fourier-transform ion-cyclotron resonance mass spectrometry (F.t./i.c.r.) [5—7]. The term Fourier-transform mass spectrometry (F.t.m.s.) is also in common use today as an exact synonym for F.t./i.c.r. and this new technique.

There is potentially some confusion in using the term F.t.m.s., as Fourier techniques have also been applied with advantage to another type of mass spectrometer called a time-of-flight (t.o.f.) mass spectrometer [8]. It should be noted that in this paper and the other papers in this issue, "Fourier-transform mass spectrometry" and "F.t.m.s." are synonymous with F.t./i.c.r. and do not refer to Fourier-transform time-of-flight (F.t./t.o.f.) mass spectrometers.

PRINCIPLES OF ION-CYCLOTRON RESONANCE

The physics of ion-cyclotron resonance is very simple and follows from the elementary principles of electromagnetism [9]. In a uniform magnetic field, B, a moving ion of charge, q, and mass, m, will be subjected to a force called the Lorentz force, which acts perpendicular to the direction of ion motion. Solution of the equation of motion for the ion shows that the ion will be constrained to a circular orbit, with radius proportional to the velocity of the ion. The ion will have a characteristic frequency, ω, called the cyclotron frequency, for its orbital motion:

0003-2670/85/$03.30

$$\omega = qB/m \quad (1)$$

For a magnetic field of 1 Tesla and a mass range of m/q = 15—1500 Daltons, the cyclotron frequencies lie between 10 kHz and 1 MHz, and are thus in the radiofrequency band of the electromagnetic spectrum.

The equation $\omega = qB/m$ is called the cyclotron equation. It follows from this equation that an ensemble of ions of differing masses will be characterized by a spectrum of cyclotron frequencies. Measurement of the cyclotron frequencies of an ensemble of ions is thus, via Eqn. 1, tantamount to measuring the masses of the ions. Any instrument which measures the masses of ions is called a mass spectrometer and Eqn. 1 provides the fundamental relationship for the operation of an i.c.r. mass spectrometer.

The measurement of cyclotron frequencies is accomplished with two operations: excitation of cyclotron motion and detection of excited cyclotron motion.

Excitation of cyclotron motion

Figure 1 shows a schematic diagram of the equipment required for i.c.r. excitation. A parallel-plate capacitor is connected to a radiofrequency oscillator which creates an alternating electric field within the capacitor. If the frequency of the alternating electric field equals the natural cyclotron frequency for a particular ion (Eqn. 1), energy will be transferred from the radiofrequency oscillator to the kinetic energy of the ion. Because the kinetic energy is related to cyclotron radius, r, by

$$\mathrm{KE} = 1/2\, m\, \omega^2\, r^2 \quad (2)$$

the radius of the ion orbit will increase. The phenomenon of transferring energy in the manner just described is called "ion cyclotron resonance" or "i.c.r. excitation". It can be used to accelerate the ion, or any charged particle for that matter, to very high translational energies [10]. When cyclotron resonance is used for accelerating particles to very high energies, the apparatus is called a cyclotron [10]. When cyclotron resonance is used to measure ion masses, the apparatus is called an ion-cyclotron resonance mass spectrometer [1, 2].

Detection of excited cyclotron motion

Prior to i.c.r. excitation, all ions are moving with random phase relative to each other. During i.c.r. excitation all ions of a given mass are accelerated together and the instantaneous average position of the ions, called a rotating electric monopole [11], moves on the spiral path shown in Fig. 1. The rotating monopole induces a charge on the plates of the capacitor [11]. When the plates of the capacitor are connected by an external circuit an alternating current, called the i.c.r. signal current, will be created in this circuit by the rotating electric monopole [11] (Fig. 2). The frequency of the signal current is the cyclotron frequency. In F.t./i.c.r. practice, the current is converted to a voltage and the i.c.r. signal voltage becomes [11]

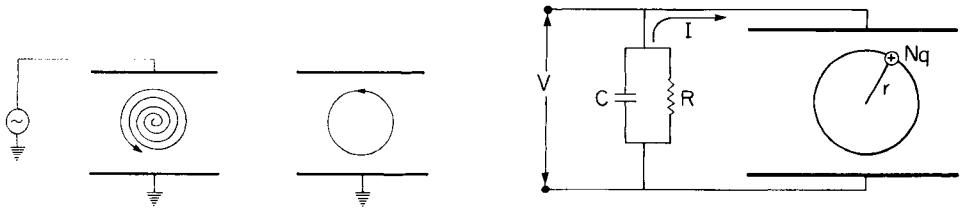

Fig. 1. Ion-cyclotron resonance excitation. An alternating electric field is created inside a capacitor and excites the cyclotron motion of an ion in the capacitor. The ion follows a spiral path as its motion is excited. After the oscillator has been turned off, the ion follows the path on the right. The coherent motion on the right is the rotating electric monopole which generates the i.c.r. signal (Fig. 2). For a magnetic field directed into the plane of the figure, a positive ion will follow the counterclockwise paths shown.

Fig. 2. Ion-cyclotron resonance detection. The rotating electric monopole induces an alternating charge in the plates of the capacitor and an alternating current, I, in the external circuit. The voltage, V, across this circuit (Eqn. 3) is the i.c.r. signal voltage.

$$V(t) = N q r/(d C) \cos \omega t \tag{3}$$

where N is the number of ions, C is the circuit capacitance and d is the capacitor spacing. It should be noted that the i.c.r. signal voltage is proportional to the number of ions and to the ion radius but is independent of the ion mass. It should also be noted that the rotating electric monopole theory [11], while developed for F.t./i.c.r., is applicable to all i.c.r. spectrometers [11]. It was the single most important theoretical concept needed for the development of F.t./i.c.r.

Conventional i.c.r. spectrometry

In conventional i.c.r. spectrometry [1, 2], a special circuit called a marginal oscillator is used to provide for simultaneous i.c.r. excitation and detection. The magnetic field is scanned to equate successively the ion-cyclotron frequencies with the fixed frequency of the marginal oscillator. Typically, about 20 min is required to scan over a mass range of 15—200 Daltons for a marginal oscillator amplitude of about 10 mV. Normally, the mass linewidth is at least one Dalton throughout the mass spectrum.

FOURIER-TRANSFORM ION-CYCLOTRON RESONANCE SPECTROMETRY

Excitation and detection in F.t./i.c.r.

In the F.t./i.c.r. instrument, all ion masses are excited, essentially at once. This can be accomplished by using a fast frequency sweep from the radiofrequency oscillator [6, 12]. Typically, a frequency sweep from 1 kHz to 1 MHz with an amplitude of a few tens of volts and a sweep time of a few milliseconds will suffice to excite all ions to a cyclotron radius of the order of a centimeter.

While a fast frequency sweep is currently the universally used F.t./i.c.r.

excitation method, pseudostochastic excitation sequences [13] may have more selectivity and may become standard in the future.

Equation 3 and the associated discussion described the generation of an i.c.r. signal voltage from excited i.c.r. motion at a single ion mass. If several ion masses have been excited there will be a composite signal

$$V(t) = \sum_{m} V_m \cos \omega_m t \tag{4}$$

which is just the sum of the individual (Eqn. 3) i.c.r. signals.

Fourier transformation

A Fourier transform (F.t.) is a mathematical recipe which analyzes any complex time signal, such as Eqn. 4, into its constituent frequency components [14]. The analysis can be graphically presented as a plot of amplitude vs. frequency called the frequency spectrum. While the mathematics of Fourier transformation is complex, modern digital computers combined with a special algorithm, called the Fast Fourier Transform [14], give rapid Fourier analysis. With special hardware, called array processors or parallel processors and/or coprocessors, a Fourier transform which analyzes for tens of thousands of individual frequencies can be done in less than a second.

The F.t./i.c.r. cell

The magnetic field constrains ion motion perpendicular to, but not parallel to, the magnetic field. Experiments in i.c.r. require that ions be held in the apparatus for at least a few milliseconds and a static electric field parallel to the magnetic field will complete the ion confinement. A pair of parallel plates called the trapping plates is added to the apparatus of Fig. 1 to create what is called the i.c.r. cell. Application of about 1 V to the trapping plates and 0 V to the other plates of the cell creates an electric potential inside the cell which traps all ions of positive electric charge. Alternatively, negative ions can be trapped with a negative trapping potential. Figure 3 shows the cubic i.c.r. cell [15] which is the most commonly used cell today.

The electric field from the trapping electric potential has a component perpendicular to the cyclotron motion. This component slightly shifts the cyclotron frequencies from those given by Eqn. 1. However, this trapping field shift is well understood [16] and corrections can be made for it.

The F.t./i.c.r. pulse sequence and the F.t./i.c.r. spectrometer

The fundamental principles described above can be combined to create a mass spectrometer as outlined in Fig. 3; the operating pulse sequence is shown in Fig. 4. Not shown in Fig. 3 is the vacuum system which encloses the i.c.r. cell and provides for introduction of the gaseous sample.

Any mass spectrometer converts neutral molecules into gaseous ions, the masses of which are then analyzed. The first step for F.t./i.c.r. operation

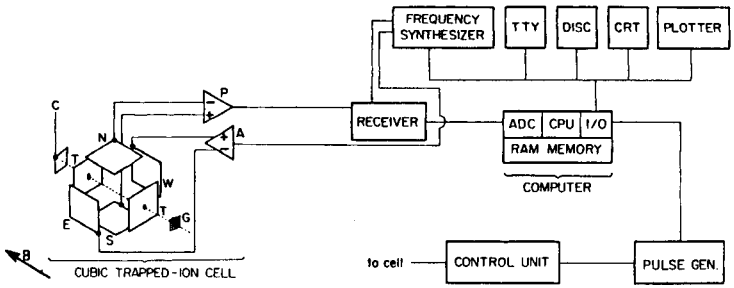

Fig. 3. Block diagram of F.t./i.c.r. spectrometer. The instrument consists of the i.c.r. cell and the associated analog and digital electronics. The cell, which most commonly is cubic in geometry, consists of the transmitter plates, E, W, the receiver plates, N, S, and the trapping plates, T; G and C are the grid and collector for the ionizing electric beam. The computer controls a frequency synthesizer which, via a power amplifier, A, applies the exciting electric field. The i.c.r. signal voltage, Eqn. 4, is amplified by the pre-amplifier, P, and digitized by the analog/digital converter, ADC. The cell is orientated such that the trapping plates are parallel to the magnetic field, B.

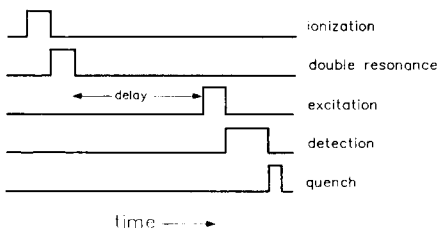

Fig. 4. The F.t./i.c.r. pulse sequence. The pulse sequence is explained in the text.

is thus ionization, which most commonly is achieved by impact on the gaseous neutral molecules by a pulse of high velocity electrons: $M + e^- \rightarrow M^+ + 2e^-$. Other ionization methods, which can have significant advantages, are described below.

The second F.t./i.c.r. pulse, which may be absent, is the double resonance pulse [17]. During this pulse, ions of a particular mass are excited at their cyclotron frequencies. Most commonly, the excitation power is high enough to cause ions to strike the plates of the cell and so be removed. Only one ion mass may be removed or a band of ions may be removed by a high-power frequency sweep. The F.t./i.c.r. third time period, which may be zero, is a delay period to allow for ion/molecule reactions [17, 18]: $M^+ + M \rightarrow$ other ions.

The next pulse is the frequency sweep excitation pulse which excites the cyclotron motion of all ions in the cell. This is followed by the detection time during which the excited cyclotron motion is detected. Finally, a quench pulse is applied to one of the trapping plates of the cell to remove all ions, prior to the start of the next pulse sequence.

The time domain signal (Eqn. 4), containing the signal from each excited ion, is acquired in the computer and is Fourier-transformed to give the frequency spectrum. Alternatively, the time signals from several successive pulse sequences can be added together to form a single time signal of higher signal-to-noise ratio. This is done when the signal-to-noise ratio of a single time signal is too low.

The above pulse sequence is the most rudimentary but also the most commonly used. More complex pulse sequences with added delay times and more pulses have been used for complex ion/molecule reaction studies [18, 19].

Performance

Any mass spectrometric technique can be characterized by the performance criteria of speed, sensitivity, resolution, mass range, convenience and versatility. These individual criteria and other aspects of F.t./i.c.r. are discussed below.

Speed. Instruments for F.t./i.c.r. give the whole mass spectrum in the time which a scanning i.c.r. spectrometer would require to scan across just a single peak in the mass spectrum. For routine mass spectral analysis, the double resonance and reaction delay time periods are set to zero. Typical times for electron-impact ionization, excitation, detection, quench and Fourier transformation would be 5 ms, 5 ms, 10 ms, and 1 ms, repeated 100 times which, with a Fourier transformation time of 1000 ms, gives a total time of about 3 s. This is comparable to the fastest of scanning mass spectrometers and is several thousand times faster than scanning i.c.r. spectrometers.

Sensitivity. Sensitivity can be defined relative to conventional i.c.r. instruments, absolutely in terms of the minimum number of ions detected or absolutely in terms of the partial pressure of or mass of or number of moles of neutral molecules. Instruments for F.t./i.c.r. are, via addition of time signals prior to Fourier transformation, up to 100 times as sensitive as conventional i.c.r. instruments. About 10 ions is the minimum number which can be detected with the current generation of instruments [20].

Partial pressures of 10^{-14} atmospheres of sample have been observed [21] by F.t./i.c.r. Sensitivity measured in terms of the minimum amount of sample required to give a signal, the most important practical definition of sensitivity, indicates that low picogram quantities of sample can be detected [22]. Improvement in this measure of sensitivity can be expected by improvements in the mass transport of the sample to the i.c.r. cell and by optimizing the fraction of neutrals which are converted into ions.

Resolution and mass range. The ultrahigh mass resolution (in excess of 10^6) and the very wide mass range of the F.t./i.c.r. instrument are the two features of the instrument which have most interested the mass spectrometry community. These features were predicted and demonstrated very early in the development of the technique [21, 23—25]. The ultrahigh resolution of the F.t./i.c.r. instrument has been used to measure the precise mass

difference between $^3H^+$ and $^3He^+$ with an accuracy of 3 parts in 10^{11}, for purposes of determining the mass of the electron antineutrino [26, 27].

Frequency, more so than most physical parameters, can be measured to very high accuracy with great ease, with the error of measurement limited only by the inherent uncertainty of the frequency itself. The accuracy with which any frequency can be determined is limited by the classical uncertainty principle, which states that the uncertainty in frequency measurement is inversely proportional to the observation time. Thus, for a 1-s observation of a 1-kHz signal, the uncertainty is 1 Hz or 1 part in 1000. For a 10-s observation, the uncertainty is 0.1 Hz or 1 part in 10 000, and so on. The uncertainty in frequency is manifested in the frequency domain by the finite linewidth of a peak in the spectrum.

At its most fundamental level, an F.t./i.c.r. spectrometer is a "frequency meter", with the "mass meter" feature of the instrument only arising via Eqn. 1. What then determines the uncertainty in measuring cyclotron frequencies? The uncertainty in i.c.r. frequencies is ultimately limited by the duration of the i.c.r. time domain signal. The uncertainty (i.e., the linewidth) can be greater if the signal is observed for less than its duration. The duration of the time signal is limited principally by the background pressure of neutral molecules with the duration being given approximately by

$$\text{Duration (s)} = 2 \times 10^{-8}/\text{pressure (Torr)} \tag{5}$$

Thus, at 10^{-7} Torr, a typical operating pressure, the F.t./i.c.r. time signal will last for 0.2 s. This gives a frequency uncertainty or frequency linewidth of a few Hz.

The F.t./i.c.r. mass linewidth Δm, and the mass resolution $m/\Delta m$ are given, respectively [25], by

$$\Delta m = m^2 \, \Delta\omega/(qB) \tag{6}$$

$$m/\Delta m = qB/(m \, \Delta\omega) \tag{7}$$

where $\Delta\omega$ is the frequency uncertainty. These equations show that mass resolution is directly proportional to the magnetic field and inversely proportional to ion mass. These predictions have been experimentally confirmed [21].

Equation 1 indicates that there is no upper mass limit for F.t./i.c.r. instruments. A more detailed analysis [16] shows that the actual upper mass limit is in excess of 100 000 Daltons. However, a practical limit in most cases is the mass at which the mass linewidth, Eqn. 6, increases to 1 Dalton. For the present generation of instruments with three Tesla magnets, this is about 10 000 Daltons. This upper limit will be raised by the availability of higher field cryomagnets.

While the discussion above involved the "approximate F.t./i.c.r. linewidth", it should be noted that the exact linewidth is known for all circumstances as is the complete F.t./i.c.r. lineshape [28]. The relationship between F.t./i.c.r. linewidths and linewidths for other mass spectrometers is also known [29].

Mass calibration. Calibrating the spectrum is very important in mass spectrometry as the exact mass of a peak can be used to determine molecular formulae. Mass calibration is particularly convenient with F.t./i.c.r. spectrometers as the measurement is one of frequency. This important feature of F.t./i.c.r. was recognized and demonstrated several years ago [21] and has been considerably improved by more accurate corrections [16] for the trapping field shift.

Discrete F.t./i.c.r. spectra

All of the discussion to this point has involved continuous time signals and continuous frequency spectra. Computers, however, deal with numbers and the actual computer data in an F.t./i.c.r. experiment are discrete data. During the detection time period, the continuous time signal, Eqn. 4, is repetitively sampled by an analog-to-digital converter (ADC) to give a series of numbers, each of which is proportional to the instantaneous amplitude of the time signal at the instant of sampling. This series of numbers is the discrete time signal which is stored in the computer. Upon command, the computer performs the numerical Fourier analysis on this discrete time signal and presents the analysis as a second series of numbers which is the discrete frequency spectrum.

There are two important constraints on the acquisition of the discrete time signal. The first is the Nyquist criterion [14] which states that the sampling rate, S, must exceed twice the bandwidth of the spectrum. The second is N, the number of words of available computer memory. These two constraints limit t, the time of observation, commonly called the acquisition time, according to $t = N/S$. As mentioned above, resolution can be limited by the observation time if this is shorter than the signal duration. The equation $t = N/S$ creates a tradeoff between the widest possible mass range and the resolution of the spectrum. There are three methods for obviating this tradeoff. The first is the spectral segment extraction or heterodyne technique [21] which allows ultrahigh-resolution mass spectra over any chosen segment of the mass spectrum. This technique is commonplace today. A second very recent technique is spectral clipping [30], which introduces some distortion but reduces memory requirements. The third and most satisfactory technique is simply to increase the size, N, of the computer memory. Memory costs will continue to decrease for the forseeable future and the tradeoff mentioned above will probably disappear in a few years.

The discrete frequency spectrum given by a numerical Fourier transform is defined only at the $N/2$ discrete frequencies given by $f_1 = i/t$ ($i = 0, 1, 2, \ldots, N/2 - 1$). Errors can arise when the continuous frequency $\omega/2\pi$ (Eqn. 1) falls between two frequencies of the discrete spectrum, as it always does. Fortunately, this source of error is understood [31, 32] and the exact frequency and intensity can be evaluated from only the finite number of points in the discrete spectrum.

Pressure requirements

All mass spectrometers operate at high vacuum, typically with pressures in the range 10^{-4}—10^{-6} Torr. It follows then that the sample must have a vapor pressure of at least this much in order to create a gaseous sample to be ionized. Unfortunately, many important compounds have high molecular weights, say above 1000 Daltons, or are polar or charged and, therefore, have negligible vapor pressures at room temperature. While sample heating to temperatures of 200°C suffices for some compounds, many compounds decompose before their vapor pressure reaches even 10^{-4} Torr.

The F.t./i.c.r. spectrometer has some advantage in this regard as the mass spectra can be obtained at sample pressures of 10^{-8} Torr, a pressure 2—4 orders of magnitude lower than that required by other mass spectrometers. Examples are known [33] of samples which decompose just above room temperature but which have vapor pressure at room temperature just sufficient for mass spectral analysis by F.t./i.c.r. but not by other mass spectrometers.

The F.t /i.c.r throughput problem and its solution

As mentioned above, F.t./i.c.r. instruments can give ultrahigh-resolution mass spectra if the background pressure of the sample is ca. 10^{-7} Torr (Eqns. 5 and 7). To keep the background below the 1% level, the residual pressure in the vacuum system should be below 10^{-9} Torr. This residual pressure can be easily reached with modern vacuum technology and a few hours pumping. The pressure dependence of F.t./i.c.r. resolution and mass range requires in general that the pressure, even for low-resolution mass spectrometry, be below 10^{-5} Torr.

The low sample pressures required for high-resolution or high-mass F.t./i.c.r. can be in conflict with other requirements of the experiment. For example, chemical ionization experiments in which the sample is ionized by ion/molecule reaction, require a high pressure of the precursor to the chemical ionizer if the ionization step is to be completed in a reasonable period of time. At a methane pressure of 10^{-5} Torr, formation of the chemical ionizer by the reaction $CH_4^+ + CH_4 \rightarrow CH_5^+$, and chemical ionization via proton transfer to the sample, M, by the reaction $CH_5^+ + M \rightarrow MH^+$, would be complete in 1 s for a sample pressure of 10^{-7} Torr, but high-resolution F.t./i.c.r. spectrometry of MH^+ would be obviated by the high background pressure of methane (Eqns. 5 and 6).

Similarly, the low pressure needed for high-resolution or high-mass F.t./i.c.r. implies evacuation of the previous sample to 10^{-9} Torr and the concomitant pumping period to reach this pressure. The F.t./i.c.r. requirement for low residual pressures, combined with the finite time required to reach these pressures, severely limits the number of samples which can be examined per day. This is the F.t./i.c.r. throughput problem.

In some cases the conflicting pressure requirements for F.t./i.c.r. experiments can be ameliorated by pulsed valve injection of a reagent gas [34, 35].

With pulsed valve injection a short pressure burst of gas is created for rapid ion/molecule reaction, which is then pumped away, allowing high-resolution F.t./i.c.r. spectrometry. These pulsed valve experiments have proven useful for complex ion/molecule studies [34] and for gas chromotography with F.t./i.c.r. [35].

The most complete solution to the throughput problem is achieved by a physical separation of the region where ions are mass-analyzed from the region where ions are created. The simplest apparatus is the Littlejohn-Ghaderi dual cell [36, 37] which has two adjacent cell regions, each like the cell in Fig. 3. A pressure differential of 1000 can be maintained between the two regions by differential pumping of the two halves of the dual cell. Ions which are formed under high pressure conditions in the source region are transferred to the low pressure region by electrical pulses applied to the cell.

The second apparatus which solves the throughput problem consists of a quadrupole mass spectrometer, interfaced to an F.t./i.c.r. spectrometer [38]. The ion source of the quadrupole spectrometer can be operated under conditions optimal for ion formation while the F.t./i.c.r. cell conditions are optimized for ion analysis. Again, differential pumping allows a large pressure drop from the quadrupole source to the i.c.r. cell [38].

Specialized ionization techniques

One of the most important mass spectrometric advances in recent years is the development of specialized techniques for direct ionization into the gas phase from an involatile solid. These techniques have had an enormous impact on the mass spectrometric analysis of involatile biological samples. In each of these techniques a high velocity beam of particles impinges on the involatile solid and in a single operational step volatilizes and ionizes the sample [X + M(solid) → M^+ (gas)]. If X is a fast beam of neutral atoms the technique is called fast atom bombardment (f.a.b.) [39]. If X is a beam of positive ions, the technique is called secondary ion mass spectrometry (s.i.m.s.) [40] and if X is a beam of photons, laser desorption ionization (l.d.i.) [41, 42]. All three techniques are applicable to F.t./i.c.r. instruments [43—45, 38].

APPLICATIONS OF F.T./I.C.R. SPECTROMETRY

Versatility

Conventional i.c.r. spectrometry is the single most versatile technique for examining gas-phase ion chemistry [1, 2]. The ion-cyclotron double resonance technique [1, 2] in particular is the mass spectrometric technique of choice for examining complex ion/molecule reaction pathways. Hundreds of gas phase acidities and basicities have been measured by i.c.r. [46, 47]. Moreover, photon impact experiments such as photodetachment [48] and photodissociation [49] are readily conducted with i.c.r. instruments. Laser

desorption of metal ions provides a general technique for studying metal ion chemistry when the experiments are done on i.c.r. instruments [44]. An important feature of F.t./i.c.r. is that all of the capability of conventional i.c.r. is retained and, moreover, is enhanced by the speed, sensitivity, convenient mass calibration, high resolution and wide mass range of the Fourier approach [21].

The slow speed, low sensitivity, low resolution and limited mass range of conventional i.c.r. instruments, however, has prevented their use as analytical mass spectrometers. The features of conventional i.c.r. combined with the spectroscopic power of the Fourier method, as well as the application on F.t./i.c.r. instruments of recent advances in mass spectrometric ionization techniques, and the development of improved devices for increasing sample throughput, promise to create an ultrahigh-performance analytical mass spectrometer of unparalleled versatility. Some of this versatility is described below. While the various features of F.t./i.c.r. are organized into subsections, each of which gives a brief discussion of a specific feature and leading references, it should be noted that many specific applications of F.t./i.c.r. take advantage of more than one of these specific features of the technique.

Ion/molecule reaction studies

The study of gas-phase ion chemistry was one of the first applications of F.t./i.c.r. to be demonstrated [18]. The wide mass range of the technique and especially the double-resonance technique [17] have been exploited in many laboratories [19, 50—54] for this traditional use of i.c.r.

Ultrahigh-resolution and high-mass applications

The ultrahigh mass resolution and the wide mass range of F.t./i.c.r. are probably the two most important features of the technique. Ultrahigh mass resolution is needed for separating isobaric ions (ions of the same nominal mass) [21, 23, 24] and for determination of molecular formulae [16, 21, 55]. These are "standard" experiments of ultrahigh-resolution mass spectrometers. In addition, ultrahigh mass resolution can be used for exact determination of atomic masses and for determination of the fundamental physical constants of nature [26, 27].

The development of f.a.b., l.d.i. and s.i.m.s. [39—42] for ionization of involatile samples has stimulated considerable interest in the mass spectrometric analysis of high-molecular-weight (say above 1000 Daltons) compounds. The inherent high upper mass limit of F.t./i.c.r. [16, 21, 23—25] makes the technique a prime candidate for the mass spectrometric technique of choice for such high mass analysis [37, 38, 43, 45]. While the most basic theoretical analysis [25] predicts an infinite upper mass limit for F.t./i.c.r., a proper consideration of the components of the trapping field still leaves an upper mass limit above 10^5 Daltons [16].

The types of high-molecular-weight compounds which will be analyzed by F.t./i.c.r. are limited only by the imaginations of users. Compounds of

biological origin such as proteins, polysaccharides, and polynucleotides, polymers, high-molecular-weight organic and organometallic compounds, complex substances such as rubbers and plastics will all be analyzed mass spectrometrically by F.t./i.c.r. [37, 38, 43, 45].

It should be noted that the mass resolution and mass range of the F.t./i.c.r. instrument are critically dependent on both computer technology and magnet technology. The performance/price ratio for both computers and cryomagnets increases each year and it follows that F.t./i.c.r. performance can be expected to improve steadily in the future. In this respect, F.t./i.c.r. differs from both quadrupole and magnetic sector mass spectrometers, both of which are based upon mature technologies.

Experiments with m.s./m.s.

A general technique for analysis of gas-phase ions is the so-called m.s./m.s. experiment in which an ion is mass-selected out of an ensemble of ions, accelerated to high velocity and collided with a suitable gas. The collision induces the ion to fragment and the mass spectrum of the collision products is characteristic of the structure of the original ion [56]. The experiment requires two mass spectrometers; one to select the first ion and one to analyze the collision products.

The experiment can be done with just a single F.t./i.c.r. instrument by adding the requisite pulses and delays to the pulse sequence [34, 37, 50, 57, 58]. After i.c.r. ejection of all ions but the desired ion, the desired ion is excited by double resonance such that its orbital radius is just less than the cell dimensions. Then, the ion is allowed to undergo high energy collisions with the collision gas. Finally, the gas is pumped away and the mass spectrum of the collision fragments is obtained by the normal F.t./i.c.r. excitation-detection sequence.

Gas chromatography/F.t./i.c.r.

A most powerful general analytical tool is the composite instrument formed from a gas chromatograph and a mass spectrometer. The high separation power of a capillary-column gas chromatograph combined with the high performance of an F.t./i.c.r. spectrometer gives an analytical instrument with many applications for mixture analysis [59, 22, 37, 60].

The F.t./i.c.r. instrument is a pulsed technique and as such is particularly well suited for g.c./m.s. applications. Electron-impact mass spectra can be obtained from (say 10 ms) temporal slices of a g.c. peak, with each mass spectrum being representative of a slice. In contrast, conventional scanning mass spectrometers have a scan time comparable to the temporal width of a g.c. peak. With a conventional scanning mass spectrometer, different parts of the mass spectrum then correspond to different parts of the g.c. peak. If the g.c. peak consisted of several partially separated components, the single mass spectrum from a scanning mass spectrometer would be related to the components in a complex and indeterminate manner. In contrast, F.t./i.c.r.

mass analysis of the same g.c. peak would show several different mass spectra which would indicate the partial separation in the g.c. peak.

At first, it might appear that the low pressure requirements of F.t./i.c.r. and the gas load from the g.c. barrier gas would make an F.t./i.c.r. instrument an unsuitable mass spectrometer for gas chromatography/mass spectrometry. However, by careful control of the g.c. flow rate and pumping speed [59], the use of pulsed valve injection of the effluent [22, 60] and the use of the dual cell [36, 37], high-sensitivity, high-mass resolution g.c./F.t./i.c.r. results can be obtained.

Photodissociation experiments and surface analysis

One of the traditional i.c.r. experiments which profits from the wide mass range of the F.t./i.c.r. experiment is the photodissociation experiment [49]. In this experiment ions are fragmented by photon impact: $h\nu + M^+ \rightarrow M_1^+, M_2^+, \ldots$. The photodissociation spectrum obtained by plotting the abundance of M^+ vs. photon wavelength and the photofragment mass spectrum are diagnostic of the structure of M^+. These experiments provide complementary structural information to the m.s./m.s. experiment. The experiments are readily performed on F.t./i.c.r. instruments [50, 61, 62]. At high mass, momentum conservation limits the amount of kinetic energy which is available for m.s./m.s.-induced fragmentation and photodissociation experiments may prove particularly valuable for structural analysis of high mass ions [62].

A novel use of F.t./i.c.r. is to analyze the components adsorbed on a surface. The technique is to desorb the surface components by pulsed laser heating and then ionize and mass analyze desorbed components by F.t./i.c.r. [63].

FUTURE DEVELOPMENTS

More detail regarding the topics mentioned above can be found in other articles in this issue. These articles also contain many leading references to the F.t./i.c.r. literature. Also noteworthy are recent review articles [64–66] which cover similar material to that in this article, but from the viewpoints of different authors.

Resolution and mass range in F.t./i.c.r. are dependent upon both magnet and computer performance and one can expect F.t./i.c.r. performance to follow the steadily increasing performance/price ratio of computers and cryomagnets. The results to date on solving the "throughput problem" [36–38] are only the first attempts and it is reasonable to expect considerable improvements in the future. Sensitivity will be improved by more efficient ionization schemes such as multiphoton ionization [22] which gives more complete conversion of the neutral sample into ions. Larger i.c.r. cells [67] will increase the sensitivity because of the larger number of ions which can be held in the cell (Eqn. 3).

New data handling methods [13, 30, 68, 69] will allow the maximum amount of spectral information to be extracted from the available discrete F.t./i.c.r. data. Finally, the specific chemical problems to which F.t./i.c.r. will be applied is limited only by the imaginations of the users and the versatility of the technique ensures that there are many new applications yet to be demonstrated.

This research was supported by the Natural Sciences and Engineering Research Council of Canada.

REFERENCES

1 J. L. Beauchamp, Ann. Rev. Phys. Chem., 22 (1971) 527.
2 T. L. Lehman and M. M. Bursey, Ion Cyclotron Resonance Spectrometry, Wiley-Interscience, New York, 1976.
3 P. L. Griffiths, Transform Techniques in Chemistry, Plenum Press, New York, 1978.
4 A. G. Marshall (Ed.), Fourier, Hadamard and Hilbert Transforms in Chemistry, Plenum Press, New York, 1982.
5 M. B. Comisarow and A. G. Marshall, Chem. Phys. Lett., 25 (1974) 282.
6 M. B. Comisarow and A. G. Marshall, Chem. Phys. Lett., 26 (1974) 489.
7 M. B. Comisarow and A. G. Marshall, Can. J. Chem., 52 (1974) 1997.
8 F. J. Korr and D. Chatfield, Presented at the American Society for Mass Spectrometry Meeting, San Diego, CA, May, 1985, paper ROC7.
9 R. P. Feynman, R. B. Leighton and M. Sands, The Feynman Lectures on Physics, Addison Wesley, Reading, MA, 1963, Vol. 2.
10 E. O. Lawrence and M. S. Livingston, Phys. Rev., 40 (1932) 19.
11 M. B. Comisarow, J. Chem. Phys., 68 (1978) 4097.
12 A. G. Marshall and D. C. Roe, J. Chem. Phys., 73 (1980) 1581.
13 A. G. Marshall, T.-C. L. Wang and T. L. Ricca, Chem. Phys. Lett., 108 (1984) 63.
14 E. O. Brigham, The Fast Fourier Transform, Prentice-Hall, Englewood Cliffs, NJ, 1974.
15 M. B. Comisarow, Int. J. Mass Spectrom. Ion Phys., 37 (1981) 251.
16 E. B. Ledford, Jr., D. L. Rempel and M. L. Gross, Anal. Chem., 56 (1984) 2744.
17 M. B. Comisarow, V. Grassi and G. Parisod, Chem. Phys. Lett., 57 (1978) 413.
18 G. Parisod and M. B. Comisarow, Adv. Mass Spectrom., 8 (1980) 212.
19 T. C. Jackson, D. B. Jacobson and B. S. Freiser, J. Am. Chem. Soc., 106 (1984) 1252.
20 M. B. Comisarow, in K. P. Wanczek (Ed.), Ion Cyclotron Resonance Spectrometry, Springer-Verlag, Berlin, 1982.
21 M. B. Comisarow, Adv. Mass Spectrom., 8 (1980) 1688.
22 T. M. Sack, D. A. McCrery and M. L. Gross, Anal. Chem., 57 (1985) 1290.
23 M. B. Comisarow and A. G. Marshall, J. Chem. Phys., 61 (1975) 293.
24 M. Comisarow, Adv. Mass Spectrom., 7 (1978) 1042.
25 M. B. Comisarow and A. G. Marshall, J. Chem. Phys., 64 (1976) 110.
26 E. Lippma, R. Pikver, E. Suurmaa, J. Past, J. Pusker, I. Koppel and A. Tammik, Phys. Rev. Lett., 54 (1985) 285.
27 E. N. Nikolaev, J. I. Neronov, M. V. Gorshkov and V. L. Ta'alroze, JETP, 39 (1984) 441.
28 A. G. Marshall, M. B. Comisarow and G. Parisod, J. Chem. Phys., 71 (1978) 4434.
29 S. L. Mullen and A. G. Marshall, Anal. Chim. Acta, 178 (1985) 17.
30 A. T. Hsu T. L. Ricca and A. G. Marshall, Anal. Chim. Acta, 178 (1985) 27.
31 M. B. Comisarow and J. Melka, Anal. Chem., 51 (1978) 2198.
32 C. Giancaspro and M. B. Comisarow, Appl. Spectrosc., 37 (1983) 153.

33 L.-Y. Hsu, W.-L. Hsu, D.-Y. Jan, A. G. Marshall and S. Shore, Organometallics, 3 (1984) 591.
34 T. J. Carlin and B. S. Freiser, Anal. Chem., 55 (1983) 571.
35 T. M. Sack and M. L. Gross, Anal. Chem., 55 (1983) 2419.
36 S. Ghaderi and D. Littlejohn, Presented at the American Society for Mass Spectrometry Meeting, San Diego, CA, May, 1985, paper ROC12.
37 R. B. Cody, J. A. Kinsinger, S. Ghaderi, I. J. Amster, F. W. McLafferty and C. E. Brown, Anal. Chim. Acta, 178 (1985) 43.
38 D. F. Hunt, J. Shabanowitz and R. T. McIver, Jr., Anal. Chem., 57 (1985) 765.
39 M. Barber, R. S. Bordoli, R. D. Sedwick and A. N. Tyler, J. Chem. Soc. Chem. Commun., (1981) 325.
40 H. Kambara and S. Hishida, Anal. Chem., 53 (1981) 2340.
41 C. J. Q. Van der Peyl, K. Isa, J. Haverkamo and P. J. Kistemaker, Org. Mass Spectrom., 16 (1981) 416.
42 R. J. Cotter, Anal. Chem., 52 (1980) 1767.
43 D. A. McCrery and M. L. Gross, Anal. Chim. Acta, 178 (1985) 91; 178 (1985) 105.
44 R. B. Cody, R. C. Burnier, W. D. Reents, T. J. Carlin, D. A. McCrery and B. S. Freiser, Int. J. Mass Spectrom. Ion Phys., 33 (1980) 37.
45 M. E. Castro and D. H. Russell, Anal. Chem., 56 (1984) 578.
46 D. H. Aue and M. T. Bowers, in M. T. Bowers (Ed.), Gas Phase Ion Chemistry, Academic Press, New York, 1979.
47 J. E. Bartmess and R. T. McIver, Jr., in M. T. Bowers (Ed.), Gas Phase Ion Chemistry, Academic Press, New York, 1979.
48 B. K. Janousek and J. I. Brauman, in M. T. Bowers (Ed.), Gas Phase Ion Chemistry, Academic Press, New York, 1979.
49 R. C. Dunbar, in M. T. Bowers (Ed.), Gas Phase Ion Chemistry, Academic Press, New York, 1979.
50 B. S. Freiser, Anal. Chim. Acta, 178 (1985) 125.
51 C. L. Johlman and C. L. Wilkins, J. Am. Chem. Soc., 107 (1985) 327.
52 C. H. dePuy, J. J. Grabowski, V. M. Bierbaum, S. Ingemann and N. N. M. Nibbering, J. Am. Chem. Soc., 107 (1985) 1093.
53 J. C. Kleingeld and N. N. M. Nibbering, Org. Mass Spectrom., 17 (1982) 136.
54 C. Dass, T. M. Sack and M. L. Gross, J. Am. Chem. Soc., 106 (1984) 5775.
55 C. L. Johlman, D. A. Laude and C. L. Wilkins, Anal. Chem., 57 (1985) 1040.
56 F. W. McLafferty (Ed.), Tandem Mass Spectrometry, Wiley, New York, 1983.
57 R. T. McIver, Jr. and W. D. Bowers, in F. W. McLafferty (Ed.), Tandem Mass Spectrometry, Wiley, New York, 1983.
58 D. H. Russell and D. L. Bricker, Anal. Chim. Acta, 178 (1985) 117.
59 E. B. Ledford, Jr., R. L. White, S. Ghaderi, C. L. Wilkins and M. L. Gross, Anal. Chem., 52 (1980) 2450.
60 D. A. Laude, Jr., C. L. Johlman, R. F. Brown, C. F. Ijamas and C. L. Wilkins, Anal. Chim. Acta, 178 (1985) 67.
61 C. H. Watson, G. Baykut, M. A. Battiste and J. R. Eyler, Anal. Chim. Acta, 178 (1985) 125.
62 W. D. Bowers, S. Delbart and R. T. McIver, Jr., J. Am. Chem. Soc., 106 (1984) 7288.
63 M. G. Sherman, J. R. Kingsley, J. C. Hemminger and R. T. McIver, Jr., Anal. Chim. Acta, 178 (1985) 79.
64 C. L. Johlman, R. L. White and C. L. Wilkins, Mass Spectrom. Rev., 2 (1983) 389.
65 M. L. Gross and D. L. Remple, Science, 226 (1984) 261.
66 A. G. Marshall, Acc. Chem. Res., 18 (1985) 316.
67 R. L. Hunter, M. G. Sherman and R. T. McIver, Jr., Int. J. Mass Spectrom. Ion Phys., 50 (1983) 259.
68 M. B. Comisarow and J. Lee, Anal. Chem., 57 (1985) 463.
69 A. Rahbee, Chem. Phys. Lett., 117 (1985) 352.

Analytica Chimica Acta, 178 (1985) 17—26
Elsevier Science Publishers B.V., Amsterdam — Printed in The Netherlands

COMPARISON OF MASS RESOLUTION CRITERIA IN MASS SPECTROMETRY

STEVEN L. MULLEN and ALAN G. MARSHALL*[a]

Department of Chemistry, The Ohio State University, 140 W. 18th Avenue, Columbus, OH 43210 (U.S.A.)

(Received 8th May 1985)

SUMMARY

For a single peak, mass spectral resolution can be expressed in terms of peak width or ratio of peak position to peak width. Alternatively, for two equally intense peaks of equal width, resolution can be defined as the minimum peak separation such that the height of the valley between the combined peaks is less than a specified ratio (1%, 10%, 50%, 100%) of the individual (or combined) peak maximum. All these definitions depend on peak shape. Conversion formulae between various mass resolution criteria are presented for each of eight spectral peak shapes: Gaussian, triangular, trapezoidal, Lorentzian (absorption-mode, magnitude-mode, and sine-apodized magnitude-mode), and sinc (absorption-mode and magnitude-mode). From these formulae, mass resolutions based upon different criteria are readily compared for the same or different line shapes.

For a given spectral line shape (e.g., Lorentzian, Gaussian), resolution is usually expressed in one of three fundamental ways: (a) peak width (in absolute or relative units); (b) ratio of peak position to peak width for a single isolated peak; or (c) ratio of peak height to the minimum separation between two equally intense peaks such that the valley between them does not exceed a specified percentage (e.g., 1%, 10%, 50%, or 100%) of the peak maximum. In mass spectrometry, all of these definitions are in common use. The first problem is thus to convert between various definitions, e.g., to establish what a mass resolution of 1000 by the 50%-valley definition would become if a 10%-valley definition were applied, or to estimate what mass separation would be required to give a 1% valley if two peaks separated by 1 amu are just barely unresolved (i.e., separated by a "100% valley").

Furthermore, mass spectral line shapes differ between different mass spectrometer configurations (e.g., quadrupole, magnetic sector, cyclotron). Ewing [1] has considered Gaussian, triangular, and trapezoidal [width at base = 2 × (width at top)] shapes. With the advent of Fourier-transform ion-cyclotron resonance mass spectrometry (F.t./i.c.r.) [2, 3], absorption-mode and magnitude-mode [4] Lorentz and since line shapes [5] must be considered. Finally, the line shape resulting from sine-apodization of

[a]Also a member of the Department of Biochemistry.

0003-2670/85/$03.30

a time-domain exponentially damped sinusoid [6] is commonly used to reduce overlap between closely spaced Lorentzian peaks.

This paper presents conversion formulae between the above mass resolution criteria, for each of the eight mass-spectral line shapes shown in Fig. 1. These formulae can be used to convert between different resolution criteria for the same line shape (i.e., same spectrometer type). Alternatively, one can compute the line width (or peak separation) required to give the same resolution (by the same criterion) from two mass spectrometers having different peak shapes. In other words, experimental results quoted in different ways for different instruments can readily be compared.

PEAK SHAPES

Figure 1 shows the eight line shapes considered. Gaussian, triangular, and trapezoidal line shapes have been used to model the experimental peak shapes observed in magnetic sector, quadrupole, and time-of-flight instruments [1]. Fourier-transform/i.c.r. produces absorption-mode and magnitude-mode (also known as absolute-value-mode) line shapes which vary between Lorentzian (high-pressure) and sinc (low-pressure) limits [5]. Magnitude-mode is ordinarily employed in F.t./i.c.r. to avoid the need for non-linear phase correction [7]. Unfortunately, a magnitude-mode F.t./i.c.r. peak is broader at half-maximum height by a factor ranging from

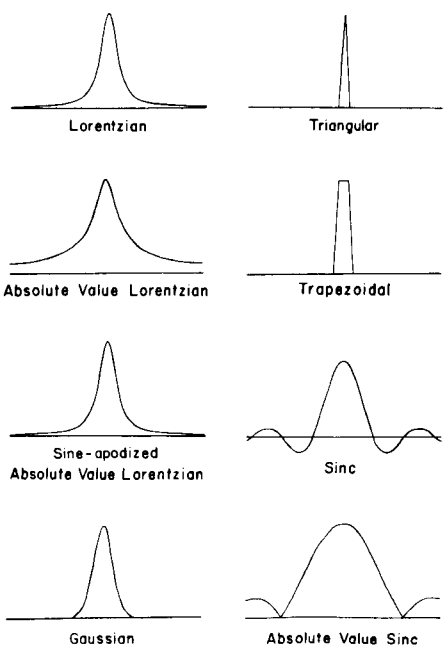

Fig. 1. Mass spectral line shapes considered.

$\sqrt{3}$ (Lorentzian) to 2 (sinc), and a magnitude-mode Lorentzian becomes extremely broad in the "wings" (i.e., far from the peak center, see Fig. 1). Thus, for nearly-Lorentzian peaks, it is common to apodize by multiplying the time-domain data (Fig. 2, middle left) by a sine wave of one-half cycle to give an apodized time-domain waveform (Fig. 2, bottom left) for which the Fourier transform to the frequency (mass) spectrum is also shown in Fig. 2 (bottom right). A related apodization is based on time-domain weighting with two quarter-wave sine curves separated by a flat segment to give an apodized time-domain waveform (Fig. 2, upper left), the Fourier transform of which is shown in Fig. 2 (upper right). The main effect of either sine-based time-domain weighting is to yield a magnitude-mode peak with a narrower base (compare upper or lower right spectra to the middle right spectrum in Fig. 2), leading to reduced overlap when closely-spaced peaks are present.

The formulae corresponding to the line shapes of Fig. 1 are listed in Table 1. Each expression is scaled in terms of the full width, Δm, at half-maximum peak height for that line shape. The sine-apodized magnitude-mode Lorentzian formula was computed analytically from the Fourier

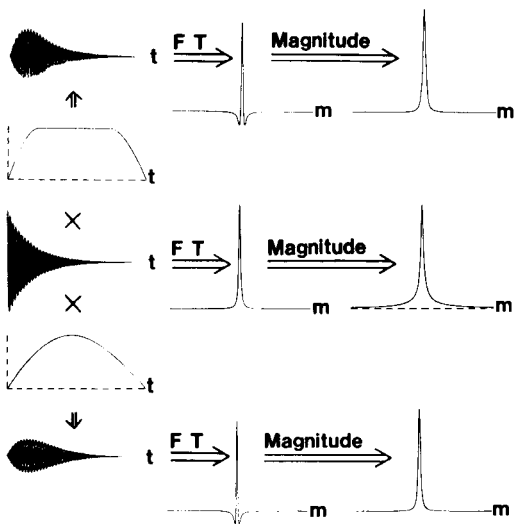

Fig. 2. Schematic diagram for sine-based apodization procedures. Middle row: Fourier transformation of an exponentially damped time-domain sinusoid leads to absorption-mode and magnitude-mode Lorentzian line shape. The time-domain waveform (bottom left) obtained by multiplying the original damped sinusoid by a half-cycle sine wave, exhibits the absorption-mode and magnitude-mode spectra shown at bottom right. Alternatively, the waveform (top left) obtained by time-domain weighting with two quarter-wave sine curves separated by a flat segment yields the absorption-mode and magnitude-mode spectra shown at top right. For a sufficiently long acquisition time, the magnitude-mode spectra obtained via either sine-based apodization are nearly identical in shape to the absorption-mode Lorentzian (middle row, second from right).

TABLE 1

Eight representative mass spectral line shapes. Each expression represents spectral amplitude, $A(m)$, as a function of mass, for a peak centered at mass, m_0, with height, h, and full width, Δm, at half-maximum height. For F.t./i.c.r. line shapes, it is assumed that $w_0 \gg \Delta w$

Gaussian	$A(m) = h \exp\{-2.7724\,[(m - m_0)/\Delta m]^2\}$
Triangular	$A(m) = 0;\ m < (m_0 - \Delta m)$ or $m > (m_0 + \Delta m)$ $A(m) = (h/\Delta m)\,[\Delta m + (m - m_0)];\ (m_0 - \Delta m) < m < m_0$ $A(m) = (h/\Delta m)\,[\Delta m - (m - m_0)];\ m_0 < m < (m_0 + \Delta m)$
Trapezoidal[a]	$A(m) = 0;\ m < (m_0 - 2\Delta m/3)$ or $m > (m_0 + 2\Delta m/3)$ $A(m) = h;\ m_0 - \Delta m/3 < m < m_0 + \Delta m/3$ $A(m) = (h/\Delta m)\,[2 + (3/\Delta m)(m - m_0)];\ (m_0 - 2\Delta m/3) < m < (m_0 - \Delta m/3)$ $A(m) = (h/\Delta m)\,[2 - (3/\Delta m)(m - m_0)];\ (m_0 + \Delta m/3) < m < (m_0 + 2\Delta m/3)$
Lorentzian (absorption)	$A(m) = h/\{1 + 4\,[(m - m_0)/\Delta m]^2\}$
Lorentzian (magnitude)	$A(m) = h/\{1 + 12\,[(m - m_0)/\Delta m]^2\}^{1/2}$
Lorentzian (sine-apodized magnitude)[b]	$A(w) = \left[\left\{\frac{[(\pi/T) - (w - w_0)]\tau}{1 + [(\pi/T) - (w - w_0)]^2\tau^2} + \frac{[(\pi/T) + (w - w_0)]\tau}{1 + [(\pi/T) + (w - w_0)]^2\tau^2}\right\}^2 + \left\{\frac{\tau}{1 + [(\pi/T) + (w - w_0)]^2\tau^2} - \frac{\tau}{1 + [(\pi/T) - (w - w_0)]^2\tau^2}\right\}^2\right]^{1/2}$
Sinc (absorption)	$A(m) = h\{\sin[3.791\,(m - m_0)/\Delta m]\}/\{[3.791\,(m - m_0)/\Delta m]\}$
Sinc (magnitude)	$A(m) = h\,2^{1/2}\{1 - \cos[7.582\,(m - m_0)/\Delta m]\}^{1/2}/[7.582\,(m - m_0)/\Delta m]$

[a](width at base) = 2 × (width at top). [b]Parametrization in terms of m, m_0, Δm, and h is extremely cumbersome in this case. The line shape is therefore expressed in terms of w, w_0, T and τ, in which w_0 is the i.c.r. frequency (rad s^{-1}), w is spectral frequency, T is acquisition period, and τ is exponential time-domain damping constant. For the alternative sine-based apodization (Fig. 2, top row), $A(w)$ is identical except that π/T is replaced by $2\pi/T$.

transform of the product of a time-domain exponentially damped sinusoid and a half-cycle sine wave.

MASS RESOLUTION CRITERIA

For a spectrum consisting of the sum of two peaks of equal width and height, the bottom of the valley between the two combined peaks must be twice the value of either component peak at the midpoint between them (see Fig. 3). A valley defined as 1% (or 10% or 50% or 100%) of the height

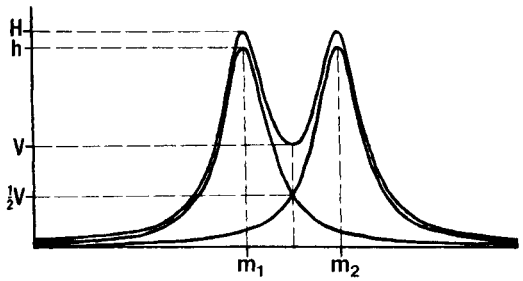

Fig. 3. Sum of two mass spectral peaks of equal width and height. The height, V, of the valley between the combined peaks can be measured with respect to either the height, h, of either component peak or the height, H, of either peak in the combined envelope. Table 3 is based on V/h = 1%, 10%, 50%, and 100%. Table 4 is based on V/H = 1%, 10%, 50%, and 100%.

of either component peak will thus result when the component amplitude of each peak has fallen to 0.5% (or 5% or 25% or 50%) of its maximum value at the mass midpoint between the two peaks. The corresponding masses are readily evaluated analytically [Gaussian, triangle, trapezoid, Lorentz (absorption-mode or magnitude-mode)] or numerically by iteration [sinc (absorption- or magnitude-mode) and sine-apodized magnitude-mode Lorentzian], and are reported in Table 2, which lists the full width at 0.5%

TABLE 2

Full line width (in units of Δm, the full width at half-maximum peak height) at specified percentage of peak height, for the line shapes of Table 1

Line shape	Percentage of peak height			
	50%	25%	5%	0.5%
Gaussian	1.000	1.4142	2.0789	2.7647
Triangular	1.000	1.4998	1.8999	1.9900
Trapezoidal	1.000	1.1667	1.3000	1.3300
Lorentzian (absorption)	1.000	1.7321	4.3589	14.1067
Lorentzian (magnitude)	1.000	2.2361	11.5326	115.4686
Lorentzian (sine-apodized magnitude)[a]	1.000	1.7320	4.3590	14.1075
Sinc (absorption)	1.000	1.3055	1.5782	1.6491
Sinc (magnitude)	1.000	1.3055	1.5782	1.6491

[a]In the Lorentzian limit (i.e., time-domain data acquired for ≥ 5 exponential decay lifetimes), either of the sine-based apodizations shown in Fig. 2 gives the same line shape, and thus the same entries in this and succeeding Tables.

(or 5% or 25% or 50%) of component peak height for each of the eight line shapes, expressed in units of Δm, the width at half-maximum height. Thus, each of these entries also represents the minimum relative separation between the two peaks, such that the valley between them will be no larger than 1% (or 10% or 50% or 100%) of the height of either component peak (columns 9, 11, and 12 of Table 3).

For an experimental mass doublet, the height of either individual component peak is not available from the observed spectrum. In this case, it is more convenient to define the valley as a specified percentage of the height of either peak in the combined (i.e., observed) spectral envelope. The mass separations (in units of Δm, determined by numerical iteration) required to give a 1% (or 10% or 50% or 100%) valley between the two observed (rather than component) peak maxima are listed in columns 9, 11, and 12 of Table 4.

RESULTS AND DISCUSSION

From the entries in Table 2, it is easy to convert between various mass resolution criteria for a given peak shape. For example, if $R_1 = m/\Delta m_1$ and $R_2 = m/\Delta m_2$, in which R_i is the resolution at mass, m, and Δm_i is the peak-to-peak mass separation for a particular valley definition, then $R_1/R_2 = \Delta m_2/\Delta m_1$. The ratio R_1/R_2 is thus the factor for converting from R_2 to R_1. The inverse ratio, $\Delta m_1/\Delta m_2$, can be thought of either as the reverse conversion factor or the conversion between mass separations corresponding to different definitions of mass resolution. The conversion factors listed in Tables 3 and 4 correspond to valley definitions based on component peak height (Table 3) and combined peak height (Table 4).

For example, (left half of Table 3), mass resolution based on the 50% definition for a Gaussian line shape is only 51.15% as good as the 1% definition. In other words, a 50% valley resolution of 1000 would be equal to a 1% valley resolution of 512. From the right side of the table, it is found that if two Gaussian peaks are separated by one amu for a 50% valley, then they would have to be separated by 1.9950 amu to give a 1% valley.

Table 2 also provides interesting comparisons between different line shapes. For example, consider a trapezoidal peak and a magnitude-mode Lorentzian peak of the same Δm (i.e., same width at half-maximum height). The Table shows that the magnitude-mode Lorentzian will be 115.5/1.33 = 86.8 times wider than the trapezoid at 0.5% of maximum peak height. In this case, the same mass resolution criterion (i.e., 1% valley) varies by almost two orders of magnitude when different line shapes are involved.

Row 5 in Tables 2—4 shows clearly that the magnitude-mode Lorentzian line shape commonly encountered in F.t./i.c.r. is a poor choice for spectra involving overlapping peaks. Fortunately, Fourier transform techniques allow for conversion from one line shape to another after the spectral data have been acquired. For example, a Lorentzian peak can be converted to a

TABLE 3

Factors for conversion between different mass resolution criteria, in which the valley between the sum of two peaks of equal height is 1%, 10%, 50%, or 100% of the height of either individual peak (see h in Fig. 3)[a].

Line shape	$\frac{R_1}{R_{10}}$	$\frac{R_1}{R_{50}}$	$\frac{R_1}{R_{100}}$	$\frac{R_{10}}{R_{50}}$	$\frac{R_{10}}{R_{100}}$	$\frac{R_{50}}{R_{100}}$	$\frac{\Delta m_1}{\Delta m_{10}}$	$\frac{\Delta m_1}{\Delta m_{50}}$	$\frac{\Delta m_1}{\Delta m_{100}}$	$\frac{\Delta m_{10}}{\Delta m_{50}}$	$\frac{\Delta m_{10}}{\Delta m_{100}}$	$\frac{\Delta m_{50}}{\Delta m_{100}}$
Gaussian	0.7519	0.5115	0.3617	0.6803	0.4810	0.7071	1.3299	1.9550	2.7647	1.4700	2.0789	1.4142
Triangular	0.9547	0.7537	0.5025	0.7894	0.5263	0.6667	1.0474	1.3268	1.9900	1.2667	1.8999	1.4998
Trapezoidal	0.9774	0.8772	0.7519	0.8974	0.7692	0.8571	1.0231	1.1400	1.3300	1.1143	1.3000	1.1667
Lorentzian (absorption)	0.3090	0.1228	0.0709	0.3974	0.2294	0.5774	3.2363	8.1445	14.107	2.5166	4.3589	1.7321
Lorentzian (magnitude)	0.0999	0.0194	0.0087	0.1939	0.0867	0.4472	10.012	51.639	115.47	5.1575	11.533	2.2361
Lorentzian (sine-apodized magnitude)	0.3090	0.1228	0.0709	0.3973	0.2294	0.5774	3.2362	8.1433	14.104	2.5170	4.3592	1.7319
Sinc (absorption)	0.9570	0.7916	0.6064	0.8272	0.6336	0.7660	1.0450	1.2633	1.6491	1.2089	1.5782	1.3055
Sinc (magnitude)	0.9570	0.7916	0.6064	0.8272	0.6336	0.7660	1.0450	1.2633	1.6491	1.2089	1.5782	1.3055

[a] R_i is mass resolution defined for an i% valley, and Δm_i the separation between the component peaks. For example, for a Gaussian shape, a mass resolution of 1000 based on 50%-valley criterion corresponds to a mass resolution of only 511.5 based on 1%-valley criterion.

TABLE 4

Factors for conversion between different mass resolution criteria, in which the valley between the sum of two peaks of equal height is 1%, 10%, 50%, or 100% of the height of either peak in the combined envelope (see H in Fig. 3)[a]

Line shape	$\frac{R_1}{R_{10}}$	$\frac{R_1}{R_{50}}$	$\frac{R_1}{R_{100}}$	$\frac{R_{10}}{R_{50}}$	$\frac{R_{10}}{R_{100}}$	$\frac{R_{50}}{R_{100}}$	$\frac{\Delta m_1}{\Delta m_{10}}$	$\frac{\Delta m_1}{\Delta m_{50}}$	$\frac{\Delta m_1}{\Delta m_{100}}$	$\frac{\Delta m_{10}}{\Delta m_{50}}$	$\frac{\Delta m_{10}}{\Delta m_{100}}$	$\frac{\Delta m_{50}}{\Delta m_{100}}$
Gaussian	0.7520	0.5065	0.1795	0.6735	0.2387	0.3544	1.3298	1.9745	5.5719	1.4848	4.1901	2.8219
Triangular	0.9547	0.7546	0.5030	0.7903	0.5269	0.6667	1.0474	1.3253	1.9879	1.2653	1.8979	1.5000
Trapezoidal	0.9774	0.8772	0.7519	0.8974	0.7692	0.8571	1.0231	1.1400	1.3300	1.1143	1.3000	1.1667
Lorentzian (absorption)	0.3063	0.1142	0.0268	0.3729	0.0876	0.2348	3.2643	8.7534	37.277	2.6815	11.420	4.2586
Lorentzian (magnitude)	0.0977	0.0166	0.0026	0.1700	0.0270	0.1585	10.234	60.193	379.73	5.8816	37.105	6.3086
Lorentzian (sine-apodized magnitude)	0.3063	0.1142	0.0268	0.3729	0.0876	0.2348	3.2643	8.7534	37.277	2.6815	11.420	4.2586
Sinc (absorption)	0.9590	0.8253	0.4138	0.8605	0.4314	0.5014	1.0427	1.2117	2.4169	1.1621	2.3179	1.9946
Sinc (magnitude)	0.9606	0.8670	0.8271	0.9025	0.8610	0.9539	1.0410	1.1534	1.0483	1.1080	1.1615	1.2091

[a] R_i is mass resolution defined for an i% valley, and Δm_i is the separation between the combined peaks. For example, for a Gaussian shape, two peaks of equal height would have to be separated by 1.9745 times as far to meet the 1%-valley criterion as to meet the 50%-valley criterion.

When two peaks are barely unresolved (100% valley), there is no detectable valley between them, and therefore no way to measure their separation. Hence, a slightly wider peak separation (99% valley) was used in order to measure the peak separation. The same comment applies for the combined peak height criterion of Table 5.

Gaussian peak by a simple series of data manipulations [8]. However, the Lorentz-to-Gauss conversion requires careful choice of weighting parameters in the apodization process, according to the absolute width of the peak(s) in question. Simpler time-domain weight functions which require no prior knowledge of the signal are the sine-based apodizations shown in Fig. 2. Comparison of the 4th and 6th rows of Tables 2—4 shows that the magnitude-mode line shape resulting from either of these apodizations is nearly indistinguishable from an absorption-mode Lorentzian, and offers a major improvement in resolution over a magnitude-mode Lorentzian, particularly in the "wings" of the peak (i.e., far from the peak center).

Table 5 shows conversion factors between resolution definitions in which the valley criterion for a doublet is based upon either the component peak height or the combined peak height. For the triangular and trapezoidal shapes, the amplitude of one peak of the doublet drops to zero before reaching the center of the other peak; thus, the maximum of either peak in the combined spectrum is the same as the height of either component peak. Both valley definitions therefore give the same resolution criteria (i.e., conversion factor of unity in Table 5) for triangular or trapezoidal peak shapes. For all other line shapes except sinc, mass resolution based upon combined peak height is as good or better than that based on original peak height. For example, a Gaussian resolution of 1000 by the 100% valley definition based on combined peak height would be only 496 if the valley had been defined relative to component peak height. Finally, the conversion factors in Table 5

TABLE 5

Conversion factors between resolution definitions based upon original height (h in Fig. 3) or combined height (H in Fig. 3)

Line shape	Factor to convert resolution from original to combined height criterion				Factor to convert resolution from combined to original height criterion			
	100% Valley	50% Valley	10% Valley	1% Valley	100% Valley	50% Valley	10% Valley	1% Valley
Gaussian	2.016	1.010	1.000	1.000	0.496	0.990	1.000	1.000
Triangular	1.000	1.000	1.000	1.000	1.000	1.000	1.000	1.000
Trapezoidal	1.000	1.000	1.000	1.000	1.000	1.000	1.000	1.000
Lorentzian (absorption)	2.639	1.073	1.007	1.002	0.379	0.932	0.993	0.998
Lorentzian (magnitude)	3.299	1.169	1.025	1.003	0.303	0.855	0.975	0.997
Lorentzian (sine-apodized magnitude)	2.639	1.073	1.007	1.002	0.379	0.932	0.993	0.998
Sinc (absorption)	1.466	0.959	0.998	1.000	0.682	1.042	1.002	1.000
Sinc (magnitude)	0.876	1.091	1.190	1.194	1.142	0.917	0.840	0.837

are most significant for the 100% valley (i.e., when contribution of one peak at the center of the other is greatest), and approach unity for the 1% valley. [The sinc results are anomalous, because the negative side lobes of the absorption-mode sinc line shape can reduce the height of the peak in the combined spectrum compared to the height of either component peak. Similarly, an additional peak appears at the midpoint between the composite peaks in a closely-spaced magnitude-mode sinc doublet.]

The series of papers of which this paper is a part is devoted exclusively to Fourier-transform ion-cyclotron resonance mass spectrometry; the history and applications of the method have recently been reviewed [9—11]. Because the line shapes encountered in F.t./i.c.r. differ markedly from those found in other types of mass spectrometry, mass resolution criteria also differ. The purpose of this paper has been to provide a basis for quantitative comparison of mass resolution criteria for different line shapes, so that measurements made on F.t./i.c.r. instruments can be critically compared to measurements made with other types of mass spectrometer.

This work was supported by grants (to A.G.M.) from NIH (GM-31683), Sohio, and The Ohio State University.

REFERENCES

1 G. W. Ewing, J. Chem. Educ., 46 (1969) A69; A149; A233.
2 M. B. Comisarow and A. G. Marshall, Chem. Phys. Lett., 25 (1974) 282.
3 M. B. Comisarow and A. G. Marshall, Chem. Phys. Lett., 26 (1974) 489.
4 M. B. Comisarow and A. G. Marshall, Can. J. Chem., 52 (1974) 1997.
5 A. G. Marshall, M. B. Comisarow and G. Parisod, J. Chem. Phys., 71 (1979) 4434.
6 P. R. Griffiths, in Chemical Infrared Fourier Transform Spectroscopy, 1975, Wiley-Interscience, New York, p. 23.
7 A. G. Marshall and D. C. Roe, J. Chem. Phys., 73 (1980) 1581.
8 A. G. Marshall, in A. G. Marshall (Ed.), Fourier, Hadamard, and Hilbert Transforms in Chemistry, 1982, Plenum, New York, pp. 1—43.
9 A. G. Marshall, Acc. Chem. Res., 18 (1985) 316.
10 M. L. Gross and D. L. Rempel, Science, 226 (1984) 261.
11 K. P. Wanczek, Int. J. Mass Spectrom. Ion Proc., 60 (1984) 11.

Analytica Chimica Acta, 178 (1985) 27—41
Elsevier Science Publishers B.V., Amsterdam — Printed in The Netherlands

CLIPPED REPRESENTATIONS OF FOURIER-TRANSFORM ION-CYCLOTRON RESONANCE MASS SPECTRA

ANNJIA T. HSU and ALAN G. MARSHALL*[a]

Department of Chemistry, The Ohio State University, 140 West 18th Avenue, Columbus, OH 43210 (U.S.A.)

TOM L. RICCA

Chemical Instrument Center, The Ohio State University, Columbus, OH 43210 (U.S.A.)

(Received 8th May 1985)

SUMMARY

Because of its high mass resolution over a wide mass range, a Fourier transform/mass spectrometry (F.t./m.s.) experiment may generate very large spectral data sets (⩾64 K each), creating severe data storage problems for g.c./F.t./m.s. and for mass spectral library storage, search and retrieval. Fortunately, the stored experimental data need not be highly precise. In this paper, it is shown that useful mass spectra can be produced from time-domain F.t./m.s. data that have been clipped to only 1 bit/word, thereby offering a potential reduction by a factor of ⩾20 in data storage requirement. In many cases, mass spectral resolution can actually be enhanced by the clipping process. Finally, it is shown that a compound can be identified quickly and accurately by comparison of its clipped representation with similarly clipped data for library compounds.

In order to take advantage of the potentially ultrahigh mass resolution [1] of Fourier-transform ion-cyclotron resonance mass spectrometry (F.t./i.c.r. or F.t./m.s.) [2—5], large data sets (⩾64 K/spectrum) may be required. Storage of large numbers of spectra is necessary in two important situations. First, a single gas chromatography experiment with F.t./i.c.r. (g.c/F.t./i.c.r.) [6] can produce about one spectrum per second for up to an hour, generating enough data to fill a 160-Mbyte storage module. Second, on-line storage of even a small spectral library for retrieval and identification becomes difficult.

Fortunately, an extraordinary reduction in data storage is made possible by the natural relation between time-domain and frequency-domain signals in Fourier transform spectroscopy. Consider a time-domain signal consisting of a sine wave at a single frequency (see Fig. 1). Conventionally, one would expect to digitize such a signal and store each time-domain point as (say) a 20-bit word. A discrete Fourier transform of the digitized time-domain data set then gives a frequency-domain spectrum consisting of a spike at the

[a]Also a member of the Department of Biochemistry.

0003-2670/85/$03.30

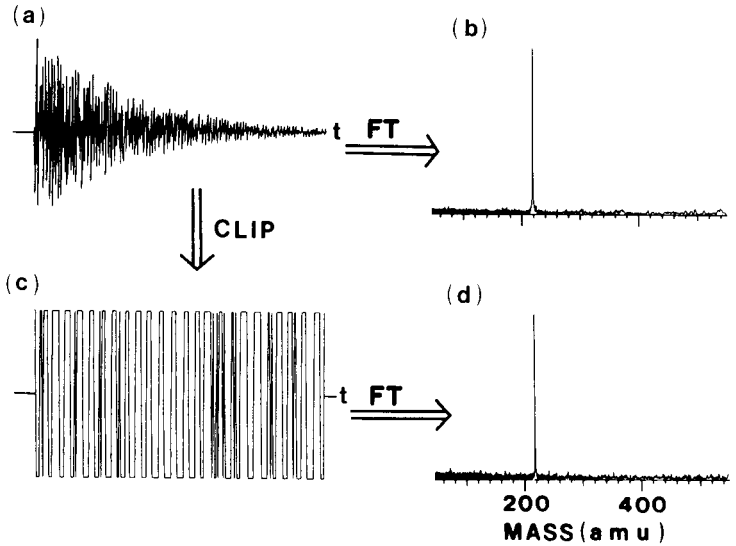

Fig. 1. Time-domain (left) and mass-domain (right) representations of a simulated single-frequency. F.t./m.s. signal, to which random noise has been added. (a) Exponentially damped sinusoidal time-domain signal, digitized with 20 bits per point. (b) Mass spectrum, obtained by magnitude-mode Fourier transform of the data shown in (a). (c) Time-domain signal from (a), clipped to one bit per point (i.e., 1 for positive-valued data; 0 for negative- or zero-valued data). (d) Mass spectrum, obtained by magnitude-mode Fourier transform of the data shown in (c).

frequency of the time-domain waveform. However, 20-bit words are not really required in order to identify a signal at that frequency. For example, it suffices to know the points at which the time-domain signal crosses zero (i.e., how many cycles occur during the detection period) [7]. In fact, if one "clips" the time-domain signal down to 1 bit (i.e., binary 1 or 0) according to the sign of the signal, then a discrete Fourier transform of the time-domain data set of 1-bit words yields a spectrum virtually identical to that obtained by Fourier transform of the time-domain data set of 20-bit words (see Fig. 1).

Surprisingly, even for signals consisting of oscillations at two or more frequencies, the Fourier transform of a clipped time-domain data set still gives a good visual representation of the "true" spectrum obtained by the Fourier transform of unclipped time-domain data (see Fig. 2). The results of the clipping process can be compared to the result of overdriving an audio-frequency amplifier: harmonic distortion (signals at multiples of the "true" frequencies), and intermodulation distortion (signals at "combination" frequencies resulting from sums and/or differences of the "true" frequencies). First applied to nuclear magnetic resonance (n.m.r.) spectrometry by Larsen and Crawford [7], the idea was later adapted to mass spectrometry [8].

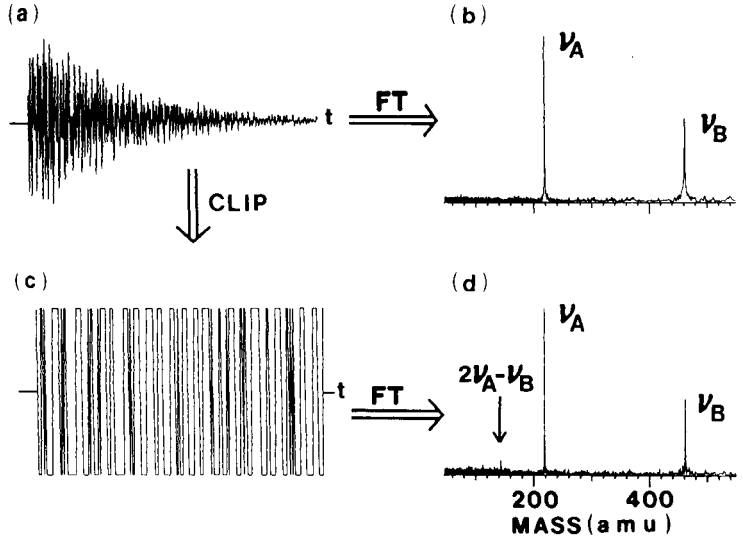

Fig. 2. Time-domain (left) and mass-domain (right) representations of a simulated two-frequency F.t./m.s. signal, to which random noise has been added. Format is as for Fig. 1.

In n.m.r., clipped time-domain data are seldom used. First, one rarely requires more than about 10^6 on-line data points at a time, even for two-dimensional n.m.r. experiments, so that there is no urgent need to reduce the data storage array size. Second, n.m.r. spectra acquired at different magnetic field strengths are qualitatively different in appearance, thereby reducing the utility of an extensive spectral library compiled at a single magnetic field strength.

In mass spectrometry, however, vast spectral libraries already exist [9]. Moreover, most mass spectral libraries are based on low-resolution nominal-mass data storage (i.e., one peak per amu), so that a stored mass spectrum consists of only ca. 1—2 K data points, and huge data arrays can again be avoided. Further, in order to generate clipped data, an ordinary mass spectrum must first be subjected to an inverse Fourier transform to yield a data set with no physical meaning.

However, Fourier transform mass spectra offer high mass resolution (and thus much larger data sets) and are acquired in the time-domain to begin with. Thus, F.t./i.c.r. time-domain data can be clipped directly, whether one chooses to transform the data to yield a mass spectrum or not. This paper presents examples and advantages for clipped representations of F.t./i.c.r. data. The main additional factor not encountered in other types of spectroscopy is the "phase" problem [10, 11], for which two alternative solutions are offered.

The clipping operation

Clipping techniques, also known as hard-limiting or one-bit quantization, have been applied to a variety of signals characterized by zero time-average value, such as time-domain speech signals. A clipped signal, $C(t)$ can be generated from a time-domain signal, $f(t)$, by the following simple recipe:

$$C(t) = f(t)/|f(t)| = \text{sgn}\,[f(t)] \tag{1}$$

An important requirement for $f(t)$ is that $\overline{< (f(t)) >} = 0$, in which the brackets denote a time-average over the data acquisition period, and the bar denotes an ensemble average over many such experiments.

The clipping operation clearly retains only the sign of the original data, $f(t)$. However, all zero-crossings of $f(t)$ are preserved in the clipped signal, $C(t)$. In order that the signal be recovered from the zero-crossings, the number of zero-crossings during the time-domain acquisition period must be at least twice the highest frequency in the final frequency-domain spectral band [12]. It is important to realize that this condition is more severe than the usual Nyquist requirement that the time-domain data be sampled at a frequency at least twice as high as the largest frequency in the spectrum, because a typical multifrequency time-domain signal does not cross zero at every data point. In any case, the clipping process is a nonlinear operation, and distortions (harmonic and intermodulation) in the frequency-domain representation of a clipped time-domain signal will be present, no matter how many clipped data points are acquired.

The phase problem

At first inspection, it might appear that one could construct a library of clipped time-domain F.t./i.c.r. signals for reference compounds, and then identify an unknown by cross-correlation (i.e., point-by-point comparison) of the clipped time-domain signal for an unknown with each of the clipped data sets in the library. However, even when the number of data points is fixed, the phase for each spectral frequency (i.e., whether a given oscillation begins as a cosine or sine or something intermediate at the beginning of the data acquisition period) can vary between different data sets for the same compound. For example, there will be a phase correction that is constant across the frequency (mass) range, according to the time delay between excitation and detection. For frequency-sweep excitation [2, 11], an additional non-linear variation of phase with frequency is produced by a combination of excitation frequency sweep rate, sweep range, and digitization rate. Thus, it is necessary to devise a way to remove phase-variation from the data, if different data sets are to be compared in a uniform way. The two approaches proposed below involve either the use of magnitude-mode in the frequency-domain (i.e., mass-domain) or autocorrelation in the time domain.

Magnitude/inversion method

One solution to the phase problem is suggested by analogy to the recovery of "pseudo-spatial" images from x-ray diffraction intensity data. In that case, the raw data exist in magnitude-mode form, in which all phase variation is absent. The "Patterson" function constructed by Fourier transformation of the magnitude-mode data is a "pseudo-spatial" image which is related to the true electron density image [13]. In F.t./i.c.r., a complex Fourier transform of a time-domain ion-cyclotron-resonance transient can be applied to obtain "absorption" and "dispersion" spectra, and then a magnitude-mode spectrum can be constructed from the square root of the sum of the squares of the absorption and dispersion data [9]. The resultant magnitude-mode display will be independent of the phase at each frequency in the spectrum.

If the magnitude-mode spectrum is then subjected to an inverse Fourier transform, a "pseudo-time domain" data set (which is independent of the phases in the original time-domain data) will be generated. For example, a time-domain sinusoid of arbitrary phase (e.g., cosine, sine, or anything in between) will yield a "pseudo-time-domain" signal which always looks like a cosine (i.e., starts with its maximum value at "pseudo-time" zero). It is as if the phase were zero-valued across the whole spectrum. The "pseudo-time-domain" signal can then be clipped and stored for library use. If a mass spectrum is later needed, the clipped "pseudo-time-domain" data can be subjected to Fourier transformation followed by magnitude-calculation to yield a magnitude-mode spectrum. These procedures are summarized below:

Time-domain data (phase-dependent)
↓ FT
Absorption and dispersion spectra (phase-dependent)
↓ magnitude-calculation
Magnitude-mode spectrum (phase-independent)
↓ inverse FT
"Pseudo-time domain" data (phase-independent)
↓ clip to 1 bit
Clipped "pseudo-time domain" data (phase-independent)
↓ FT + magnitude-calculation (optional)
Magnitude-mode display of clipped "pseudo-time-domain" data

Autocorrelation: direct method

For a causal time-domain signal [i.e., $f(t) = 0$ for $t < 0$] of duration, T, the autocorrelation function, $G(\tau)$, for $f(t)$ is defined [14] by

$$G(\tau) = \int_0^T f(t)\, f(t + \tau)\, dt \qquad (2)$$

It is readily shown that for any linear system (i.e., when response varies linearly with excitation), the autocorrelation function and the power spectrum, $P(\omega)$, are related by a Fourier transform:

$$P(\omega) = (2/\pi) \int_0^T G(\tau) \cos(\omega\tau)\, d\tau \qquad (3)$$

An autocorrelation function is inherently phase-independent: e.g., the autocorrelation functions for a time-domain sine wave and a time-domain cosine wave are identical. Thus, a magnitude-mode spectrum can be obtained from a time-domain signal in either of two ways: (a) by Fourier transformation followed by magnitude-calculation, or (b) by autocorrelation followed by Fourier transformation (see Eqn. 3) and then taking the square root of each power spectrum data point. In either case, a phase-independent display is obtained.

One way to exploit this phase-independence is to construct an autocorrelation function directly from the original time-domain data, and then clip the autocorrelation function to one bit per data point. The clipped, autocorrelated data can be stored for library retrieval and comparison to other data sets, and visualized (if necessary) by subsequent retrieval and Fourier transformation to give a "pseudo" power spectrum, from which a "pseudo" magnitude-mode spectrum can be obtained by taking a point-by-point square root of the power spectrum, if desired. (Magnitude-mode display is usually preferred to a power spectrum, because the peak heights more accurately reflect the relative numbers of ions for each mass peak.) The data reduction for this method is summarized below:

Time-domain data (phase-dependent)
↓ autocorrelate
Time-domain autocorrelation function (phase-independent)
↓ Clip to 1 bit
Clipped time-domain autocorrelation function (phase-independent)
↓ FT
"Pseudo" power spectrum

Autocorrelation: power/inversion method

Another means for generating the autocorrelation function is suggested by Eqn. 3. Beginning again from the time-domain signal, one can apply a Fourier transform, and then take the point-by-point sum of the squares of the absorption and dispersion data sets to yield a power spectrum. Inverse Fourier transformation of the power spectrum then provides the autocorrela-

tion function, which can then be clipped as in the previous method. The procedure is summarized below:

Time-domain data (phase-dependent)

↓ FT

Absorption and dispersion spectra (phase-dependent)

↓ square each data point;
point-by-point add (absorption)^2 + (dispersion)^2

Power spectrum (phase-independent)

↓ Inverse FT

Time-domain autocorrelation function (phase-independent)

↓ Clip to 1 bit

Clipped time-domain autocorrelation function

↓ FT

"Pseudo" power spectrum

Table 1 shows why the power/inversion method is preferred over the direct method of computing an autocorrelation function. Direct computation of a discrete autocorrelation function for an N-point time-domain data set is a lengthy process. Specifically, $f(t)$ is first aligned along itself and then multiplied point-by-point for each of the N points. Then the function is shifted by one data point with respect to a twin of itself, and the next point-by-point multiplication requires only $(N-1)$ points, because one knows in advance that the first data point is zero. The number of calculations thus becomes $N + (N-1) + (N-2) + \ldots + 2 + 1 = N(N-1)/2$ multiplications and additions. When the number of data points is large (ca. 10^4), the number of computational steps approaches 10^8. However, the Cooley-Tukey algorithm [15] provides a discrete fast Fourier transform requiring on the order of $N \log_e(N)$ computations for an N-point time-domain data set. Even with the additional steps of the power/inversion method, the total number of computational steps is still on the order of only

TABLE 1

Approximate number of computational steps required for the various data reductions proposed in the text, for an 8 K time-domain data set

Method	Formula for number of computational steps	Actual number of steps for 8 K time-domain data set
Magnitude/inversion	$N \ln(N) + 2N + N \ln(N)$	1.64×10^5
Autocorrelation: direct	$N(N-1)/2$	3.36×10^7
Autocorrelation: power/inversion	$N \ln(N) + N + N \ln(N)$	1.56×10^5

10^5. Thus, the power/inversion method produces an autocorrelation function about 200-fold faster than by the direct discrete autocorrelation method.

EXPERIMENTAL

Both experimental and theoretical work for this paper was done with a Nicolet FTMS-1000 Fourier transform mass spectrometer, operating at 3.02 tesla, equipped with a 1280 computer and co-processor. Simulated noise for the theoretical plots was produced from the RND command in BASIC. For experimental spectra, background subtraction in the time domain was used to remove artifacts resulting from residual oscillations in the electronics. Sample pressure was ca. 1.5×10^{-8}. All spectra were produced via "direct" (as opposed to "heterodyne") mode. For library spectra (Table 2), time-domain 32 K data sets were collected with a bandwidth of 1.33 MHz (for an acquisition time of 12.5 ms), but only the first 1 K of data were retained, so that library comparisons could all be done in core memory for convenience.

RESULTS AND DISCUSSION

Phase-independent spectra based on data clipped according to each of the three algorithms presented in the Theory section are shown in Figs. 3—5.

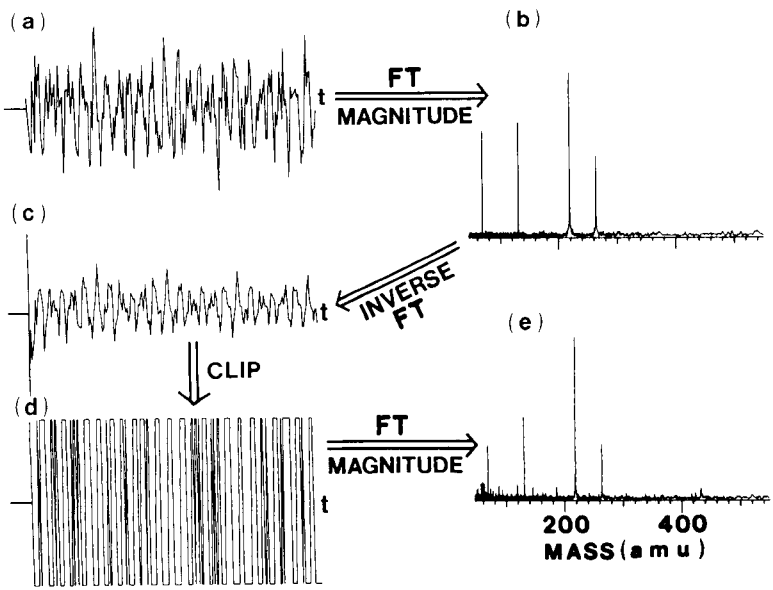

Fig. 3. Time-domain (left) and mass-domain (right) representations of a theoretical multiple-frequency F.t./m.s. signal, to which random noise has been added. (a) Same as Fig. 1(a). (b) Same as Fig. 1(b). (c) The "pseudo-time domain" signal, obtained by inverse Fourier transform of the magnitude-mode spectrum shown in (b). (d) "Pseudo-time-domain" signal from (c), clipped to one bit per point (i.e., 1 for positive-valued data; 0 for negative- or zero-valued data). (e) "Pseudo" mass spectrum, obtained by magnitude-mode Fourier transform of the data shown in (d).

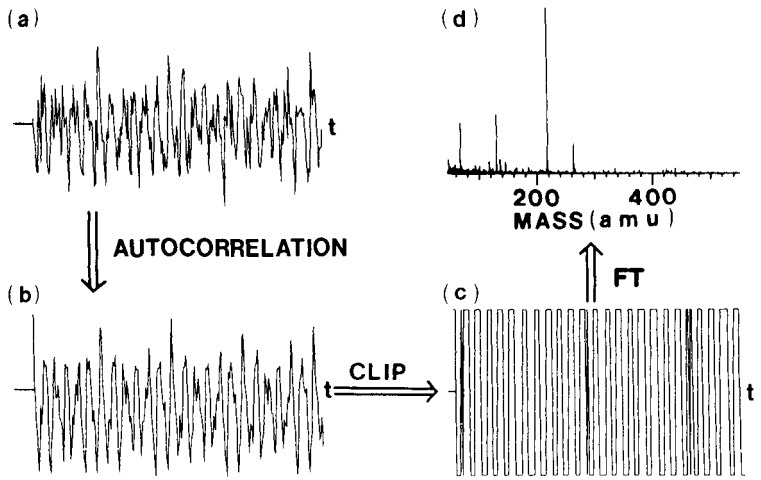

Fig. 4. Time-domain (left) and mass-domain (right) representations of a theoretical mixed-frequency F.t./m.s. signal, to which random noise has been added. (a) Same as Fig. 1(a). (b) Time-domain signal, obtained by direct autocorrelation of (a). (c) Autocorrelation function (b) clipped to one bit per point. (d) "Pseudo-power" spectrum, obtained by Fourier transform of the data shown in (c).

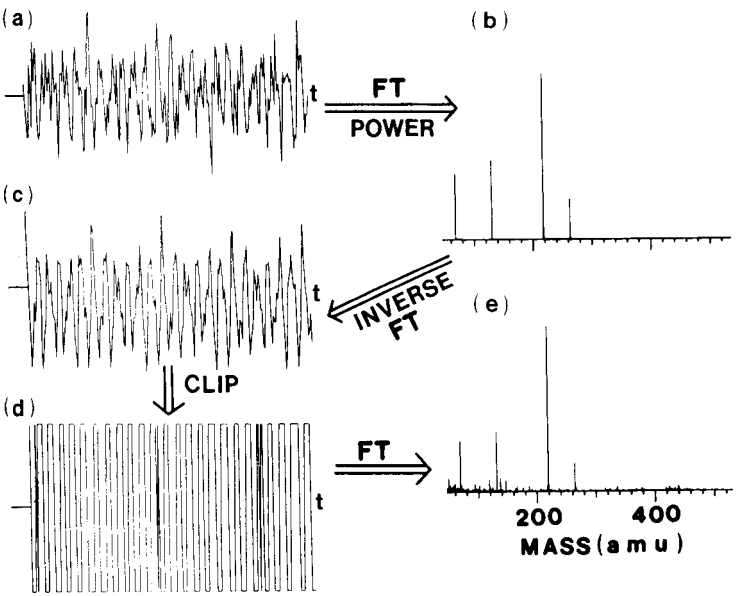

Fig. 5. Time-domain (left) and mass-domain (right) representations of a theoretical multiple-frequency F.t./m.s. signal, to which random noise has been added. (a) Same as Fig. 1(a). (b) Power spectrum of the data shown in (a), obtained by Fourier transform followed by point by point addition of (absorption)^2 + (dispersion)^2. (c) Time-domain autocorrelation function, obtained by inverse Fourier transform of the power spectrum shown in (b). (d) Autocorrelation function, (c), clipped to one bit per point. (e) "Pseudo-power" spectrum, obtained by Fourier transform of (d).

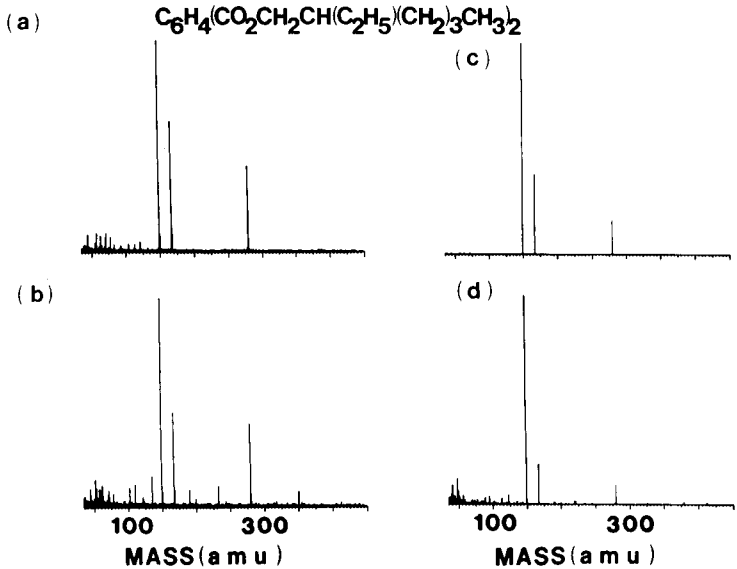

Fig. 6. Experimental Fourier-transform mass spectra of bis(ethylhexyl) phthalate: (a) magnitude-mode spectrum, from Fourier transform of time-domain digital data (20 bit/word). (b) "Pseudo" magnitude-mode spectrum, from clipped (1 bit/word) "pseudo-time-domain" data produced by the magnitude/inversion method. (c) Power spectrum, computed by squaring each data point in (a). (d) "Pseudo" power spectrum, obtained from clipped autocorrelation function (power/inversion method).

Spurious small intermodulation peaks produced by the (non-linear) clipping operation are observed in the spectra produced by all three methods (Figs. 3e, 4d, and 5e). As expected, the "pseudo-power" spectra obtained by direct autocorrelation (Fig. 4d) and by the power/inversion method (Fig. 5e) are identical. However, the computation time for the power/inversion method is vastly less, as discussed above.

Further examples of clipped mass spectral representations based on the magnitude/inversion or power/inversion methods are shown in Figs. 6–8 for organic and organometallic samples. In spite of the additional intermodulation peaks in the spectrum generated by the magnitude/inversion method, the characteristic major peaks of bis(ethylhexyl) phthalate are readily recognized (Fig. 6b). However, it is more difficult to identify the characteristic masses in the spectrum produced via the power/inversion method (Fig. 6d), because the intensity of one of the intermodulation peaks is nearly the same as for the (true) peak at 279 amu. Thus, it appears that a spectrum obtained by clipping the phase-independent time-domain signal gives a more accurate representation of the true spectrum than that obtained by clipping the time-domain autocorrelation function.

Signal-to-noise ratio

Figures 7 and 8 show normal magnitude-mode (top) and magnitude/

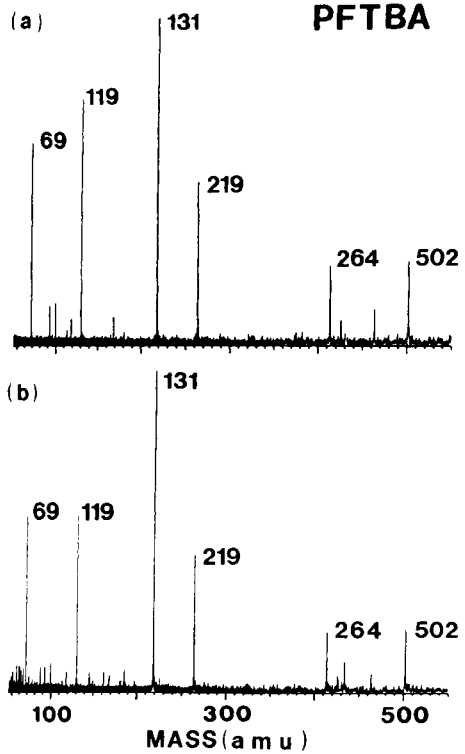

Fig. 7. Experimental Fourier-transform mass spectra of perfluorotri-n-butylamine (PFTBA): (a) magnitude-mode spectrum, from Fourier transform of time-domain digital data (20 bit/word); (b) "pseudo" magnitude-mode spectrum, from clipped (1 bit/word) "pseudo-time-domain" data produced by the magnitude/inversion method.

inversion clipped representations (bottom) of the mass spectra of two compounds. Although the signal-to-noise ratios for the clipped and normal mass spectral representations are similar for PFTBA (Fig. 7), the signal-to-noise ratio is significantly poorer for the clipped representation than for the normal F.t./i.c.r. mass spectrum of Ir(cyTTP)H_2Cl (Fig. 8).

When (as in Fig. 7) the time-domain acquisition period is short compared to the time-domain damping constant (i.e., "low-pressure" limit [16]), then clipping decreases the signal and noise to a similar extent, and the signal-to-noise ratio of a magnitude/inversion clipped representation is essentially the same as for a magnitude-mode Fourier transformation of the raw time-domain data. However, when (as in Fig. 8), the time-domain acquisition period is long enough that the signal has dropped below the noise level by the end of the acquisition period (i.e., "high-pressure" limit [16]), then clipping effectively reduces the signal more than the noise, and the magnitude/inversion clipped spectral representation exhibits poorer signal-to-noise ratio than a magnitude-mode Fourier transformation of the raw time-domain data.

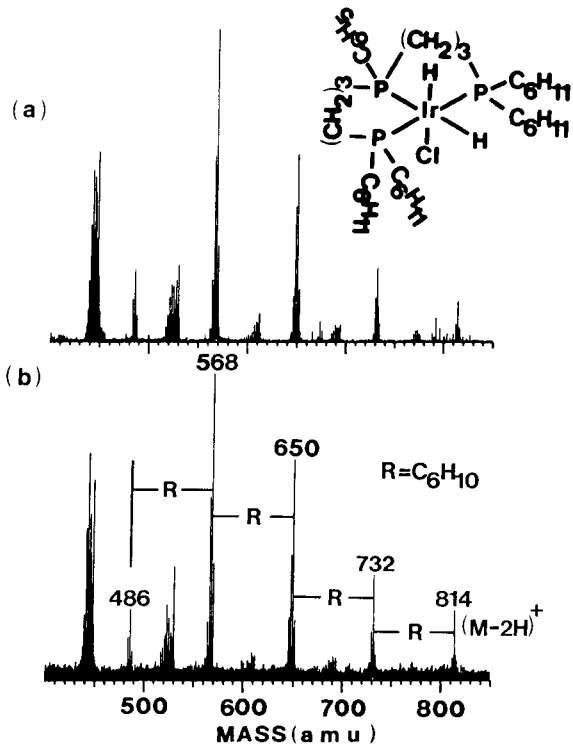

Fig. 8. Experimental Fourier-transform mass spectra of Ir(CyTTP)H_2Cl, in which CyTTP denotes $(C_6H_5)P[CH_2CH_2CH_2P(C_6H_{11})_2]_2$. Format is as for Fig. 7.

Resolution enhancement

An interesting consequence of the clipping procedure appears most clearly in Fig. 9. The line width in the clipped spectrum is actually narrower than in the spectrum obtained by direct Fourier transformation of the (unclipped) time-domain data. The reason is that the clipping operation, in the absence of noise, eliminates any damping in the time-domain. Thus, the clipping operation in the time-(or "pseudo-time") domain effectively enhances mass resolution in the frequency domain.

Effect of noise on distortion

One might expect that the nonlinear clipping operation in the time- (or "pseudo-time-") domain should introduce both harmonic and intermodulation distortion in the Fourier spectrum of a clipped time-domain transient signal. In fact, harmonic distortion peaks are clearly visible in the clipped representation of a noiseless time-domain single-frequency oscillation (compare Fig. 10a and b). However, when a small level of noise is added to the time-domain data prior to clipping, the harmonic peaks in the clipped representation become so small that they are no longer visible above the

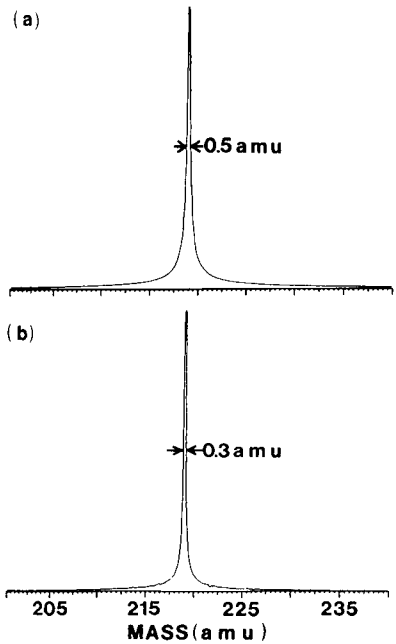

Fig. 9. (Left.) Fourier-transform mass spectra for a theoretical noiseless single-frequency time-domain exponentially-damped sinusoidal i.c.r. signal: (a) magnitude-mode Fourier transform of unclipped time-domain data (20 bit/word); (b) magnitude-mode Fourier transform of clipped time-domain data (1 bit/word).

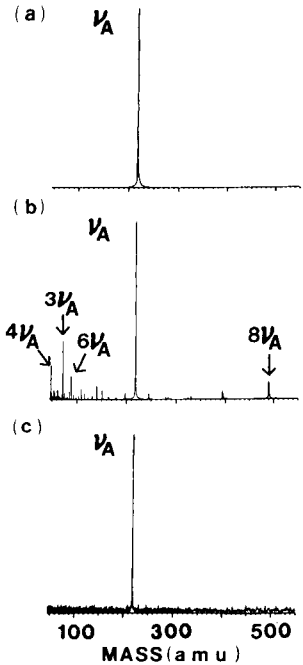

Fig. 10. (Right.) Fourier-transform mass spectra for a theoretical noiseless single-frequency time-domain exponentially-damped sinusoidal i.c.r. signal: (a) magnitude-mode Fourier transform of unclipped time-domain data (20 bit/word); (b) "pseudo" magnitude-mode spectrum for the same (noiseless) time-domain data, obtained via the magnitude/inversion method; (c) "pseudo" magnitude-mode spectrum for the same time-domain data to which random noise had been added, obtained via the magnitude/inversion method.

noise (see Fig. 10c). It is believed that the addition of noise increases the number of zero-crossings so that the number of zero-crossings more nearly approaches the limit of twice the highest frequency in the spectral bandwidth [17]. Fortunately, the noise need only amount to a few bits (which will almost always be the case in actual experiments) in order to produce the desired zero-crossings.

Library search based on clipped representations of F.t./m.s. data

Although Fourier transformation of a clipped time- (or "pseudo-time") domain signal gives a distorted mass spectrum one should be able to compare clipped time (or "pseudo-time") data sets for knowns and unknowns with (in principle) undistorted reliability. In order to test this idea, F.t./i.c.r. data sets for a small number of related dialkyl phthalates were acquired,

TABLE 2

Library search/identification of phthalate diesters based on cross-correlation of clipped phase-independent time-domain F.t./m.s. signals. A perfect match of one 1024-point data set with itself would give a cross-correlation value of 1024 (see text)

Compound	Cross-correlation with library clipped data set for di-n-octyl phthalate
Di-n-octyl phthalate	994[a]
	959[a]
Di-n-butyl phthalate	926
Diethyl phthalate	903
Butylbenzyl phthalate	857
bis(2-ethylhexyl) phthalate	824
Perfluoro-tri-n-butylamine	508
Dimethyl phthalate	500

[a]The two values are derived from independent F.t./m.s. data acquired on different days at different filament current. The values are less than 1024 (perfect match) because of noise.

subjected to the magnitude/inversion clipping procedure, and stored as a reference library. An independent data set for one of the compounds (di-n-octyl phthalate) taken several days later was processed similarly, and stored as an "unknown". The "unknown" data set was then cross-correlated with each of the "knowns", by an exclusive/nor operation: that is, if a given "pseudo-time" data bit was the same in both (clipped) data sets, it was scored as "1", whereas if the data bit was opposite in the two data sets, it was scored as a "0". Thus, for 1024-point data sets, a perfect match would give a cross-correlation value of 1024. Actual agreement of two independent data sets will of course be somewhat smaller because of finite noise in the data, as seen in Table 2. Nevertheless, Table 2 shows that the correct reference compound can be distinguished from several other related compounds, based upon cross-correlation of their clipped F.t./i.c.r. representations. Apart from the vastly reduced storage requirements for clipped F.t./i.c.r. data, an additional advantage for library search/retrieval is that the cross-correlation procedure for clipped data is extremely fast.

Limitations of the clipped representation method

The principal problem for any mass spectral library is the comparison of data sets collected from different instruments or under different conditions; F.t./i.c.r. is no exception. For comparison of clipped representations, mass spectra should be acquired at similar analyzer pressure, as facilitated by use of a dual-section cell [18]. It will obviously help if the cell dimensions and voltages (both d.c. and r.f.) are similar. Because the spectra are inherently expressed on a frequency-scale (which is converted to a mass scale for display purposes), point-by-point comparison of F.t./i.c.r. data sets (whether magnitude-mode frequency-domain or clipped time-domain) requires that

the data sets be of equal size (say 64 K), and span the same mass range, so that the mass scales are equal. For F.t./i.c.r. spectrometers operating at different magnetic field strengths (and thus different i.c.r. frequency for a given m/z ratio), one would vary the digitizing rate (and, in heterodyne mode, the reference frequency), in order to correct for difference in magnetic field strength.

In conclusion, the value of the clipped representation technique will depend upon whether it is better to know a little (1 bit/word) about all of the mass spectrum, or a lot ($\geqslant$20 bit/word) about a few (say $<$100) selected m/z values. When mass resolution is relatively low (as in quadrupole instruments), the total mass spectral data set is small (ca. 1 K data points), and the data compression offered by clipping is of limited value [7]. However, for the ultrahigh mass resolution offered by F.t./i.c.r. instruments, much more data ($\geqslant$64 K/spectrum) is involved, and clipping may prove more advantageous for storing and/or comparing large numbers of mass spectra.

The authors thank C. R. Weisenberger for helpful suggestions and discussion. This work was supported by grants (to A.G.M.) from the U.S.A. Public Health Service (National Institutes of Health 1 R01 GM-31683-02), the National Science Foundation (CHE-8218998), and The Ohio State University.

REFERENCES

1 M. B. Comisarow and A. G. Marshall, J. Chem. Phys., 62 (1975) 293.
2 M. B. Comisarow and A. G. Marshall, Chem. Phys. Lett., 25 (1974) 282; 26 (1974) 489.
3 A. G. Marshall, Acc. Chem. Res., 18 (1985) 316.
4 M. L. Gross and D. L. Rempel, Science, 226 (1984) 261.
5 K.-P. Wanczek, Int. J. Mass Spectrom. Ion Proc., 60 (1984) 11.
6 E. B. Ledford, Jr., R. L. White, S. Ghaderi, C. L. Wilkins and M. L. Gross, Anal. Chem., 52 (1980) 2450.
7 R. D. Larsen and E. F. Crawford, Anal. Chem., 49 (1977) 508.
8 R. B. Lam, S. J. Foulk and T. L. Isenhour, Anal. Chem., 53 (1981) 1679.
9 See, e.g., Mass Spectral Library, Chemical Information Systems, Inc., 7215 York Road, Baltimore, MD 21212.
10 M. B. Comisarow and A. G. Marshall, Can. J. Chem., 52 (1974) 1997.
11 A. G. Marshall and D. C. Roe, J. Chem. Phys., 73 (1980) 1581.
12 H. B. Voelcker and A. A. G. Requicha, IEEE Trans. Commun., 21 (1973) 738.
13 A. G. Marshall, Biophysical Chemistry, Wiley, New York, 1978, Chap. 22.
14 R. Bracewell, The Fourier Transform and Its Applications, McGraw-Hill, New York, 1965, pp. 40–46.
15 J. W. Cooley and J. W. Tukey, Math. Comp., 19 (1975) 9.
16 A. G. Marshall, M. B. Comisarow and G. Parisod, J. Chem. Phys., 71 (1979) 4434.
17 A. Sekey, IEEE Trans. Audio. Electroacoust., 18 (1970) 43.
18 S. Ghaderi and D. P. Littlejohn, Paper ROC12, 33rd Am. Soc. for Mass Spectrom. Ann. Conf., San Diego, CA, May, 1985.

Analytica Chimica Acta, 178 (1985) 43—66
Elsevier Science Publishers B.V., Amsterdam — Printed in The Netherlands

DEVELOPMENTS IN ANALYTICAL FOURIER-TRANSFORM MASS SPECTROMETRY

ROBERT B. CODY*, JAMES A. KINSINGER and SAHBA GHADERI

Nicolet Analytical Instruments, 5225 Verona Rd., Madison, WI 53719 (U.S.A.)

I. JONATHAN AMSTER and FRED W. McLAFFERTY

Department of Chemistry, Baker Laboratory, Cornell University, Ithaca, NY 14853 (U.S.A.)

CHARLES E. BROWN

Department of Biochemistry, Medical College of Wisconsin, 8701 Watertown Plank Road, Milwaukee, WI 53226 (U.S.A.)

(Received 19th August 1985)

SUMMARY

Development of a differentially-pumped, dual-cell geometry, coupled with the evolution of pulsed-laser desorption and Cs^+-secondary-ion mass spectrometric (s.i.m.s.) desorption methods, has improved the analytical utility of Fourier-transform mass spectrometry (F.t.m.s.). A survey of applications and performances obtained in our laboratories is presented. Among the topics covered are ultra-high-resolution electron-impact and chemical-ionization mass spectra, gas chromatography/F.t.m.s. performance, pulsed Cs^+-s.i.m.s./F.t.m.s. with cooled liquid matrices and solid samples, laser desorption/F.t.m.s. and accurate mass measurements taken under each of these modes of operation.

Fourier-transform mass spectrometry (F.t.m.s.) has emerged as one of the most exciting recent developments in mass spectrometry. Since the concept was first demonstrated by Comisarow and co-workers [1—8], the potential of the technique as a method for analytical mass spectrometry has been evident. Characteristics of F.t.m.s. that are particularly attractive include ultra-high mass resolution [8—10], simultaneous ion detection over a wide mass range, the ability to trap ions for very long times, accurate mass measurement [11—14], and the capability of performing both chemical ionization [15,16] and collisional activation [17—22] at low pressures. Recent reviews have considered in detail the potential analytical applications of F.t.m.s. [23—26].

Despite these desirable characteristics, the requirement that mass analysis be accomplished at low pressures (less than 10^{-7} Torr) in order to obtain high resolution has slowed the development of Fourier-transform mass spectrometry as a viable analytical method. Two solutions to the problem of performing the mass analysis at low pressures are proposed. The first is to use a pulsed sample introduction and/or ionization method. Ions can be trapped

0003-2670/85/$03.30

for several seconds, while waiting for neutral molecules to be pumped out of the system. When a low enough pressure has been attained, mass analysis can be performed. This solution can be accomplished by the use of a pulsed valve to introduce gas-phase compounds [27, 28], provided that the sample has sufficient volatility. If the sample consists of a solid with a low vapor pressure, a pulsed desorption technique such as pulsed laser desorption [29] or pulsed cesium ion secondary ion mass spectrometry (s.i.m.s.) [30] can be applied. Both neutral species and ions are produced by these techniques but the desorbed ions may be trapped in the analysis cell, while desorbed neutral species are pumped out or stick to the walls.

The second solution to the requirement for low pressures consists of separating the ion souce from the mass analyzer. This is the approach that has been traditionally used in mass spectrometry, and is the preferred solution for situations in which pulsed sample introduction or desorption is difficult, impossible, or impractical, such as heated direct-insertion probe work. In fact, best results for desorption techniques have come from combining pulsed s.i.m.s. or laser desorption with differential pumping in the dual-cell instrument.

Separation of the source from the analyzer can be accomplished by a tandem quadrupole-F.t.m.s. design, as reported by Hunt et al. [31], or by the use of the differentially pumped, dual-cell design developed at Nicolet Analytical Instruments [32—34]. In this paper, progress in developing and applying both of these solutions (pulsed ionization and separation of the source from the analyzer) is discussed, with emphasis on pulsed laser desorption and cesium-ion s.i.m.s., and the use of the dual-cell design for chemical determinations by F.t.m.s. This paper is intended to be a "survey" of applications and results obtained in our laboratories. More details on the construction and operation of the dual-cell instrument and the desorption interfaces will be published separately.

EXPERIMENTAL

Most of the laser desorption experiments were conducted on a Nicolet FTMS-1000, single-cell Fourier-transform mass spectrometer equipped with a Tachisto TAC-II, Model 215G pulsed CO_2 laser and a Nicolet laser desorption interface. High-resolution laser desorption experiments were conducted on a standard Nicolet FTMS-2000 Fourier-transform mass spectrometer equipped with a laser desorption interface. A more complete description of this equipment will be published elsewhere.

Cesium-ion desorption experiments were done on a modified FTMS-1000 instrument. The Cs^+ gun was designed at Nicolet to fit the requirements of the F.t.m.s. geometry. The Cs^+ source filament was purchased from Antec Co. of California. The gun was mounted at a distance of 60 cm from the cell along the z axis of the superconducting magnet. The vacuum chamber of the F.t.m.s. instrument was modified to allow differential pumping of the Cs

source. This arrangement was used to avoid pressure increase in the analyzer cell caused by cesium neutral molecules evaporating from the source. Cesium ions generated in pulsed mode were accelerated at energies between 5 and 10 keV along the magnetic field flux lines passing through the Cs^+ source. The ion beam was focused and aligned to pass through the cell via the apertures at the center of the trapping plates, and struck the tip of the solids-sample probe. The solids probe was inserted from the opposite side of the vacuum chamber and situated so that its tip was exposed into the analyzer cell. The probe tip was held at the trapping potential. The Cs^+ pulse duration and duty cycle was adjustable via the F.t.m.s. computer keyboard. In this study, pulse durations as short as 100 μs and as long as 1 ms were used. The Cs^+ emission current was controlled by the cesium power supply designed for this application. This power study also provides different potentials for acceleration, gating, and focusing of the ion beam. Typical cesium ion emission currents used were between 200 nA to 2 μA.

The remainder of the experiments described in this paper were done on a prototype Nicolet FTMS-2000 dual-cell Fourier-transform mass spectrometer. A diagram of the cell arrangement is presented in Fig. 1. The key feature of this system is the incorporation of a conductance limit (see figure) between the two trapping regions. The purpose of the conductance limit is to separate the vacuum chamber and cell into two separate pressure regions. Pressures on the source side can be as high as is necessary or as needed while maintaining ultra-low pressures (10^{-8}—10^{-9} Torr) on the analyzer side, which is necessary for the best performance of ultra-high-resolution Fourier-transform mass spectrometers. By utilizing the 3-T magnetic field to trap ions along the magnetic flux lines collinear with the electron beam path, it is possible to transfer ions from one side of the cell to the other.

Operation of the dual-cell instrument is very similar to the single-cell F.t.m.s. The initial step is to quench the cell to remove all ions by applying appropriate positive and negative potentials to the three trapping plates. For electron impact and chemical ionization, a beam of electrons is allowed to pass through both cells. Ion formation occurs along the path of the electrons.

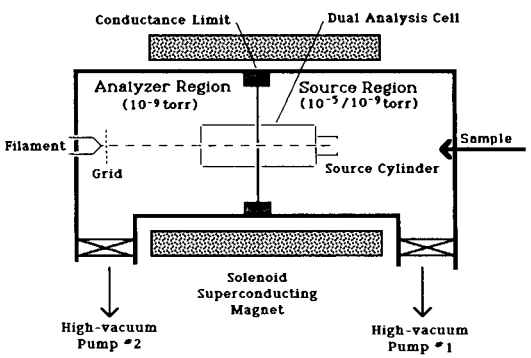

Fig. 1. Diagram of the dual-cell arrangement.

Those ions produced between the two extreme trapping plates are trapped within the cells. The center trap plate (the conductance limit) is kept at ground potential during ion formation and, therefore, does not impede ion motion. Owing to their initial translational energies, ions move between the trap plates (along the z axis) with a frequency in the kilohertz range. Because the pressure in the source region may be considerably higher (e.g., 2×10^{-6} Torr) than the analyzer (e.g., 2×10^{-9} Torr), the average number of ions formed per centimeter of electron beam path is much greater (e.g., 1000 times) than the number of ions produced per centimeter of beam path in the analyzer cell. As the ions move between the two cells, the ion population density equilibrates. By bringing the conductance limit to trap potential, two separate but identical packets of ions are formed. When the excitation and detection sequences are applied to the ion packet in the low-pressure analysis region, measurements with high resolution and high sensitivity are achieved. This procedure increases the number of ions over what would be obtained if one were required to operate under the low pressure conditions by a factor (e.g., 500 in this example) that is one half the ratio of the pressures. An increase in sensitivity is accomplished by two factors: (1) more ions are produced and detected; (2) ions are detected at higher resolution which, in F.t.m.s. instruments, can result in higher sensitivity [35]. This characteristic is particularly important in g.c./m.s. operation.

An increase in g.c./m.s. performance can also be obtained by taking advantage of the fact that the source cell also contains excitation and receiver plates. During the ionization period, ions are formed from all species present in the cells, including the helium carrier gas. The dominant helium ion is of no use in the analysis. By applying the resonant frequency of He^+ to the excitation plates of the source side of the dual-cell arrangement, helium ions are excited to a larger orbit and cannot pass through the conductance limit into the analyzer side. The helium ejection procedure, which is always being applied to the source cell, results in improved sensitivity and resolution by reducing the space charge in the analysis cell.

Sensitivity is further enhanced by introducing the g.c. column into a small cylinder kept at the trapping potential, adjacent to the source trap plate and centered on the z axis. This area has a high local pressure. Because the cylinder is kept at the trapping potential, ions formed in the cylinder migrate through the source trap plate and eventually into the analysis region. It is thus possible to utilize the sample more efficiently, producing a larger number of ions from the g.c. effluent.

ULTRA-HIGH RESOLUTION

Electron impact

The first test of the dual-cell design provided striking results. By operating the instrument in the heterodyne (high-resolution) mode, it was possible to detect the $C_3F_5^+$ ion in the electron-impact spectrum of perfluorotributyl-

amine with a mass resolution of 4×10^6 (FWHH definition) at a source pressure of approximately 5×10^{-7} Torr (Fig. 2) and an analyzer pressure of 4×10^{-9} Torr. The peak is approximately 33×10^{-5} mass units wide at half height, or approximately 1/17 the rest mass of an electron.

A somewhat more interesting example is shown in Fig. 3, which shows the molecular ions from methyl salicylate and tetramethoxysilane. These two ions differ in mass by only 3×10^{-3} mass units, and are separated with a mass resolution of 1×10^6. Using either one of the peaks as a calibrant mass for a one-point calibration produces a measured mass for the other peak which differs from the calculated mass by only 10 parts in 10^9. The one-point calibration procedure may be thought of as being analogous to peak matching in conventional mass spectrometry. A third example is shown in Fig. 4. This spectrum shows a triplet at nominal mass 356 in the electron-impact spectrum of tin bromide. The peaks in this triplet are detected with clear baseline separation at a resolution of 8.33×10^5. To our knowledge, this triplet has not previously been observed by mass spectrometry.

Chemical ionization

The dual-cell design allows chemical ionization to occur at higher pressures in the source region, with mass analysis occurring at lower pressures in the

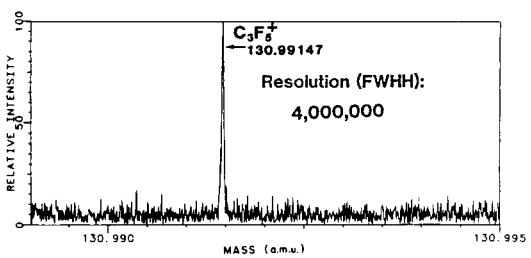

Fig. 2. $C_3F_5^+$ peak detected at a resolution of 4×10^6 (FWHH definition).

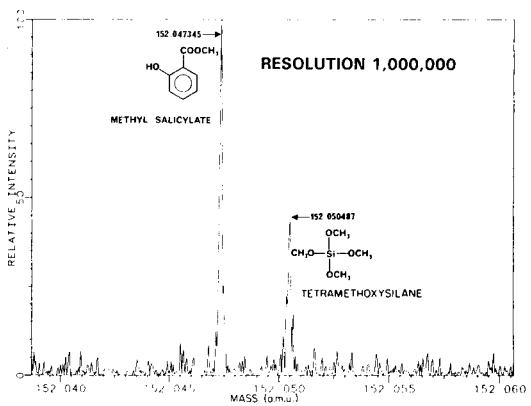

Fig. 3. Molecular ions from methyl salicylate and tetramethoxysilane detected at a resolution of 1×10^6.

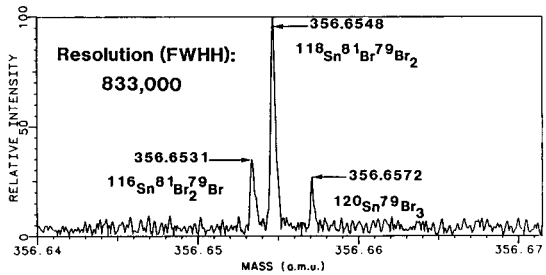

Fig. 4. $SnBr_3^+$ isotopic triplet at a resolution of 8.33×10^5.

analyzer region. Chemical ionization can be achieved in the source region either with a reagent gas such as methane or isobutane, or without a reagent gas ("self-c.i."). If a reagent gas is used, a pulsed valve on the source side can be used to maximize the reagent gas pressure during the ionization period. This permits the chemical-ionization reactions to occur at higher pressures than if a static pressure of the reagent gas were used. The result is a higher ionization efficiency and a shorter reaction time, without raising the pressure on the analyzer side during detection.

Preliminary experiments involving chemical ionization on the dual-cell instrument consisted of performing the ionization reactions with the ions trapped on the source side, and then dropping the potential on the conductance limit to zero volt for a period of 100—750 μs to allow the ions produced by the c.i. reactions to move into the analyzer region. Double resonance ejection of all ions trapped in the analyzer region preceded the ion transfer event to ensure that only ions formed in the source region were detected. Reagent ions, such as $C_4H_9^+$, could be ejected during the transfer event to maximize dynamic range.

An example of the extremely high mass resolution that can be obtained in the c.i. mode is shown in Fig. 5, which represents the $(M + H)^+$ ion from acetone, detected with a resolving power of 1.5×10^6. Only one transient signal was collected, with a reaction time of 500 ms, at source and analyzer pressures of respectively 1×10^{-6} and 8×10^{-9} Torr. The experiment was done by allowing trapped fragment ions produced by electron impact to

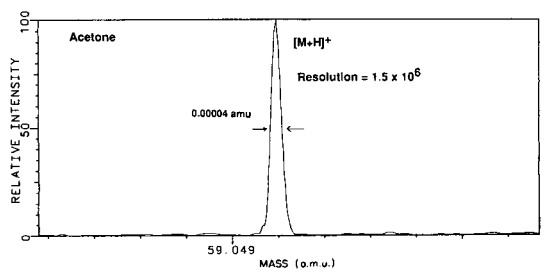

Fig. 5. $(M + H)^+$ ion from self-chemical ionization of acetone, at a resolution of 1.5×10^6

react with neutral sample molecules in the source region of the dual cell of the FTMS-2000, and then transferring the resulting ions to the analyzer side for detection. An example of the use of ultra-high-resolution self-c.i. to separate ions from two components is shown in Fig. 6. Self-c.i. of a mixture of mesitylene and acetophenone (both with nominal masses of 120 a.m.u.) results in complete protonation of acetophenone, and partial protonation of mesitylene after a reaction time of 450 ms and at a source pressure of 4×10^{-6} Torr. Acquisition of the spectrum at a resolution of 2×10^5 results in complete separation of the $(M + H)^+$ peaks from both acetophenone and mesitylene (Fig. 6A). More importantly, the ^{13}C-isotope peak from the unreacted molecular ion of mesitylene is completely separated from the $(M + H)^+$ peak of mesitylene. These peaks differ (Fig. 6B) by 4.4×10^{-3} a.m.u.

Detection limits of g.c./F.t.m.s. under high resolution conditions

One of the potential strengths of F.t.m.s. has been the viability of g.c./m.s. with high resolution and high sensitivity. Because F.t.m.s. does not use slits to obtain high resolution, the possibility exists for obtaining high-resolution mass spectra on very small quantities of sample. This would be very useful for analysis of complex mixtures by g.c./m.s.

It is clear that one of the major factors affecting detection sensitivity for F.t.m.s. is ionization efficiency. To make use of F.t.m.s. for low detection limits, an efficient ionization method is needed. Sack et al. [36] have reported detection limits for napthhalene of about 10 pg at a mass resolution of about 2×10^4 by using multiphoton ionization with a pulsed-valve

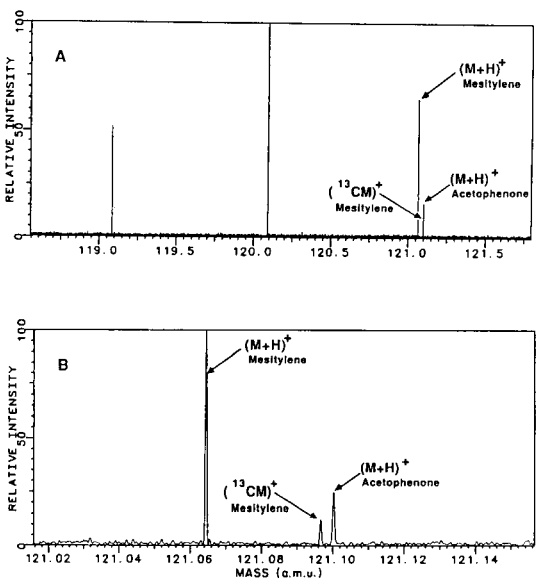

Fig. 6. (A) Self-chemical-ionization spectrum of acetophenone and mesitylene at a resolution of 2×10^5. (B) Enlarged view of m/z 121 region.

g.c./F.t.m.s. interface. This is a convincing demonstration of the combination of the high ionization efficiency of multiphoton ionization methods with the high sensitivity at high resolution possible by F.t.m.s.

To obtain the lowest possible detection limits with electron-impact ionization, we have added a "source cylinder" which confines the sample eluting from the column in a higher pressure region, directly in the path of the electron beam. This increases the efficiency of ionizing the sample by electron impact. The "source cylinder" can be considered as a separate cell in addition to the source and analyzer ion-trapping cells, because it can be operated at the trap potential. Ions can be trapped in the source cylinder, and transferred to the source and analyzer trapping cells in a manner similar to that used for ion transfer between the source and analyzer cells. Operating the electron beam at a high emission current also increases the number of ions formed by electron-impact ionization of the sample. A high emission current is practical when a small quantity of sample is present, because few ions are formed, and space charge effects are not likely to occur. In g.c./F.t.m.s., the helium used as a carrier gas results in the presence of helium ions in large abundance.

Results of a preliminary study of the detection limit for naphthalene detected by electron-impact g.c./F.t.m.s. are reported here. A 1-μl splitless injection was made with a 125 pg μl^{-1} solution of naphthalene in heptane. The g.c. column (a 25-m BP-1 column) was programmed from 70 to 300°C at a rate of 8°C min^{-1}, with a 1-min hold time at 70°C. The injection temperature was 325°C, with a 300°C transfer-line temperature.

Figure 7 shows the background-subtracted mass spectrum for the naphthalene eluting at 10.5 min. The spectrum was taken over a 120—130 a.m.u. mass range with a mass resolution of 15 000. Ten transients were collected for each spectrum, with the mass spectrometer operated in the heterodyne mode. The electron beam was turned on for 25 ms per transient. The total acquisition time per spectrum was 1.5 s. The signal-to-noise ratio for the molecular ion is about 10:1. Based on this figure, the detection limit under these conditions would be 25 pg with a signal-to-noise ratio of 2:1.

Although these detection limits are somewhat higher than those reported

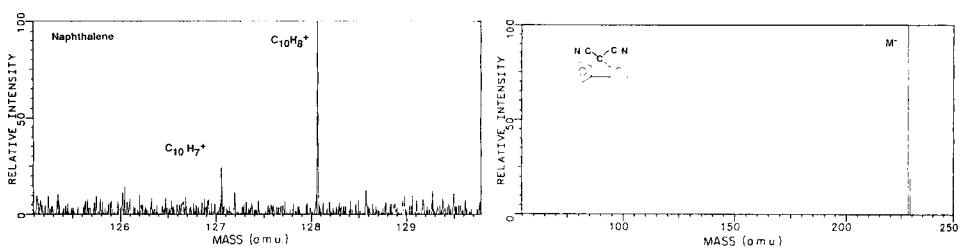

Fig. 7. Background-subtracted mass spectrum of naphthalene molecular ion at the 125 pg level, detected at a resolution of 1.5×10^4.

Fig. 8. Negative-ion g.c./F.t. mass spectrum of a 9,9-dicyanofluorene.

by Sack et al. [36], the difference is probably due to the somewhat greater ionization efficiency of multiphoton ionization compared to electron impact. We are currently investigating how variations in the experiment sequence (beam duration, number of data points, etc.) can be used to reduce detection limits at high resolution.

Negative-ion g.c./F.t.m.s.

Negative-ion detection can be accomplished in a manner similar to that used for chemical ionization. Low-energy electrons which enter the source region may lose energy by collisions with neutral species present in the source region. If the resulting electron energy is less than the (negative) trapping potential, the electrons will remain trapped in the source, and can continue to lose kinetic energy by further collisions. A large number of thermal electrons is then available for electron capture by compounds eluting from the g.c. column. Following ion formation in the source region by electron capture, negative ions can be transferred to the analyzer cell by lowering the potential on the conductance limit to zero for a period of approximately 500 μs. Mass analysis is then performed on the analyzer side at low pressures.

To test this procedure, a compound known to have a high electron-capture cross-section was injected onto an OV-1 column with a 100-μm diameter. The compound, 9,9-dicyanofluorene has a molecular weight of 228 a.m.u. The compound was dissolved in chloroform at a concentration of approximately 50 ng μl^{-1}; 1 μl was injected into the splitless injector port on the g.c. Electrons with energies less than 2 eV were trapped by the −2 V trap potentials on the source trap and conductance limit. After allowing a 750-ms reaction period, ions formed by electron capture in the source region were transferred to the analyzer side for detection. The total time to collect one transient was 800 ms. Two transients were averaged for each spectrum collected. The compound eluted from the column at 12 min after injection (Fig. 8), and the mass spectrum shows only the M^- ion at mass 228 and the isotope peak at *m/z* 229. It is believed that this preliminary experiment demonstrates the feasibility of performing electron-capture/g.c./F.t.m.s. on the dual-cell instrument. Further investigation should provide more information about performance and should establish the optimum conditions.

SECONDARY-ION MASS SPECTROMETRY (S.I.M.S.)

The most commonly used techniques for desorption ionization of solid samples involve bombarding the surface with accelerated particles. Recently, Castro and Russell [30] demonstrated the use of combined cesium ion s.i.m.s./F.t.m.s. to analyze vitamin B12. Their initial results were intriguing, if somewhat complex. Several ionic species were observed, including a cesium-bound dimer $(2M + Cs - 2CN)^+$ at *m/z* 2792. Later investigations by the same group [37] have shown the dependence of the method upon primary-ion beam current, and the duration of irradiation of the surface by the

cesium ion beam. At low primary-ion beam currents (10^{-8} A cm^{-2}), spectra of β-cyclodextrin showed primarily $(M + H)^+$. As the primary ion density is increased, ions of the type $(M + Na)^+$, $(M + xNa-(x - 1)H)^+$, and fragments dominate the spectrum. Thus, low primary ion densities (static s.i.m.s. conditions) are clearly preferable for organic analysis by cesium s.i.m.s./F.t.m.s.

Hunt et al. [31] have reported the use of a liquid s.i.m.s. source combined with a tandem quadrupole-F.t.m.s. for the desorption of several polypeptides, including angiotensin. Some preliminary experiments with cooled liquid matrix s.i.m.s. and solid matrix s.i.m.s., as well as the use of s.i.m.s. to generate high mass CsI clusters are reported here.

Cooled liquid matrix s.i.m.s./F.t.m.s.

Because our initial experiments with s.i.m.s. were done with a single-cell system, the increased pressure produced by the liquid matrix presented a serious obstacle. To minimize the problems presented by the use of a glycerol, the probe tip containing the sample dissolved in glycerol was cooled to −27°C by using a fluorocarbon refrigerant sprayed into the cooling "spout" on the direct-insertion probe. By warming the probe until a slight pressure increase was observed, it was possible to obtain the spectral characteristic of two antibiotics.

The positive-ion liquid s.i.m.s./F.t. mass spectrum of erythromycin is shown in Fig. 9. The sample is dissolved in glycerol, with added cesium iodide. The base peak in the spectrum is $(M + Cs)^+$ at m/z 866.4. In addition, peaks from cesium and cesium iodide are observed at m/z 133, 393, 653, and 912. The peaks at mass 301 and 303 are due to Cs_2Cl^+. Although a small peak from the the glycerol $(M + H)^+$ ion is visible at m/z 93, the expected glycerol chemical background is virtually absent. Figure 10 shows the liquid s.i.m.s./F.t. mass spectrum of the cyclic decapeptide gramicidin S. The $(M + H)^+$ peak at m/z 1142 is virtually the only peak in the spectrum. No significant fragmentation is evident. A later repetition of this experiment produced essentially the same results, but with the additional appearance of an $(M + Na)^+$ peak at mass 1164. The presence of sodium is attributed to trace contamination remaining from the previous sample, a sodium salt of an alkylbenzene

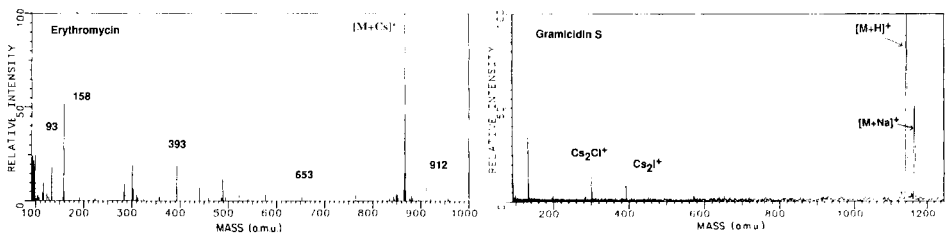

Fig. 9. Cooled liquid s.i.m.s./F.t. mass spectrum of erythromycin, with added cesium iodide.

Fig. 10. Cooled liquid s.i.m.s./F.t. mass spectrum of gramicidin S.

sulfonate, which was analyzed as a solid matrix (see following discussion), and remained after a hasty cleaning of the target surface.

These preliminary results are of interest because we were unable to obtain spectra from these compounds in a solid matrix under these conditions. Cesium-s.i.m.s./F.t. mass spectra of gramicidin obtained as a solid matrix were only obtained when (1) the primary beam density was lowered significantly (static s.i.m.s. conditions), and (2) the sample was deposited on the surface by electrospraying. Although the higher pressures from the evaporation of the glycerol result in the loss of resolution in the single-cell system, this limitation should be removed by operating the s.i.m.s. source on a dual-cell system. The absence of a significant chemical background is unexpected. The only explanation offered is that the reduction of the chemical background results from cooling the liquid matrix.

Solid matrix cesium s.i.m.s.

These initial successes with s.i.m.s. of organic compounds in the solid state involved organic salts. Figure 11A shows the cesium-ion spectrum of the sodium salt of a benzothioazole sulfonate deposited onto the tip of the stainless-steel probe from a solution in methanol. The M^- ion is the largest peak in the spectrum, followed by I^- at mass 127 (a trace impurity from CsI). Several fragments from the monomeric anion are observed including $(M - SO_2)^-$ at m/z 150, $(M - SO_3)^-$ at m/z 134, and SO_3^- at m/z 80. The sodium-bound dimer $(2M + Na)^-$ at m/z 451 is present at an abundance of 7% (relative to the mask peak), and loss of SO_2 produces $(2M + Na - SO_2)^-$ at m/z 387 with 15% abundance.

This same compound was also examined by laser desorption/F.t.m.s., which produces a very similar negative-ion spectrum (Fig. 11B). It is interesting to note that the positive-ion laser desorption spectrum produced by this compound is dominated by $(M + 2Na)^+$ at m/z 260, with a small peak due to $(M + Na + K)^+$ appearing at m/z 276 (Fig. 11C). In contrast, the positive-ion cesium secondary-ion mass spectrum shows only Na^+, with no ions characteristic of the organic portion of the molecule.

Attempts to obtain secondary-ion mass spectra of the antibiotic gramicidin S were unsuccessful at first. Several different sample preparation methods were tried, including deposition by evaporation from solution in methanol, addition of ammonium chloride (which has been shown to enhance protonation in organic s.i.m.s. [38, 39]), and rubbing the sample onto the target surface. Only when the sample was deposited on the surface by electrospraying [40] from a solution in methanol was it possible to obtain a spectrum from gramicidin S. The spectrum shown in Fig. 12 shows a strong $(M + Na)^+$ ion at mass 1164. The sodium is believed to come from trace cations present on the surface. More information is necessary to draw correlations with the work of Castro and Russell. Nevertheless, these results illustrate the importance of the sample preparation method chosen for solid s.i.m.s. of larger organic molecules.

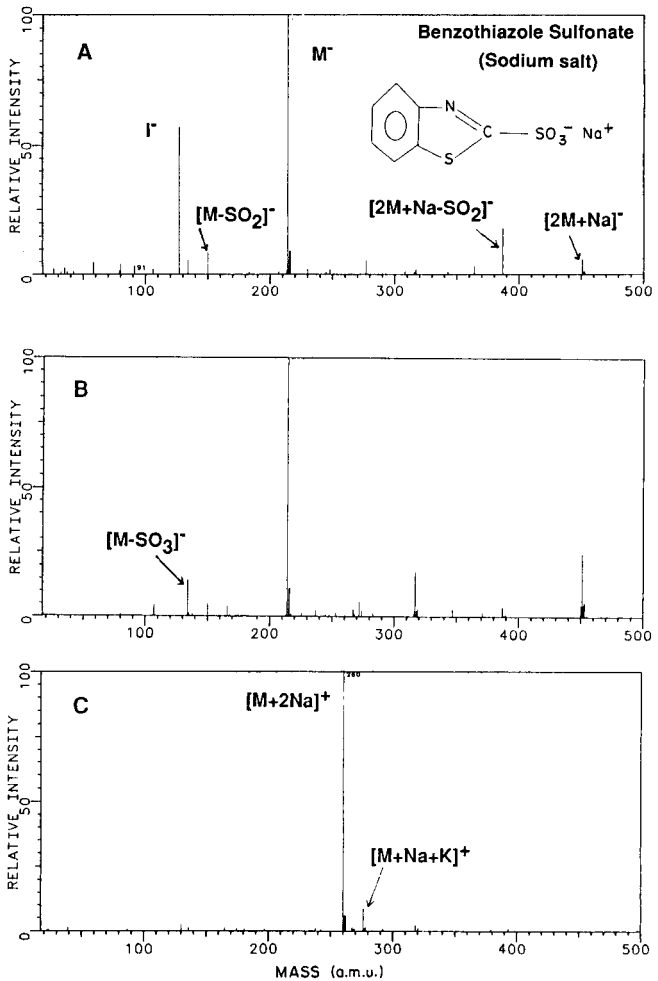

Fig. 11. (A) Negative-ion solid matrix s.i.m.s./F.t. mass spectrum of a benzothiazole sulfonate (sodium salt). (B) Negative-ion laser desorption spectrum of the same compound. (C) Positive-ion laser desorption spectrum for the same compound.

Solid s.i.m.s. has also demonstrated the ability of F.t.m.s. to detect high masses. The mass spectra of CsI clusters up to 16 241 a.m.u. (a 5 X 5 X 5 cube) were obtained (Fig. 13). Under these conditions, both positive and negative clusters were observed with approximately equal intensity. The intensity distribution can be readily explained by the magic number associated with cesium iodide clusters [59].

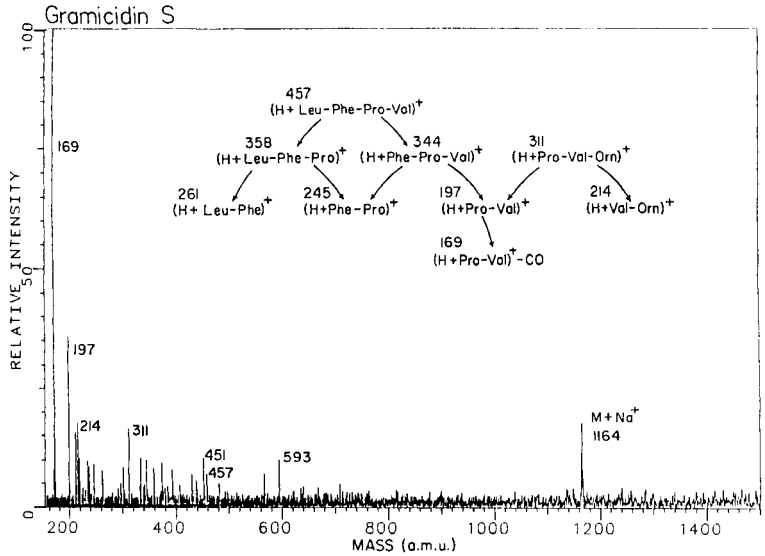

Fig. 12. Solid matrix Cs^+-s.i.m.s./F.t. mass spectrum of gramicidin S (static s.i.m.s. conditions).

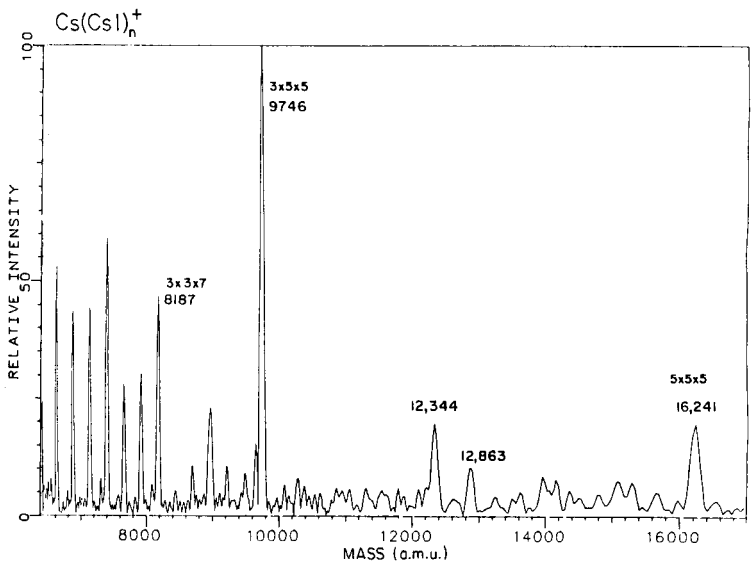

Fig. 13. Secondary-ion mass spectrum of Cs ion clusters at high mass.

LASER DESORPTION/F.T.M.S.

Pulsed laser desorption has proven to be one of the most useful recent developments in analytical F.t.m.s. Initially, the combination of pulsed laser

desorption with ion cyclotron resonance and F.t.m.s. was applied by Freiser and co-workers [41, 42] to the study of gas-phase reactions of laser-generated metal ions. Differences in reactivity between specific metal ions and compounds containing various functional groups have suggested the use of metal ions as chemical-ionization reagents [43, 44].

The application of pulsed laser desorption to the determination of organic compounds by F.t.m.s. was first reported by McCrery et al. [29], who reported the observation of $(M-H)^-$ ions from several low-molecular-weight organics, and demonstrated the potential for high-resolution laser desorption (l.d.)/F.t.m.s. by detecting the carboxylate anion from succinic acid with a mass resolution of 1×10^5.

With the intention of providing a routine soft ionization method for F.t.m.s., we have chosen to pursue the development of a laser desorption/F.t.m.s. interface. Over the past two years several hundred samples have been examined with the laser desorption technique, including synthetic organic compounds [45—47], inorganics and organometallics [48, 49], polymers [50—52], pharmaceuticals [45—47, 53—55], and surface samples. Using the laser desorption interface (which was developed at Nicolet with support from a joint grant with U.C. Riverside), Wilkins et al. [56] have demonstrated the generation and detection of several high mass ions, including ions in the 1000—7000 a.m.u. range generated from the laser desorption ionization of a poly(perfluoroether). This work certainly demonstrates the potential of combined l.d./F.t.m.s. for higher mass materials. Marshall et al. [57] have applied the l.d./F.t.m.s. interface to a variety of compounds, including several organometallics. A comparison of l.d./F.t.m.s. with fast atom bombardment (f.a.b.) has shown significantly less fragmentation for the l.d./F.t.m.s. technique [58]. All of these results indicate that l.d./F.t.m.s. is making a significant contribution to analytical mass spectrometry.

The pulsed-laser desorption technique consists of focussing the output of a high-power pulsed laser onto the surface of a sample, and using mass spectrometry to monitor the ions generated. The need to generate the entire mass spectrum from a single laser pulse has resulted in the need for a compatible mass spectrometric method. Time-of-flight mass spectrometry has been the method of choice to date, but the poor mass resolution presently available from time-of-flight has placed limitations on the applicability of the technique. Fourier-transform mass spectrometry shares many of the desirable characteristics of time-of-flight mass spectrometry, including rapid detection of ions from a single laser pulse over a wide mass range, but F.t.m.s. has the additional capabilities of ion trapping and extremely high mass resolution.

While laser desorption can be used to examine virtually any sample that can be placed in front of the laser beam, the best results we have obtained have been when the sample is deposited as a thin film on the surface of the stainless-steel sample mount. The sample can be deposited by a variety of means. In most cases, compounds have been dissolved in methanol, water, dichloromethane or other solvents, and the solution has been deposited on

the target from a pipette, allowing the solvent to evaporate. Electro-spraying the sample onto the target has also been used, and may give better results than evaporation in some cases. Generally, a "dopant" such as potassium bromide is added to the surface prior to sample deposition, in order to enhance cationization (see discussion below).

The positive-ion l.d./F.t.m.s. spectrum of the polypeptide "substance P" provides an example (Fig. 14). The pseudomolecular ion at mass 1385.6 is consistent with potassium attachment to the neutral peptide, which has the formula $C_{63}H_{98}N_{18}O_{13}S$. In addition to the pseudomolecular ion, several fragment ions are present which provide sequence information. Interestingly, the fragments which are indicative of loss of proline are weak or absent, while fragments indicative of other amino acid losses are relatively high in abundance. We do not currently understand the reason for this.

Effect of adding dopants in laser desorption

The cationization process plays a very important role in l.d./m.s. and the addition of dopants such as sodium chloride or tartaric acid has often been used to enhance this process [60—63]. We have found that the addition of an excess of potassium bromide increases the extent of cationization for most of the neutral, polar organic compounds studied. The presence of a strong $(M + K)^+$ peak in the positive-ion spectrum, coupled with the presence of an M^- or $(M - H)^-$ peak in the negative-ion l.d./F.t. mass spectrum is useful in confirming the molecular weight of a sample. Potassium attachment is often easily identified by the increase in the (M + 2) peak intensity produced by the ^{41}K isotope. Potassium bromide is relatively unreactive, and is thus a "safe" choice of additive. Its addition to an organic salt (a "pre-formed ion") or a compound which gives a strong M^+ peak has no deleterious effect on the spectrum obtained.

If no dopant is added, molecular weight information is often difficult to obtain because pseudomolecular ions may be weak or absent. Cationization may also take place with trace metals present as contaminants on the surface,

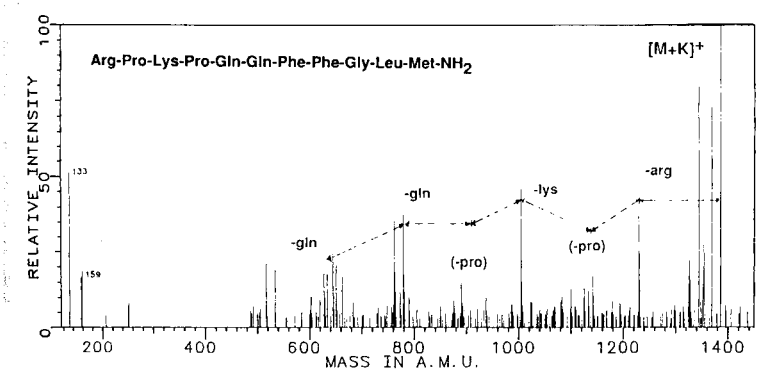

Fig. 14. Positive-ion l.d./F.t. mass spectrum of substance P.

producing a mixture of protonation, sodium, potassium, and even cesium and rubidium attachments. Other dopants have been tested. Tartaric acid seems to enhance the formation of $(M + H)^+$ ions for many compounds (especially polypeptides). However, tartaric acid may be sufficiently reactive to cause decomposition or increased fragmentation, or even clustering reactions. Perhaps the best way to illustrate the effect of additives on laser desorption spectra is with an example.

We have investigated the structures of various opiates with a variety of analytical techniques, including cross polarization/magic angle/spinning sample nuclear magnetic resonance spectroscopy and l.d./F.t.m.s. Interest in these compounds is due to the fact that morphine is metabolized primarily via conjugation with UPD-glucuronic acid and formation of sulfate esters and is excreted via the liver and kidney. The relative preponderance of formation of glucuronide vs. sulfate ester and of biliary excretion vs. urinary excretion varies from species to species. Morphine has two hydroxyl groups, a phenolic hydroxyl at C-3 and an aliphatic hydroxyl at C-6. Both conjugation and sulfate ester formation occur predominantly at the 3-position of morphine in the liver and kidney, and this has been considered a detoxification mechanism in vivo. However, morphine 6-sulfate is a potent analgesic after intracerebroventricular administration, and it has been suggested that this sulfate ester may mediate some of the effects of morphine within the central nervous system [53]. In order to test this hypothesis, a sensitive assay for morphine and the sulfate esters was needed. Laser desorption/F.t.m.s. was a promising approach for making these measurements.

Morphine, morphine 3-sulfate and morphine 6-sulfate all yield l.d./F.t. mass spectra, but the identities of the desorbed ions depend on the matrix composition of the sample target [53]. Morphine yields both positive and negative ions in the presence of KBr (Table 1). The potassium adduct of the molecular ion is observed in the positive-ion spectrum (Fig. 15a). In the presence of tartaric acid, morphine yields primarily positive ions, and there is increased fragmentation with loss of hydrogen and water (Fig. 15B). In the absence of KBr or tartaric acid, morphine does not yield readily detectable molecular ions. Morphine 3-sulfate yields both positive dipotassium adduct ions and negative ions in the presence of KBr. There is fragmentation with loss of hydrogen and water. Tartaric acid does not facilitate desorption of morphine 3-sulfate ions. Morphine 6-sulfate yields only negative ions in the presence of both KBr and tartaric acid. These differing matrix effects on desorption provide a tool for distinguishing morphine, morphine 3-sulfate and morphine 6-sulfate in tissue extracts. By recording separate l.d./F.t. mass spectra in the presence of KBr and tartaric acid, one can readily confirm the presence of morphine by its distinctive fragmentation pattern in the presence of tartaric acid. In addition, morphine 3-sulfate and morphine 6-sulfate, which have identical molecular weights, can be distinguished by the effect of tartaric acid on their ability to desorb and by the charges on the ions they produce.

TABLE 1

Pseudomolecular ions detected by laser desorption/Fourier-transform mass spectrometry

Opiate	Solvent	Ions		
		m/z	Charge	Identity
Morphine	KBr/MeOH/H_2O	324	positive	morphine + K^+
		284	negative	morphine $- H^+$
	tartaric acid/MeOH	286	positive	morphine + H^+
		284	positive	$(\text{morphine} - H)^+$
		268	positive	morphine + $H^+ - H_2O$
Morphine 3-sulfate	KBr/MeOH/H_2O	442	positive	(morphine 3-sulfate) + $2K^+ - H^+$
		424	positive	(morphine 3-sulfate) + $2K^+ - H^+ - H_2O$
		364	negative	(morphine 3-sulfate) $- H^+$
		346	negative	(morphine 3-sulfate) $- H^+ - H_2O$
Morphine 6-sulfate	KBr/MeOH/H_2O	364	negative	(morphine 6-sulfate) $- H^+$
		346	negative	(morphine 6-sulfate) $- H^+ - H_2O$
	tartaric acid/H_2O	364	negative	(morphine 6-sulfate) $- H^+$
		346	negative	(morphine 6-sulfate) $- H^+ - H_2O$

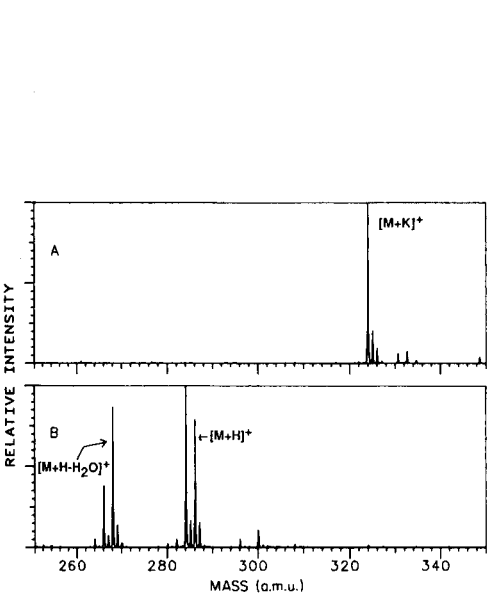

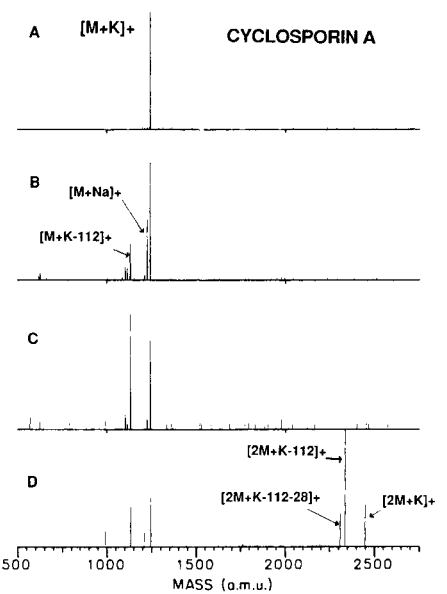

Fig. 15. Positive-ion l.d./F.t. mass spectra: (A) morphine + KBr; (B) morphine + tartaric acid.

Fig. 16 (A—D). Positive-ion l.d./F.t. mass spectra of cyclosporin A as laser power density is increased from low power density (A) to high power density (D). See text for details.

Effect of laser power

The laser power density has a significant effect on the degree of fragmentation observed for a given compound. The immunosuppressive drug, cyclosporin A, provides an interesting example. This cyclic peptide produces a spectrum at low laser power densities which is virtually devoid of fragmentation, showing only $(M + K)^+$ at nominal mass 1241 (Fig. 16A). Increasing the laser power density by opening the iris aperture or increasing the high voltage setting on the laser produces a fragment at mass 1129 (Fig. 16B). Increasing the power density still more increases the abundance of fragment ions relative to the pseudo-molecular ions (Fig. 16C). Opening the aperture to its widest setting produces potassium-bound dimers (Fig. 16D). The reason for this dimer formation is not well understood at this time.

This ability to control the degree of fragmentation should prove useful for analytical purposes. The observation of dimer formation at high laser power densities is very interesting, and should be of use in comparing laser desorption taken at relatively low power densities (such as those reported in this paper) with those taken under microprobe conditions, where higher power densities are more commonly used.

Resolution

The mass resolution obtained on laser-desorption spectra when the dual-cell design is used seems to be dependent on exactly the same factors that affect electron-impact spectra, i.e., the pressure in the analysis region, and the number of ions trapped in the analysis cell. A resolution of 2.6×10^6 has been obtained for laser-desorbed potassium at mass 39, and a resolution of 1.5×10^5 for the cyclic peptide antibiotic gramicidin S at mass 1180 [34]. Differential pumping allows separation of the ions and neutral species produced by each laser pulse. The same tuning conditions used for high-resolution electron-impact spectra may be used to obtain high-resolution spectra for laser-desorbed ions at both low and high mass.

Because of the extremely large number of ions produced by each laser pulse, the major adjustment needed to collect high-resolution l.d./F.t. mass spectra was to select conditions that limited the number of ions that were trapped in the analyzer region to avoid space-charge effects. Thus, after ions had been formed by the laser pulse, and trapped on the source side, the conductance limit was dropped to zero volt for only 100 μs. Trap potentials were lowered to 0.3 V for the remainder of the experiment sequence, thus limiting the number of ions trapped.

A spectrum showing the pseudomolecular ions resulting from potassium attachment to gramicidin S is shown in Fig. 17. The mass resolution is approximately 1.5×10^5 (FWHH definition). The duration of the transient signal was 16 s. Only one transient was collected. A resolution of 1.5×10^5 at this mass corresponds to a resolution of 1.35×10^6 at mass 131. This corresponds reasonably well with the 4×10^6 resolution actually measured at mass 131 (see previous discussion), and suggests that there are no unexpected phenomena inherent in l.d./F.t.m.s. that might act to limit resolution at

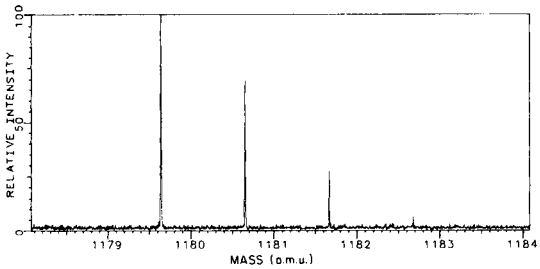

Fig. 17. Pseudomolecular ions, $(M + K)^+$, for gramicidin S at a resolution of 1.5×10^5.

higher masses. An extrapolation of this resolution to higher mass suggests that it should be possible to obtain unit resolution up to 13 000 a.m.u. by F.t.m.s. with a 3-T magnetic field. Much higher masses could be reached at unit resolution if the magnetic field were to be increased. Because the work by Wilkins et al. [56] with laser desorption, and the work performed in these laboratories with cesium-ion s.i.m.s. (see above) has shown that high mass ions can be detected by F.t.m.s., this extrapolation should not be considered unreasonable.

Application to intractable polymers

One type of analysis for which l.d./F.t.m.s. has proven particularly useful has been the characterization of intractable (i.e. insoluble and nonvolatile) polymers such as poly(*p*-phenylene) (PPP). PPP is a highly conjugated polymer that is resistant to oxidation, thermal degradation, and radiation. It can be made electrically conductive by doping and thus has attracted considerable attention in both basic research and commercial development. Several different procedures have been used for preparation of PPP, and the electrical conductivities of the products from these different synthetic routes vary considerably. It is important that the chemical structures of the PPP samples from different synthetic routes be known in order to understand the physical bases of conductivity in these polymers, yet their intractability severely curtails the analytical techniques that can be applied. With l.d./F.t.m.s., molecular ions of the individual oligomers in each sample have been detected with better than unit mass resolution [50, 52]. The products of the synthetic routes tested thus far are PPP oligomers with an average of 10—14 rings per molecule and varying amounts of halogen substitution at the end rings (1—8%). Furthermore, the mass spectra provide evidence for a termination reaction that yields polynuclear structures when PPP is synthesized from benzene with aluminum chloride/copper(II) chloride [50, 52]. In Fig. 18 the effect of reaction temperature on the proportion of oligomers that become monochlorinated during polymerization of benzene under these conditions is readily apparent. A major advantage of l.d./F.t.m.s. for characterizing intractable PPP samples is that sample preparation can be accom-

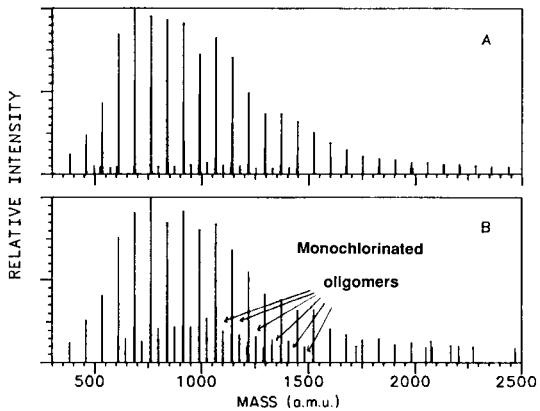

Fig. 18. Positive-ion l.d./F.t. mass spectra of samples prepared from benzene with $AlCl_3$/$CuCl_2$ at reaction temperatures of (A) 20°C and (B) 80°C.

plished simply by compressing the sample onto the probe tip with a 10-pound sledge hammer, thereby obviating any necessity of dissolving the sample.

Applications to inorganic and surface analysis

Laser desorption can be used to examine a solid surface in order to obtain information about surface composition or to identify the nature of contaminants or impurities. This is often accomplished with laser microprobe instruments involving time-of-flight analyzers [64, 65]. The l.d./F.t.m.s. interface can also be applied to surface analysis. Figure 19 shows a negative-ion l.d./F.t. mass spectrum of a section of a magnetic storage disk which has been coated with a fluorocarbon lubricant. The presence of the lubricant is clearly indicated by a series of characteristic negative ions. The peaks at m/z 185, 301, 351, 467, 517, 583, 633, 661, 683, and 849 are all characteristic negative ions that might be expected from a poly(perfluoroether).

Information provided by accurate mass measurements can be used to identify suspected contaminants. For example, a small peak at nominal mass 445 was suspected to be the $(M - H)^-$ peak from pentaphenyl ether, a common mass spectrometric contaminant. The measured mass was 445.144598,

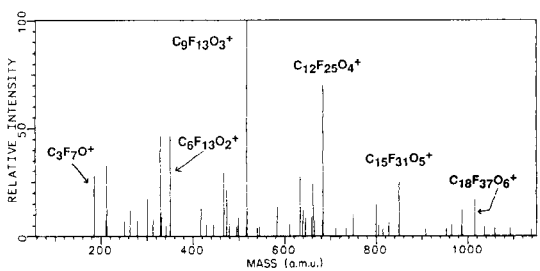

Fig. 19. Negative-ion l.d./F.t. mass spectrum of lubricant on the surface of a magnetic storage disk.

which differed from the calculated mass 444.144533 by only −0.14 parts in 10^6, confirming the nature of the suspected contaminant.

Another example is provided by the l.d./F.t.m.s. analysis of a sample of the mineral zircon ($ZrSiO_4$). The positive-ion spectrum (Fig. 20) shows a Zr^+ isotope cluster at m/z 90—94. In addition, ZrO^+ (m/z 106—110), $[ZrO(OH)]^+$ at m/z 123—127, and $(ZrO(OH)(H_2O)_n)^+$ for $n = 1$—3 can be seen. The presence of silicon is indicated by the Si^+ and $SiOH^+$ peaks at m/z 28 and 45. Uranium is present in the sample at approximately 100 mg kg^{-1}. Its presence is detected by ejecting the zirconium and its oxide peaks below mass 200, to increase the dynamic range. The $^{238}U^+$ peak then becomes visible (inset, Fig. 20).

ACCURATE MASS MEASUREMENTS

In F.t.m.s., mass is measured by the measurement of ion frequencies. The fact that frequencies can be measured very precisely and accurately has led to a great deal of interest in the application of F.t.m.s. methods to accurate mass measurement [11—14]. Indeed, the high resolution capabilities of F.t.m.s. must be paired with accurate mass measurement capability in order to utilize the instrument fully for analytical purposes. The stability of the fields produced by the superconducting magnets used in F.t.m.s. instruments has led to the development of methods for making accurate mass measurements in the absence of an internal calibrant [12, 58].

We have made use of the mass measurement equation described by Ledford et al. [14] to measure ion masses under all of the modes of analysis described in this paper, including electron impact, electron capture (e.c.), chemical ionization (c.i.), cesium s.i.m.s., laser desorption (l.d.), and g.c./m.s. Measurements were usually made in the direct mode over a wide mass range, using an internal calibrant. Generally, for electron-impact and chemical-ionization experiments, the electron beam current was kept low to minimize space-charge effects, and signal averaging was used to maximize signal-to-noise. Six to ten calibrant peaks provided a calibration over a mass range of 600 a.m.u.

In the heterodyne (high-resolution) mode, a single calibrant peak could be used to measure neighboring masses. Measurements taken for laser desorption experiments were usually taken from one laser shot, or the average measure-

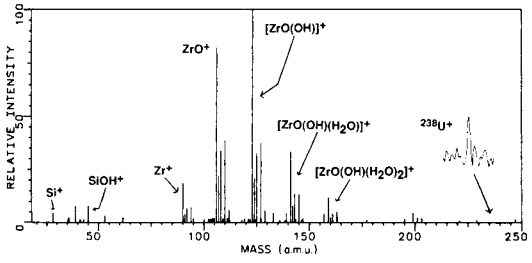

Fig. 20. Positive-ion l.d./F.t. mass spectrum of a sample of zircon.

ment from up to ten individual laser shots. Although an internal calibrant is to be preferred whenever possible, some of the measurements were taken in the absence of calibrant. The magnetic field produced by the superconducting magnet was sufficiently stable to allow correct nominal mass measurements for almost a year, based on a single calibration with perfluorotributylamine.

Table 2 shows some typical values for measurements made under each of these modes. Mass measurements generally differed by less than 10 parts in 10^6 from the calculated masses, and the errors in most measurements were less than 5 parts in 10^6. The largest errors occur when the mass resolution in direct mode is insufficient to resolve known doublets. Measurements made in heterodyne mode were usually less than 2 parts in 10^6 different from calculated values, with some differences as low as 0.07.

One of the more useful features of the system is the ability to make accurate mass measurements in the chemical-ionization mode. It is relatively easy to select conditions for low-pressure self-c.i. or reagent gas c.i., where ions produced by electron impact on a relatively unreactive compound, such as perfluorotributylamine, are relatively unreactive during the chemical-ionization process and can be used to calibrate the instrument to measure the $(M + H)^+$ ions from the sample.

CONCLUSION

Advances in instrument design, and the development of new ionization sources, have made it possible to apply Fourier-transform mass spectrometry to a wide variety of analytical problems. Further advances in instrumentation, and a better understanding of fundamental principles should contribute to the rapid growth of this fascinating mass spectrometric technique.

TABLE 2

Typical values for measurements made under s.i.m.s., l.d., c.i., self-c.i. and e.c. modes

Sample	Ion	Mode	Calibrant	Calculated mass (a.m.u.)	Measured (a.m.u.)	Differe (ppm)
Benzenethiosulfate	$C_7H_4S_2O_3N^-(M^-)$	s.i.m.s.	CsI	213.963812	213.962575	−5.80
Gramicidin S	$C_{60}H_{92}N_{12}O_{10}K^+$ $(M + K)^+$	l.d.	PEG1000	1179.669097	1179.679376	+8.70
Erythromycin	$C_{37}H_{67}NO_{13}K^+$ $(M + K)^+$	l.d.	PEG1000	772.424403	772.42449	−0.11
Insol. deriv., PAH[a]	$C_{48}H_{30}O_6$ (M^+)	l.d.	PEG600	702.203691	702.2011576	−3.60
6-Hydroxymelatonin sulfate	$C_{13}H_{14}O_6N_2S$ (M^-)	l.d.	(None)	327.065088	327.065026	−0.20
T2 toxin, TFA[b]	$C_{26}H_{34}O_{10}F_3$ $(M + H)^+$	i-C_4H_{10} c.i.	PFTBA	563.209860	563.207253	−4.63
Isophorone	$C_9H_{15}O$ $(M + H)^+$	self-c.i. (res. = 25 000)	PFTBA	139.112209	139.112177	−0.80
Drug sample, TFA[b]	$C_{23}H_{20}NO_8F_3$ (M^-)	e.c.	PFTBA	495.114652	495.1148635	+0.42

[a]Polynuclear aromatic hydrocarbon. [b]Trifluoroacetate derivative.

The 9,9-dicyanofluorene was obtained from J. Throck Watson of Michigan State University. The 6-hydroxymelatonin sample was provided by Sandy Markey of the National Institute of Health.

REFERENCES

1 U.S. Patent Number 3, 937, 955, February 10, 1976.
2 M. Comisarow and A. G. Marshall, Chem. Phys. Lett., 25 (1974) 282.
3 M. Comisarow and A. G. Marshall, Chem. Phys. Lett., 26 (1974) 489.
4 M. Comisarow and A. G. Marshall, J. Chem. Phys., 62 (1975) 293.
5 M. Comisarow and A. G. Marshall, J. Chem. Phys., 64 (1976) 110.
6 M. G. Parisod and M. B. Comisarow, Chem. Phys. Lett., 62 (1979) 303.
7 A. G. Marshall and M. B. Comisarow, J. Chem. Phys., 71 (1979) 4434.
8 M. B. Comisarow, Adv. Mass Spectrom., 7B (1978) 1042.
9 M. Allemann, H. P. Kellerhals and K. P. Wanczek, Int. J. Mass Spectrom. Ion Processes, 46 (1983) 139.
10 R. Cody, Anal. Chem., 57 (1986) in press.
11 R. L. White, E. B. Ledford, S. Ghaderi, C. L. Wilkins and M. L. Gross, Anal. Chem., 52 (1980) 2525.
12 R. L. White, E. C. Onyirinka and C. L. Wilkins, Anal. Chem., 55 (1983) 339.
13 T. Francl, M. G. Sherman, R. L. Hunter, M. J. Locke, W. D. Bowers and R. T. McIver, Jr., Int. J. Mass Spectrom. Ion Processes, 54 (1983) 189.
14 E. Ledford, Jr., D. L. Rempel and M. L. Gross, Anal. Chem., 56 (1984) 2744.
15 R. L. Hunter and R. T. McIver, Jr., Anal. Chem., 51 (1979) 699.
16 S. Ghaderi, P. S. Kulkarni, E. B. Ledford, Jr., C. L. Wilkins and M. L. Gross, Anal. Chem., 53 (1981) 428.
17 R. B. Cody and B. S. Freiser, Int. J. Mass Spectrom. Ion Processes, 41 (1982) 199.
18 R. B. Cody, R. C. Burnier and B. S. Freiser, Anal. Chem., 54 (1982) 96.
19 R. B. Cody and B. S. Freiser, Anal. Chem., 54 (1982) 1431.
20 R. R. White and C. L. Wilkins, Anal. Chem., 54 (1982) 2211.
21 R. B. Cody, R. C. Burnier, C. J. Cassady and B. S. Freiser, Anal. Chem., 54 (1982) 2225.
22 D. L. Bricker, T. A. Adams, Jr. and D. H. Russell, Anal. Chem., 55 (1983) 2417.
23 M. L. Gross and D. L. Rempel, Science, 226 (1984) 261.
24 C. L. Johlman, R. L. White and C. L. Wilkins, Mass Spec. Rev., 2 (1983) 389.
25 C. L. Wilkins and M. L. Gross, Anal. Chem., 53 (1981) 1661A.
26 E. B. Ledford, Jr., S. Ghaderi, C. L. Wilkins and M. L. Gross, Adv. Mass Spectrom., 8B (1981) 1707.
27 T. J. Carlin and B. S. Freiser, Anal. Chem., 55 (1983) 955.
28 T. M. Sack and M. L. Gross, Anal. Chem., 55 (1983) 2419.
29 D. A. McCrery, E. B. Ledford, Jr. and M. L. Gross, Anal. Chem., 54 (1982) 1435.
30 M. E. Castro and D. H. Russell, Anal. Chem., 56 (1984) 578.
31 D. F. Hunt, J. Shabanowitz, R. T. McIver, Jr., R. L. Hunter and J. E. P. Syka, Anal. Chem., 57 (1985) 768.
32 U.S. Patent Application, Serial No. 610502.
33 S. Ghaderi and D. P. Littlejohn, Paper presented at 33rd Annual Conference on Mass Spectrometry and Allied Topics, San Diego, CA, 1985.
34 R. Cody, Anal. Chem., 57 (1986) in press.
35 R. L. White, E. B. Ledford, Jr., S. Ghaderi, C. L. Wilkins and M. L. Gross, Anal. Chem., 52 (1980) 1527.
36 T. M. Sack, D. A. McCrery and M. L. Gross, Anal. Chem., 57 (1985) 1290.
37 M. E. Castro, L. M. Mallis and D. H. Russell, J. Am. Chem. Soc., 107 (1985) 5652.
38 L. K. Liu, K. L. Busch and R. G. Cooks, Anal. Chem., 53 (1981) 109.

39 K. L. Busch, B. H. Hsu, Y. X. Xie and R. G. Cooks, Anal. Chem., 55 (1983) 1157.
40 C. J. McNeal, R. D. Macfarlane and E. L. Thurston, Anal. Chem., 51 (1979) 2036.
41 R. B. Cody, R. C. Burnier, W. D. Reents, Jr., T. J. Carlin, D. A. McCrery, R. K. Lengel and B. S. Freiser, Int. J. Mass Spectrom. Ion Processes, 33 (1980) 37.
42 R. C. Burnier, T. J. Carlin, W. D. Reents, Jr., R. B. Cody, R. K. Lengel and B. S. Freiser, J. Am. Chem. Soc., 101 (1979) 7127.
43 R. C. Burnier, G. D. Byrd and B. S. Freiser, Anal. Chem., 52 (1980) 1641.
44 D. A. Peake and M. L. Gross, Anal. Chem., 57 (1985) 115.
45 R. E. Hein and R. B. Cody, presented at the 31st Annual Conference on Mass Spectrometry and Allied Topics, Boston, MA, 1983.
46 R. B. Cody and R. E. Hein, Anal. Chem., in press.
47 R. B. Cody, J. A. Kinsinger, S. Ghaderi and R. E. Hein, presented at the 33rd Annual Conference on Mass Spectrometry and Allied Topics, San Diego, CA, 1985.
48 D. Busch, C. Cairns, W. K. Lin, K. A. Goldsby, R. B. Cody and A. G. Marshall, unpublished results.
49 R. B. Cody and M. B. Comisarow, unpublished results.
50 C. E. Brown, P. Kovacic, C. A. Wilkie, R. B. Cody and J. A. Kinsinger, J. Polym. Sci., Polym. Lett. Ed., 23 (1985) 453.
51 D. Battiste, C. E. Brown, J. A. Kinsinger and R. B. Cody, unpublished results.
52 C. E. Brown, P. Kovacic, J. Smukalla, C. A. Wilkie, R. B. Cody and J. A. Kinsinger, presented at the 33rd Annual Conference on Mass Spectrometry and Allied Topics, San Diego, CA, 1985.
53 C. E. Brown, S. C. Roerig, V. T. Berger, R. B. Cody and J. M. Fujimoto, J. Pharm. Sci., 74 (1985) 821.
54 R. B. Cody, K. Faull, unpublished results.
55 Nicolet Instrument Corporation, FTMS Application Report No. 84.
56 C. L. Wilkins, D. A. Weil, C. L. C. Yang and C. F. Ijames, Anal. Chem., 57 (1985) 520.
57 A. G. Marshall, S. L. Mullen, R. E. Shomo and C. R. Weisenberger, presented at the 33rd Annual Conference on Mass Spectrometry and Allied Topics, San Diego, CA, 1985.
58 C. L. Johlman, D. A. Laude, Jr. and C. L. Wilkins, Anal. Chem., 57 (1985) 1040.
59 T. M. Barlak, J. R. Wyat, R. J. Colton, J. J. DeCorpo and J. E. Campana, J. Am. Chem. Soc., 104 (1982) 1212.
60 F. W. Stoll and F. Rollgen, Z. Naturforsch. A, 37A (1982) 9.
61 G. J. Q. Van der Peyl, K. Isa, J. Haverkamp and P. Kistemaker, Org. Mass Spectrom., 16 (1981) 416.
62 R. Stoll and F. W. Rollgen, Org. Mass Spectrom., 14 (1979) 642.
63 E. D. Hardin, T. P. Fan, C. R. Blakley and M. L. Vestal, Anal. Chem., 56 (1984) 2.
64 R. J. Conzemius and J. M. Capellen, Int. J. Mass Spectrom. Ion Processes, 34 (1980) 197.
65 R. J. Conzemius, D. S. Simons, Z. Shankai and G. D. Byrd, in R. Gooley (Ed.), Microbeam Analysis, San Francisco Press, San Francisco, 1983, p. 301.

Analytica Chimica Acta, 178 (1985) 67—77
Elsevier Science Publishers B.V., Amsterdam — Printed in The Netherlands

PULSED-VALVE CHEMICAL IONIZATION FOR GAS CHROMATOGRAPHY/FOURIER-TRANSFORM MASS SPECTROMETRY

DAVID A. LAUDE, Jr., CAROLYN L. JOHLMAN, ROBERT S. BROWN
CARL F. IJAMES, and CHARLES L. WILKINS*

Department of Chemistry, University of California, Riverside, CA 92521 (U.S.A.)

(Received 8th May 1985)

SUMMARY

The pressure requirements for chemical ionization g.c./F.t.m.s. which restrict mass resolution and accuracy are overcome through use of a pulsed valve that provides momentary reagent gas pressures. For alternate electron impact (EI)/chemical ionization (c.i.) g.c./F.t.m.s., similar resolution for both e.i. and c.i. data is demonstrated. The efficiency of chemical ionization with the pulsed valve is similar to static high pressure c.i. measurements of several model compounds. Results from the analysis of peppermint oil and a fuel additive illustrate the potential information available from a single g.c./F.t.m.s. experiment.

The well-documented high resolution capability of Fourier-transform mass spectrometry (F.t.m.s.) is directly related to the increased ion residence times observed at low measurement pressures [1, 2]. Important mass spectrometric techniques, including collision-induced dissociation (CID) [3], g.c./F.t.m.s. [4, 5] and chemical ionization (c.i.) [6, 7], are conventionally performed at pressures in excess of 10^{-7} Torr, degrading F.t.m.s. performance. These high pressures are avoided through the use of pulsed introduction methods which permit momentary high pressures prior to ion excitation and detection at optimal lower pressures. Carlin and Freiser [8] first demonstrated the feasibility of using a pulsed valve for high-resolution CID/F.t.m.s. experiments and obtained a resolution of 43 000 for the *m/z* 117 ion from the proton-bound dimer of acetone with a 0.9 T magnet. Sack and Gross [9] and McCrery et al. [10] extended application of the pulsed valve to chemical ionization F.t.m s. Sack and Gross [11] also demonstrated the use of a pulsed valve for introduction of the g.c. effluent to the F.t.m.s. and improved g.c./F.t.m.s. performance significantly; for example, a resolution of 103 000 for benzene molecular ion (*m/z* 78) was obtained at 1.2 T.

In this laboratory, the development of g.c./F.t.m s. has included demonstration of high-resolution peak switching [4], integrated electron impact/chemical ionization (e.i./c.i.) g.c./m.s. [7], and wide-band accurate mass analysis [12, 13]. Previously, integrated e.i./c.i. measurements were achieved by using a constant reagent gas pressure of 2.5×10^{-7} Torr. Although suc-

0003-2670/85/$03.30

cessful, this approach has three distinct disadvantages directly related to the high reagent gas pressure: (1) potential "crossover" contamination of e.i. and c.i. spectra; (2) degraded mass spectral resolution; and (3) difficulty in optimizing parameters for accurate mass measurement. The conflict between pressure requirements for efficient chemical ionization and the need for high resolution and mass measurement accuracy is resolved through the use of a pulsed valve for introduction of the reagent gas. Equivalent g.c./F.t.m.s. base pressures for both e.i. and c.i. spectra should permit optimum F.t.m.s. spectral parameters to be used for chemical-ionization mass spectra. The present data demonstrate that it is possible to obtain wide-band high-resolution e.i. and c.i. spectra from a single g.c./F.t.m.s. run.

EXPERIMENTAL

The major components of the g.c./F.t.m.s. included a Hewlett-Packard 5880A gas chromatograph interfaced with a Nicolet FTMS-1000 Fourier-transform mass spectrometer, operating at 3.0 T with a 2.54 × 2.54 × 7.62 cm^3 cell. The calculated vacuum system pumping speed was 120 l s^{-1} for helium at 150°C. The spectrometer was controlled by a Nicolet 1280 computer using Nicolet-developed software. Data were stored on a 300 Mbyte removable platter storage module.

A capillary split injector with ca. 10:1 split ratio was used for sample injection onto a (60 m × 0.323 mm i.d.) J+W DB-5 bonded phase capillary column. Helium carrier gas flow at 45°C was 3.0 ml min^{-1}. Because of the large pressure differential between the g.c. and the spectrometer, the post-column g.c. effluent was split at a Swagelok tee by narrow-diameter fused silica tubing. A 19 mm × 5 μm i.d. fused silica restrictor reduced the F.t.m.s. pressure to 4.5×10^{-8} Torr, sufficient for high resolution and accurate mass analysis. (The estimated split of 200:1 at the restrictor significantly decreases the F.t.m.s. sensitivity; despite this, low nanogram detection limits have been experimentally determined.)

The post-restrictor m.s. transfer line of 100 cm × 0.25-in. o.d. glass-lined stainless-steel tubing was maintained under vacuum. No degradation in chromatographic resolution was observed despite this large dead volume because of the low pressure conditions. Temperatures at the restrictor and along the transfer line were 250°C. The spectrometer was maintained at 91°C to minimize background from diffusion pump oil.

A three-way solenoid valve (Series-9, General Valve Corporation) mounted on the solid probe inlet was used for all c.i. experiments with methane as the reagent gas. An energizing circuit was designed to apply variable voltage (31—90 V) to the valve. Under typical operating conditions, a software-controlled trigger pulse of 0.5—3 ms, depending on the voltage employed, opened the valve to introduce the methane reagent gas; maximum pressures of $1—10 \times 10^{-7}$ Torr above the g.c./F.t.m.s. base pressure were obtained. A profile of the methane gas density as measured from the ion gauge is

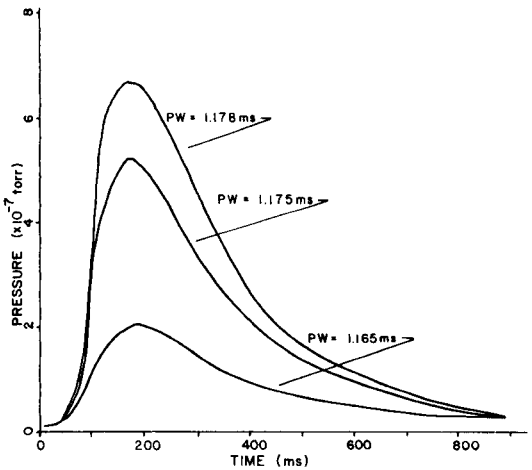

Fig. 1. Profiles of methane pressure obtained from oscilloscopic trace of the ion gauge reading after triggering the pulse valve. The software-controlled pulse width (*PW*) was varied for each trace. The profile with *PW* = 1.165 ms yielded the highest c.i. reagent ion concentrations and was used for data presented in Table 1.

presented in Fig. 1 for a voltage of 60 V and various pulse widths. Maximum pressure at the cell was attained at about 100 ms after the trigger and the system returned to base pressures in approximately 700 ms. Although the methane concentration increased with an increase in pulse width, the pump-down time was essentially constant over the narrow pressure range utilized. The pulse-valve reproducibility was found to be ±5%.

Optimum pulsed-valve c.i. conditions were determined empirically by varying a delay between the trigger and electron beam to maximize methane concentration in the cell, and a delay after ionization to produce large CH_5^+ (*m/z* 17) and $C_2H_5^+$ (*m/z* 29) ions. An initial delay of 75—100 ms produced the highest concentration of methane at the cell, and a 100—300-ms reaction time delay following a 315-nA, 5-ms electron beam produced the reagent ions. The concentration of methane in the cell was critical in maximizing reagent ion fluxes. If too much methane was introduced, inefficient trapping decreased the abundance of the *m/z* 17 and 29 ions. For example, the pulse width of 1.165 ms in Fig. 1 produced the optimum momentary pressure of 2.5×10^{-7} Torr methane, while the higher methane pressures from longer pulse widths resulted in decreased reagent ion yields.

Figure 2 is a timing diagram of the alternate e.i.-c.i. pulse sequence used in the study. The EI mode produced 70-eV mass spectra which were used in mass spectral library searches. Minimal delays of 3 ms were imposed following the quench and ionization pulses as electronic settling times. Total experiment time depended on bandwidth and number of data points but typically ranged from 10 to 40 ms for a wide-band experiment. Ensemble averaging of nine 64 K spectra was performed over a 1.0-s period prior to data storage.

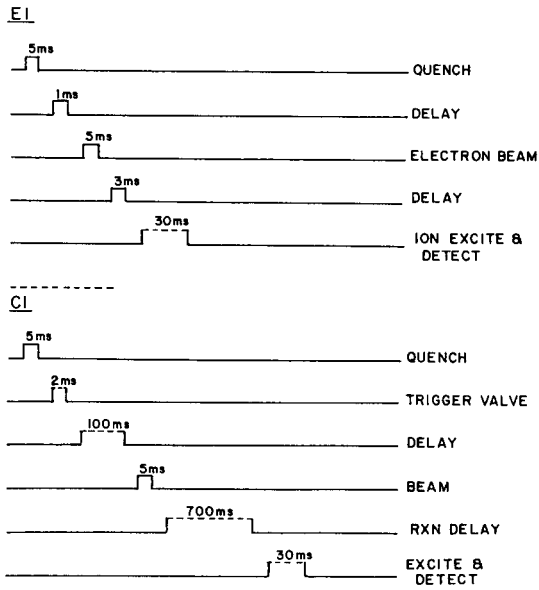

Fig. 2. The software-controlled pulse sequence for all pulsed-valve e.i.-c.i. g.c./F.t.m.s. work. Dashed lines indicate variable event times. Typical values for all events are included.

The c.i. mode differed from the e.i. both in the length of delays used and by the presence of reagent gas. For these measurements, a synchronized trigger pulse opened the pulsed valve momentarily to admit methane prior to a 100-ms delay and ionization. A 700-ms reaction delay permitted efficient c.i. and ensured that the base g.c./F.t.m.s. pressure for maximum resolution was achieved prior to ion excitation and detection. A single c.i. spectrum was then stored on disk. The total c.i. experiment time of approximately 1 s in combination with the 1-s e.i. data acquisition produced a total time (equivalent to the chromatographic time resolution) of 2 s. For the 0.323-mm i.d. column used, this was sufficient for the typical g.c. peak widths of 6—15 s.

All g.c./F.t.m.s. separations were run in a wide-band mode with 8 or 64 K data collected over a 1.0 or 1.1 MHz bandwidth. (At 3.0 T, low mass cutoffs for 1.0 and 1.1 MHz are m/z 45 and 41, respectively.) All spectra were baseline-corrected, sine-bell apodized, augmented with an equivalent number of zeroes and magnitude-mode Fourier-transformed. To demonstrate the wide-band resolution and accurate mass measurement capabilities for pulsed-valve experiments, 64 K data files were acquired as 6-component equivolume mixtures were analyzed.

Details of the accurate mass experiment conditions and data processing are available elsewhere [12]. Peppermint oil and a fuel additive were analyzed as part of a g.c./i.r./m.s. measurement demonstrating the utility of the pulsed valve for alternate e.i./c.i. Because only nominal mass resolution was required for these analyses, 8 K data files were acquired to minimize data storage.

RESULTS AND DISCUSSION

Previous applications of the integrated e.i.-c.i. F.t.m.s. experiments required a constant reagent gas pressure in excess of 2×10^{-7} Torr to ensure sufficient c.i. within the time constraints of the g.c. separation. As a result, the high mass resolution potential of the g.c./F.t.m.s. experiment could not be realized. The momentary high reagent gas pressures provided by use of a pulsed valve for efficient c.i. would ideally permit equivalent base pressures for e.i. and c.i. data acquisition. Figures 3 and 4 demonstrate this capability in the wide-band g.c./F.t.m.s. separation of a 6-component mixture. Resolution as a function of mass is compared in Fig. 3 for e.i. and c.i. spectra obtained in a single pulsed-valve g.c./F.t.m.s. separation. Although not equivalent (average e.i. resolution was 16% higher), the pulsed c.i. resolution data are far superior to the resolution data for the static experiment, which are included for comparison (average c.i. resolution was 86% higher than the static c.i. results). The decrease in resolution of 16% for the pulsed experiment is likely due to sub-optimal trapping conditions at long delays for the c.i. spectra, rather than higher pressures.

As seen in the inserts for Fig. 4, with resolution in excess of 12 000 for both e.i. and c.i. spectra, the $C_4H_9^+$ and $C_3H_5O^+$ ions at *m/z* 57 are baseline-separated. These resolution data are from a wide-band measurement (1.0 MHz with low mass cutoff of 46 and 64 K data points collected) and should not be confused with data obtained from high-resolution heterodyne-mode measurements where the bandwidth is substantially decreased. The data are representative of resolution obtainable at 3.0 T for wide-band

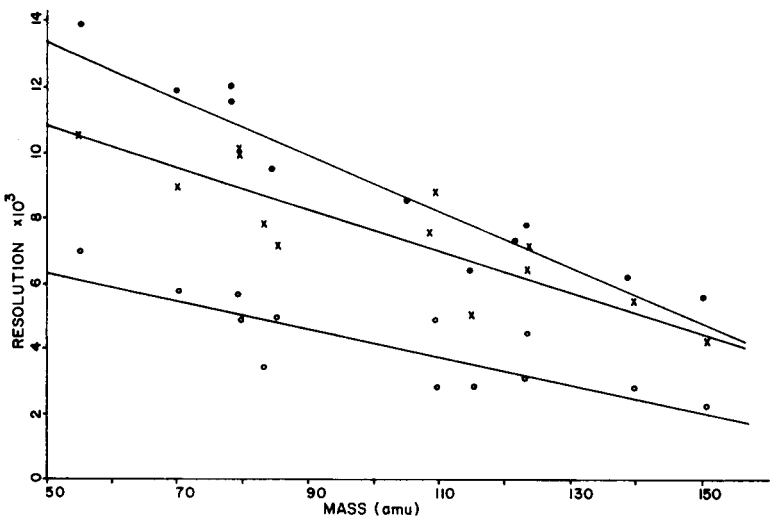

Fig. 3. Representative resolution values from a 6-component g.c./F.t.m.s. separation are plotted for; (○) c.i. data with 2.5×10^{-7} Torr methane present; (×) c.i. data from a pulsed-valve e.i./c.i. run with base pressures at 4.5×10^{-8} Torr; (●) e.i. data from a pulsed-valve e.i./c.i. run at 4.5×10^{-8} Torr. 64 K data were collected over a 1.0-MHz bandwidth (low mass cutoff of 46) followed by a single zero fill. Linear least-squares fits of the three experiments are included.

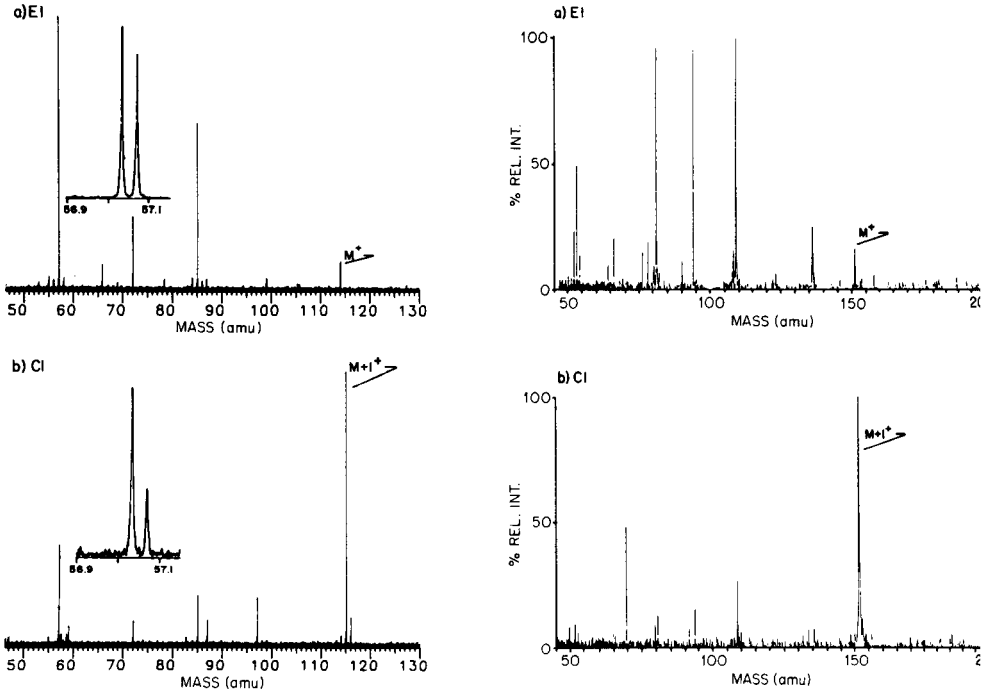

Fig. 4. Comparative e.i. and c.i. spectra of 3-heptanone from the pulsed-valve e.i.-c.i. analysis described in Fig. 3. The inserts, expanded regions from *m/z* 56.9 to 57.15, demonstrate the equivalent resolution of two nominal mass 57 peaks, $C_4H_9^+$ and $C_3H_5O^+$, obtained for both e.i. and c.i. spectra.

Fig. 5. Comparative e.i. and c.i. spectra of piperitone, a minor component taken from the g.c./i.r./m.s. peppermint oil analysis. The m.s. search result obtained from the e.i. data is substantiated by molecular-weight c.i. information. The low-resolution spectra were obtained from 8 K data acquired over a 1.1-MHz bandwidth.

spectra under typical g.c./F.t.m.s. conditions. Because a simple restrictor is used at the g.c./F.t.m.s. interface, sensitivity and resolution are inversely related. Although resolution would increase at lower pressures, a compromise value of 4.5×10^{-8} Torr was chosen. Alternatives to the restrictor which improve detection limits yet retain resolution include use of a pulsed valve to introduce g.c. column effluent [11] or ideally, a differentially pumped cell which permits all g.c. effluent to be introduced into the m.s. vacuum system without loss of mass resolution.

To test the efficiency of the pulsed valve for chemical ionization, a comparison was made with static system c.i. at various reagent gas pressures. Results of this comparison are presented in Table 1 for a 6-component mixture; the fraction of molecular species in the spectrum was calculated for each compound. In all cases, the pulsed c.i. experiment was equivalent or superior to the static result at 2.5×10^{-7} Torr. Beyond a total pressure of 2.5×10^{-7} Torr for the pulsed measurement, the efficiency of chemical

TABLE 1

Efficiency of methane chemical ionization at various pressures

Compound	Efficiency[a] at different total pressures[b] (Torr)			
	2.5×10^{-7}	8.5×10^{-8}	4.5×10^{-8} [c]	Pulsed
Benzaldehyde	0.50	0.45	0.29	0.68
Ethyl acetate	0.63	0.64	0.64	0.73
Cyclohexane	0.57	0.39	0.30	0.71
p-Fluoroacetophenone	0.66	0.53	0.40	0.61
3-Heptanone	0.33	0.21	0.11	0.28
Ethyl benzoate	0.51	0.53	0.32	0.51

[a]The efficiency is given as the fraction of molecular species relative to the total ion intensity. [b]The total pressure given includes a background pressure of 4.5×10^{-8} Torr with the difference being the pressure contribution from methane. A profile of the pulsed experiment, with a maximum pressure of 2.5×10^{-7} Torr, is found in Fig. 1 for a pulse width of 1.165 ms. [c]Data are for self-c.i. of the eluent.

ionization did not improve substantially. As expected, the lengthy delay time permitted self-c.i. to occur to some extent for each compound; these data are also included in Table 1.

To demonstrate the practical utility of the pulsed valve experiments, pulsed-valve alternate e.i./c.i. was utilized in the on-line g.c./i.r./m.s. analysis of real mixtures, peppermint oil and a fuel additive; representative examples from those g.c./F.t.m.s. data illustrate the information available from a single measurement. The e.i. and c.i. spectra for a relatively minor component of the peppermint oil separation are found in Fig. 5. From the e.i. spectrum (Fig. 5a) a m.s. library search identified piperitone as the unknown. The large $M + 1$ ion at m/z 153 from the c.i. spectrum (Fig. 5b) confirmed the molecular weight of 152.

Figure 6 is the e.i. reconstruction from the e.i./c.i. g.c./F.t.m.s. separation of a gasoline additive. Especially with complex mixtures, the time resolution of the g.c. experiment is crucial to avoid peak overlap; here a time resolution of 2 s (1 s each for the e.i. and c.i. experiment), although not optimum, is sufficient for the g.c. peak widths of 6—15 s and permits the separation and quantitation of over 80 components. Representative examples of e.i./c.i. spectra are presented in Figs. 7 and 8 (g.c. peaks labeled 1 and 2, respectively, in Fig. 6). For this separation, the early eluting peaks (prior to 13 min) are generally branched alkanes that yield $M - 1$ ions in the c.i. spectra. The $M - 1$ ions are observed to increase in units of 14 amu with increasing elution time so that information on molecular weight can be predicted for those compounds not yielding chemical ionization quasi-molecular ions. In Fig. 7, the c.i. data ($M - 1$ equal to m/z 113) is indicative of a C_8 hydrocarbon; the top m.s. search result is 2-ethyl-3-methylpentane with a molecular weight of 114.

The later eluting peaks in the fuel additive are alkylbenzenes which yield

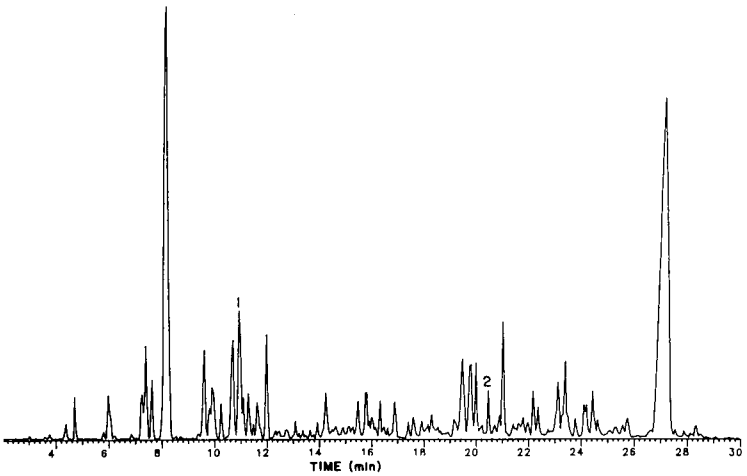

Fig. 6. Reconstruction of the e.i. g.c./F.t.m.s. from the pulsed-valve e.i./c.i. analysis of a commercial fuel additive. Time resolution for the reconstruction was 2 s. Spectra for the first and second labeled peaks are found in Figs. 7 and 8, respectively.

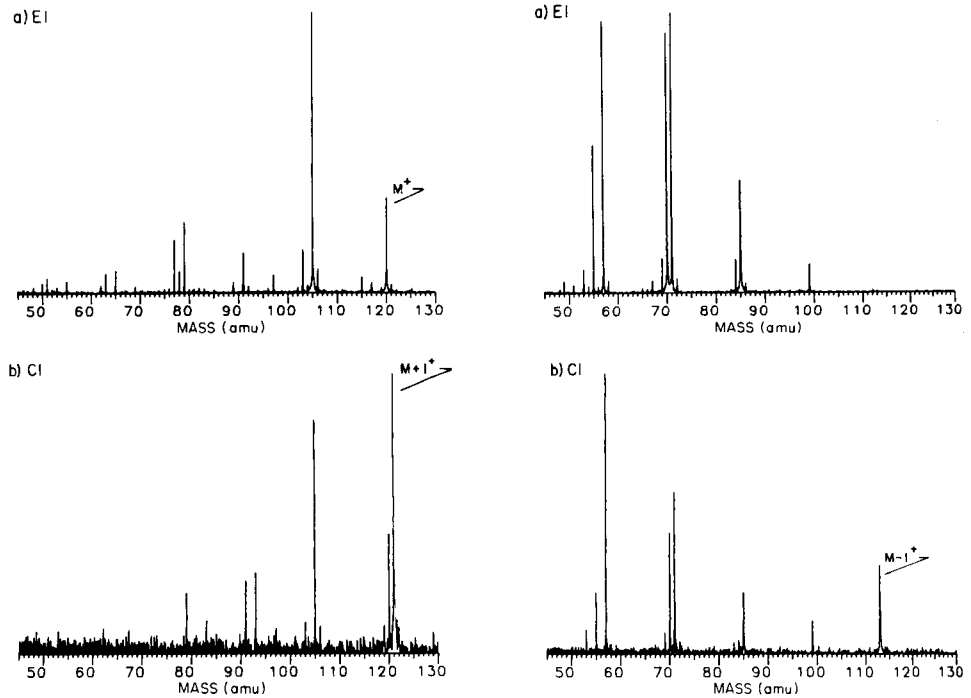

Fig. 7. Mass spectra of an early eluting aliphatic component from the pulsed-valve e.i./c.i. separation of the fuel additive. The C_8 hydrocarbon was identified as 3-methyl-2-ethylpentane.

Fig. 8. Mass spectra of an aromatic component from the fuel additive separation. In conjunction with i.r. data the compound was identified as 1,3,4-trimethylbenzene.

strong $M + 1$ ions increasing in mass by increments of 14 amu. The c.i. spectrum presented in Fig. 8 confirms a molecular weight of 120. The major limitation of g.c./m.s., analysis of isomers, was highlighted in the search results for this compound, as all structural isomers of propylbenzene in the library yielded excellent matches with the unknown. Ultimately, infrared spectral data were required to confirm 1,3,4-trimethylbenzene as the identify of the unknown. Both c.i. spectra in Figs. 7 and 8 appear to contain some e.i. fragmentation produced by the electron beam during formation of methane reagent ions. Although unnecessary for the present analysis, ejection sweeps after the electron beam would have removed any sample ions formed.

The information potential of the g.c./F.t.m.s. experiment is increased considerably by the accurate mass measurement capabilities of F.t.m.s. As has been demonstrated recently [12, 13], accurate mass measurement values in the low ppm error range can be obtained in a wide-band electron-impact experiment. Examples of the accurate mass data routinely available are

TABLE 2

Accurate mass measurement data for 6-component mixture[a]

Compound	Measured mass	Error (ppm)	Compound	Measured mass	Error (ppm)
Benzaldehyde	50.01551	2.8	*p*-Fluoroacetophenone	75.02326	4.5
	51.02338	1.8		83.02935	2.3
	74.01554	1.4		95.02920	0.5
	77.03893	2.5		123.02359	3.9
	105.03354	4.7		138.04698	4.1
	106.04133	5.0	Trichloroethylene	47.97667	0.2
Cyclohexane	41.03934	5.2		59.97669	0.2
	51.02364	3.2		61.97377	0.6
	53.03924	2.1		94.94551	0.2
	55.05495	3.1		96.94251	0.7
	56.06281	3.7		98.93966	0.2
	67.05507	4.3		129.91391	3.6
	69.07076	4.8		131.91104	2.9
	77.27473	2.2		133.90846	0.2
	81.06982	7.4	Ethyl benzoate	77.03897	5.1
	83.08666	7.0		105.03370	2.0
	84.09430	4.7		122.03621	0.2
3-Heptanone	72.05768	2.2		150.06674	5.3
	81.07051	1.0	Overall avg.		2.7
	84.05724	3.2			
	85.06541	0.8			
	99.08109	1.0			
	114.10457	0.9			

[a]64 K data were collected over a 1.1-MHz bandwidth in e.i. mode at a pressure of 2.5×10^{-8} Torr.

presented in Table 2 for the six-component mixture. The utility of these accurate mass data has recently been demonstrated in this laboratory through use of a post-search filter algorithm which eliminates m.s. search results with incorrect molecular or fragment ion formulae. If a search result has an incorrect composition, mass errors are typically on the order of ppm. Table 3 presents an example of the post-search filter applied to one of the six compounds, ethyl benzoate. Although placed in the third search result position prior to the filter, the post-search accurate mass analysis readily eliminates the top two search results and correctly elevates ethyl benzoate to the first position.

Although application of accurate mass analysis to c.i. data would be complicated in a high-pressure static experiment, pulsed-valve accurate mass results for c.i. data should be comparable to the e.i. data in Table 2. The unambiguous molecular formula information which would be directly obtained would be invaluable in the analysis of unknowns. Preliminary results, to be presented elsewhere, indicate the feasibility of this experiment.

Support from the National Science Foundation under NSF Grants CHE-80-18245, CHE-82-08073, and a Department Research Instrument Grant, CHE-82-17610, are gratefully acknowledged.

TABLE 3

Accurate mass measurement analysis of ethyl benzoate

Mass spectral search result

Search position	*Compound name*	*Molecular formula*
1	benzoic acid, formyl ester	$C_8H_6O_3$
2	benzoic acid, 2-methylhydrazine	$C_8H_{10}N_2O$
3	benzoic acid, ethyl ester	$C_9H_{10}O_2$
4	diazine(4-nitrophenyl)phenyl	$C_{12}H_9N_3O_2$
5	benzoic acid, 2-propanyl ester	$C_{10}H_{10}O_2$

Post-search filter

From unknown spectrum, peak at *m/z* 150.06674

Search position	*Nom. mass*	*Elem. comp.*	*Exact mass*	*Error (ppm)*	*Result*
1	150	$C_8H_6O_3$	150.03114	−237.1	eliminate
2	150	$C_8H_{10}N_2O$	150.07876	80.1	eliminate
3	150	$C_9H_{10}O_2$	150.06753	5.2	correct M.F.

Filtered search results

Search position	*Compound name*	*Molecular formula*
1	benzoic acid, ethyl ester	$C_9H_{10}O_2$
2	diazine(4-nitrophenyl)phenyl	$C_{12}H_9N_3O_2$
3	benzoic acid, 2-propanyl ester	$C_{10}H_{10}O_2$

REFERENCES

1 A. G. Marshall, M. B. Comisarow and G. J. Parisod, J. Chem. Phys., 71 (1979) 4434.
2 R. L. White, E. C. Onyiriuka and C. L. Wilkins, Anal. Chem., 55 (1983) 339.
3 R. B. Cody, R. C. Burnier and B. S. Freiser, Anal. Chem., 54 (1982) 96.
4 E. B. Ledford, R. L. White, S. Ghaderi, C. L. Wilkins and M. L. Gross, Anal. Chem., 52 (1980) 2450.
5 R. L. White and C. L. Wilkins, Anal. Chem., 54 (1982) 2443.
6 S. Ghaderi, P. S. Kulkarni, E. B. Ledford Jr., C. L. Wilkins and M. L. Gross, Anal. Chem., 53 (1981) 428.
7 D. A. Laude, Jr., G. M. Brissey, C. F. Ijames, R. S. Brown and C. L. Wilkins, Anal. Chem., 56 (1984) 1163.
8 T. J. Carlin and B. S. Freiser, Anal. Chem., 55 (1983) 571.
9 T. M. Sack and M. L. Gross, presented at the 31st Annual Conference of Mass Spectrometry and Allied Topics, Boston, MA, May, 1983.
10 D. A. McCrery, T. M. Sack and M. L. Gross, Spectrosc. Int. J., 3 (1984) 57.
11 T. M. Sack and M. L. Gross, Anal. Chem., 55 (1983) 2419.
12 C. L. Johlman, D. A. Laude, Jr. and C. L. Wilkins, Anal. Chem., 57 (1985) 1040.
13 D. A. Laude, Jr., C. L. Johlman, J. R. Cooper and C. L. Wilkins, Anal. Chem., 57 (1985) 1044.

Analytica Chimica Acta, 178 (1985) 79—89
Elsevier Science Publishers B.V., Amsterdam — Printed in The Netherlands

SURFACE ANALYSIS BY LASER DESORPTION OF NEUTRAL MOLECULES WITH DETECTION BY FOURIER-TRANSFORM MASS SPECTROMETRY

M. G. SHERMAN, J. R. KINGSLEY, J. C. HEMMINGER and R. T. McIVER, Jr.*
Department of Chemistry, University of California, Irvine, CA 92717 (U.S.A.)
(Received 8th May 1985)

SUMMARY

Molecules chemisorbed on a platinum single crystal are desorbed by a pulsed laser, ionized by an electron beam or multiphoton ionization, and detected by Fourier-transform mass spectrometry (F.t.m.s.). Laser desorption of ethylene, methanol, cyanogen, benzene and naphthalene is described. In all cases, molecular ions are the major peaks observed in the mass spectra, and the minor peaks correspond to known electron-impact fragments of the adsorbates. For the systems investigated thus far, the laser-desorption F.t. mass spectra are less complex and easier to interpret than the spectra produced by secondary-ion mass spectrometry, which are complicated by the rapid ion/-molecule reactions that can occur directly above the surface between adsorbates and substrate atoms. In the laser-desorption method, these complications are avoided because the ions are formed after the desorbed molecules have moved away from the surface and have expanded into the vacuum. The sensitivity of the laser-desorption F.t.m.s. method is tested. For carbon monoxide adsorbed on platinum, the detection limit is ca. 5×10^{-6} monolayer per cm^2. For naphthalene, a single laser pulse at 248 nm produces abundant molecular ions even when the electron beam is turned off. The ions appear to be produced by resonance-enhanced multiphoton ionization rather than a thermal process. In these experiments, multiphoton ionization of naphthalene at 248 nm is about 35-fold more sensitive than electron ionization.

A primary goal of many modern studies of surface chemistry has been the identification of surface chemical species (both stable molecules and intermediates) and the measurement of the time dependence of the concentrations of these species. The primary tools used in such experiments have been temperature-programmed reaction methods (t.p.r.) secondary-ion mass spectrometry (s.i.m.s.), and vibrational or photoelectron spectroscopy.

The t.p.r. technique usually involves ramping the sample temperature at a rate of 5—100 K s^{-1} while desorbed molecules are monitored with a quadrupole mass spectrometer [1, 2]. Often the species which desorb from the surface are not those present at the beginning of the experiment because a thermally-activated process (diffusion-controlled recombination, direct decomposition, etc.) may occur as the temperature is increased. For example, at room temperature, naphthalene adsorbs on platinum as an intact molecule, but only molecular hydrogen is observed in t.p.r. experiments

0003-2670/85/$03.30

because the naphthalene decomposes as the temperature is increased [3]. Other limitations are related to the basic characteristics of the quadrupole mass spectrometer that detects the desorbed molecules. The mass resolution of a quadrupole typically used in t.p.r. experiments is not sufficient to resolve chemically-distinct ions of the same nominal mass, such as CO^+ and $C_2H_4^+$. Also, a quadrupole mass spectrometer is a single-channel detector that must be scanned to obtain a complete mass spectrum. This results in lower sensitivity because the dwell time at a particular mass is a small fraction of the total scan time.

The use of vibrational or photoelectron spectroscopy in surface analysis is often limited because the spectra do not provide an unambiguous identification of the species present [4, 5]. This is especially true for reactive systems with multiple species on the surface. In addition, the relatively long time (several seconds) required to obtain the spectrum of a surface species at low concentration often precludes kinetic measurements.

With s.i.m.s., high-energy atomic ions are focused on a surface, and secondary ions ejected from the surface are mass-analyzed [6, 7]. Thus, s.i.m.s. has proved to be a very powerful and sensitive surface analysis method. One problem, however, is that ions sputtered from the surface react rapidly in the gas phase with sputtered neutral species and produce complicated mass spectra that cause ambiguities in the identification of the surface species.

Recently, a new surface analysis technique was described in which a pulsed laser is used to desorb neutral molecules from a surface and Fourier-transform mass spectrometry (F.t.m s.) is applied to detect the ions that are produced by electron impact of the desorbed neutral species [8]. An important feature of this approach is that the desorption and ionization steps are separated. This reduces complications that are thought to be caused by ionic reactions which occur directly above the surface. The first publication also showed that F.t.m.s. is well suited as the detection method for these pulsed-laser experiments because a complete mass spectrum can be obtained for each laser pulse. The F.t.m.s. method shares this advantage with time-of-flight mass spectrometry (t.o.f.), but far higher mass resolution can be achieved with F.t.m.s.

New results for laser desorption of several organics from a platinum single crystal are described in this paper. The laser-desorption F.t.m.s. results are compared with those obtained by s.i.m.s., and the limits of detection are discussed.

EXPERIMENTAL

During the last years, an F.t.m.s. instrument specifically designed for laser-induced thermal desorption from single-crystal metal surfaces has been constructed in this laboratory. The high resolution capabilities of F.t.m.s. were demonstrated and the detection of carbon monoxide desorbed from a platinum single crystal by a laser pulse was reported [8].

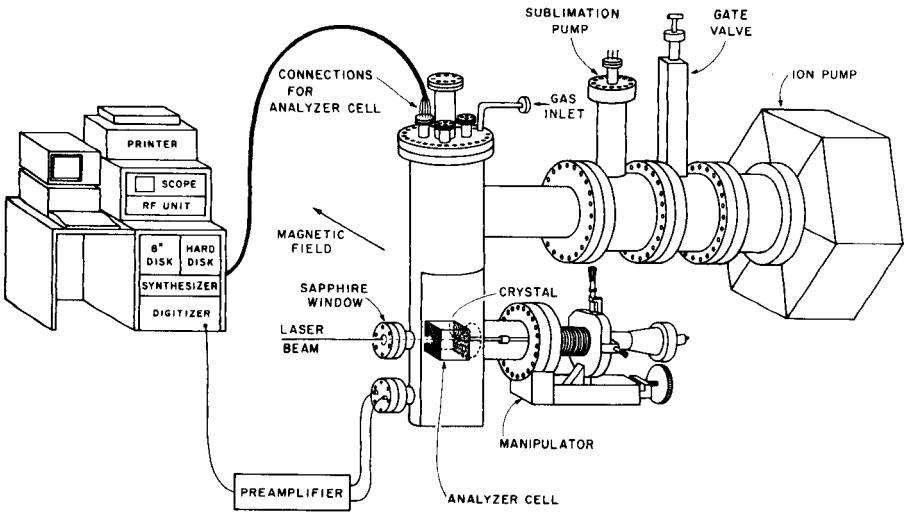

Fig. 1. Perspective drawing of the laser-desorption F.t.m.s. instrument showing the relative positions of the crystal, laser beam and analyzer cell.

Figure 1 is a perspective drawing of the vacuum chamber, F.t.m.s. analyzer cell, sample manipulator, and data system. A gate valve and titanium sublimation pump are mounted between the main chamber and the ion pump (150 l s^{-1}). The chamber has a base pressure of 3×10^{-8} Pa after bake-out. Gases are introduced through sapphire-sealed leak valves from a separate gas handling manifold that is pumped by an oil diffusion pump. A Pt(s) [7(111) × (100)] single crystal is positioned in front of a hole in one of the plates of the F.t.m.s. analyzer cell, and the laser beam enters the chamber through a sapphire window directly opposite the crystal. Presently, an excimer laser (Lambda Physik EMG 103 MSC) is used, operated at a wavelength of 248 nm with krypton fluoride. The F.t.m.s. analyzer cell has cubic geometry with inside dimensions of 6.35 cm. Four of the electrodes are made with stainless steel mesh (22 lines/cm) that is supported by Macor insulators, and the other two electrodes (trapping plates) are copper that has been plated with silver and flashed with rhodium. The analyzer cell is centered between the pole caps of an electromagnet (Varian Assoc., V-7300) operated at 1.1 T. There is a rhenium filament (not shown in Fig. 1) mounted on one of the analyzer cell plates, and a 1—10-μA electron beam is accelerated across the analyzer cell, in the same direction as the magnetic field and 3.1 cm in front of the crystal.

For these studies, an IonSpec model 2000 F.t.m.s. data system was used to control the analyzer cell, detect the ions, and plot the data. The IonSpec data system (IonSpec Corp., 1 Longstreet, Irvine, CA 92714) is based on an IBM Instruments computer (CS-9002) with 1 Mbyte of system memory. A floating-point array processor is utilized to calculate the Fourier transform

of the ion image current signal. Typically, an F.t.m.s. signal consisting of 16 K data points is Fourier-transformed and a new mass spectrum is displayed every 4.5 s.

Figure 2 shows the sequence of events for a laser-desorption F t.m.s. experiment. First, a focused laser beam traverses the analyzer cell and strikes the crystal normal to the surface. Approximately half the laser energy is absorbed at the surface of the crystal [9]; during the 20-ns period of the laser pulse, the surface temperature increases rapidly. As desorbed neutral molecules move away from the crystal, they pass through an electron beam and a very small number (approximately 10^{-4}%) are ionized. The ions are trapped in the analyzer cell by the combined effects of the magnetic field and static voltages applied to each of the cell plates. Finally, the ions are accelerated by a radiofrequency pulse and detected by the image current their coherent cyclotron motion induces to flow between the cell plates. Fourier-transform analysis of the ion-current signal yields the mass spectrum.

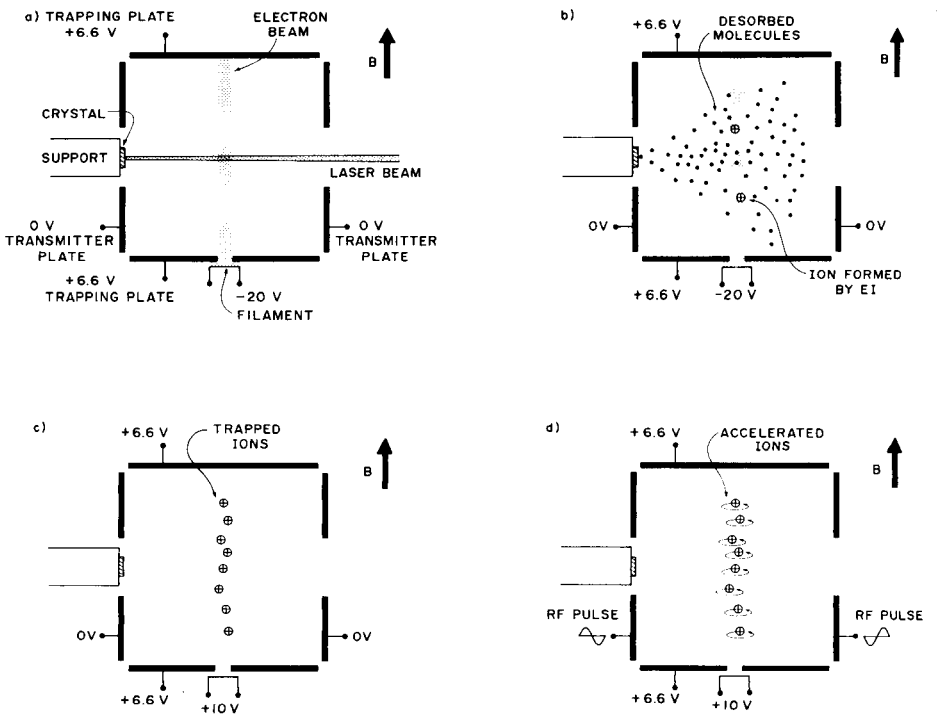

Fig. 2. Sequence of events in a laser-desorption F.t.m.s. experiment: (a) laser beam enters the analyzer cell and strikes the crystal; (b) desorbed molecules are ionized by an electron beam; (c) ions are trapped in the analyzer cell by the magnetic and electric fields; (d) ions are accelerated by a radiofrequency pulse and their coherent cyclotron motion is detected.

Under normal operating conditions, the laser output is 260 mJ/pulse. The output beam is reflected by two dielectric-coated mirrors and then transmitted through quartz plates to drop its energy to 150 mJ/pulse. After reflecting off a third aluminium-coated mirror, the beam is adjusted to a circular cross-section of 4-mm radius by an adjustable iris. The beam is then split with a 1.0-mm thick Suprasil fused-quartz window so that 89% of the light is transmitted to the analyzer cell and 8% is passed to a power meter that monitors each laser pulse. The transmitted light is reflected off a fourth aluminum-coated mirror and then focused by a lens (0.25-m focal length) that is positioned directly in front of the sapphire window on the vacuum chamber. The reflected beam passes out of the vacuum chamber through the same sapphire window.

Prior to each experiment, the platinum crystal was cleaned by heating it for 5 min in oxygen (2×10^{-4} Pa) at 1100 K. The gate valve was closed during the oxygen exposure, and then opened while the crystal was annealed at 1300 K to remove residual oxygen. The crystal was then cooled to the temperature of interest. Once the temperature of the crystal had stabilized, an adsorbate of interest was admitted to the vacuum chamber through a variable leak valve. A typical exposure lasted for 250 s, then the leak valve was closed, and the remaining gas was pumped away. Once the pressure in the vacuum chamber had stabilized, the laser-desorption experiments were begun.

RESULTS AND DISCUSSION

Initial experiments involved laser desorption of carbon monoxide from a platinum single crystal [8]. Since then, several different organic adsorbates have been investigated. Figure 3 shows F.t.m.s. data for laser desorption of ethylene, methanol, cyanogen, and benzene from a Pt(s) [7(111) × (100)] crystal. Various exposure levels and substrate temperatures were used, but in all cases a single laser pulse of 4.0 mJ (incident at the crystal) at a wavelength of 248 nm was applied. Assuming a pulse duration of 20 ns and a beam radius of 0.4 mm, the average power density is calculated to be 40 MW cm^{-2}. The narrow-band detection mode of F.t.m.s. was used in order to maximize the detection sensitivity in the region around the molecular ions of interest. In the narrow-band mode, the mass resolution is very high. Figure 3 shows that the molecular ions of nitrogen, ethylene and carbon monoxide are easily resolved. N_2 and CO are present as residual gases in the vacuum chamber. Mass resolution greater than 50 000 is routinely available with this instrument when the narrow-band detection mode is used. For complete mass spectra covering a range of several hundred mass units, the broad-band mode must be used. Figure 4 (to be discussed later) shows the data obtained in the broad-band mode. Presently, the mass resolution available with the broad-band mode is a few thousand because of limitations in the software for calculating the Fourier transforms. This problem will be remedied by a new fast Fourier-transform program that can calculate 128 K transforms.

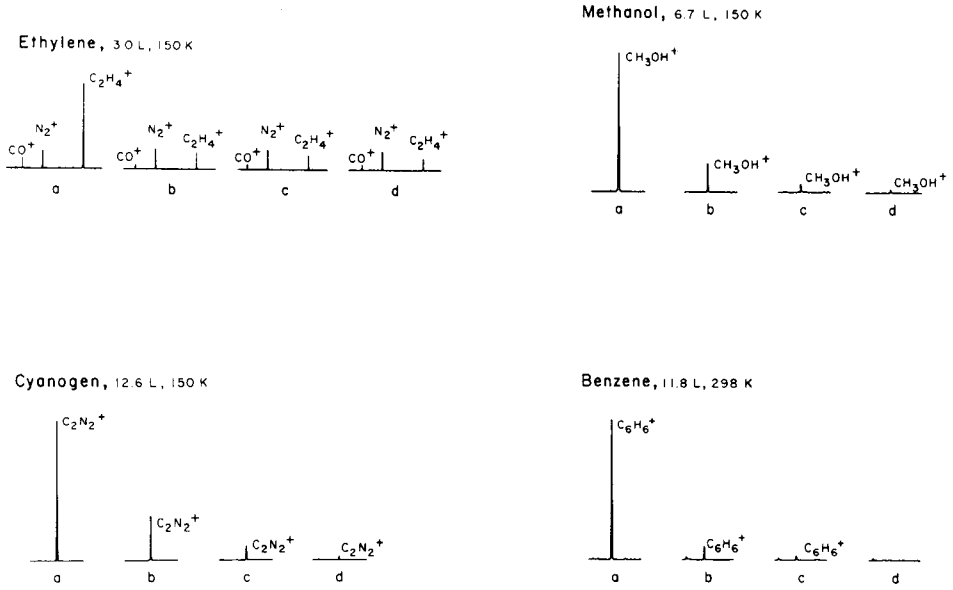

Fig. 3. Fourier-transform mass spectra for various adsorbates on a platinum crystal. In each case, (a) shows the result of the first laser pulse, (b) is taken after a second laser pulse of the same energy applied to the same spot about 1 min later, (c) is after the third laser pulse, and (d) is the background spectrum under the same conditions with the laser off.

Figure 3 shows four mass spectra that were obtained for different adsorbates. There are two important conclusions that can be drawn from these spectra. First, most of the adsorbed molecules are removed by the first laser pulse. Typically, a second laser pulse at the same spot produces a signal that is only 20% as large as the first, and the third laser pulse produces an even smaller signal. These observations are consistent with those reported by Wedler and Ruhmann [10] for CO adsorbed on an Fe (110) surface and with the experiments of Viswanathan et al. [11] with CO on Cu (100). Apparently, during the 1-min delay between laser pulses, the adsorbates do not diffuse across the surface and repopulate the area that was cleaned by the first laser pulse. A second observation is that molecular ions of the adsorbates are the predominant peaks in the Fourier-transform mass spectra. Figure 3 shows only the molecular ion region for each adsorbate, but other experiments performed with broad-band F.t.m.s. detection showed only a few minor peaks that were readily assigned as electron-impact fragments of the adsorbates. In the case of ethylene, these experiments were done at 140 K, and under these conditions ethylene is known to exist as an undissociated, molecular-bonded species on the surface [12]. We observe *m/z* 28.031, $C_2H_4^+$, as the main peak. In s.i.m s. experiments under the same conditions, Creighton and White [12] reported results only for CH_2^+ because C_2 ions from ethylene could not be resolved by their quadrupole mass

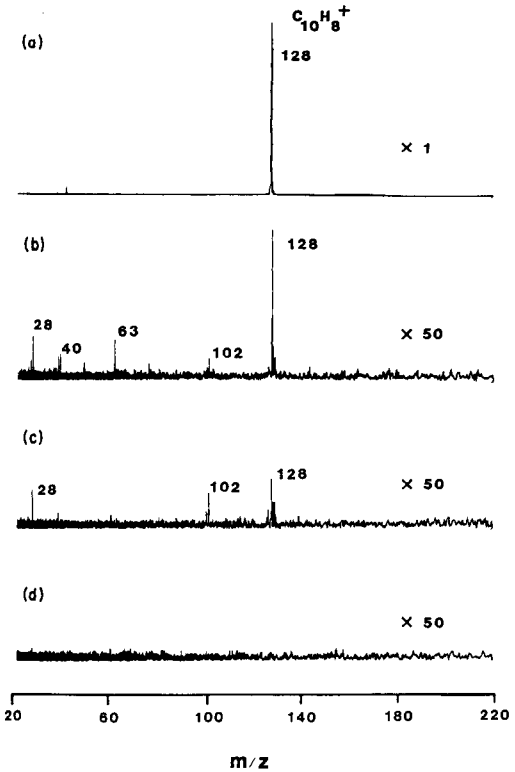

Fig. 4. Fourier-transform mass spectra (broad-band mode) for laser desorption of naphthalene from a Pt crystal. The dose was 4.7 L at 298 K. (a—d) As in Fig. 3. The signal at *m/z* 28 is due to laser-desorbed CO.

spectrometer from possible aluminum (*m/z* 26.981) and silicon (*m/z* 27.976) impurities in the platinum crystal. With F.t.m.s. these ions can be resolved, and Al or Si ions were not observed in the laser-desorption experiments. Benninghoven et al. [13] in an s.i.m.s. study of ethylene on a nickel surface found a surface atom—adsorbate cluster ion, $NiC_2H_4^+$. For benzene on Ni (001), Winograd and Karwacki [14] reported that $NiC_6H_6^+$ forms by cationization of benzene with Ni^+ ions over the surface of the solid.

Ions are produced at the surface during an s.i.m.s. experiment, and many of the secondary ions are produced by rapid ion/molecule reactions (clustering, charge exchange, and displacement) that occur directly above the surface between adsorbates and the substrate ions. In the present experiments with ethylene, methanol and cyanogen, F.t.m.s. signals were not observed after a laser pulse if the electron beam was turned off. It can be concluded that with these adsorbates only neutral molecules are desorbed at the low laser powers used. This may account for the differences between the present results and the s.i.m.s. results. It appears that cationization ions

do not form in these laser-desorption F.t.m.s. experiments because the ions are formed after the desorbed molecules have moved away from the surface and have expanded into the vacuum to a much lower density.

Laser-desorption Fourier-transform mass spectra for naphthalene on the platinum crystal are shown in Fig. 4. These data were acquired in the broad-band detection mode so that for each laser pulse a mass spectrum was recorded for ions in the mass range m/z 20—220. The analog-to-digital converter was operated at 2 MHz for a detection period of 8 ms. The mass resolution is much lower in Fig. 4 than in Fig. 3 because the detection period is shorter. Figure 4(a) shows that the first laser pulse produces a very large molecular ion signal for naphthalene. Figure 4(b) was obtained under the same conditions after a second laser pulse at the same spot, and shows that most of the naphthalene (98%) was removed by the first laser pulse. Several small peaks clustered around m/z 39, 63, and 102 are seen in Fig. 4(b) and (c). These are observed as electron impact fragments of gaseous naphthalene at 30 eV when it is leaked into the vacuum chamber. However, these peaks are probably related to laser-induced decomposition of naphthalene on the crystal because their relative abundance does not parallel that of the naphthalene molecular ion signal. In particular, m/z 102 in Fig. 4(c) may correspond to thermal elimination of C_2H_2 from adsorbed naphthalene.

Temperature-programmed reaction experiments with naphthalene on this crystal have been reported by Dahlgren and Hemminger [3]. They reported that only molecular hydrogen desorbs because naphthalene decomposed as the temperature of the crystal is increased at a rate of 13 K s^{-1}. In contrast, with the rapid temperature jump used in the present experiments (5×10^{10} K s^{-1}) desorption of intact naphthalene molecules occurs faster than the competing thermal decomposition channel.

Multiphoton ionization

It was found that ethylene, methanol and cyanogen adsorbed on platinum are not ionized directly by the laser at 246 nm, but benzene and naphthalene behave differently. For benzene, the laser alone produced an F.t.m.s. ion signal at m/z 78 that was approximately one-tenth the size of that shown in Fig. 3(a). And for naphthalene, it was found that most of the ions are produced by the laser alone; turning off the electron beam produced a negligible decrease in the signal for the molecular ion at m/z 128. The tentative conclusion is that the ions are made by multiphoton ionization of the adsorbates rather than a thermal process. Evidence is as follows. First, multiphoton ionization of background molecules is ruled out by two lines of evidence: (a) ions are not observed when the focal point of the laser beam is moved several centimeters away from the surface of the crystal; and (b) the F.t.m.s. signals in Fig. 4 are very small after three laser pulses at the same spot on the surface. If multiphoton ionization of background naphthalene was occurring, Fig. 3(c) would still show a large signal for m/z 128. Second, ions are not observed in the absence of the electron beam at a

laser wavelength of 350 nm (XeF) when the same pulse energy is directed at the crystal. Because the temperature jumps produced by 248-nm and 350-nm radiation are presumably similar, the production of ions does not appear to be related to the surface temperature of the crystal. Third, the ionization potentials of benzene (9.50 eV) and naphthalene (8.12 eV) are such that two photons at 350 nm are not sufficient for ionization whereas two photons at 248 nm are sufficient. This too points to an electronic process rather than a thermal process for the formation of ions.

Multiphoton ionization of adsorbed molecules has been previously reported. Lubman and Naaman [15] found a greatly enhanced yield of photoelectrons following multiphoton ionization of molecules adsorbed on the electrodes of an ionization cell. Opsal and Reilly [16] and Meek et al. [17] observed an unusually sharp peak for m/z 78 in their t.o.f. mass spectrometer when a laser was focused on the surface of a grid that had been sprayed with benzene. Egorov et al. [18] reported increased detection sensitivity by accumulating the molecules on a cooled substrate and subsequent pulsed desorption and photoionization with a u.v. laser.

More experiments are planned to determine the mechanism of this process. Two simple mechanisms can be imagined. One might involve thermal desorption of the neutral molecules followed by multiphoton ionization as they depart from the surface. All this would occur during the 20-ns period of one laser pulse, during which the adsorbates could move approximately 8 μm away from the surface. Another mechanism might involve resonant absorption to an excited electronic state while the molecules are still adsorbed on the surface. In this case the ejected electron would pass directly to the crystal and an ion would desorb. This second mechanism is unlikely because of rapid quenching of the molecular electronically excited state on the surface.

Sensitivity of F.t.m.s.

The naphthalene molecular ion signal in Fig. 4(a) has a signal-to-noise ratio of about 1600:1. This was produced by just one laser pulse. Assuming a coverage of one monolayer, it is estimated that approximately 3×10^{-4} of a monolayer could be detected.

Another measure of the sensitivity of the laser-desorption F.t.m.s. method is provided by Fig. 5 which shows the F.t.m s. signal for CO^+ as a function of exposure to the crystal to carbon monoxide. For these experiments a single laser pulse having a radius of 0.3 mm was used for each desorption. The laser power was maintained at 37 MW cm^{-2}, and under these conditions about half the CO is removed by the first laser pulse. Figure 5 shows a linear relationship between CO^+ signal and the CO dose. At the low exposures utilized in these experiments, the surface coverage is proportional to the dose and the sticking probability is approximately unity. Using this approximation, the surface coverage can be calculated from the kinetic theory of gases using the relationship that a pressure of 1 atm corresponds to a collision

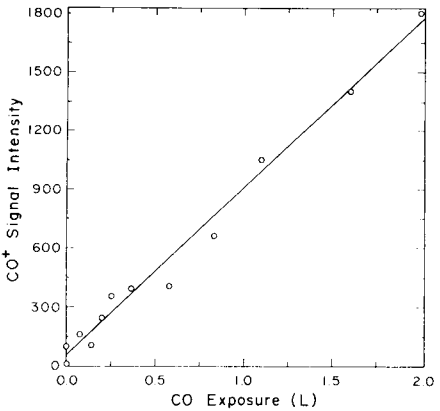

Fig. 5. Dependence of the F.t.m.s. signal for CO^+ on exposure of CO to a clean Pt single crystal at 298 K.

frequency at a surface of 3×10^{23} collisions s^{-1} cm^{-2}. Thus a dose of 0.1 Langmuir (1×10^{-6} Torr for 1 s) corresponds to a coverage of 4×10^{13} molecules cm^{-2}. Furthermore, because saturation coverage (1 monolayer) for carbon monoxide on platinum is approximately 5×10^{14} molecules cm^{-2}, a dose of 0.1 L corresponds to about 0.08 of a monolayer. Extrapolation of the data in Fig. 5 to a signal-to-noise ratio of 2:1 gives a detection limit of 0.002 monolayer for CO on platinum. If these results are normalized to a laser beam having an area of 1 cm^2, the detection limit is 5×10^{-6} monolayer cm^{-2} for one pulse of the laser.

These results for the sensitivity of the laser-desorption F.t.m.s. method are comparable to the value of 0.005 monolayer for carbon monoxide on nickel that has been reported by Hall and DeSantolo [19]. In their work, a quadrupole mass spectrometer was used with an electron-impact source placed 8 cm from the crystal. Laser-desorbed molecules fill the vacuum chamber and are pumped away in 20 ms.

Further improvements in the sensitivity of these experiments are planned. Presently a very simple, low-current electron beam is used, but a larger electron beam, one with greater current and a larger cross-sectional area, would be able to ionize more of the desorbed molecules. About one order of magnitude may be realized in this way before the space charge limit of the F.t.m.s. analyzer cell is reached.

Conclusions

Several experimental innovations have been described in this paper. First, laser desorption of neutral molecules followed by electron impact ionization is shown to be a promising method for detecting molecular adsorbates. By separating the desorption and ionization processes, rapid ionic reactions directly above the surface are avoided, and easily interpretable mass spectra are obtained. Second, multiphoton ionization of aromatic adsorbates by

the u.v. laser is shown to be an efficient process. And third, Fourier-transform mass spectrometry has been shown to have various features which are desirable for these experiments. For example, because F.t.m.s. detects the cyclotron frequency of ions in a homogeneous magnetic field, the mass resolution is high and independent of the spatial distribution and velocity distribution of the ions. Also a complete mass spectrum can be obtained for each laser pulse. Finally, the ion detection sensitivity is high because all ions formed by the electron beam are trapped in the analyzer cell and detected.

We are grateful for support from the Petroleum Research Fund administered by the American Chemical Society, a Faculty Research Grant from the University of California, Irvine, and the National Science Foundation under grant CHE8511999. The array processor used in calculating the Fourier transforms was purchased with funds provided to R.T.M. by the Chevron Research Company. J. C. Hemminger is an Alfred P. Sloan Fellow, 1984—86.

REFERENCES

1 T. E. Madey and J. T. Yates, Jr., Surf. Sci., 63 (1977) 203
2 L. A. Petermann, Prog. Surf. Sci., 3 (1973) 1.
3 D. Dahlgren and J. C. Hemminger, Surf. Sci., 134 (1983) 836.
4 H. Ibach and D. L. Mills, Electron Energy Loss Spectroscopy and Surface Vibrations, Academic Press, New York, 1982.
5 G. Ertl and J. Kuppers, Low Energy Electrons and Surface Chemistry, Weinheim, Verlag Chemie, 1974.
6 B. J. Garrison and N. Winograd, Science, 216 (1982) 805.
7 A. Benninghoven, in A. Benninghoven (Ed.), Ion Formation from Organic Solids, Springer Series in Chemical Physics, Springer-Verlag, New York, 1983, Vol. 25, p. 64.
8 M. G. Sherman, J. R. Kingsley, D. A. Dalgren, J. C. Hemminger and R. T. McIver, Jr., Surf. Sci., 148 (1985) L25.
9 D. E. Gray (Ed.), American Institute of Physics Handbook, McGraw-Hill, San Francisco, 1972, Sect. 6, p. 157.
10 G. Wedler and H. Ruhmann, Surf. Sci., 121 (1982) 464.
11 R. Viswanathan, D. R. Burgess, Jr., P. C. Stair and E. Weitz, J. Vac. Sci. Technol., 20 (1982) 605.
12 J. R. Creighton and J. M. White, Surf. Sci., 129 (1983) 327.
13 A. Benninghoven, P. Beckmann, D. Greifendorf and M. Schemmer, Surf. Sci., 114 (1982) L62.
14 N. Winograd and E. J. Karwacki, Anal. Chem., 55 (1983) 790.
15 D. M. Lubman and R. Naaman, Chem. Phys. Lett., 95 (1983) 325.
16 R. B. Opsal and J. P. Reilly, Chem. Phys. Lett., 99 (1983) 461.
17 J. T. Meek, S. R. Long, R. B. Opsal and J. P. Reilly, Laser Chem., 3 (1983) 19.
18 S. E. Egorov, V. S. Letokhov and A. N. Shibanov, Chem. Phys., 85 (1984) 349.
19 R. B. Hall and A. M. DeSantolo, Surf. Sci., 137 (1984) 421.

Analytica Chimica Acta, 178 (1985) 91—103
Elsevier Science Publishers B.V., Amsterdam — Printed in The Netherlands

LASER DESORPTION/FOURIER-TRANSFORM MASS SPECTROMETRY FOR THE STUDY OF NUCLEOSIDES, OLIGOSACCHARIDES, AND GLYCOSIDES

DAVID A. McCRERY and MICHAEL L. GROSS*
Department of Chemistry, University of Nebraska, Lincoln, NE 68588 (U.S.A.)
(Received 28th March 1985)

SUMMARY

Laser desorption/Fourier-transform mass spectrometry (l.d./F.t.m.s.) has been used to investigate the feasibility of desorbing nucleosides, oligosaccharides, and glycosides into the gas phase. Nucleosides were desorbed as $(M - H)^-$ ions or as $(M + H)^+$ or more readily as alkali metal ion cationized species. Monosaccharides also could be desorbed as $(M - H)^-$ but not di- or tri-saccharides. At higher laser irradiance, very abundant cationized oligosaccharides were observed. This was particularly true when the Nd:YAG laser was operated in a non-Q-switched mode to give a longer lasting laser pulse. Ions of non-reducing sugars cleaved at the glycosidic bond, but those of reducing sugars underwent ring cleavage reactions. Various glycosides including quercitrin, rutin, xanthorhamnin, digoxin, digitoxin, and erythromycin were also successfully desorbed as cationized species by using l.d./F.t.m.s. Digoxin and digitoxin $(M + Na)^+$ ions fragment differently than the $(M + H)^+$ ions, presumably because the sodium ion is primarily affiliated with the sugar moiety whereas H^+ is bound on the steroid portion of the molecule.

This paper describes the utility of laser desorption/Fourier-transform mass spectrometry (l.d./F.t.m.s.) for investigating various biomolecules including saccharides, nucleosides, and glycosides. These molecules tend to exist as neutral species in the solid state, and the most efficient mechanism for vaporization/ionization appears to be thermal desorption and cationization (see below). In the accompanying paper, the precision or reproducibility of l.d./F.t.m.s. is discussed in terms of various desorption mechanisms proposed in the literature.

Laser desorption/mass spectrometry (l.d./m.s.) dates from 1963 [1], and the first application to organic salts was in 1970 [2]. Posthumus et al. [3] demonstrated that high-power lasers could be used to generate molecular ion species for several classes of biomolecules. Reviews of the work published until 1979 [4] and the experimental arrangements currently used [5] have appeared recently.

Lasers, and particularly pulsed lasers, are attractive sources of energy for vaporizing solid molecular samples. They can be viewed as sources for rapid delivery of thermal energy. Fast heating is known to lead to preferential evaporation over thermal degradation [6, 7]. The mass analyzer most often

0003-2670/85/$03.30

used in laser-desorption experiments is the time-of-flight (t.o.f.) mass spectrometer. The t.o.f. instrument can acquire a full mass spectrum for a single laser shot and can be used for elegant microsecond time-resolved experiments [8, 9]. However, its disadvantages are its limited mass resolution (<1000 for l.d./m.s.) and inability to store and manipulate ions.

Fourier-transform mass spectrometry provides an alternative approach [10]. Its inherent multichannel advantage coupled with long term (up to tens of second) ion storage allow a complete mass spectrum to be recorded for each laser pulse. The possibility for study of l.d.-produced ions by using collisional activation or laser photodissociation are other advantages which accrue to long term ion storage. Of additional analytical importance is the extremely high resolving powers of F.t.m.s. [10].

The first demonstration of l.d./F.t.m.s. was made in 1982 [11], and that has been followed by a comparative study of the effectiveness of l.d./F.t.m.s. and fast atom bombardment for determining organic phosphonium salts [12]. In the latter study, the very high mass resolving power of F.t.m.s. in the l.d. mode was documented; however, good high resolution is only possible today in a narrow-mass-band mode to be contrasted with the wide-band measurements reported here. The high mass capabilities of l.d./F.t.m.s. were recently demonstrated convincingly by Wilkins et al. [13] in a study of both synthetic and biologically important polar molecules. These early studies serve as impetus for more systematic investigations such as those presented here and in the following paper.

EXPERIMENTAL

Equipment

Laser-desorption spectra were obtained with a Fourier-transform mass spectrometer constructed in this laboratory and controlled with a Nicolet FTMS-1000 computer and data acquisition system. The magnetic field strength was 1.2 T. The analyzer cell was the conventional cubic design with 2.54-cm dimensions, used for nucleosides, or 5.08-cm dimensions, used for the saccharides and glycosides. Approximately 10 μg of sample in methanol was placed on a copper probe tip (3.3 mm diameter) of a direct insertion probe and the solvent evaporated. The probe tip was placed in the analyzer cell through a 6.35-mm diameter hole at the edge of the cell formed by the transmitter and excitation plates. The laser beam, from a Quanta-Ray DCR-2 Nd:YAG laser, entered the cell along the opposing diagonal striking the sample normal to the surface. The focused beam diameter was ca. 0.5 mm and the power density was in the range of $1—100 \times 10^6$ W cm^{-2}. The wavelength was 1.064 μm and the pulse duration was 8—9 ns in the Q-switched mode.

The current optical arrangement uses an ultraviolet (u.v.)-grade fused silica prism (Esco Products) and the principles of total internal reflection to steer the laser output with 90% transmission. The focusing lens and the optical

window (Esco Products) are also made of u.v.-grade fused silica. The prism was mounted on a tilt-table at 67.5° and affixed to an optical rail with a vertically-adjustable mounting post and rotationally-adjustable base. The lens was in a gimbal mount and was attached (via a linearly-adjustable mounting) to the flange containing the optical window. The mounting was constructed to prevent the lens from rotating. Total transmission through the three optical pieces was 70%. Glass neutral density filters (Schott Optical) were used to attenuate the laser beam.

During the course of the investigation it was discovered that the probe tip could be inserted into the corner of the cell so that it extended down to approximately the radius of the cell. The sensitivity was improved (2—3 times) when the probe tip extended into the cell.

Chemicals

Guanosine, 1-methylguanosine, adenosine, thymidine, uridine, 3-methyluridine, 5-hydroxyuridine, pseudouridine, and cytidine were purchased from Sigma Chemical Co. The N^6,N^6-dimethyladenosine was from P-L Biochemicals (Milwaukee, WI), and the dihydrouridine was from Calbiochem (San Diego, CA). The 2′-*O*-methylguanosine and 2′-*O*-methyluridine were gifts from Dr. G.B. Chheda, Roswall Park Memorial Institute, Buffalo, NY, and the uridine-5-oxyacetic acid was from Dr. S. Nishimura, National Cancer Center Research Institute, Tokyo, Japan. The oligosaccharide erythromycin was from Sigma Chemical Co. The plant glycosides were donated by Professor J. H. Looker (University of Nebraska), and digitoxin and digoxin were from Applied Science (State College, PA).

RESULTS AND DISCUSSION

Nucleosides

The specific need for mass spectrometric techniques in nucleic acid research has been stated with references to oligonucleotides and nucleobases modified by carcinogens [14]. Several desorption techniques have been used successfully to determine oligonucleotides [15—19], their salts [20], and nucleosidic antibiotics [21]. The aim of the present research is to explore the use of l.d./F.t.m.s. as a viable approach for determining nucleosides, the ultimate goal being application to more complex systems. With further development of m.s./m.s. techniques, mixture analysis may also be feasible.

Negative ions. The compounds studied are listed in Table 1, and a summary of the negative-ion spectra for all compounds is in Table 2. Uridine (compound 7) serves as a representative compound to illustrate the general characteristics of negative-ion l.d. mass spectra (see Fig. 1). The appearance of the spectrum is similar to that obtained by using fast atom bombardment (f.a.b.) and a sector mass spectrometer [15]. Normally prominent are ions resulting from deprotonation, $(M - H)^-$, and from cleaving off the sugar moiety. The most abundant ion in almost every case results from cleavage of

TABLE 1

Nucleosides used in this investigation

No.	Compound	R_1	R_2	R_3	
1	Guanosine	H	H	H	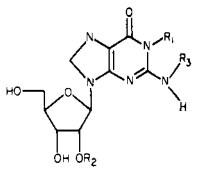
2	1-Methylguanosine	CH_3	H	H	
3	2'-*O*-Methylguanosine	H	CH_3	H	
4	Adenosine	H	H	OH	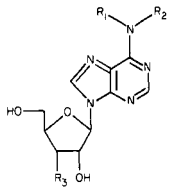
5	N^6,N^6-Dimethyladenosine	CH_3	CH_3	OH	
6	Thymidine	CH_3	H	H	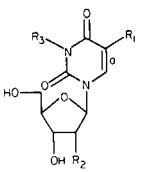
7	Uridine	H	OH	H	
8	Dihydrouridine[a]	H	OH	H	
9	3-Methyluridine	H	OH	CH_3	
10	2'-*O*-Methyluridine	H	OCH_3	H	
11	5-Hydroxyuridine	OH	OH	H	
12	Uridine-5-oxyacetic acid	OCH_2CO_2H	OH	H	
13	Pseudouridine	(see structure)			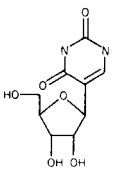
14	Cytidine	(see structure)			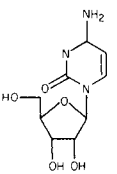

[a]Double bond "a" is reduced.

the base/sugar bond with negative charge retention on the base portion of the molecule. At lower abundances are fragments resulting from further loss of HNCO from $(M - H)^-$ and from cleavage of the base/sugar bond with negative charge retention on the sugar portion of the molecule (see Table 2).

Both purine and pyrimidine nucleosides fragment to lose HNCO from the base moiety. There are two possible cleavages which could occur (see Fig. 1). Using 4-thiouridine and 2-thiouridine, Crow et al. [15] showed that the 2,3-cleavage is more likely (labeled 1 in Fig. 1). This fragmentation is analogous to the retro-Diels-Alder reaction which is characteristic of the electron ionization and fragmentation of pyrimidines [22]. In addition, $(NCO)^-$, m/z 42, appears in all l.d. mass spectra. When the oxygen at position two was replaced with a sulfur, NCS^- was observed [15].

TABLE 2

Summary of major ions observed in negative-ion l.d./F.t. mass spectra[a]

Compound number	$(M-H)^-$	$(M-H-HNCO)^-$	A	$(B-H)^-$	Sugar	Other
1	282(5)	239(3)	—	150(100)	133(20)	—
2	296(20)	256(15)	206(20)	164(100)	133(15)	—
3	296(47)	—	206(28)	150(37)	—	115(100)
4	—	223(6)	176(5)	134(100)	133(18)	—
5	294(5)	251(11)	204(12)	162(100)	—	—
6	241(5)	—	—	125(100)	—	—
7	243(4)	200(6)	153(11)	111(100)	—	—
8	245(16)	—	155(22)	113(70)	—	141(5) 174(45)
9	—	214(11)	167(10)	125(100)	133(6)	—
10	257(56)	214(50)	—	111(100)	—	—
11	259(20)	—	169(16)	127(100)	133(12)	—
12	317(20)	—	—	185(65)	133(13)	141(13) 126(40) 259(24) 167(14)
13	243(13)	—	153(100)	111(10)	133(10)	183(9)
14	242(10)	199(5)	152(20)	110(100)	133(6)	—

[a]Format: mass (relative abundance). B = base.

A common natural modification of nucleosides is methylation at the 2′-*O* position of the sugar moiety to give, for example, 2′-*O*-methylguanosine, **3**, and 2′-*O*-methyluridine, **10**. Another likely modification site is one of the nitrogens of the base portion of the molecule. An immediate indication that methylation is not on the sugar comes from observing the mass of $(B-H)^-$ ions (B = base). The spectra of 1-methylguanosine, **2**, and 3-methyluridine, **9**, clearly have absolute mass shifts of 14 for $(B-H)^-$ when compared to the

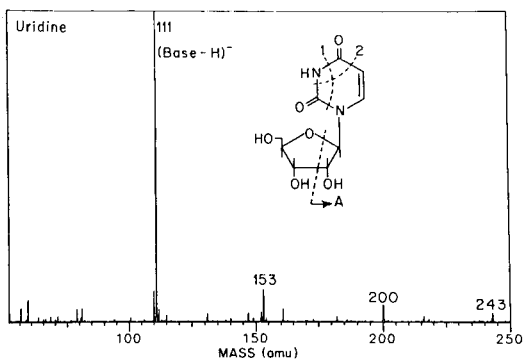

Fig. 1. Negative-ion l.d./F.t.m.s. spectrum of uridine obtained from one shot of the laser. Cleavage A produces *m/z* 153.

corresponding ions from 3 and 10, respectively (see Table 2). Another example is N^6,N^6-dimethyladenosine, 5.

The double bond in uridine and other pyrimidines apparently inhibits fragmentation from the other side of the ring. Dihydrouridine, 8, does not contain this double bond and the loss of CO-NH-CO from $(M - H)^-$ is relatively facile.

All the nucleosides studied here are *N*-nucleosides except for one. Pseudouridine, 13, is an isomer of uridine, 7, the base/sugar bond being a C—C bond instead of a C—N bond (see Table 1 for structures). As can be seen in Table 2, the fragmentation is strongly affected by the greater strength of the C—C bond. For pseudouridine, the base/sugar bond cleavage is not as prominent, the decompositions being dominated by cleavage A. This change also applies to the collisionally-activated decompositions following f.a.b. desorption [15].

Shot-to-shot spectral reproducibility under these experimental conditions was poor (the relative abundances of major ions can vary by as much as ±50%). The high power densities required (ca. 1×10^8 W cm^{-2}) to observe ion signals may contribute to the poor precision. This issue is addressed in the following paper.

Positive ions. If no alkali metal salts were added, cationization of neutral nucleosides was found to depend on the presence of metal salts. Cationized species in the form of $(M + Na)^+$, $(M + K)^+$, and even $(M + Cu)^+$ (a copper probe tip was used) were observed. In addition, $(M + H)^+$ was observed for several species, most notably N^6,N^6-dimethyladenosine. As illustrated in Fig. 2, the base peak in the positive-ion spectra of nucleosides (without added alkali metal salts) generally corresponds to $(BH_2)^+$. The presence of $(M + H)^+$ indicates that more than a simple laser-induced thermal process is occurring at these irradiances [5]. Protonated molecular species have also been observed by Fan et al. [23] who used similar pulsed laser irradiances.

It should be noted that the mass resolution is not particularly impressive because of the use of a wide mass-band detection mode and possibly because

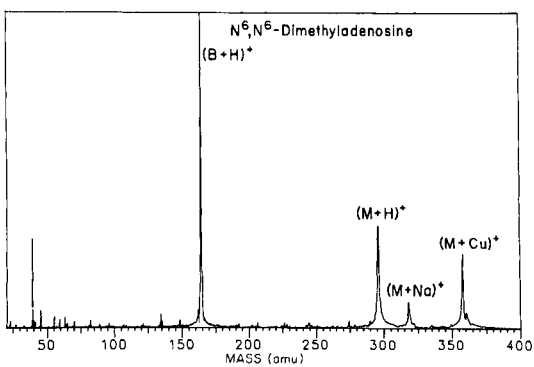

Fig. 2. Positive-ion l.d./F.t.m.s. spectrum of N^6,N^6-dimethyladenosine obtained from one shot of the laser.

of excessive space charge. The threshold for l.d. in terms of laser power is sharp, and it is difficult to control the number of ions. The resolution of other spectra reported in this paper is also limited by these considerations.

Saccharides

Monosaccharides were some of the first organic compounds investigated by using l.d./m.s. Like nucleosides, they exhibit abundant $(M - H)^-$ ions and produce fragment ions resulting from losses of water and CH_2OH groups. The determination of disaccharides, however, is a problem because they do not yield $(M - H)^-$ ions. The most prominent cleavage is at the glycosidic bond and the resulting spectrum resembles that of a monosaccharide. It became apparent that cationization of the parent molecule, probably with an alkali metal ion, is a necessity for the study of oligosaccharides.

When sodium chloride was mixed with a saccharide and the mixture submitted to l.d., the ions observed were due solely to sodium chloride (e.g., Na^+, Na_2Cl^+, etc.) at the irradiances used for the nucleosides. No $(M + Na)^+$ was observed, even at laser irradiances where Na^+ ion production was abundant and Cu^+ ions (from the copper probe tip) were produced. It was discovered that slightly higher power densities were necessary for $(M + Na)^+$ ions to be observed. In fact, at about 3-times the irradiance used for the nucleoside study, $(M + Na)^+$ ions were more abundant than the Na^+ (or K^+) ions (see Fig. 3). In all other reported l.d. spectra of sugars (with and without

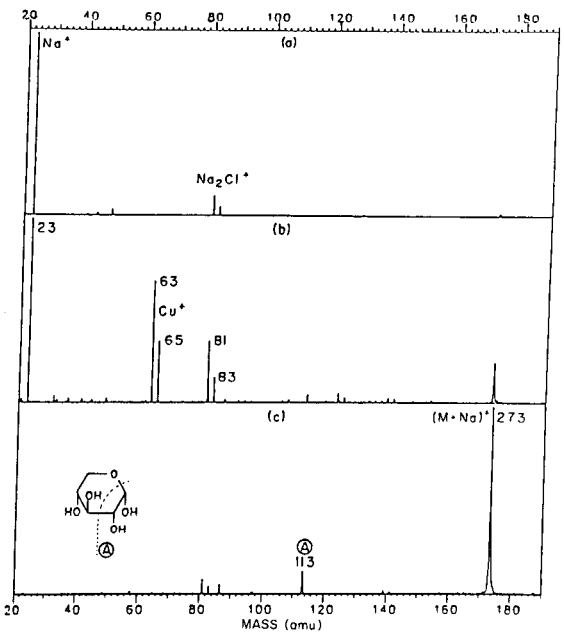

Fig. 3. Positive-ion l.d./F.t.m.s. spectrum of xylose (mixed with NaCl) taken at various irradiances: (a) 1.3×10^8 W cm^{-2}; (b) 2.7×10^8 W cm^{-2}; (c) 3.8×10^8 W cm^{-2} (values are approximate).

added sodium chloride), the Na^+ and K^+ ion abundances are generally 1—2 orders of magnitude greater than the cationized molecular ion and its fragments. The reason for the increased yield of the cationized molecular ion over Na^+ and Na_2Cl^+ is not well understood. At first it was reasoned that it was due to ion/molecule reactions between trapped Na^+ and Na_2Cl^+ ions and desorbed neutral sugar molecules occurring in the "diffuse" gas phase of the analyzer cell. This, however, was later discounted (see following paper). Another explanation is that at high irradiances those Na^+ ions which do not undergo stabilizing ion/molecule reactions are of such high kinetic energy that they are not trapped by the low trapping fields (0.2—1 V was the voltage applied to the trapping electrodes) used in these experiments. Further investigations are required.

Disaccharides, both reducing (e.g., sucrose) and non-reducing (e.g., lactose, maltose, melibiose) sugars, also underwent cationization under these l.d. conditions and showed the same dependence on irradiation. The fragmentations of the two groups of sugars were totally different, however. Whereas the non-reducing sugars were cleaved at the glycosidic bond, the reducing sugars underwent fragmentations of the sugar moiety and lost predominantly CH_2O groups. This behavior was surprising and has not been reported previously. Cationized trisaccharides were also determined with very good signal/-noise ratios (see Fig. 4).

The best operating conditions for shot-to-shot reproducibility of natriated molecular ions were not at these high irradiances, however. It was discovered that abundant gas-phase cationized species were also obtained if the irradiance was decreased while at the same time the time of irradiance was increased. This was accomplished by operating the laser in a Q-switch-off mode. In this mode, the power density of the focused (1-mm diameter) laser beam was reduced to about 1×10^6 W cm^{-2}, but the duration of the non-Q-switched beam was about 150 μs; thus, lower peak powers but higher average powers were delivered in the non-Q-switched mode. The improvement in performance is believed to be due to longer desorption times for the neutral molecules and

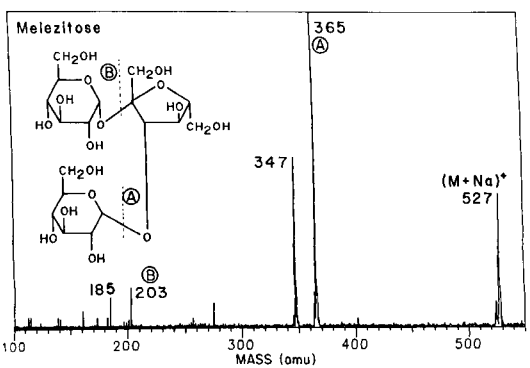

Fig. 4. Positive-ion l.d./F.t.m.s. spectrum of melezitose (mixed with NaCl) obtained from one shot of the laser.

perhaps to less thermal damage to the molecules than that produced at the higher irradiances. It should be noted that natriated molecules were not observed at irradiances of about 1×10^6 W cm^{-2} when the laser was Q-switched (beam duration of about 10 ns). At the lower irradiances, it was also possible to observe sample transient signals for multiple shots on the same spot. At the higher irradiances, generally only the first laser burst at a given spot produced a spectrum of ions which could be easily ascribed to the sample. Later laser shots gave sample, decomposed sample, and substrate ions.

Glycosides

The success with the oligosaccharides prompted the extension to more complex glycosides; Table 3 lists the glycosides used and their structures. Spectra were obtained for 1:1 mixtures of glycoside and sodium chloride dissolved in methanol and laid down on the copper probe tip. Major cleavages are indicated in the Table. The laser was operated in the non-Q-switched mode and the power density was $1-5 \times 10^6$ W cm^{-2}.

Quercitrin, rutin and xanthorhamnin are closely related flavanoid glycosides. Quercitrin (Table 3) is comprised of the flavone quercetin bonded to 6-deoxymannose. The natriated molecular ion, m/z 471, is the most abundant ion in the positive-ion spectrum (see Fig. 5). An ion at $(M + Na - 16)^+$ is also present (m/z 455) apparently from a deoxy homolog. Other substance-specific fragments include m/z 425 (loss of CH_2O possibly from the benzenediol side group) and m/z 367 (cleavage A in Table 3). Also observed are ions $(M - H + 2\ Na)^+$ and $(M + K)^+$.

The negative-ion spectrum of quercitrin is dominated by m/z 301 (from the flavone portion of the molecule) (Fig. 5 and Table 3). A deprotonated $(M - H)^-$ ion is also observed along with a very low abundance $(M - H)^+$ from the deoxy homolog. The ions with masses below m/z 301 can be interpreted to show that the chemical modification to produce the homolog occurs in the flavone group. The ion m/z 285 may be due to the homolog or to cleavage on the other side of the oxygen between the flavone and the sugar.

Rutin is comprised of quercetin bonded to the disaccharide rutinose (see Table 3). Significant substrate-specific positive ions observed were $(M + Na)^+$, m/z 369 (cleavage A), m/z 347 (cleavage B), and m/z 331 (cleavage C). The negative-ion spectrum did not show a deprotonated molecular ion and otherwise looked like that of quercitrin.

Xanthorhamnin is composed of the flavone rhamnetin (7-methylquercitin) bound to the trisaccharide rhamninose (Table 3). The positive-ion spectrum shows that only a few ions are formed, including $(M + Na)^+$ at m/z 793 and a more abundant natriated homolog m/z 807. The most abundant ion is due to cleavage next to the sugar/flavone bond, with Na^+ and charge retention on the sugar. Because there is no corresponding ion for the homolog, the additional methyl group must reside on the flavone portion of the molecule.

TABLE 3

Glycosides used in this investigation

No.	Compound	
1	Quercitrin $C_{21}H_{20}O_{11}$ 448.10 amu	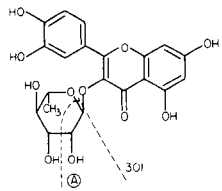
2	Rutin $C_{27}H_{30}O_{16}$ 610.15 amu	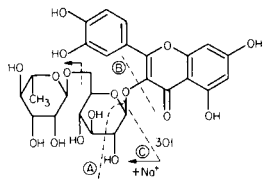
3	Xanthorhamnin $C_{34}H_{42}O_{20}$ 770.23 amu	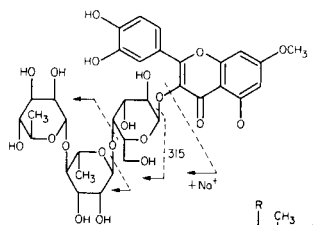
4	Digitoxin (R = H) $C_{41}H_{64}O_{13}$ 764.43 amu	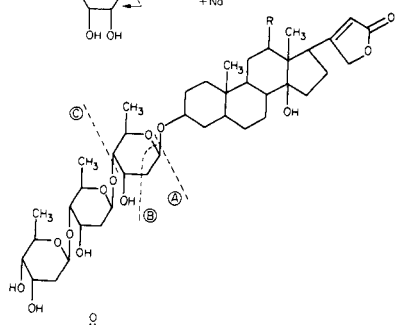
5	Digoxin (R = OH) $C_{41}H_{64}O_{14}$ 780.43 amu	
6	Erythromycin $C_{37}H_{67}NO_{13}$ 733.92 amu	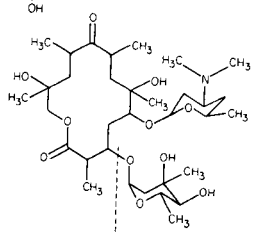

Other cleavages are indicated in Table 3. In the negative-ion mode, ions $(M - H)^-$, $(homolog - H)^-$, and the charged flavone moieties of each, with the ions from xanthorhamnin dominant, were observed. Evidence that the additional methyl group resides on the quercetin-based flavone portion of the molecule is the appearance of the $(flavone - H)^-$ ions at masses 315 and 329 for xanthorhamnin and its homolog, respectively.

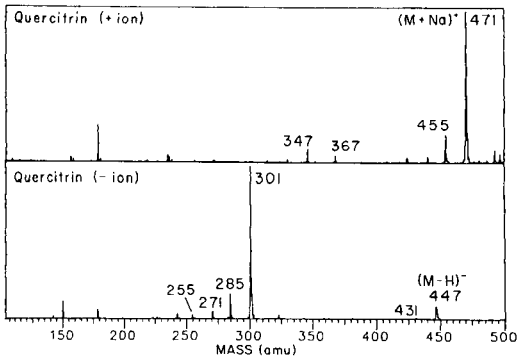

Fig. 5. The l.d./F.t.m.s. spectra of quercitrin obtained from one shot of the laser: (a) positive-ion mode (mixed with NaCl); (b) negative-ion mode.

Higher mass compounds that have been successfully determined are digitoxin (764.4 amu) and digoxin (780.4 amu) (see Table 3), which differ at C_{14} in the steroid portion of the molecule. Both undergo cationization when desorbed in the presence of sodium chloride (see Fig. 6). The most abundant ions are from the saccharide chain, consistent with the fact that the sodium is bonded to the sugar portion of the molecule. This is in striking contrast to protonation which occurs on the steroid portion [24]; i.e., the $(M + H)^+$ fragments to give only steroid-containing ions resulting from the stepwise losses of the sugar moieties. It is suggested that some relatively simple modification of the sample or matrix in desorption ionization may allow tuning of the type of fragmentation desired.

Erythromycin A (see Table 3) is composed of the aglycone erythronolide and sugar moieties desosamine and cladinose. When mixed with sodium chloride and desorbed, the most abundant positive ion is $(M + Na)^+$, followed by $(M + Na - H_2O)^+$, $(M + Na -$ cladinose$)^+$, and $(M + Na -$ cladinose $- H_2O)^+$.

In summary, improved and more routine performance of l.d./F.t.m.s. since

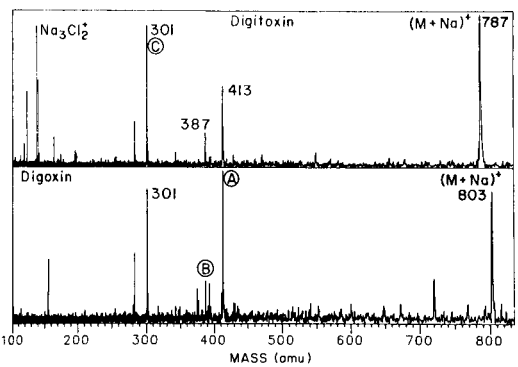

Fig. 6. Positive-ion l.d./F.t.m.s. spectrum of (a) digitoxin and (b) digoxin obtained from one shot of the laser. Both samples were mixed with NaCl.

the initial demonstration has been achieved. Increased sensitivity and the capability to study complex biomolecules have now been demonstrated. These advantages have also been realized by several other groups [13, 25—29]. In our experience, l.d. is less routine than f.a.b. possibly because of the lack of a matrix, resulting in thermal damage and lower reproducibility of mass spectra. However, pulsed l.d. is very compatible with F.t.m.s. The F.t.m.s. features of multichannel advantage, high mass resolution [12], high upper mass limit [13], and collisional activation [12] have been preserved in the l.d./F.t.m.s. combination. Improvements in sample preparation and sample handling should follow from a better understanding of mechanism and lead to more routine utilization of l.d./F.t.m.s.

This work was supported by grants from the National Science Foundation (CHE-8018245) and the National Institutes of Health (GM-30604).

REFERENCES

1 R. E. Honig and J. R. Woolston, Appl. Phys. Lett., 2 (1963) 138.
2 F. J. Vastola, R. O. Mumma and A. J. Prione, Org. Mass Spectrom., 3 (1970) 101.
3 M. A. Posthumus, P. G. Kistemaker, H. L. C. Muezelaar and M. C. Ten Noever de Brauw, Anal. Chem., 50 (1978) 985.
4 R. J. Conzemius and J. M. Capellen, Int. J. Mass Spectrom. Ion Phys., 34 (1980) 197.
5 F. Hillenkamp, in A. Benninghoven (Ed.), Ion Formation from Organic Solids, Springer-Verlag, Berlin, 1983.
6 R. J. Beuler, E. Flanagan, L. J. Greene and L. J. Friedman, J. Am. Chem. Soc., 96 (1974) 3990.
7 G. D. Daves, Jr., Acc. Chem. Res., 12 (1979) 359.
8 J.-C. Tabet and R. J. Cotter, Int. J. Mass Spectrom. Ion Proc., 54 (1983) 151.
9 R. B. van Bremen, M. Snow and R. J. Cotter, Int. J. Mass Spectrom. Ion Phys., 49 (1983) 35.
10 M. L. Gross and D. L. Rempel, Science, 226 (1984) 261.
11 D. A. McCrery, E. B. Ledford, Jr. and M. L. Gross, Anal. Chem., 54 (1982) 1435.
12 D. A. McCrery, D. A. Peake and M. L. Gross, Anal. Chem., 57 (1985) 1181.
13 C. L. Wilkins, D. A. Weil, C. L. C. Yang and C. F. Ijames, Anal. Chem., 47 (1985) 520.
14 M. Linscheid, Trends Anal. Chem., 2 (1983) 32.
15 F. W. Crow, K. B. Tomer, M. L. Gross, J. A. McCloskey and D. E. Bergstrom, Anal. Biochem., 139 (1984) 243.
16 C. J. McNeal, K. K. Ogilvie, N. Y. Theriault and M. J. Nemer, J. Am. Chem. Soc., 104 (1982) 976 and 981.
17 S. D. Negra, Y. M. Ginot, Y. LeBeyec, M. Spiro and P. Vingy, Nucl. Instrum. Methods, 198 (1982) 159.
18 L. Grotjahn, R. Frank and H. Blocher, Nucleic Acids Res., 10 (1982) 4671.
19 R. Beavis, W. Ens, M. J. Nemer, K. K. Ogilvie, K. G. Standing and J. B. Westmore, Int. J. Mass Spectrom. Ion Phys., 46 (1983) 475.
20 G. Sindona, N. Ucella and K. J. Wedawek, J. Chem. Res., (1982) 184.
21 E. Takahashi and T. Beppu, J. Antibiot., 35 (1982) 939.
22 J. A. McCloskey, in P. O. P. Ts'o (Ed.), Basic Principles in Nucleic Acid Chemistry, Academic Press, New York, 1974, Vol. 1, p. 209.
23 T. P. Fan, E. D. Hardin and M. L. Vestal, Anal. Chem., 56 (1984) 1870.
24 F. W. Crow, K. B. Tomer and J. H. Looker, in 32nd Annual Conference on Mass Spectrometry and Allied Topics, San Antonio, TX, 1984, p. 679.

25 R. E. Hein and R. B. Cody, in 31st Annual Conference on Mass Spectrometry and Allied Topics, Boston, MA, 1983, p. 800.
26 A. G. Marshall, T.-C. L. Wang, S. L. Mullen and I. Santos, in 32nd Annual Conference on Mass Spectrometry and Allied Topics, San Antonio, TX, 1984, p. 589.
27 M. L. Coates and C. L. Wilkins, presented at the 33rd Annual Conference on Mass Spectrometry and Allied Topics, San Diego, CA, 1985, Paper TPA6.
28 A. G. Marshall, presented at the 33rd Annual Conference on Mass Spectrometry and Allied Topics, San Diego, CA, 1985, Paper MPH5.
29 C. E. Brown, R. B. Cody and J. A. Kinsinger, presented at the 33rd Annual Conference on Mass Spectrometry and Allied Topics, San Diego, CA, 1985, Paper MPH6.

Analytica Chimica Acta, 178 (1985) 105—116
Elsevier Science Publishers B.V., Amsterdam — Printed in The Netherlands

REPRODUCIBILITY AND EXTENT OF FRAGMENTATION OF LASER-DESORBED IONS
Relation to Mechanism of Desorption

DAVID A. McCRERY and MICHAEL L. GROSS*
Department of Chemistry, University of Nebraska, Lincoln, NE 68588 (U.S.A.)
(Received 28th March 1985)

SUMMARY

The reproducibility of decomposition patterns of laser desorbed propyltriphenylphosphonium ions and $(M + Na)^+$ ions of sucrose is evaluated. These compounds were chosen because they desorb by two different mechanisms commonly ascribed to "thermal" desorption. The phosphonium ions desorb directly whereas sucrose requires cationization with an alkali metal ion. Samples were either pipetted or electrosprayed onto both "smooth" and "rough" copper probe tips. The precision of two ratios of ion abundances are slightly worse for laser desorption of the phosphonium ions than for ions produced by electron ionization of toluene and 2,5-dibromotoluene. Little improvement was obtained by turning to electrospray as a means of depositing the sample. Worse precision was found for ion abundance ratios obtained from the laser desorption of $(M + Na)^+$ of sucrose which had been pipetted onto the probe. The precision was improved by using the electrospray deposition method. Fragmentation of the phosphonium ions was greater if desorption was from a "rough" probe tip whereas less decomposition of the $(M + Na)^+$ of sucrose occurred with desorption from a "rough" tip. The trends in precision and extent of fragmentation are rationalized in terms of mechanisms of ion desorption. Chemical ionization of laser-desorbed neutral species was found to be impossible under the experimental conditions used.

In the preceding paper [1], the applicability of laser desorption/Fourier-transform mass spectrometry (l.d./F.t.m.s.) for determining certain biomolecules such as nucleosides, oligosaccharides, and glycosides was demonstrated. In this paper, the issues of precision or reproducibility of mass spectral patterns produced by l.d. and the relation between precision and mechanism of desorption are addressed.

The deposition of thin films of involatile organic material so that reproducible measurements are assured is a difficult task. This is particularly true for techniques which may exhibit a sensitivity to sample preparation or sample surface, such as in mass spectrometry where field desorption [2], ^{252}Cf-plasma desorption [3], ion bombardment [4], and laser desorption [5] are used for sample volatilization and ionization. Various techniques have been used for sample deposition including solvent evaporation, high-temperature vacuum evaporation, and electrospraying.

In previous studies of pulsed-laser desorption F.t.m.s. in this laboratory,

0003-2670/85/$03.30

laser shot-to-shot spectral reproducibility, measured by comparing the ratio of the abundances of a fragment ion and its parent, ranged from 20—30% to >60% depending on the nature of the sample and on sample preparation. The spectra were least reproducible when solutions of sample concentrations were high or when cationization of neutral compounds was required to observe positive ions. In the work reported here, laser shot-to-shot spectral reproducibility was investigated systematically by measuring ion abundance ratios after application of solutions of low sample concentration. Comparisons were made between two methods of sample deposition (pipetting with solvent evaporation and electrospraying). In addition, experiments were conducted for two compounds from which gas-phase ions were prepared by two different means (direct desorption of ions from the crystal lattice and cationization of a neutral molecule). The influences of two types of substrate surfaces were investigated also.

Precision of mass spectra of laser-desorbed ions may be influenced by the mechanism of the desorption processes. Three mechanisms have been proposed. Two of the mechanisms for desorption of ions are referred to as "thermal" because the results are consistent with classical, non-laser radiative heating. Direct thermal evaporation of ions from the solid states applies to l.d. of quaternary ammonium salts, for example [6—8]. Thermal evaporation of neutral molecules such as saccharides accompanied by cationization with alkali metal ions may be a second "thermal" mechanism [6, 9—11]. A wide variety of evidence can be cited in support of the "thermal" description [4, 9, 12—17]. A third mechanism involves a collective, non-equilibrium process occurring in the condensed phase [18]. This is the process which is characteristic of laser microprobes which use highly focused laser beams and thin layers of sample [18—22]. It is possible that more than one mechanism may operate concurrently, given the thermal gradient starting from the center of the laser spot and moving outward [21].

EXPERIMENTAL

Equipment

An electrospray apparatus was built similar to that described by McNeal et al. [23]. The electrodes consisted of a syringe needle, the probe tip having the surface to be covered, and an aluminum "ground plate" that surrounded the probe tip. A Hamilton 701RN 10-μl syringe was fitted with a removable, 26-gauge side port (style 5) needle and was held vertically within an aluminum plate. The plate was attached through a 50-MΩ current limiting resistor to the positive terminal of a home-built high-voltage power supply. The 0.33-cm diameter probe tip to be loaded was mounted on a grounded aluminum plate and was placed through a hole of a second grounded plate, thus providing a larger ground plane for the counter electrode. While this decreased the sample transfer efficiency (the area of the probe tip was approximately 6% of the total area covered by the sprayed

sample), it greatly improved the quality of the spray and led to a more uniform coating on the probe surface. The apparatus was enclosed in a bakelite box with a Lucite window to minimize turbulence which may disturb the spray. The positions of both electrodes could be adjusted from outside the box via insulated mechanical feedthroughs.

The solution to be electrosprayed was loaded into the syringe such that solution remained in the needle and then the syringe was placed in the electrospray apparatus with the plunger removed. As noted by Murphy et al. [24], it was important to avoid air gaps in the liquid column because the electrospray event became irreproducible when the gaps reached the needle tip.

A drop of sample solution would form readily on the needle tip and large droplets often emerged prior to the establishment of a stable current when the voltage (5 kV) was applied. Therefore, the probe tip was initially positioned to one side of the needle, exposing the needle to the ground plate surrounding the tip. After the high-voltage supply had been turned on and the spray had stabilized onto the ground plate, the probe tip was brought into position under the needle (11 mm below). When the desired amount of material was sprayed (monitored by observing the miniscus in the syringe), the probe tip was again moved to one side and the voltage supply turned off. Large droplets and erratic deposition also occurred at this time if there was sample remaining in the syringe.

Flow rate affected the performance of the electrospray; large flow rates sometimes led to large droplets and erratic currents. The solution was delivered in 3-μl aliquots (15 μl total), between syringe markings 4 and 1. This allowed sample time to establish a steady electrospray and to move the probe tip in and out of position. Time of delivery for the 3-μl aliquot was roughly 47 s.

For manual application, the sample solution was pipetted onto the probe tip in 3-μl aliquots by using a micropipet. In these studies, 12 μl of solution containing 1 $\mu g\ \mu l^{-1}$ of sample was applied.

Laser-desorption spectra were obtained with a Fourier-transform mass spectrometer constructed in this laboratory and interfaced to a Quanta-Ray DCR-2 Nd:YAG laser. Both were controlled with a Nicolet FTMS-1000 computer and data acquisition system [1]. The magnetic field strength was 1.2 T. The analyzer cell was the conventional cubic design with 5.08-cm dimensions. The surface of the copper probe tip was either sanded with polishing paper (3 μm) to produce a "smooth" surface or etched in nitric acid to produce a "rough" probe surface. The "smooth" surface of the probe tip was not a highly polished surface, and many surface scratches were visible. It was, however, much smoother than the etched surface.

Methods

Reagents used in these studies were 2,5-dibromotoluene, n-propyltri-

phenylphosphonium bromide (Aldrich Chemical Co.), sucrose (grade 1, Sigma Chemical Co.), sodium chloride, toluene, and methanol (reagent grades, Fisher Scientific Co.). Sample solutions were made by dissolving 1 mg of sample (1 mg each of sucrose and sodium chloride) in 1 ml of methanol. Samples were deposited on the probe tip by pipetting and solvent evaporation or by electrospraying (see above).

Phosphonium ion mass spectra were obtained under the following conditions: wavelength, 1.06 μm, beam duration, $\approx$9 ns; focal spot, $\approx$0.5 mm; power density, 1—10 $\times$ 10^7 W cm^{-2}. Sucrose data were obtained under the same conditions except that the beam duration was $\approx$150 μs (non-Q-switched), and power density was 1—5 $\times$ 10^6 W cm^{-2}. Production of (sucrose + Na)$^+$ was enhanced by working in the non-Q-switched mode, presumably because of longer irradiation times and, hence, longer ion and neutral desorption times.

Thymidine was desorbed in the presence of methane or ammonia (chemical ionization reagent gases introduced into the cell to a pressure of 1×10^{-6} Torr) which had been ionized by electron ionization. The electron beam was on for 15 ms at 2.5-μA emission current and a delay time of 100 ms was used to allow production of abundant reagent ions (CH_5^+, $C_2H_5^+$, or NH_4^+). After this delay time, the laser was fired to desorb the thymidine. The cell and vacuum chamber of the mass spectrometer were heated to 80—100°C to inhibit condensation of the thymidine.

RESULTS AND DISCUSSION

Electron ionization spectra

Measurements of the precision of relative abundances of ions obtained with a steady pressure of neutral sample molecules and electron ionization (e.i.) served as "benchmarks" for judging the l.d. results. Toluene and 2,5-dibromotoluene served as convenient compounds for this purpose. Experiments were done under conditions that mimicked l.d. conditions in terms of mass resolution (1000—2000) and absolute ion abundance for the most numerous ion species. Results of these "benchmark" investigations indicated that quite good relative ion-abundance reproducibility should be expected if the masses and the abundances of the ions are similar to one another (see *m/z* 91: *m/z* 92 in Table 1). The relative standard deviations (RSD) of the abundance ratios worsen as the difference in ion abundances or in ion masses widens (see *m/z* 91: *m/z* 93 and *m/z* 89: m/z 169 in Table 1). Also, the RSD is $\approx$8% for ions of similar, but low, abundances (e.g., *m/z* 65: *m/z* 63 in the spectrum of toluene).

Laser-desorption spectra

Laser desorption can be expected to give more sparse spectra than electron ionization and a wide range of relative ion abundances. On the basis of the e.i. results, then, an RSD in the range of 10% for ion-abundance

TABLE 1

Abundance ratios for ions produced by electron ionization of toluene and 2,5-dibromotoluene

Compound	Lines used	Average abundance ratio	RSD[a]
Toluene	*m/z* 91: *m/z* 92	1.8	1.3
	m/z 91: *m/z* 93	15.7	10.0
2,5-Dibromotoluene			
	m/z 89: *m/z* 169	0.37	5.6
	m/z 169: *m/z* 171	0.95	3.4
	m/z 171: *m/z* 250	0.40	3.0

[a]Relative standard deviation (%) for N = 100 measurements.

ratios may be expected in l.d. experiments. This simplistic view disregards any difference in ion production between e.i. and l.d. and how that production may influence detection. Also, ions are formed along an axis in the center of the analyzer cell by using e.i., whereas ions are "injected" from the corner of the cell in our approach to l.d. In addition, it is known that the number of ions in the F.t.m s. analyzer cell can affect the quality of the tuning characteristics of the cell and the transient signal observed. This, in turn, may affect the relative abundances of ion species, although the extent of this effect still requires investigation.

Phosphonium salts

n-Propyltriphenylphosphonium bromide represents a class of compounds for which direct desorption of ions from the crystal lattice occurs (see Fig. 1 for the l.d. mass spectrum) [25]. Relative ion-abundance reproducibility was

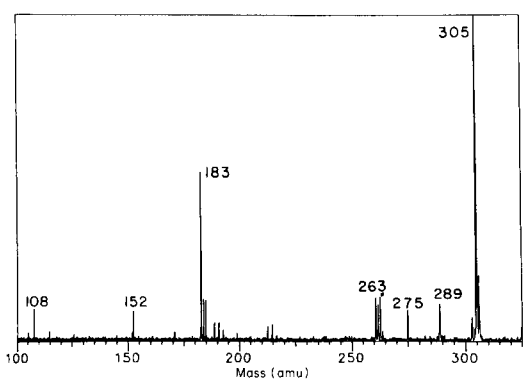

Fig. 1. Laser-desorption Fourier-transform mass spectrum of $(n\text{-}C_3H_7)P(C_6H_5)_3Br$ desorbed with one shot of the laser (positive ion).

compared for laser desorption of samples deposited under four different experimental conditions: pipetting sample material onto (1) "smooth" and (2) "rough" probe surfaces, and electrospraying sample material onto (3) "smooth" and (4) "rough" probe surfaces.

Results from experiments (1) and (2) have RSD values that are slightly greater (see Table 2) than those estimated from the e.i. experiments. The lower RSD values obtained for the ratio *m/z* 263: *m/z* 289 are probably because the relative abundances are quite close. From these results, it would appear that the nature of the probe surface has little effect on spectral reproducibility under these experimental conditions. The substrate surface did, however, affect the amount of fragmentation. Higher relative abundances of fragment ions were generated when using the 'rough" probe tip (compare ratios *m/z* 289: *m/z* 305 in Table 2).

A possible mechanism for phosphonium ion volatilization and fragmentation is

$$\text{n-PrPPh}^+_{3\,(s)} \xrightarrow{h\nu} (\text{n-PrPPh}^+_3)^*_c \rightarrow \text{n-PrPPh}^+_{3\,(g)}\ (m/z\ 305)$$
$$\searrow\ m/z\ 289,\ m/z\ 263,\ \text{etc.}$$

where subscripts s, c, and g represent solid, condensed (selvedge), and diffuse gaseous regions, respectively. The extent of fragmentation should be a function of the internal energy of $(\text{n-PrPPh}^+_3)^*_c$, which in turn should depend on temperature. By increasing the surface roughness, local "hot spots" at surface protrusions lead to a greater population of $(\text{n-PrPPh}^+_3)^*_c$ with higher internal energies than those desorbed from a smooth surface. The higher internal energies lead to more fragment species, as was observed experi-

TABLE 2

Abundance ratios for ions desorbed from n-propyltriphenylphosphonium bromide

Lines used	Average ion abundance ratio	RSD[a]
(1) Pipetted onto "smooth" probe surface		
m/z 263: *m/z* 289	1.11	15
m/z 289: *m/z* 305	0.13	20
(2) Pipetted onto "rough" probe surface		
m/z 263: *m/z* 289	1.11	15
m/z 289: *m/z* 305	0.24	21
(3) Electrosprayed onto "smooth" probe surface		
m/z 263: *m/z* 289	0.89	22
m/z 289: *m/z* 305	0.13	18
(4) Electrosprayed onto "rough" probe surface		
m/z 263: *m/z* 289	1.04	20
m/z 289: *m/z* 305	0.16	29

[a]Relative standard deviation (%) for $N = 15$.

mentally (Table 2). The average amount of fragmentation increases 85% for pipetted samples and 27% for electrospray deposited samples on rough surfaces. The difference in fragmentation enhancement is attributed to the greater sample thicknesses achieved with pipetting because sample transfer is more efficient than with electrospraying (see Experimental). The rate of heating may also have an effect on fragmentation, as will be discussed later.

Reproducibility measurements for electrosprayed samples were just slightly worse, though generally still within the range of 20% RSD. This can be understood if the phosphonium salt precipitates from solution to form a reasonably uniform layer and the uniformity is not improved with electrospraying. By using solutions of higher concentration, the similarity in sample deposits could be observed visually with the aid of a microscope. The precision of the spectra obtained for the electrosprayed sample may, in fact, be a little worse because of inexperience with the technique. The experimental results do indicate, however, that phosphonium salts may prove to be suitable compounds for testing whether improvements have been achieved by adopting different sample treatment and deposition schemes.

Sucrose

Sucrose, to which was added sodium chloride, was used as an example of compounds that require cationization for ions to be observed readily in the positive ion mode (see Fig. 2). As might be expected, the co-desorption of two materials and the requirement that an ion/molecule reaction occur to form a natriated species lead to less reproducible abundance ratios than those of desorbed phosphonium ions (compare data in Tables 2 and 3). This is reflected principally in the ratio of *m/z* 203: *m/z* 365 which is the ratio of the abundance of a fragment species to its parent. The lower precision, however, is expected in part because of the mass difference of the ion abundances ratioed. Ions of widely different masses are subject to vagaries

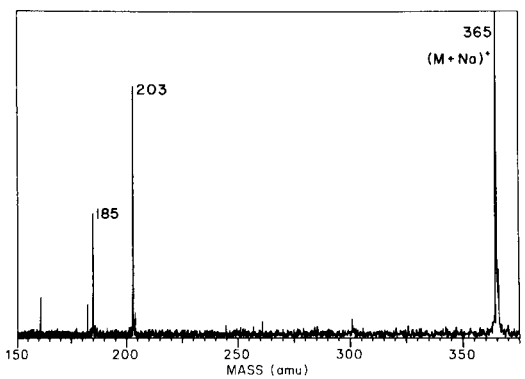

Fig. 2. Laser-desorption Fourier-transform mass spectrum of sucrose mixed with NaCl desorbed with one shot of the laser (positive ion).

TABLE 3

Abundance ratios for ions desorbed from sucrose mixed with NaCl

Lines used	Average ion abundance ratio	RSD[a]
(1) Pipetted onto "smooth" probe surface		
m/z 185: *m/z* 203	0.67	19
m/z 203: *m/z* 365	0.60	45
(2) Pipetted onto "rough" probe surface		
m/z 185: *m/z* 203	0.68	22
m/z 203: *m/z* 365	0.65	38
(3) Electrosprayed onto "smooth" probe surface		
m/z 185: *m/z* 203	0.55	14
m/z 203: *m/z* 365	0.42	31
(4) Electrosprayed onto "rough" probe surface		
m/z 185: *m/z* 203	0.56	25
m/z 203: *m/z* 365	0.22	39

[a] Relative standard deviation (%) for $N = 15$.

of ion excitation, a subject currently under study in this laboratory. One cause of poor precision may be mass-dependent z-excitation. The RSD values and extent of fragmentation are similar for the two surfaces (smooth and rough), indicating that the sample layer is sufficiently thick to negate any strong influence that the substrate texture may have.

Electrospraying may be expected to improve the co-deposition, and hence the co-desorption, of the two compounds. This expectation was realized by electrospraying the sucrose/NaCl mixture onto the smooth probe tip (see Table 3). Reproducibility of the ratio *m/z* 203: *m/z* 365 improved by about 30%. When the etched probe tip was used, however, performance was slightly worse; the RSD values are similar to those obtained when the sample was pipetted. This may be attributed to the influence of the rough probe surface when the sample layer was thin, as a reduction in performance was not observed for thick layers produced by pipetting the sample solution onto the probe tip. The precision is worse presumably because of the wide variety of desorption sites on the rough surface.

An unexpected observation is the reduction in the amount of fragmentation, reflected in *m/z* 203: *m/z* 365 [compare (*3*) and (*4*) in Table 3). This observation is surprising in light of experiments with phosphonium ions wherein fragmentation increased when the rough probe surface was used in place of the smooth surface (see Table 2). The reduction in sucrose fragmentation, however, can be attributed to the same cause as that which led to an increase in phosphonium ion fragmentation (i.e., the development of local "hot spots" at the protrusions on the rough surface) This can be explained in terms of the following mechanism:

$$\text{sucrose}_{(s)} \begin{cases} \nearrow \text{sucrose}_{(c)} \rightarrow (\text{sucrose} + \text{Na})^+_{(c)} \rightarrow (\text{sucrose} + \text{Na})^+_{(g)} \\ \searrow C_6H_{12}O_{6\,(s)} + C_6H_{10}O_{5\,(s)} \rightarrow C_6H_{12}O_{6(c)} + C_6H_{10}O_{5(c)} \end{cases}$$

$$\left.\begin{matrix} C_6H_{12}O_{6(c)} \\ + \\ C_6H_{10}O_{5(c)} \end{matrix}\right\} \xrightarrow{Na^+} \begin{matrix} (C_6H_{12}O_6 + Na)^+_{(c)} \rightarrow (C_6H_{12}O_6 + Na)^+_{(g)} \\ + \qquad\qquad\qquad + \\ (C_6H_{10}O_5 + Na)^+_{(c)} \rightarrow (C_6H_{10}O_5 + Na)^+_{(g)} \end{matrix}$$

The mechanism of sucrose volatilization is, obviously, different from that for phosphonium ions. It was observed in these investigations [1] that desorption of Na^+ preceded natriated sucrose. Thus, the volatilization of neutral sucrose and its decomposition to $C_6H_{12}O_6$ and $C_6H_{10}O_5$ are in competition (the evidence presented here does not permit a distinction to be made between decomposition of sucrose in the solid state or in the selvedge). The volatilization of intact sucrose molecules is favored when the rate of heating is high [10, 11], as is the case when the probe surface is rough. In contrast, phosphonium ions are desorbed at lower temperatures, and decompose in the selvedge or the gas phase. The extent of decomposition depends on their internal energy content which in turn is a function of the temperature of the substrate at the desorption site. Desorption of the phosphonium ions is more nearly a "thermal" process, and this conclusion is consistent with the lower average power needed for desorbing these preformed ions. However, the effects of reactions with the copper substrate cannot be ruled out, but these decompositions seem unlikely.

The pipetted samples formed thick layers and the surface of the sucrose (where molecules will escape to the gas phase) was remote from the substrate surface. The degree of fragmentation for both the smooth and rough probes is essentially the same because the thick sample layer effectively dampens any increase in the rate of heating at the sample surface. The situation is different for the electrosprayed samples because the sample layer is thin and heat transfer from the substrate to the sucrose surface will be much more efficient. This is particularly evident when the rough probe is irradiated. Substrate protrusions will attain higher temperatures at a faster rate, thus enhancing the formation of intact sucrose. As a result, less fragmentation is observed (see Table 3).

Possibility of ion/molecule reactions following laser desorption

In the foregoing discussion of the mechanism for ion production in the laser desorption of sucrose, it was not considered that natriated sucrose could be produced by ion/molecule reactions occurring in the "diffuse" gas-phase between Na^+ and Na_2Cl^+, etc. and neutral sucrose. If diffuse or low-pressure ion/molecule reactions can take place involving neutral sucrose, then the possibility is opened for laser-desorption/chemical-ionization F.t.m.s. These issues are considered in this section.

The cationization of sucrose has been suggested to be a thermal process (under conditions similar to those used here) and it has been demonstrated that this process can occur via gas-phase ion/molecule reactions [9, 15, 26]. Strong evidence for a thermal process is also found in studies in which rather long ion emission times occur following short laser pulses [27, 28]. In addition, neutral species are desorbed for much longer periods of time (hundreds of microseconds) following the laser pulse [29]. In a recent, elegant study, results were presented which point to cationization in a low-temperature plasma just above the substrate surface [30].

When a high-amplitude r.f. burst at the cyclotron frequency of *m/z* 365, $(M + Na)^+$, was applied to the cell milliseconds after the laser pulse, no new formation of $(M + Na)^+$ was observed (60-ms delay between laser pulse and detect event). The natriation of the neutral sucrose molecules must occur, therefore, shortly after laser irradiation, most likely in or near the selvedge where a high cross-section for collisions exist. The natriated molecular ion is not regenerated in the "diffuse" region of the analyzer cell despite the abundant population of Na^+ and Na_2Cl^+ ions trapped in the cell and the apparent high instantaneous pressure produced by laser irradiation.

A complementary experiment involved the ejection of Na^+ and its cluster ions. Double resonance ejection of these ion species milliseconds after the laser burst did not affect $(M + Na)^+$, again indicating that a diffuse c.i. process does not contribute significantly to the population of cationized neutrals observed in the l.d. mass spectrum.

The issue of diffuse c.i. was investigated further by desorbing thymidine in the presence of the reagent gases methane and ammonia. Similar observations were made for both cases, so only results obtained with methane are presented. For methane at a pressure of 1×10^{-6} Torr, a delay of 100 ms after electron ionization is sufficient to reach a steady-state population of reagent ions, CH_5^+ and $C_2H_5^+$. If the vacuum region was sufficiently heated to evaporate thymidine directly from the probe ($\approx$100°C), a c.i. spectrum of thymidine (reaction time about 350 ms) was obtained. The ions which resulted were $(M + H)^+$, *m/z* 243, 100%; *m/z* 225, 18%; *m/z* 207, 14%; *m/z* 155, 10%; *m/z* 127, 63%; *m/z* 117, 14%; *m/z* 99, 6%.

Laser-desorption experiments were done at 80°C to prevent thermal evaporation of thymidine prior to laser irradiation and to inhibit condensation of thymidine neutral species on the analyzer cell. The laser was fired about 115 ms after the electron beam to allow reagent-ion formation, and spectra were taken over a time range of 30—350 ms. There was no evidence for protonated thymidine resulting from a diffuse c.i. process occurring after the laser shot. The most abundant species observed as a result of l.d. was H_3O^+ from protonation of water. In fact, H_3O^+ became the most abundant ion at long times. The presence of H_3O^+ can be explained by invoking longer desorption times for water, thus allowing c.i. to occur. If thymidine neutral species were present in sufficient quantity and for a sufficient period of time for protonation to occur, it is expected that they would be protonated preferentially to water.

Most cationization of nonvolatile sample material probably occurs in the region near the selvedge under the experimental conditions of F t.m.s., despite the sometimes large abundance of Na^+ and Na_2Cl^+ trapped in the analyzer cell. Either few intact neutral molecules are desorbed (unlikely in view of the results of Cotter [28]) or their lifetime is too short (about 100 μs [29]) for ion/molecule reactions to occur. The open nature of the F.t.m.s. analyzer cell contributes to the difficulty of maintaining a sufficiently high average sample pressure for a significant number of ion/molecule reactions to occur. Even when the pumping speed was decreased (to about 10%) to prolong neutral residence time, protonation of thymidine was not observed. Application of l.d./c.i. in F.t.m.s. will require the use of gas-tight cells, such as those previously proposed [31].

This work was supported by grants from the National Science Foundation (CHE-8018245) and the National Institutes of Health (GM-30604).

REFERENCES

1 D. A. McCrery and M. L. Gross, Anal. Chim. Acta, 178 (1985) 91.
2 H. D. Beckey, Principles of Field Ionization and Field Desorption Mass Spectrometry, Pergamon, Oxford, 1977.
3 R. D. Macfarlane and D. F. Torgerson, Science, 191 (1976) 920.
4 A. Benninghoven and W. Sichtermann, Anal. Chem., 50 (1978) 1180.
5 M. A. Posthumus, P. G. Kistemaker, H. L. C. Muezelaar and M. C. Ten Noever de Brauw, Anal. Chem., 50 (1978) 985.
6 R. Stoll and F. W. Röllgen, Org. Mass Spectrom., 16 (1981) 72.
7 U. Schade, R. Stoll and F. W. Röllgen, Org. Mass Spectrom., 16 (1981) 441.
8 R. J. Cotter and A. L. Yergey, J. Am. Chem. Soc., 103 (1981) 1596.
9 G. J. Q. van der Peyl, K. Isa, J. Haverkamp and P. G. Kistemaker, Org. Mass Spectrom., 16 (1981) 416.
10 R. J. Beuler, E. Flanagan, L. J. Greene and L. Friedman, J. Am. Chem. Soc., 96 (1974) 3990.
11 G. D. Daves, Jr., Acc. Chem. Res., 12 (1979) 359.
12 J.-C. Tabet and R. J. Cotter, Int. J. Mass Spectrom. Ion Proc., 54 (1983) 151.
13 F. J. Vastola and A. I. Pirone, Adv. Mass Spectrom., 4 (1968) 35.
14 R. B. van Bremen, M. Snow and R. J. Cotter, Int. J. Mass Spectrom. Ion Phys., 49 (1983) 35.
15 G. J. Q. van der Peyl, J. Haverkamp and P. J. Kistemaker, Int. J. Mass Spectrom. Ion Phys., 42 (1982) 125.
16 F. Heresch, E. R. Schmid and J. F. K. Huber, Anal. Chem., 52 (1980) 1803.
17 R. Stoll and F. W. Röllgen, Org. Mass Spectrom., 14 (1979) 642.
18 B. Jost, B. S. Schueler and F. R. Krueger, Z. Naturforsch. Teil A: 37 (1982) 18.
19 E. Unsold, F. Hillenkamp and R. Nitsche, Analusis, 4 (1976) 115.
20 K.-D. Kupka, F. Hillenkamp and Ch. Schiller, Adv. Mass Spectrom., 8A (1980) 935.
21 D. M. Hercules, R. J. Day, K. Balasanmugan, T. A. Dang and C. P. Li, Anal. Chem., 54 (1982) 280A.
22 B. Lindner and U. Seydel, Anal. Chem., 57 (1985) 895.
23 C. J. McNeal, R. D. Macfarlane and E. L. Thurston, Anal. Chem., 51 (1979) 2036.
24 R. C. Murphy, K. L. Clay and W. R. Matthews, Anal. Chem., 54 (1982) 336.
25 D. A. McCrery, D. A. Peake and M. L. Gross, Anal. Chem., 57 (1985) 1181.

26 R. Stoll and F. W. Röllgen, Z. Naturforsch. Teil A: 37 (1982) 9.
27 D. Zakett, A. E. Schoen and R. G. Cooks, J. Am. Chem. Soc., 103 (1981) 1295.
28 R. J. Cotter, Anal. Chem., 52 (1980) 1767.
29 R. B. van Bremen, M. Snow and R. J. Cotter, Int. J. Mass Spectrom. Ion Phys., 49 (1983) 35.
30 G. J. Q. van der Peyl, W. J. van der Zande and P. G. Kistemaker, Int. J. Mass Spectrom. Ion Proc., 62 (1984) 51.
31 E. B. Ledford, Jr., S. Ghaderi, C. L. Wilkins and M. L. Gross, Adv. Mass Spectrom., 8B (1980) 1707.

Analytica Chimica Acta, 178 (1985) 117—124
Elsevier Science Publishers B.V., Amsterdam — Printed in The Netherlands

COLLISIONAL ACTIVATION BY FOURIER-TRANSFORM MASS SPECTROMETRY
A Study of Target Gas Excitation

D. H. RUSSELL and D. L. BRICKER
Department of Chemistry, Texas A & M University, College Station, TX 77843 (U.S.A.)
(Received 17th May 1985)

SUMMARY

Studies on the charge-transfer reactions between translationally excited polyatomic ions and the neutral target gas used for collisional activation/collision-induced dissociation are described. These studies demonstrate an additional area where Fourier-transform mass spectrometry can be used to probe the fundamentals of ion/neutral interactions, viz., target gas excitation which competes with collision-induced dissociation.

Since the original paper by Cody et al. [1] describing the experimental sequence for performing collision-induced dissociation (CID) with Fourier-transform mass spectrometry (F.t.m.s.), several papers dealing with this subject have appeared in the literature. For example, Cody and Freiser [2] and White and Wilkins [3] have demonstrated high-resolution mass analysis of the CID product ions, and Carlin and Freiser [4] have reported on the increased resolution afforded by using pulsed values for introducing the collision gas. The use of pulsed valves may have particular advantages for studies where sequential CID processes are involved, i.e., m.s./m.s./m.s. or $(MS)^3$ [5]. Nibbering [6] has demonstrated that sequential CID steps, i.e., $(MS/MS)^n$ up to $n = 5$, can be used to examine the occurrence of consecutive dissociation reactions. Such studies may have practical analytical applications which go beyond studies of relatively simple ion/molecule reaction product ions. However, at this point it is unclear how the translational energy imparted to an ion will affect the ion/molecule chemistry and the nature, e.g., internal energy and structure, of the product ions.

The early CID/F.t.m.s. studies were limited to reactions of species with low translational energies (up to ca. 100 eV). The restriction to low-energy CID is due to the fact that as the energy of the ion increases so does its radius of cyclotron orbit. At some point, depending upon the design of the ion cell [1], the ion will strike the walls of the ion cell and be neutralized. Thus, the energy at which CID can be performed is limited by the radius of the ion cell and the magnetic field strength [1]. In addition, the maximum energy that an ion can receive has an m^{-1} dependence. In this laboratory, the design of larger ion cells for performing CID has been studied. These

0003-2670/85/$03.30

larger ion cells made it possible to demonstrate keV-energy CID for charge-stripping on $C_6H_6^+$ (benzene) [7], and at these higher energies it is possible to perform CID on ions which cannot be studied at low collision energies [7].

This report is concerned with additional processes which can be studied at the higher translational energies available with larger ion cells. In particular, the occurrence of charge-transfer reactions between the incident ion and the target gas can be studied quite easily. Such studies are impossible with conventional tandem mass spectrometers; however, a clear understanding of the collisional activation/collision-induced dissociation process, i.e., limits on the CID efficiency and ion-loss mechanisms, is not possible until such information is available.

EXPERIMENTAL

The experimental procedures and instrumentation used for this study were described earlier [7]. The large-radius ion cells used for this work are constructed exactly as the original ion cell supplied by Nicolet Analytical Instruments. The experimental pulse sequences employed for CID were as described by Cody et al. [1] and the necessary software for these experiments was supplied by Nicolet. The samples used for this work were obtained from standard commercial sources and used without extensive purification.

The C_6D_6 (benzene; Merck Isotopes) and the other samples were introduced into the vacuum system by using variable leak valves (Varian Vacuum Division-model 951-5106). The sample pressures were maintained at total pressures of less than 1×10^{-7} Torr. To minimize the charge-transfer reaction between $C_6D_6^+$ and C_6D_6, the pressure of benzene-d_6 was kept below 2×10^{-8} Torr. The $C_6D_6^+$ ions were produced by a short pulse (typically 3—5 ms) of low-energy electrons (11—13 eV), and the $C_6H_6^+$ ions formed during this step were ejected by applying a low amplitude (5 V peak-to-peak) radio-frequency (r.f.) signal corresponding to the cyclotron frequency of the *m/z* 78 ion.

The translationally excited $C_6D_6^+$ ions were generated by applying a low amplitude (10—15 V peak-to-peak) r.f. signal slightly "off-resonance" of *m/z* 84. In our instrument, the cyclotron frequency of *m/z* 84 is ca. 1660 kHz, and the acceleration frequencies for *m/z* 84 were typically 1652—1658 kHz. The translational energy of the *m/z* 84 ion can be varied by changing the duration (t) of the applied r.f. signal (E_{tr} increases as t^2). A typical value for t in these experiments is 1—10 ms, depending on the applied frequency. These instrumental parameters were chosen in order to minimize the time required to accelerate the *m/z* 84 ion, thereby reducing the probability of collisions occurring during the acceleration step.

In the experiments involving argon as the collision gas, the Ar^+ formed by electron impact ionization was ejected by applying an r.f. signal corres-

ponding to the cyclotron frequency of *m/z* 40. The spectra obtained in this manner were compared with the spectra obtained by using ionizing energies below the ionization energy of argon. In all other experiments, any interfering ions were removed by sweeping the r.f. oscillator over the range of masses to be ejected.

RESULTS AND DISCUSSION

The F.t.m.s./CID spectrum of benzene $C_6H_6^+$ ions has been reported previously [7]. In the previous work the translational energy of the $C_6H_6^+$ ions undergoing CID was approximately 1.5—2 keV (ion cell radius of 2.0 cm), and the threshold energy for CID was estimated to be approximately 500 eV. While the relative abundance of the CID product ions did not change at energies above threshold, the CID efficiency increased exponentially as the energy of the incident ion was increased. The increase in the CID efficiency with increasing translational energy is inconsistent with work performed on ion beam instruments which shows that the efficiency of keV-energy CID is much less than that of low energy (10—100 eV) CID [8, 9].

In the CID/F.t.m.s. spectra obtained with a larger-radius ion cell (2.88 cm), an intense signal is observed at *m/z* 40 (Ar^+) when argon is used as the collision gas (Fig. 1), and at the maximum translation energies available with this ion cell (ca. 3.2 keV at *m/z* 78) a signal is observed at *m/z* 20 (Ar^{2+}). The occurrence of a charge-transfer reaction between $C_6H_6^+$ and argon

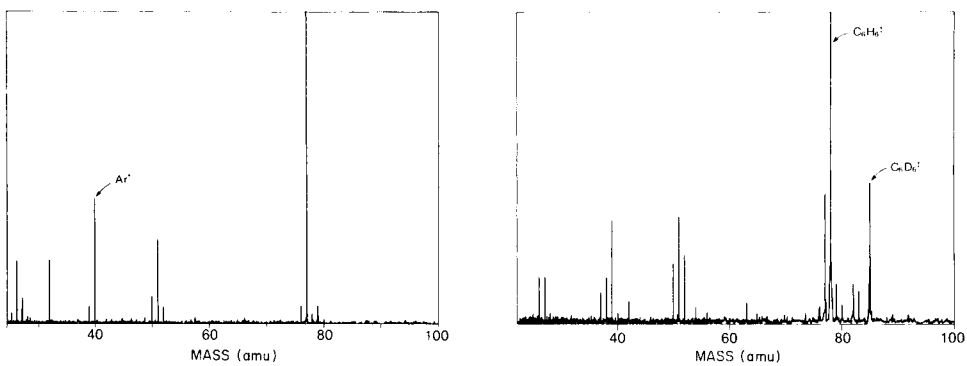

Fig. 1. Collision-induced dissociation F.t.m.s. spectrum of benzene with argon collision gas. The partial pressure of benzene is 2×10^{-8} Torr and the total pressure is 1.2×10^{-7} Torr.

Fig. 2. Spectrum (F.t.m.s.) produced by charge-transfer ionization of C_6H_6 (benzene) with $C_6D_6^+$ (benzene) incident ions. Partial pressure of C_6D_6 is 2×10^{-8} Torr and the total pressure is 1×10^{-7} Torr. Ionizing energy is 12 eV (nominal) and trapping voltage is 2.5 V. The r.f. excitation frequency corresponds to *m/z* 86 and the excitation time was 5 ms at an amplitude of 20 V (peak-to-peak).

$$[C_6H_6^+]^* + Ar \rightarrow C_6H_6 + Ar^+ \quad (1)$$

is rather surprising, i.e., reaction 1 is endothermic by approximately 6 eV (IE ($C_6H_6^+$) = 9.24 eV; IE (Ar) = 15.76 eV [10]), and the formation of Ar^{2+} has an energy requirement of 43.39 eV [10]. One would suspect that during the lifetime of the collision complex, $[C_6H_6^+—Ar]^*$, the charge density would be centered predominantly around the benzene molecule. Although some charge density could develop around the argon atom during the ion/neutral interaction, upon separation of the collision partners the charge density would rapidly develop around the species of lowest ionizing energy. This idea, commonly referred to as the adiabatic condition or Massey's adiabatic criteria [11], is known to be valid under conditions where the time of interaction is long in comparison to the time of the transition. However, in well-defined systems it is known that the cross-section for charge transfer rises exponentially with increasing energy (velocity) of the incident ion [12], i.e., as the energy of the incident ion increases, the cross-section for the non-adiabatic process increases.

The observed charge-transfer reaction between $C_6H_6^+$ and argon (reaction 1) led us to investigate charge-transfer reactions of translationally excited polyatomic ions. The first system studied was benzene C_6H_6/C_6D_6

$$[C_6D_6^+]^* + C_6H_6 \rightarrow C_6D_6 + C_6H_6^+ \quad (2)$$

In this system the resonant charge-transfer reaction (reaction 2) should be the favored process. If $C_6D_6^+$ (benzene) is collisionally activated by a keV-energy collision on C_6H_6 (benzene) neutral species, abundant fragment ions are observed which arise by fragmentation of the $C_6H_6^+$ ions, i.e., fragments which originate from dissociative charge transfer of the target neutral molecules (see Fig. 2). Thus, the charge-transfer reaction between $C_6D_6^+$ and neutral C_6H_6 does not proceed (exclusively) by a resonant charge-transfer reaction, i.e., upon charge transfer, energy in excess of the dissociation threshold is deposited into the newly formed ion. At translational energies in excess of 500 eV, it can be estimated that the cross-section for dissociative ionization of C_6H_6 is 10 times greater than the cross-section for CID of the incident $C_6D_6^+$ ion. In Fig. 2 low abundance signals are observed at *m/z* 42, 54, and 56. These signals correspond to $C_3D_3^+$, $C_4D_3^+$, and $C_4D_4^+$ ions which are formed by dissociative charge transfer between $C_6D_6^+$ and residual C_6D_6 neutral species (see Experimental).

To test the generality of the dissociative charge-transfer reaction, studies were performed on the $C_6D_6^+$ (benzene) and 2,4-hexadiyne and 1,5-hexadiyne systems. Figure 3A contains the spectrum obtained when $C_6D_6^+$ is translationally excited to ca. 1.5 keV and then allowed to react with 2,4-hexadiyne. Similarly, the spectrum contained in Fig. 3B is for the $C_6D_6^+$/1,5-hexadiyne system. In each spectrum the fragment ions arise by fragmentation of the neutral C_6H_6 target gas molecules. In each example, the experimental parameters, e.g., pressure of each neutral species, collision energy, and reaction time are similar. There are two major points regarding each of

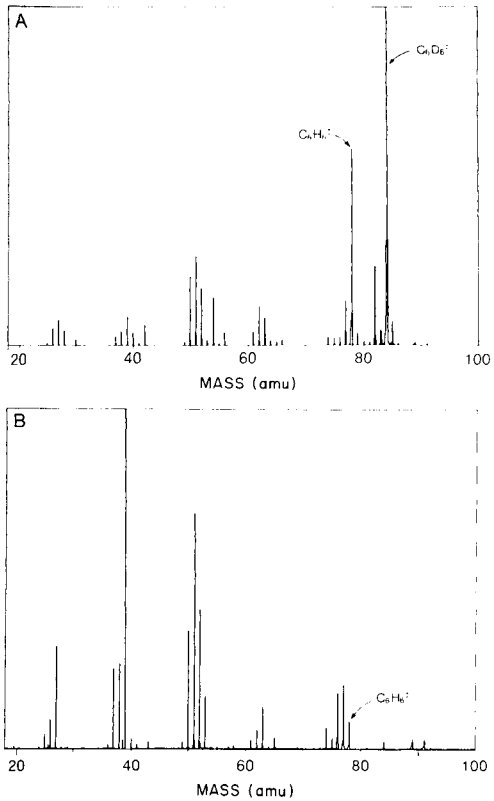

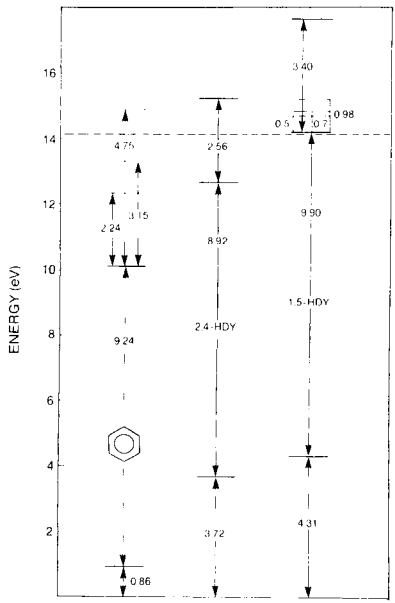

Fig. 3. Spectrum (F.t.m.s.) produced by charge-transfer ionization of C_6H_6 (A, 2,4-hexadiyne; B, 1,5-hexadiyne) with $C_6D_6^+$ incident ions. All other experimental parameters are the same as for Fig. 2.

Fig. 4. Diagram of energy levels for the C_6H_6 systems. The data for this figure were taken from Refs. 10, 13, and 16. The dashed line represents the minimum energy dissociation channel (e.g., loss of H).

the two spectra: (1) the mass spectra are dramatically different, and (2) the cross-sections for charge transfer and dissociative charge transfer are significantly different for each system.

The differences in the dissociative charge-transfer mass spectra for 2,4- and 1,5-hexadiyne are rather surprising. For example, the 70-eV mass spectra of 2,4- and 1,5-hexadiyne are very similar and indistinguishable from the mass spectrum of benzene. Photoion/photoelectron coincidence data reported by Baer et al. [13] do reveal some differences in the fragment ion branching ratios for the different $C_6H_6^+$ ions. For example, Baer et al. reported that the relative abundance for $C_3H_3^+$ from 1,5-hexadiyne increases (relative to $C_4H_4^+$) as the total energy of the dissociating $C_6H_6^+$ increases, whereas the ratio $C_3H_3^+/C_4H_4^+$ for 2,4-hexadiyne is relatively small even at

high internal energies. There are still some open questions regarding the dissociation dynamics of $C_6H_6^+$ ions [14, 15]. In particular, the issue of dissociation from isolated states (either excited electronic states or different structural forms) has not been completely resolved [14, 15]. The data reported here suggest that the 2,4- and 1,5-hexadiyne $C_6H_6^+$ ions formed by dissociative charge transfer do not structurally equilibrate to a common structure prior to dissociation.

The relative cross-sections for dissociative charge transfer for benzene, 2,4-, and 1,5-hexadiyne differ dramatically. Based on measurements of the relative abundance of the $C_6H_6^+$ ions formed by the charge-transfer reaction (measured relative to $C_6D_6^+$), it can be estimated that the reaction cross-sections follow the order benzene > 2,4-hexadiyne > 1,5-hexadiyne. Similarly, the cross-sections for dissociative charge transfer follow the order 1,5-hexadiyne > 2,4-hexadiyne > benzene. The cross-sections for charge transfer and dissociative charge transfer are consistent with the existing models for keV-energy ion/molecule reactions, i.e., the reaction can be described by a two-step model [11]. If it is assumed that the $C_6H_6^+$ ions (products of reaction 2) are formed initially in an excited electronic state, and undergo internal conversion followed by vibrational predissociation, then the observed trend in the reaction cross-sections would be predicted. For example, 1,5-hexadiyne $C_6H_6^+$ has three low-lying excited states within 1 eV of the ground state and a second series of excited states at approximately 3.4 eV above the ground-state ion [16]. In contrast, the 2,4-hexadiyne $C_6H_6^+$ ion manifold is quite simple with states at 2.56 eV and 6.1 eV (15.2 and 18.7 eV) total energy, respectively [17]. Benzene $C_6H_6^+$ has two excited states (2.24 eV and 3.15 eV) which lie below the dissociation threshold (ca. 4 eV) and a third excited state which is approximately 1 eV above the dissociation threshold, e.g., 4.7 eV above the ground-state ion [16]. For convenience, these data are summarized in Fig. 4.

The data for charge transfer and dissociative charge transfer are consistent with the notion that the relative cross-sections for reaction are proportional to the energy defects within the ion manifolds. If charge-transfer ionization of benzene proceeds by an electronic transition, then formation of the low-lying electronic states (those below the dissociation threshold) will have the largest cross-sections. Thus the cross-section for charge transfer (formation of $C_6H_6^+$) will be greater than the cross-section for dissociative charge transfer. Compare the relative abundances of *m/z* 78 and the fragment ions in Fig. 2. Similarly, the energy of the excited state of 2,4-hexadiyne $C_6H_6^+$ is relatively high (ca. 2.5 eV above the ground state) and this will favor non-dissociative charge transfer to produce $C_6H_6^+$; however, the cross-section for dissociative charge transfer will be larger than that for benzene. In contrast, excitation to the low-lying excited states of 1,5-hexadiyne $C_6H_6^+$ (which lie at energies near the dissociation threshold) will have a large cross-section and dissociative charge transfer will be the favored process.

The dissociative charge-transfer mass spectrum of 1,5-hexadiyne is extremely interesting and raises several questions. For example, the abundance of the $C_6H_x^+$ (x = 2—6) is much less than the same fragment ions for benzene and 2,4-hexadiyne. Several years ago, Gross and Aerni [17] reported on the kinetic shift associated with H-loss from 1,5-hexadiyne $C_6H_6^+$ ions, but in their experiment abundant $C_6H_5^+$ ions were observed. Conversely, in the present experiment the dominant fragment ions are the C_3 and C_4 fragment ions. This system is presently being investigated in much greater detail in an attempt to understand these differences.

Conclusions

The results reported above clearly demonstrate the occurrence of target gas excitation for keV-energy collisional activation. That is, the cross-section for charge transfer and dissociative charge transfer are relatively large. In fact, at the collision energies used for these studies the cross-sections for the charge-transfer reactions are much larger (at least a factor of 10 larger) than the cross-section for CID. Although it is generally assumed that target gas excitation for keV-energy collisions is an unimportant process [18], work done in this laboratory on the CID of chlorophyll-*a* $[M + H]^+$ ions suggests that the major fraction of the energy lost by the incident ion upon collisional activation is due to target gas ionization. The general interpretation of the CA/CID studies on chlorophyll-*a* are consistent with the charge transfer reactions studied in the present work. Owing to the fact that target gas excitation could serve as the major limiting factor for structural characterization of large molecules by CID, it is imperative that a more detailed understanding of these processes be developed [19]. Studies of target gas excitation/ionization are not possible with conventional sector-type tandem mass spectrometers. High-energy (keV) ion/molecule reactions can now be studied with F.t.m.s. and the products of charge-transfer reactions can be studied directly. Consequently, new information concerning target gas excitation can be obtained and this information will aid in developing a clearer understanding of keV-energy ion/neutral interactions.

This work was supported by the U.S. Department of Energy, Division of Chemical Sciences, Office of Basic Energy Sciences (DE-AS05-82ER13023). Some of the equipment used was purchased with funds provided by the National Science Foundation (CHE-8418457). A portion of the funds for purchase of the FTMS-1000 system was obtained from the Texas A & M University Center for Energy and Mineral Resources, The Texas Agriculture Experiment Station, and The Office of University Research.

REFERENCES

1 R. B. Cody, R. C. Burnier and B. S. Freiser, Anal. Chem., 54 (1982) 96.
2 R. B. Cody and B. S. Freiser, Anal. Chem., 54 (1982) 1431.

3 R. L. White and C. L. Wilkins, Anal. Chem., 54 (1982) 2211.
4 T. J. Carlin and B. S. Freiser, Anal. Chem., 55 (1983) 571.
5 R. B. Cody, R. C. Burnier, C. J. Cassidy and B. S. Freiser, Anal. Chem., 54 (1982) 2225.
6 N. M. M. Nibbering, Nachr. Chem. Tech., 32 (1984) 1044.
7 D. L. Bricker, T. A. Adams, Jr. and D. H. Russell, Anal. Chem., 55 (1983) 2417.
8 R. A. Yost and C. G. Enke, Anal. Chem., 51 (1979) 1251A.
9 D. J. Douglas, J. Phys. Chem., 86 (1982) 185.
10 H. M. Rosenstock, K. Draxl, B. W. Steiner and J. T. Herron, J. Phys. Chem. Ref. Data, 6, Suppl. 1 (1977).
11 R. G. Cooks, in R. G. Cooks (Ed.), Collision Spectroscopy, Plenum Press, New York, 1978, pp. 383, 294–302.
12 J. B. Hasted, J. Appl. Phys., 30 (1959) 25.
13 T. Baer, G. D. Willett, D. Smith and J. S. Phillips, J. Chem. Phys., 70 (1979) 4076.
14 H. M. Rosenstock, J. Dannacher and J. F. Liebman, Radiat. Phys. Chem., 20 (1982) 7.
15 R. E. Krailler, D. H. Russell, M. F. Jarrold and M. T. Bowers, J. Am. Chem. Soc., 107 (1985) 2436.
16 G. Bieri, F. Burger, E. Heilbronner and J. P. Maier, Helv. Chim. Acta, 60 (1977) 2213.
17 M. L. Gross and R. J. Aerni, J. Am. Chem. Soc., 95 (1973) 7875.
18 G. M. Neumann and P. J. Derrick, Org. Mass Spectrom., 19 (1984) 165.
19 S. A. McLuckey, C. E. D. Ouwerkerk, A. J. H. Boerboom and P. G. Kistemaker, Int. J. Mass Spectrom. Ion Proc., 59 (1984) 85.

Analytica Chimica Acta, 178 (1985) 125—136
Elsevier Science Publishers B.V., Amsterdam — Printed in The Netherlands

INFRARED MULTIPHOTON AND COLLISION-INDUCED DISSOCIATION STUDIES OF SOME GASEOUS ALKYLAMINE IONS

C. H. WATSON, G. BAYKUT, M. A. BATTISTE and J. R. EYLER*
Department of Chemistry, University of Florida, Gainesville, FL 32611 (U.S.A.)
(Received 26th July 1985)

SUMMARY

Collision-induced dissociation and infrared multiphoton dissociation of ions formed in di- and tri-ethylamine, di- and tri-n-propylamine, and di-isopropylamine were investigated by Fourier-transform ion-cyclotron resonance mass spectrometry. Molecular ions of all amines except di-n-propylamine produced similar fragment ions when subjected to either dissociation technique. The initial fragmentation involved C_α—C_β bond cleavage, loss of an alkyl radical, and formation of an immonium ion. Subsequent fragmentations of the immonium ions produced by both dissociation mechanisms involved McLafferty-type rearrangements and loss of alkenes. The molecular ion of di-n-propylamine fragmented by a different mechanism when subjected to infrared irradiation. Protonated molecules of di- and tri-n-propylamine yielded C_3H_6 and an ammonium ion upon infrared multiphoton dissociation, while protonated molecules of the other amines did not dissociate when this technique was applied. In contrast, collision-induced dissociation produced fragmentation for all protonated molecules. Explanation of the different fragmentations observed for the two dissociation techniques is given in terms of a mechanism involving a tight transition state for protonated di- and tri-n-propylamine dissociation.

Infrared multiphoton dissociation (i.r.m.p.d.) of gaseous ions was first observed using an ion-cyclotron resonance (i.c.r.) mass spectrometer and a low-power continuous wave (c.w.) CO_2 laser [1, 2]. A recent review [3] summarizes most experimental results up to 1983. The i.c.r. technique has several advantages for studying i.r.m.p.d. Foremost among these is the ability to trap ions for long periods of time [4] to allow absorption of many infrared photons; often 5—20 photons must be absorbed before dissociation occurs [3]. With the development of Fourier-transform ion-cyclotron resonance (F.t.i.c.r.) [5, 6] mass spectrometry, it is now possible to detect simultaneously an entire mass spectrum, greatly facilitating the study of different photodissociation pathways. Such photodissociation pathways resulting from visible and ultraviolet (u.v.) irradiation have proven quite useful for structure elucidation of gaseous ions [7, 8]. Recent results from this laboratory (to be reported elsewhere) have demonstrated the utility of i.r.m.p.d. for solving gas-phase ionic structure problems, most notably for isomeric differentiation.

Collision-induced dissociation (c.i.d.) is the most widely used mass

0003-2670/85/$03.30

spectrometric technique for ion structure determination [9]. Collisions of ions with (usually) inert target molecules can produce excited ions which lose excess energy by dissociating. While quadrupole and sector-type mass spectrometers have been used for most c.i.d. experiments to date, the technique has recently been developed as a standard analytical tool on F.t.i.c.r. mass spectrometers [10] as well.

In recent studies of some oxygen-containing hydrocarbon systems, primarily esters and ethers, the sole fragment produced by i.r.m.p.d. was always the same as the most intense ion observed following c.i.d. While such behavior would be expected for many ionic systems, it should not hold true in all cases. The relatively slow excitation process in i.r.m.p.d. experiments leads to dissociation via the channel of lowest activation energy. In c.i.d. a range of internal energies is imparted to an ion during the short collision duration, and of the resulting fragment ions, the one of highest intensity need not be obtained via the pathway of lowest activation energy. This is particularly to be expected if substantial rearrangement occurs during the fragmentation (i.e., if the entropy of activation is high). Quite significant differences between c.i.d. and i.r.m.p.d. have been observed for alkylamine ions, and the results of applying the two dissociation techniques to this class of ions are reported here.

The only bond cleavage observed during the earlier i.r.m p.d. investigations involved C—O, and not C—C or C—H bonds. Available thermochemical data showed that these were the weakest bonds in the ions under study. Thus the dissociation of lowest overall endothermicity (corresponding to breaking the weakest bond in the ion) correlated directly with the dissociation pathway with lowest activation energy (observed in i.r.m.p.d. experiments). Extension of the validity of this behavior to nitrogen-containing hydrocarbons was sought, to see if C—N bonds would again cleave preferentially to C—C bonds.

Infrared multiphoton dissociation of triethylamine and benzylamine ions produced by multiphoton ionization has been reported [11, 12], and metastable ions produced by multiphoton ionization have been compared to those obtained using electron impact ionization [13]. One other i.r.m p.d. study [14] of the ethylisopropylammonium ion gave useful mechanistic information about the ethylisopropylamine proton-transfer system. The present work reports i.r.m.p.d. and c.i.d. results for molecular, protonated, and fragment ions of various tri- and di- n-propyl-, isopropyl-, and ethylamines. Results for i.r.m.p.d. and c.i.d. of the various alkylamines are discussed in light of the earlier studies [11—14].

EXPERIMENTAL

Figure 1 shows the experimental apparatus used for i.r.m.p.d. studies. The CO_2 laser beam was reflected from two gold plated glass mirrors through a zinc selenide window into the vacuum system of a modified Nicolet

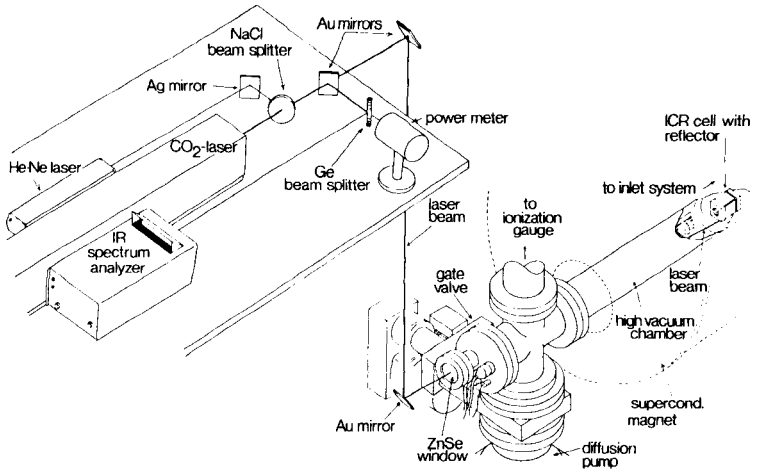

Fig. 1. Laser table and cutaway view of relevant portions of the F.t.i.c.r. instrumentation. The He/Ne laser was used only for alignment of the CO_2 laser and the NaCl beam splitter was removed during ion irradiation.

FT/MS-1000 mass spectrometer. For monitoring laser power and wavelength, a mirror supported by a kinematic mount was inserted into the beam path. This reflected the laser beam to a germanium beam splitter which allowed it to be directed to both a power meter and a spectrum analyzer. For the work reported here, a fixed wavelength (10.61 μm) and high output power (ca. 50 W measured at the laser) were used.

The 2.54-cm cubic F.t.i.c.r. analyzer cell was modified by adding a 15-mm diameter hole covered by wire mesh to one transmitter plate (see Fig. 2). This modification caused no significant deterioration of the ion signal. The actual laser irradiance inside the cell was difficult to measure because mul-

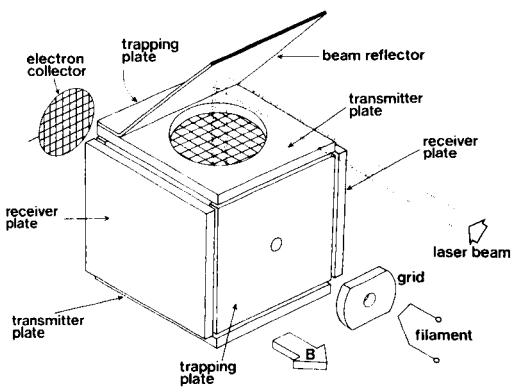

Fig. 2. Cubic i.c.r. cell modified for irradiation of trapped ions. Direction of the magnetic field (B) is as indicated.

tiple internal reflections from the polished stainless steel cell plates are possible. To estimate the laser power entering the cell, the cell mounting flange (including the ZnSe window, see Fig. 1), support rod, and cell were removed from the vacuum chamber. The transmitter plate opposite the one through which the laser beam enters the cell was removed, and the beam was reflected from the gold mirrors, passed through the ZnSe window, reflected from the cell beam reflector (see Fig. 2) and passed through the transmitter plate mesh while outside of the vacuum system. The laser power exiting the (open) analyzer cell under these conditions, identical to those used in actual experimentation, was 20 W (approximately a factor of 2.5 less than the direct output of the laser). Assuming one internal reflection from the transmitter plate which had been removed for the above measurement, and a 1-cm^2 cross-sectional area for the laser beam, an estimate of the actual irradiance to which the ions were subjected is 40 W cm^{-2}. For favorable cases, 100% dissociation was observed, indicating complete overlap of the laser beam and the trapped ion cloud.

A typical i.r.m.p.d. experiment consisted of ion formation by electron impact (50 eV for 5 ms) followed by a reaction delay (0—1000 ms) to build up a significant concentration of protonated molecules via fragment ion/molecule reactions. The reaction delay was not necessary when molecular ion dissociation was being investigated. The ion of interest was next isolated by ejection of all other ions, followed by gated laser irradiation of 200—2000 ms. Immediately after laser irradiation the ions were detected.

Collision-induced dissociation experiments were done similarly to those involving i.r.m.p.d. except that an oscillating voltage, with a frequency equal to the cyclotron frequency of the ion to be accelerated, applied to opposing cell plates (typically for 100 μs) was used instead of laser irradiation to excite the ion to higher translational energies and a collision time of typically 10 ms was then allowed for dissociation. Sample pressure was maintained at ca. 4.0×10^{-6} N m^{-2} (3×10^{-8} Torr), as measured on an ionization gauge. Argon or xenon was added as collision gas until the total pressure was in the $7—13 \times 10^{-5}$ N m^{-2} ($5—10 \times 10^{-7}$ Torr) range. The maximum kinetic energy to which ions can be accelerated in F.t.i.c.r./c.i.d. experiments before they strike the walls of the analyzer cell is given [10] by $KE_{max} = e^2r^2B^2/(2m)$, where e is the charge of an electron, r is the cyclotron radius, B is the magnetic field, and m is the mass of the ion. In the experiments reported here, $B = 3$ T, $r = 1.27$ cm, and thus $KE_{max} = 486$ eV for protonated tripropylamine (m/z 144). To maximize the intensities of observed fragment ions, most c.i.d. experiments were done by exciting parent ions to kinetic energies very near the maximum allowable (400—800 eV depending on ion mass).

All chemicals were obtained commercially and sample purity was determined by electron-impact mass spectrometry. No further sample purification was necessary except for several freeze-pump-thaw cycles to remove non-condensible gases.

RESULTS AND DISCUSSION

Both the i.r.m.p.d. and c.i.d. of molecular ions, protonated molecules, and selected fragment ions of tri-n-propyl-, triethyl-, di-n-propyl-, di-isopropyl-, and diethyl-amine were studied. Results are listed in Table 1. For molecular ions, C—C bond cleavage and production of an immonium ion were observed for both means of dissociation. Protonated molecules, however, showed somewhat different behavior. Their dissociation generally involved C—N bond cleavage with some type of rearrangement when induced by laser irradiation, while c.i.d. proceeded via C—C bond cleavage and production of an immonium ion, or C—N bond cleavage and formation of an alkyl ion. Daughter ions, produced by either i.r.m.p.d. or c.i.d., fragmented further, typically by a mechanism similar to that which led to their formation.

TABLE 1

Results for i.r.m.p.d. and c.i.d. of selected alkylamines[a]

Amine Type of Ion (Mode of Formation)	Ion	I.r.m.p.d. fragments (m/z)	C.i.d. fragments (m/z)
Tripropylamine			
M^+ (e.i.)	$(C_3H_7)_3N^+$ (m/z 143)	114	114, 86, 43
F^+ (i.r.m.p.d./c.i.d.)	$(C_3H_7)_2NCH_2^+$ (m/z 114)	86	86, 43
F^+ (i.r.m.p.d./c.i.d.)	$C_3H_7(CH_3)NCH_2^+$ (m/z 86)	58	58, 44, 43
$(M + 1)^+$ (i.m.r.)	$(C_3H_7)_3NH^+$ (m/z 144)	102	114, 43
F^+ (i.r.m.p.d.)	$(C_3H_7)_2NH_2^+$ (m/z 102)	60	60, 43
Triethylamine			
M^+ (e.i.)	$(C_2H_5)_3N^+$ (m/z 101)	86	86
$(M + 1)^+$ (i.m.r.)	$(C_2H_5)_3NH^+$ (m/z 102)	n.s.f.	74, 58, 29
Di-n-propylamine			
M^+ (e.i.)	$(C_3H_7)_2NH^+$ (m/z 101)	58	72, 58, 30, 29
$(M + 1)^+$ (i.m.r.)	$(C_3H_7)_2NH_2^+$ (m/z 102)	60	60, 43, 41, 30, 27
Di-isopropylamine			
M^+ (e.i.)	$[(CH_3)_2CH]_2NH^+$ (m/z 101)	86	86, 44, 43, 27
$(M + 1)^+$ (i.m.r.)	$[(CH_3)_2CH]_2NH_2^+$ (m/z 102)	n.s.f.	86, 60, 44, 43
Diethylamine			
M^+ (e.i.)	$(C_2H_5)_2NH^+$ (m/z 72)	58	58, 30, 29
$(M + 1)^+$ (i.m.r.)	$(C_2H_5)_2NH_2^+$ (m/z 74)	n.s.f.	58, 30, 29

[a]The following notation is used in Table 1: M^+ = molecular ion; $(M + 1)^+$ = protonated molecule; F^+ = fragment ion; (e.i.) refers to ions formed by electron impact; (i.r.m.p.d./c.i.d.) refers to ions formed by either i.r.m.p.d. or c.i.d.; (i.r.m.p.d.) refers to ions formed solely by i.r.m.p.d.; (i.m.r.) refers to ions formed by ion/molecule reactions; n.s.f. = no significant fragmentation was observed (fragment peak had S:N < 2). The fragment ion of highest intensity produced by c.i.d. is underlined. High-resolution experiments showed that m/z 44 fragment ions produced by c.i.d. were $C_2H_6N^+$, m/z 43 ions were $C_3H_7^+$, m/z 30 CH_4N^+, m/z 29 $C_2H_5^+$, and m/z 27 $C_2H_3^+$.

Detailed discussion of all dissociations is given below. Reactions observed only in i.r.m.p.d. are labeled with a "P" (e.g., P1); reactions observed only in c.i.d. are labeled with a "C" (e.g., C2); and reactions observed in both processes with "P/C" (e.g., P/C3).

Molecular ions

Both i.r.m.p.d. and c.i.d. were observed for the molecular ions produced by electron impact on tri-n-propyl-, triethyl-, di-n-propyl-, di-isopropyl-, and diethyl-amine. In every case, i.r.m.p.d. produced only one fragment, which, except for di-n-propylamine, was also the most intense ion observed following c.i.d. For most cases, production of the primary fragment ion could be explained by C—C bond cleavage, with formation of a stable immonium ion. Further dissociation of major fragments, usually producing yet another immonium ion, was generally observed. However, a different mechanism must be used to explain secondary fragmentations than that which holds for production of the original immonium ion. For the fragment ions, dissociation is postulated to occur via a mechanism involving hydrogen transfer and C—N bond cleavage.

The molecular ion of tripropylamine exhibits C_α—C_β bond cleavage to produce a *m/z* 114 ion (presumably of an immonium structure) during both i.r.m.p.d. and c.i.d.:

$$(C_3H_7)_3N^+ \rightarrow (C_3H_7)_2N{=}CH_2^+ + C_2H_5 \qquad \text{(P/C1)}$$

m/z 143 *m/z* 114

The same subsequent fragmentation of this immonium ion is produced by both c.i.d. and i.r.m.p.d., but dissociation in this case occurs via a mechanism different from that which holds for the molecular ion. The *m/z* 114 ion dissociates to produce a *m/z* 86 ion, which in turn dissociates further to produce a *m/z* 56 ion:

$$(C_3H_7)_2NCH_2^+ \rightarrow (C_3H_7)(CH_3)N{=}CH_2^+ + C_2H_4 \qquad \text{(P/C2)}$$

m/z 114 *m/z* 86

$$(C_3H_7)(CH_3)NCH_2^+ \rightarrow (CH_3)_2N{=}CH_2^+ + C_2H_4 \qquad \text{(P/C3)}$$

m/z 86 *m/z* 58

Reactions P/C2 and P/C3 are both postulated to involve γ-hydrogen transfer followed by ethene expulsion via a McLafferty-type rearrangement [15—17]:

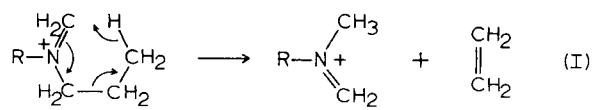

(I)

Similar rearrangements and fragmentations observed in slow metastable decompositions of immonium ions have been discussed by Bowen [18].

Some additional fragments, listed in Table 1, were also produced by c.i.d. of the *m/z* 86 ion.

Molecular ions of triethyl-, diethyl-, and di-isopropyl-amine all fragment by i.r.m.p.d. and c.i.d. through a mechanism similar to that observed for tri-n-propylamine: C—C bond cleavage with formation of alkyl radicals and immonium ions:

$$(C_2H_5)_3N^+ \rightarrow (C_2H_5)_2N{=}CH_2^+ + CH_3 \qquad \text{(P/C4)}$$

m/z 101 *m/z* 86

$$(C_2H_5)_2NH^+ \rightarrow (C_2H_5)HN{=}CH_2^+ + CH_3 \qquad \text{(P/C5)}$$

m/z 73 *m/z* 58

$$[(CH_3)CH]_2NH^+ \rightarrow [(CH_3)_2CH]HN{=}CHCH_3^+ + CH_3 \qquad \text{(P/C6)}$$

m/z 101 *m/z* 86

No further photodissociation of the *m/z* 86 immonium ion produced in reaction P/C4 was observed, consistent with the γ-hydrogen transfer mechanism depicted in I. The activation energy barrier for direct C—N bond cleavage apparently is too high to be overcome during the i.r.m.p.d. process.

Photodissociation of the triethylamine ion using a pulsed CO_2 laser has been reported by Haas and Lifshitz [13]. Fragmentation as shown in reaction P/C4 was seen. Subsequent dissociation of the *m/z* 86 photoproduct ion to form a *m/z* 58 ion, which fragmented further to produce *m/z* 30 and *m/z* 28 ions was seen by those workers. Similar photo-fragment ion dissociation was not observed in this work, probably because the relatively low irradiance of the c.w. CO_2 laser was not sufficient to excite these ions over apparently high barriers to dissociation.

Dissociation of the molecular ion of di-n-propylamine cannot be explained by a mechanism similar to that used for the other molecular ions studied. An ion with *m/z* 58 was produced by both i.r.m.p.d. and c.i.d.:

$$(C_3H_7)_2NH^+ \rightarrow C_3H_8N^+ + C_3H_7 \qquad \text{(P/C7)}$$

m/z 101 *m/z* 58

The *m/z* 58 ion was the only fragment observed following i.r.m.p.d., but it was seen as a minor product following c.i.d., while a *m/z* 72 ion $[(C_3H_7)HN{=}CH_2^+]$ was the most intense fragment, consistent with c.i.d. results for the other molecular ions (C—C bond cleavage and immonium ion formation). No detailed explanation for the different i.r.m.p.d. behavior of the di-n-propylamine molecular ion can be given at this time.

Protonated molecules

Numerous fragment ions were formed during electron impact ionization of the alkylamines studied in this work. Proton-transfer reactions of these fragments with alkylamine neutrals produced protonated molecules. Infrared laser irradiation of these ions resulted in C—N bond cleavage with hydrogen shift and loss of an alkyl group, producing an ammonium ion. In

marked contrast, the major ion observed following c.i.d. was either an immonium ion resulting from C—C bond cleavage and loss of an alkyl radical, or an alkyl ion produced by C—N bond cleavage. This behavior was observed in both tri-n-propylamine and di-n-propylamine.

Tri-n-propylamine is protonated by ion/molecule reactions of the electron impact fragments $C_7H_{16}N^+$ and $C_5H_{12}N^+$:

$$C_7H_{16}N^+ + (C_3H_7)_3N \rightarrow (C_3H_7)_3NH^+ + C_7H_{15}N \quad (1)$$

m/z 114 *m/z* 144

$$C_5H_{12}N^+ + (C_3H_7)_3N \rightarrow (C_3H_7)_3NH^+ + C_5H_{11}N \quad (2)$$

m/z 86 *m/z* 144

When subjected to maximum laser irradiance (ca. 40 W cm^{-2}) the protonated molecular ion fragments to produce a *m/z* 102 ion

$$(C_3H_7)_3NH^+ \rightarrow (C_3H_7)_2NH_2^+ + C_3H_6 \quad (P1)$$

m/z 144 *m/z* 102

which photodissociates to produce a *m/z* 60 ion.

$$(C_3H_7)_2NH_2^+ \rightarrow (C_3H_7)NH_3^+ + C_3H_6 \quad (P2)$$

m/z 102 *m/z* 60

This process is assumed to occur analogously to the reaction P1. A *m/z* 102 ion was also observed in the c.i.d. spectrum as a very minor peak. Experiments at lower collision energies with a triple quadrupole mass spectrometer [19] confirmed this result.

Reaction P1 involves cleavage of a C—N bond and transfer of a hydrogen to the nitrogen atom. Considerable evidence has been massed by earlier workers that this dissociation occurs via a loose complex. Stretching of the C—N bond gives rise to a complex (b) in which an incipient carbonium ion is coordinated to an amine. Slight rearrangement in (b) leads to (c), where an amine and olefin are bound to a common proton. Dissociation of (c) then occurs, and the proton remains with the neutral of highest proton affinity, in this case the amine:

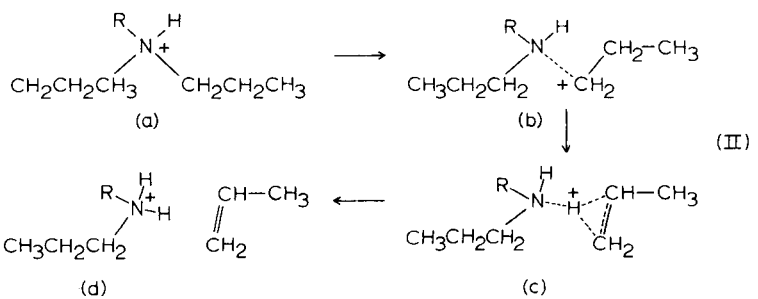

This type of mechanism is discussed extensively by Moylan and Brauman [14] in explaining pulsed CO_2 laser i.r.m.p.d. of protonated ethylisopropylamine, and was also frequently invoked by Bowen [18] to explain metastable decomposition of immonium ions.

Alternatively, a mechanism which involves C—N bond cleavage and transfer of a γ-hydrogen could explain the dissociation observed for protonated tri-n-propylamine:

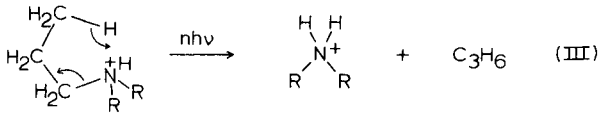

(III)

Further support for this mechanism is provided by experimental results for i.r.m.p.d. of protonated triethylamine and di-isopropylamine. For these ions, which have no available γ-hydrogens, no significant dissociation was observed upon irradiation. However, dissociation of these ions via the proton-bridged loose complex mechanism shown in scheme II should be almost as facile as dissociation of protonated tri-n-propylamine.

The c.i.d. of protonated tri-n-propylamine gave rise to different products than i.r.m.p.d.

$$(C_3H_7)_3NH^+ \rightarrow C_3H_7^+ + (C_3H_7)_2NH \qquad \text{(C1)}$$

m/z 144 *m/z* 43

$$(C_3H_7)_3NH^+ \rightarrow (C_3H_7)_2NCH_2^+ + C_2H_6 \qquad \text{(C2)}$$

m/z 144 *m/z* 114

Reaction C1 involves a simple C—N bond cleavage and requires an overall enthalpy of 368 kJ mol^{-1}. The second reaction, however, is more complicated. A hydrogen migration from N to a β-C is necessary to form the *m/z* 114 immonium ion and an ethane molecule. A possible mechanism is

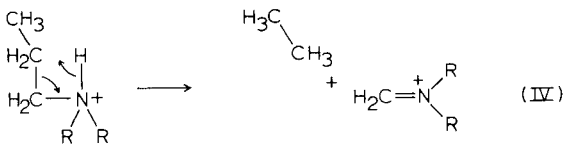

(IV)

Di-n-propylamine is protonated by ion/molecule reactions involving the fragment ions $CH_2NH_2^+$, $C_2H_6N^+$, and $C_3H_7NHCH_2^+$, formed by electron impact:

$$CH_2NH_2^+ + (C_3H_7)_2NH \rightarrow (C_3H_7)_2NH_2^+ + CH_3N \qquad (3)$$

m/z 30 *m/z* 102

$$C_2H_6N^+ + (C_3H_7)_2NH \rightarrow (C_3H_7)_2NH_2^+ + C_2H_5N \qquad (4)$$

m/z 44 *m/z* 102

$$(C_3H_7)NHCH_2^+ + (C_3H_7)_2NH \rightarrow (C_3H_7)_2NH_2^+ + C_3H_7NCH_2 \quad (5)$$
$$m/z\ 72 \qquad\qquad m/z\ 102$$

Protonated di-n-propylamine photodissociates by reaction P2 producing a m/z 60 $(C_3H_7)NH_3^+$ ion. Collision-induced dissociation of protonated di-n-propylamine produces $C_3H_7^+$ (m/z 43) and $C_3H_7NH_3^+$ (m/z 60). Formation of the m/z 60 $C_3H_7NH_3^+$ ion is postulated as taking place via a mechanism identical to the i.r.m.p.d. of this ion shown in reaction P2.

No photodissociation of protonated di-isopropylamine or diethylamine was observed. Because these ions contain no γ-hydrogens, the observed results are more consistent with the mechanism shown in scheme III than that shown in scheme II. More definitive evidence as to the importance of γ-hydrogen transfers would be provided by study of alkylamines labeled with deuterium at that position. Limited deuterium-labeling experiments were done by transferring a deuteron from D_3O^+ to the amines. The deuterium atom was retained on the amine after alkene loss, indicating no hydrogen transfer between the nitrogen and carbon atoms in the protonated amines. As would be expected, this type of experiment gives no information as to whether scheme II or scheme III is operative. The deuterium atom was lost in reaction C2, supporting the validity of scheme IV. Experiments involving synthesis and study of alkylamines with deuterium on the γ-carbon in order to elucidate the proposed mechanisms further are currently underway.

Infrared multiphoton dissociation proceeds only via the fragmentation pathway of lowest activation energy. Collisional and radiative energy loss processes compete with absorption of infrared photons during the several hundred milliseconds of irradiation time usually required when a gated c.w. CO_2 laser is used in this process. This limits the amount of internal energy which can be deposited into an ion to ca. 160—250 kJ mol^{-1}. If the barriers to fragmentation for all pathways are higher than this range, no dissociation is observed. Such appears to be the case for protonated di- and tri-ethylamine and di-isopropylamine. For protonated di- and tri-n-propylamine, C—N bond cleavage with accompanying hydrogen transfer to the nitrogen atom, whether it takes place via scheme II or scheme III, has sufficiently low activation energy that it can be observed by i.r.m.p.d. Results on collision-induced dissociation for these two ions show formation of alkyl ions via direct C—N bond cleavage as the major fragmentation process. These fragmentations have a higher energy, but lower entropy, of activation and should be favored in c.i.d., which can impart much higher internal energies to ions than i.r.m.p.d. [Fragmentation ratios for c.i.d. experiments can vary dramatically with collision energy. The results reported here correspond to energies in the range 400—800 eV. In one series of experiments involving protonated tri-n-propylamine ion, kinetic energies were successively lowered to the 5—20 eV range. At these ion collision energies, the m/z 102 ion, observed exclusively following i.r.m.p.d., was the major c.i.d. fragment, although quite low in intensity when compared to its formation by i.r.m.p.d.

or to the *m/z* 43 ion formed at higher collision energies.] The fact that the only fragment ion produced by infrared irradiation is either not formed (in protonated tri-n-propylamine dissociation) or seen only as a minor fragment (in protonated di-n-propylamine dissociation) during the c.i.d. process lends further support to the fragmentation mechanism shown in scheme III, which involves a tight transition state. In cases where c.i.d. results only were observed (protonated di- and tri-ethylamine and di-isopropylamine) the major fragment ion was often produced by a high-energy process (e.g., 368 kJ mol^{-1} [20, 21] for reaction C1), attesting to the higher range of internal energies deposited in the ions during the c.i.d. process.

Earlier work from these laboratories demonstrated the potential of i.r.m.p.d. for isomeric differentiation. It is interesting to note that both parent and protonated di-n-propylamine and di-isopropylamine ions exhibit substantially different photodissociation behavior (Table 1). As can be seen in Table 1, c.i.d. can be used for isomeric differentiation as well.

In summary, significant differences between i.r.m.p.d. and c.i.d. were seen for protonated amines, but unprotonated molecular ions behaved similarly under both dissociation processes. In contrast to the work on oxygenated compounds where C—O bonds and not C—C bonds were broken, some of the amines in this study preferentially underwent C—C and not C—N bond cleavage. Extension of these studies to other classes of heteroatom-containing compounds is planned further to compare and contrast i.r.m.p.d. and c.i.d.

Purchase of the F.t.i.c.r. mass spectrometer was made possible by funds from the DOD-University Instrumentation Program. This research was supported in part by the Office of Naval Research.

REFERENCES

1 R. L. Woodin, D. S. Bomse and J. L. Beauchamp, J. Am. Chem. Soc., 100 (1978) 3224.
2 D. S. Bomse, R. L. Woodin and J. L. Beauchamp, J. Am. Chem. Soc., 101 (1979) 5503.
3 L. R. Thorne and J. L. Beauchamp, in M. T. Bowers (Ed.), Gas Phase Ion Chemistry, Vol. 3, Academic Press, New York, 1984, p. 41.
4 M. Allemann, Hp. Kellerhals and K.-P. Wanczek, Chem. Phys. Lett., 75 (1980) 328.
5 M. B. Comisarow and A. G. Marshall, Chem. Phys. Lett., 25 (1974) 282.
6 C. L. Johlman, R. L. White and C. L. Wilkins, Mass Spectrom. Rev., 2 (1983) 389.
7 R. C. Dunbar, in M. T. Bowers (Ed.), Gas Phase Ion Chemistry, Academic Press, New York, 1979, p. 181; and in M. A. Almoster-Ferreira (Ed.), Ionic Processes in the Gas Phase, NATO/ASI Series, De Riedel, Dordrecht, The Netherlands, 1984, p. 179.
8 F. M. Griffiths, F. M. Harris and J. H. Beynon, Int. J. Mass Spectrom. Ion Phys., 42 (1982) 77.
9 K. Levsen and H. Schwarz, Mass Spectrom. Rev., 3 (1983) 1251.
10 R. B. Cody and B. S. Freiser, Int. J. Mass Spectrom. Ion Phys., 41 (1982) 199; Anal. Chem., 54 (1982) 2225.
11 Y. Haas, H. Reisler and C. Wittig, J. Chem. Phys., 77 (1982) 5527.

12 J. H. Cantanzarite, Y. Haas, H. Reisler and C. Wittig, J. Chem. Phys., 78 (1983) 5506.
13 Y. Haas and C. Lifshitz, Chem. Phys. Lett., 97 (1983) 467.
14 C. R. Moylan and J. I. Brauman, J. Am. Chem. Soc., 107 (1982) 5527.
15 F. W. McLafferty, Anal. Chem., 31 (1959) 82.
16 F. P. Boer, T. W. Shannon and F. W. McLafferty, J. Am. Chem. Soc., 90 (1968) 7239.
17 J. S. Smith and F. W. McLafferty, Org. Mass Spectrom., 5 (1971) 483.
18 R. D. Bowen, J. Chem. Soc., Perkin Trans. II, (1982) 409; (1980) 1219.
19 J. V. Johnson and R. A. Yost, University of Florida, unpublished work.
20 D. H. Aue and M. T. Bowers, in M. T. Bowers (Ed.), Gas Phase Ion Chemistry, Vol. 2, Academic Press, New York, 1979, p. 1.
21 J. L. Franklin, J. G. Dillard, H. M. Rosenstock, J. T. Herron, K. Draxl and F. H. Field, Ionization Potentials, Appearance Potentials and Heats of Formation of Gaseous Ions, NSRDS-NBS 26, Washington, D.C., 1969.

Analytica Chimica Acta, 178 (1985) 137—158
Elsevier Science Publishers B.V., Amsterdam — Printed in The Netherlands

APPLICATIONS OF LASER IONIZATION/FOURIER-TRANSFORM MASS SPECTROMETRY TO THE STUDY OF METAL IONS AND THEIR CLUSTERS IN THE GAS PHASE

BEN S. FREISER
Department of Chemistry, Purdue University, West Lafayette, IN 47907 (U.S.A.)
(Received 22nd July 1985)

SUMMARY

Recent software and hardware modifications of the Nicolet FTMS-1000 Fourier-transform mass spectrometer have made it possible to conduct research in what can be termed a "complete gas-phase chemical laboratory". Selected ions of interest can be mixed with various reagents and their detailed chemistries monitored through a series of as many as eight reaction sequences. At any point in these sequences, ion structures can be elucidated and fundamental kinetic and thermodynamic parameters of the reactions can be determined. These powerful new techniques have been applied to examine the gas-phase chemistry and photochemistry of metal ions, metal ion clusters, and metal ion complexes, all of which have a bearing on the fundamentals of organometallic chemistry and catalysis.

In addition to the spectacular instrumental developments in mass spectrometry over the past two decades, there has also been a growing emphasis on the chemistry associated with mass spectrometry. The ion source can be regarded as a reaction chamber in which chemical reactions can permit enhanced selectivity above and beyond the instrumentation itself. The beginnings of this more chemical approach can be traced to the landmark paper by Munson and Field [1] in 1966 introducing chemical ionization. Nevertheless, the search for new and useful reagent ions is still in its infancy and will continue to be an area of increasing importance in mass spectrometry.

In this context, it is significant that the precursor instrument to Fourier-transform mass spectrometry (F.t.m.s.), namely the ion-cyclotron resonance (i.c.r.) spectrometer, rose to prominence in the late sixties and seventies as a method of choice for studying ion/molecule reactions. Early on, however, the limitations of i.c.r. spectrometry (i.e., low mass range, low mass resolution, and slow scanning speeds) seemed to present an insurmountable barrier for its serious consideration as an analytical mass spectrometer, and it earned its reputation as a "physical-organic or inorganic chemist's tool". Since these instrumental limitations have been more than overcome with the advent of F.t./i.c.r. or F.t.m.s., the unusual capability and versatility of F.t.m.s. for studying ion/molecule reactions will emerge and be recognized as providing

0003-2670/85/$03.30

important and useful features for analytical applications. In this paper, some highlights from our studies of metal ions, metal ion complexes, and metal ion clusters in the gas phase are presented in the hope of providing a basic understanding and appreciation of both the methodology and the chemistry involved in these studies.

LASER GENERATION OF METAL IONS

Several of the preceding papers in this issue demonstrate and discuss the utility of using laser desorption in conjunction with F.t.m.s. for analyzing organic samples. The application of a pulsed-laser source in this laboratory has proven to be a convenient and powerful method of generating metal ions for subsequent gas-phase studies [2]. As shown schematically in Fig. 1, by focussing the beam of a high-powered pulsed laser onto an untreated metal target, a plume of material is ejected from the surface. This phenomenon, known as laser ionization in the event that ions are produced or laser ablation in general, can be seen visually as a "spark" and is attributed to the rapid heating of the surface [3]. The process is dependent on laser power, with a threshold on the order of 10^7—10^8 W cm^{-2}, but is apparently independent of wavelength and readily occurs, for example, using the fundamental, doubled, tripled, and quadrupled beam of a Nd:YAG laser at 1066 nm, 533 nm, 355 nm and 267 nm, respectively. Although at threshold laser energies the plume consists predominantly of neutral metal atoms, these species rapidly condense on the first surface they strike and are not observed on the time scale of the present experiments as discussed below. By far the most abundant positive ion produced is the monatomic, singly charged metal ion, while the electron is the predominant negatively-charged species generated. Atomic metal anions, M^-, as well as metal cluster ions, M_n^+ and M_n^-, have also been observed using laser ionization [4, 5] but, unfortunately, are not produced in sufficient abundance to be studied by F.t.m.s. Alternative routes for generating atomic metal anions and metal

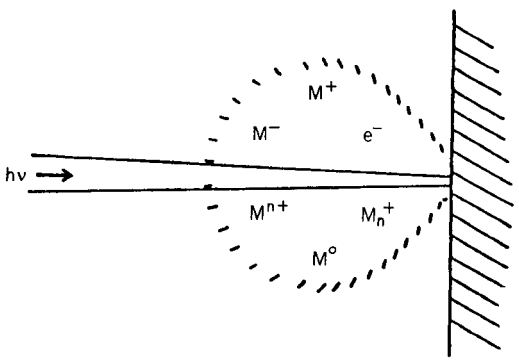

Fig. 1. Schematic depiction of laser ablation.

cluster ions involving either chemical sequences or new target geometries, however, have been developed and will be discussed.

Laser ionization thus provides a convenient method for generating virtually any positive atomic metal ion from the pure metal for subsequent gas-phase chemical studies, and has a number of clear advantages over other commonly used techniques. Electron impact on a volatile metal carbonyl compound such as $Fe(CO)_5$, for example, produces not only Fe^+ but also high abundances of $Fe(CO)_n^+$ with $n = 1—5$ [6, 7]. In addition, if one wants to study the chemistry of Fe^+ with an organic substrate, the neutral carbonyl, which is highly reactive with the ions present, can obscure the chemistry. Finally, a convenient volatile metal complex for a more exotic metal may not be available. Surface ionization of metal atoms, produced by heating metal salts, has also been used quite successfully in ion-beam studies [8—10] but requires a somewhat cumbersome changing of the metal salts to study different metals. In addition, some of the more exotic metal ions are again difficult to produce by this method. In summary, while these other techniques continue to be quite useful, laser ionization can be readily interfaced to F.t.m.s. and offers a "clean" and convenient source of metal ions, the selection of which is rapidly accomplished by simply changing the focus of the laser onto a different target.

Interest in studying metal ions is twofold. First, fundamental studies of metal ions in the gas phase provide kinetic, mechanistic and thermodynamic information of relevance to such areas as organometallic chemistry, atmospheric chemistry, corrosion chemistry, and catalysis. Secondly, metal ions hold promise as selective chemical ionization reagents.

METAL IONS AS SELECTIVE CHEMICAL IONIZATION REAGENTS

The most commonly recognized ionization method in mass spectrometry is electron impact (e.i.) in which a sample is bombarded with electrons (usually at 70 eV). Electron impact on compound AB, for example, produces the fragments A^+ and B^+, and in fortunate cases, the molecular ion AB^+:

$$AB \xrightarrow{e^-} A^+, B^+, AB^+$$

Both the advantage and the disadvantage of electron impact is that it is a universal, non-selective ionization method whereby any sample that can be volatilized can be ionized. While under many circumstances this may be desirable, clearly a complex mixture would produce a complex spectrum. Furthermore, it is often the case that electron impact, especially at 70 eV, imparts enough energy to the parent molecular ion to cause decomposition and, thus, its absence from the spectrum. In contrast, chemical ionization (c.i.) is a two-step process:

$$R \xrightarrow{e^-} R^+; R^+ + AB \rightarrow \text{product ions}$$

The first step involves the generation of a reagent ion, R^+, generally by electron impact on a reagent gas, R. The second and key step is that the reagent ion then undergoes an ion/molecule reaction with the sample, AB, to produce product ions. In this way, the sample is not ionized by electron impact, but rather by a chemical reaction. Careful choice of the reagent ion can in theory, therefore, permit this reaction to be as selective or universal as desired. While several reagent gases have been used for chemical ionization, most of these have come under the category of either proton or charge-transfer reagents [11]. Fourier-transform mass spectrometry offers the potential of a much greater flexibility in the choice of reagent ions which can be used [12, 13]. In particular, the array of metal ions available should exhibit a far wider variety of reactivities which would be particularly useful for selective chemical ionization. A systematic study of metal ions with various classes of organic molecules was therefore undertaken. The goal of this research is to identify trends in reactivity, i.e., reaction mechanisms useful in interpreting the chemical ionization spectra of unknown compounds and to test for the functional group selectivity of the various metal ions. The feasibility of these goals, thus far, has been demonstrated in extensive fundamental studies on Cu^+ with esters and ketones [14], on Fe^+ with ethers [15], ketones [15] and hydrocarbons [16], on Ti^+ [16], Rh^+ [17], V^+, and Y^+ [18] with hydrocarbons, and on Fe^+ and Co^+ with sulfur containing compounds [19].

To exemplify these ideas, some preliminary results on two alkane mixtures and two isomeric esters are presented [20]. Saturated hydrocarbons can undergo random rearrangements under e.i. conditions and thereby lose some structural information in addition to having molecular ion peaks of low intensity [21]. Chemical ionization studies of large alkanes [22] have shown that molecular weight information can be enhanced by using methane as a reagent gas. Figure 2A shows the 70-eV e.i. spectrum of a 1:1 mixture of n-octane and n-decane. The pattern of peaks 14 mass units apart is typical of long hydrocarbon chains and verifies the presence of alkanes in this mixture. Figure 2B—D illustrates three metal ion c.i. spectra for this same mixture. The Fe^+ spectrum indicates the presence of an alkane chain by the orderly sequence of peaks that result from the ability of this ion to cleave C—C bonds [16, 23]. The other metal ions, Nb^+ and Rh^+, are more selective for C—H cleavages followed by dehydrogenation [17, 20]. As a result, both of these spectra produce C_8 and C_{10} ligands bound to the metal as the major products which provide molecular weight information. The C_7 peak in the Rh^+ spectrum comes from the n-decane and is characteristic of long-chain alkanes [17].

Petroleum distillates contain a mixture of alkanes, alkenes, aromatics, and many other types of hydrocarbons in lesser amounts. Identification of the components in fuels, for example, has been a major focus of analytical mass spectrometry. The lighter components of gasoline consist mostly of alkanes and these are easily admitted into the FTMS-1000 instrument for analysis

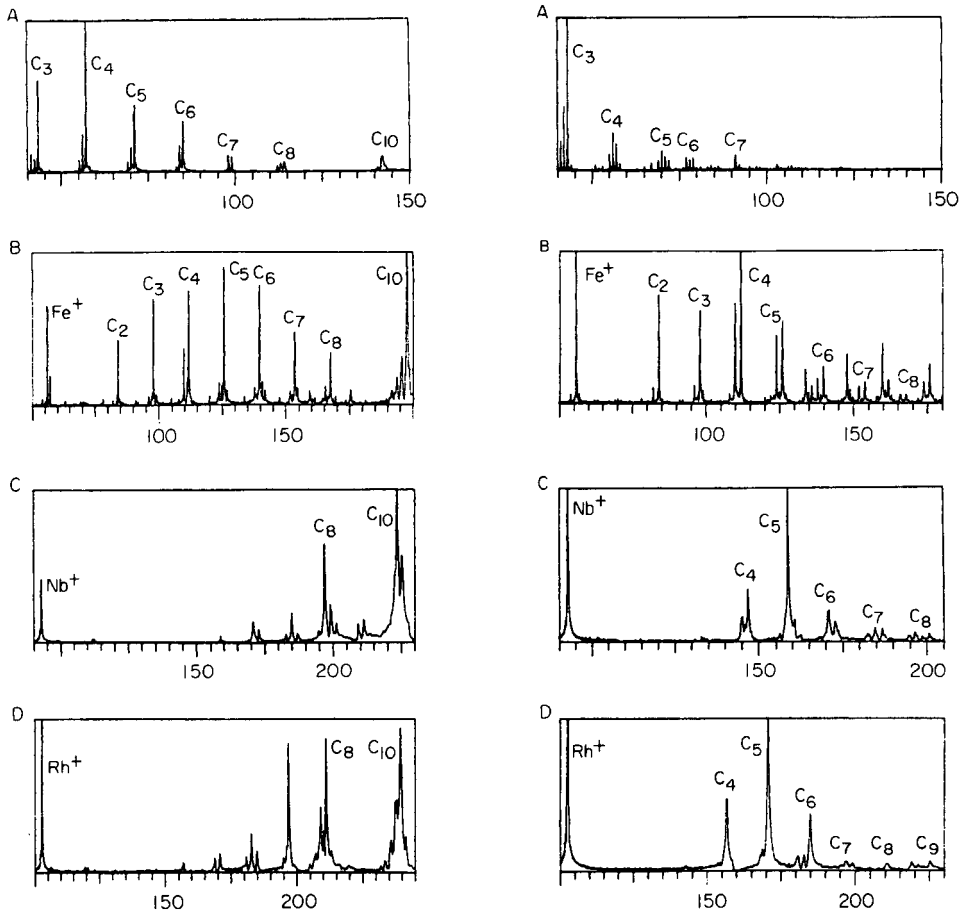

Fig. 2. (A) Electron impact spectrum for a 1:1 mixture of n-octane and n-decane at 1×10^{-7} Torr and 70 eV (no delay, 40 scans). (B) Fe^+ chemical ionization spectrum of the mixture; C_n corresponds to $(Fe + C_n)^+$ (500 ms, 15 scans). (C) Nb^+ chemical ionization spectrum of the mixture; C_n corresponds to $(Nb + C_n)^+$ (500 ms, 15 scans). (D) Rh^+ chemical ionization spectrum of the mixture; C_n corresponds to $(Rh^+ + C_n)^+$ (500 ms, 15 scans). Spectra obtained from [20].

Fig. 3. (A) Electron impact spectrum of a gasoline sample at 1×10^{-7} Torr and 70 eV (no delay, 40 scans). (B) Fe^+ chemical ionization spectrum; C_n corresponds to $(Fe + C_n)^+$ (500 ms, 15 scans). (C) Nb^+ chemical ionization spectrum; C_n corresponds to $(Nb + C_n)^+$ (500 ms, 15 scans). (D) Rh^+ chemical ionization spectrum; C_n corresponds to $(Rh + C_n)^+$ (500 ms, 15 scans). Spectra obtained from [20].

by simply connecting a gasoline sample to one of the leak valves. Figure 3A is the 70-eV e.i. spectrum of a commercial gasoline sample admitted in this manner. The spectrum shows the alkyl series from C_3 through C_7. Some aromatic species are also present as seen from $C_7H_8^+$ (m/z 92) and $C_6H_6^+$ (m/z

78) probably produced from toluene and benzene, respectively, which are commonly found in gasoline. The c.i. spectrum for Fe^+ in Fig. 3B shows a similar pattern as it did with the octane/decane mixture but now stopping at C_9. Also, two peaks out of sequence correspond to toluene and benzene attached to the metal which indicates that Fe^+ is a useful c.i. reagent ion for detecting aromatics. The Nb^+ and Rh^+ spectra are similar both qualitatively and quantitatively (Fig. 3C and D). The major peaks observed, corresponding to attachment of C_4—C_9 ligands, provide a good indication that the sample consists mainly of C_4—C_9 alkane species because neither Nb^+ nor Rh^+ tend to cleave C—C bonds. There is less information, however, about the presence of aromatics. Finally, the complete absence of NbO^+ (*m/z* 109) indicates that no oxygen-containing compounds are present in significant amounts in this mixture [20].

The e.i. spectra of ethyl isovalerate and isoamyl acetate are very distinct from one another as shown in Fig. 4. Yet, the molecular ion of the latter is not observable and renders such a spectrum by itself virtually useless in identifying this compound. The Cu^+ ion was previously shown to be very predictable in its cleavage of esters [14] and this behavior is again demonstrated by the spectra in Fig. 5. These spectra were taken after 1 s to enhance the Cu^+-monomer complex (*m/z* 193) which provides molecular

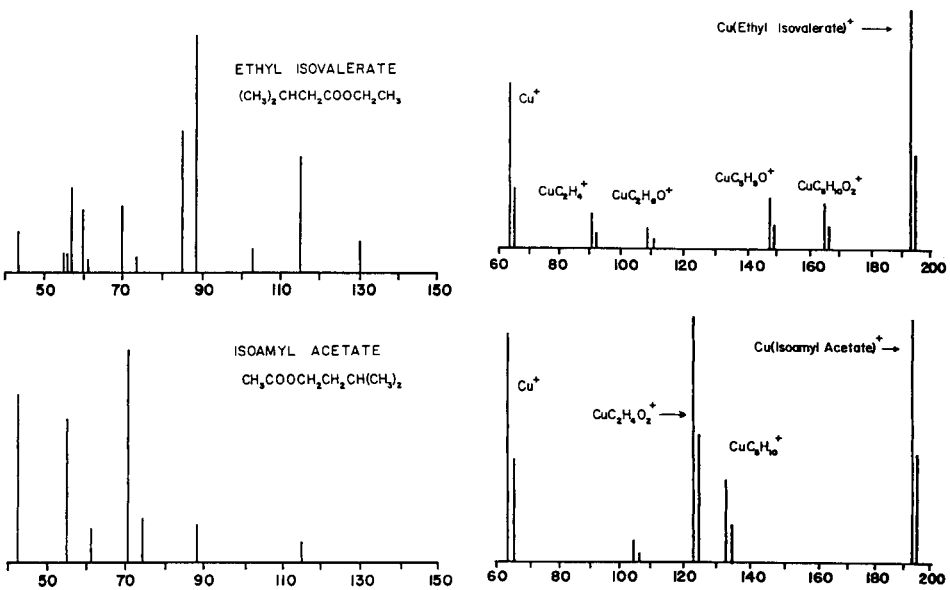

Fig. 4. Electron impact spectra of ethyl isovalerate and isoamyl acetate at 1×10^{-7} Torr with 70-eV electron beam. Spectra obtained from [20].

Fig. 5. Cu^+ chemical ionization spectra of ethyl isovalerate and isoamyl acetate. Pressure 1×10^{-7} Torr, trapping time 1 s. Spectra obtained from [20].

weight information. Overall, the Cu^+ spectra have fewer peaks and can readily be interpreted. For ethyl isovalerate, two different competing cleavage processes are obvious from the loss of 28 and 102 and the loss of 46 and 84. Each pair is complementary because the combined masses add up to the molecular weight of the sample. These losses and the corresponding molecular formulae are summarized as follows:

$$Cu^+ + C_7H_{14}O_2 \longrightarrow \begin{cases} \rightarrow CuC_5H_{10}O_2^+ + C_2H_4 \\ \rightarrow CuC_2H_4^+ + C_5H_{10}O_2 \\ \rightarrow CuC_5H_8O^+ + C_2H_6O \\ \rightarrow CuC_2H_6O^+ + C_5H_8O \end{cases}$$

The isoamyl acetate case is even simpler with only two fragment ions, suggesting a single competitive cleavage process:

$$Cu^+ + C_7H_{14}O_2 \longrightarrow \begin{cases} \rightarrow CuC_5H_{10}^+ + C_2H_4O_2 \\ \rightarrow CuC_2H_4O_2^+ + C_5H_{10} \end{cases}$$

The small ion at *m/z* 105 is $CuC_2H_2O^+$, which results from a less competitive fragmentation pathway for acetates. Its complement, $CuC_5H_{12}O^+$ (*m/z* 151), is not observed. Based on the trends established for the reactions of Cu^+ with esters [14], these spectra unambiguously characterize both samples as esters of molecular weight 130. As for structural information, the Cu^+ reactions readily identify the position of the ester linkage in each case. However, the actual structure of the alkyl groups cannot be determined from these spectra alone. For example, amyl acetate would have the same spectrum as isoamyl acetate in its reactions with Cu^+. But, by using other metal ions that can interact with the alkyl groups by cleaving C—C bonds (e.g., Fe^+), information about the carbon skeletal structure of the ester can be obtained.

Results have also been reported from a number of other laboratories [6—9]. Chemical ionization with Co^+, for example, has been applied to bifunctional compounds [24], Li^+ has been shown to be particularly useful for yielding molecular weight information [25], and in a recent elegant experiment, Fe^+ was found to be useful for locating double bonds in a variety of long chain compounds [26]. Applications involving "real life" samples will clearly continue to receive greater attention. Finally, in view of the large data sets generated from the variety of metal ions and organics studied, pattern recognition techniques can be applied as a powerful means for data analysis, as will be reported elsewhere. Thus, metal-ion c.i. yields additional complementary information to that obtained by e.i. and provides an unprecedented "tunability" by taking advantage of the vastly different reactivities of the metal ions.

TANDEM MASS SPECTROMETRY BY F.T.M.S.

One of the techniques currently on the forefront of mass spectrometry research is m.s./m.s. (mass spectrometry/mass spectrometry) in analogy to g.c./m.s. [27—29]. Figure 6 illustrates one of the basic differences between performing this experiment using the more conventional tandem instruments as opposed to using F.t.m.s. In a tandem m.s./m.s. experiment the ions are manipulated in space. An ion generated in the source is selected using the first sector or quadrupole (MS_1) and undergoes a collision in the reaction chamber, and the product ions from that collision are analyzed using MS_2. This is the basis, for example, for the popular triple quadrupole instrument as well as instruments employing magnetic and electrostatic analyzers. Clearly, additional sectors or quadrupoles would be required for m.s./m.s./m.s. or beyond. In F.t.m.s., however, the ions are constrained in space, and different experiments are done in time. A typical pulse-timing sequence is shown in Fig. 6. In this experiment the ion formation pulse triggers the laser to generate metal ions. After ion formation, a series of radiofrequency (r.f.) pulses (often referred to as double resonance pulses) of varying amplitude, frequency, and duration occur to manipulate the ions as discussed below, and finally a detection pulse permits a "snapshot" of the products generated. This pulse sequence is readily modified under computer control and, therefore, different experiments require changes in software rather than hardware.

All of the r.f. pulses are generated from a frequency synthesizer which is under computer control. This device calculates voltage as a function of time to achieve the desired frequency and sends the signal to the cell. The r.f. from the frequency synthesizer is used for three functions: (1) detection,

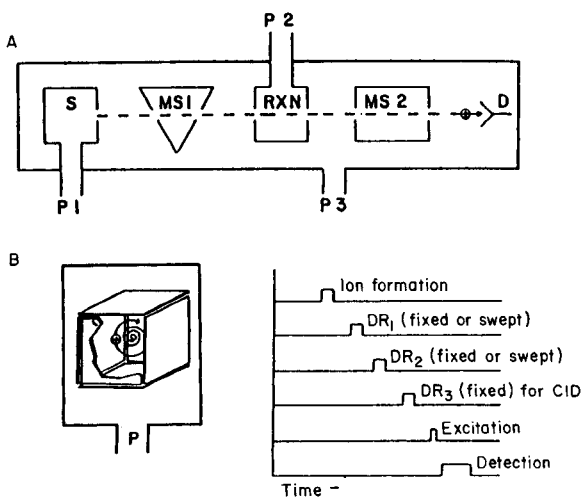

Fig. 6. Comparison of a generalized tandem mass spectrometer (A) and the F.t.m.s. (B). Also shown is a typical F.t.m.s. pulse timing sequence.

(2) ejection, and (3) collision-induced dissociation (c.i.d.). Ejection is achieved when a high amplitude r.f. signal is applied at the cyclotron frequency of an ion, causing the orbit of the ion to expand rapidly and resulting in the annihilation of the ion against one of the cell plates [30, 31]. A single frequency can be applied to eject selectively one ion or a swept frequency can be applied to eject several ions. The spectrum shown in Fig. 7 illustrates the power of this technique to determine reactant ion/product ion relationships. Laser ionization of a titanium target in the presence of water generates Ti^+ and TiO^+ [20]. Because titanium is such a reactive metal, it is not clear whether the TiO^+ arises from a gas-phase reaction of Ti^+ with water or whether it is being generated directly from the surface as a result of a surface reaction. Titanium has several isotopes (^{46}Ti 7.93%, ^{47}Ti 7.28%, ^{48}Ti 73.94%, ^{49}Ti 5.51%, ^{50}Ti 5.34%) and while *m/z* 46 and *m/z* 50 are observed, during this experiment the isotopes at masses 47—49 were continuously ejected. Not only are these species absent from the spectrum in Fig. 7, but the corresponding oxide ions are also missing. This provides unambiguous evidence that the TiO^+ is a result of the gas-phase reaction

$$Ti^+ + H_2O \rightarrow TiO^+ + H_2$$

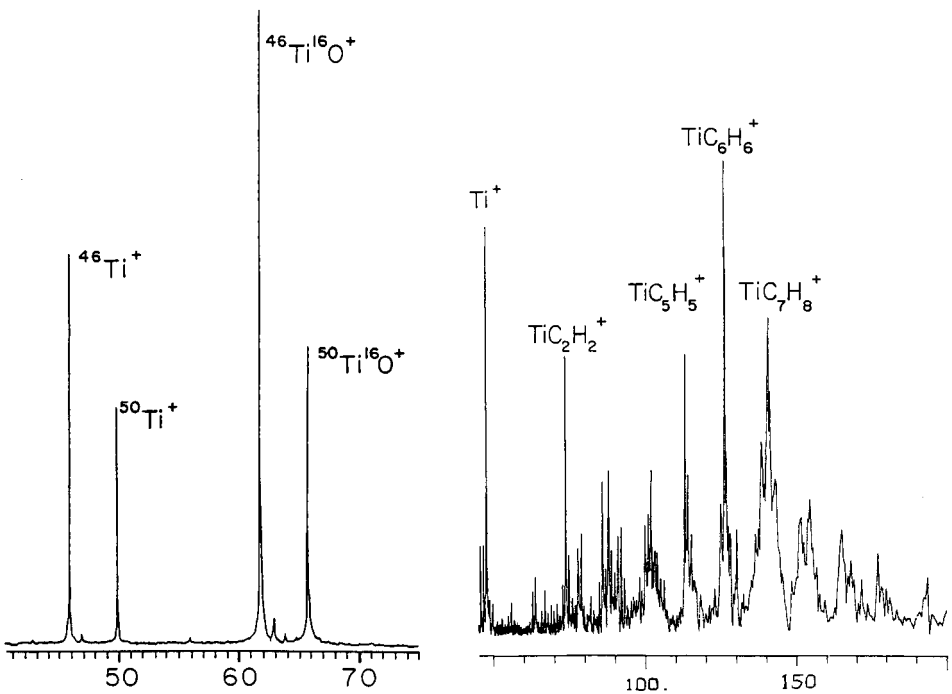

Fig. 7. Spectrum obtained from reaction of Ti^+ and H_2O (1.0-s trap). Continuous ejection of the isotopes of Ti^+ at *m/z* 47—49 provides unambiguous evidence that TiO^+ is generated in a gas-phase reaction as opposed to a surface reaction. Spectrum obtained from [20].

Fig. 8. Laser ionization spectrum from a contaminated titanium target. A trapping time of 100 ms was used and no reagent gas was present. Spectrum obtained from [20].

It is not due to direct formation from the surface because in the latter case, ejection of Ti^+ would have had no effect on TiO^+. For example, Fig. 8 shows a spectrum obtained from a titanium target in the absence of a reagent gas taken after a 10-h bakeout [20]. In this case, ejection of Ti^+ had no effect on the other ions in the spectrum indicating that they were not the products of normal gas-phase ion/molecule reactions, but were either desorbed directly from the surface or were formed in fast ion/molecule reactions in the high-pressure selvedge produced above the surface during desorption [32]. This same target had been used the day before to generate Ti^+ in the presence of alkanes and this spectrum clearly demonstrates that a nonvolatile layer of hydrocarbon material remained on the surface. Metal surfaces are known to adsorb hydrocarbons rapidly from sample gases or even pump oil vapors to form a carbonaceous overlayer [33]. Of particular interest are the three major peaks with masses corresponding to aromatic ligands bound to Ti^+ such as cyclopentadienyl, benzene, and toluene which indicates dehydrocyclization as a possible mechanism for this surface event [34]. While these contaminants usually disappear after a few laser shots, in some instances certain ions such as $TiC_2H_2^+$ are observed for several laser shots. In general, however, problems with "sticky" samples and reactive metals can be circumvented by cleaning the surface with several rapid laser pulses followed by a single pulse from which the mass spectrum is recorded. Ion ejection is also applied routinely to confirm the origin of the observed ions.

In collision-induced dissociation (c.i.d.), an ion is accelerated into a target gas causing it to fragment and thus yield its mass spectrum. Combined F.t.m.s./c.i.d. is readily accomplished by, once again, applying an r.f. pulse at the frequency appropriate to affect a particular mass ion [35, 36]. By using an r.f. pulse of moderate amplitude, the kinetic energy and radius of the ion increase at such a rate as to favor collisions with argon, which is present in excess at ca. 5×10^{-6} Torr, over ejection. Collision-induced dissociation is one of the most powerful and certainly most widely used tools in mass spectrometry for ion structure determination [27—29]. This technique has been particularly useful in our work in which knowledge of the product ion structure yields insight into the reaction mechanism. For example, c.i.d. was used to distinguish the four isomeric $NiC_4H_8^+$ ions generated in the following reactions [37]:

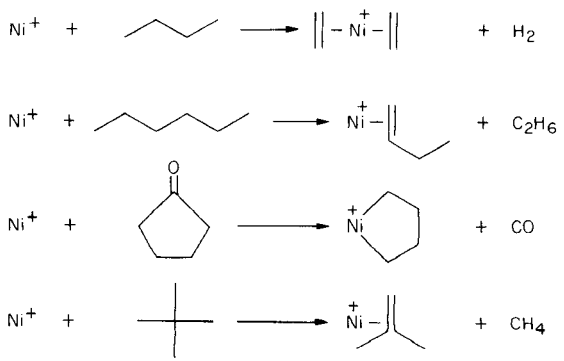

TABLE 1

Neutral losses from c.i.d. of $NiC_4H_8^+$ complexes[a,b]

Structure	H_2	C_2H_4	C_4H_8	Structure	H_2	C_2H_4	C_4H_8
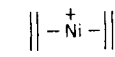	—	X	X		X	X	X
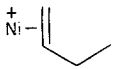	X	—	X		—	—	X

[a] C.i.d. fragments observed at 15 eV kinetic energy. [b] Argon added for total pressure of 1×10^{-5} Torr.

As shown in Table 1, the bis-ethene product in the first reaction loses one and two ethenes upon c.i.d., while the butene complex in the second reaction loses H_2 to form a stable butadiene complex, and so forth. The particular significance of these results is that they provide direct evidence for initial C—C insertion as opposed to C—H insertion which is in direct contrast to the behavior observed for bare metal atoms and transition metal complexes in solution [38].

In addition to structural elucidation, we have shown that c.i.d. is a powerful and convenient tool for synthesizing unusual ions in situ. This technique has been used extensively, for example, to generate and study atomic transition metal anions which could not be formed reproducibly or in sufficient yields by direct laser ionization [39]. Figure 9 demonstrates this capability for generating Fe^-. In this example $Fe(CO)_5$ is added to the cell; typical of metal carbonyls, $Fe(CO)_5$ has a large cross-section for dissociative electron capture and produces a large signal of $Fe(CO)_4^-$ (Fig. 9A). Next, c.i.d. results in the sequential loss of CO ligands producing a variety of products including Fe^-, and finally the Fe^- is isolated by ejecting all of the other species present. Thus, the chemistry of Fe^- can readily be studied; for example, it reacts with CO_2 to generate FeO^-. From data such as these an estimate of the

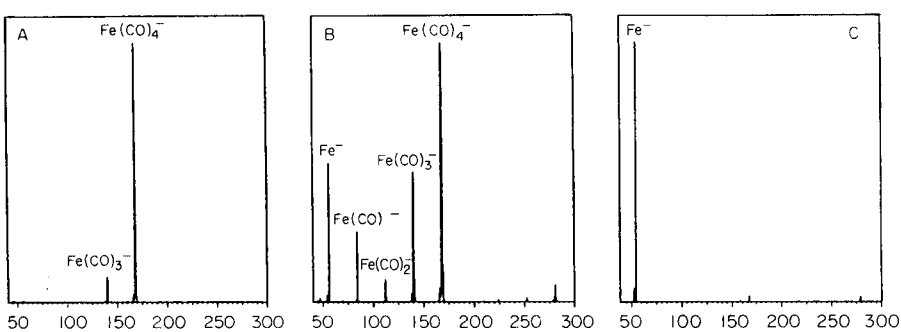

Fig. 9. Multistep synthesis of Fe^- (see text). Reprinted with permission [39b].

bond dissociation energy $D^0(Fe^-—O)$ = 139 ± 13 kcal mol^{-1} has been assigned. Comparing this value to D^0 $(Fe^+—O)$ = 68 kcal mol^{-1} [40] and D^0 (Fe—O) = 98 kcal mol^{-1} [41, 42] indicates an increasing bond order as electrons are added to the system. These techniques should add greatly to our knowledge of atomic metal anions for which there is a paucity of thermodynamic and reactivity information.

PULSED-VALVE CHEMISTRY: STUDY OF MX^+

Thus far, the study of atomic metal cations and anions has been discussed. A logical extension to this work is to investigate the influence of various ligands on the observed chemistry. In order to run such experiments properly, however, it was necessary to develop a method for manipulating the concentrations of neutral species with as much ease as the ion concentrations could be manipulated. Because the cell is in a single vacuum chamber, the use of differential pumping is not feasible. It became apparent, however, that because the entire experiment is pulsed, neutral gases could be pulsed in as well [43]. Figure 10, in which an analogy is drawn to a conventional experiment in an organic or inorganic laboratory, illustrates this idea. The experiment begins with a synthesis step to generate the desired metal/ligand complex, followed by a separation step in which that ion is isolated from all others, a reaction step, and finally a product analysis step. With this flexibility, F.t.m.s. may be dubbed "the complete gas phase chemical laboratory".

The effect of oxygen on metal-ion reactivity is of particular interest, because oxides have been observed to exhibit catalytic activity. Figure 11 shows a sequence of reactions in which FeO^+ is generated and its reactions with neopentane are studied [44]. In the first step, Fe^+ is permitted to react with a mixture of nitrous oxide and neopentane. The nitrous oxide is admitted to the cell, concurrently with the laser generation of Fe^+, through a pulsed valve achieving a maximum pressure of about 10^{-5} Torr. The neopentane is present in the system at a static pressure of about 2×10^{-7} Torr. Pulsing in the gas allows the system to be maintained at a lower pressure during most of the reaction sequence; this enables ions to be trapped more

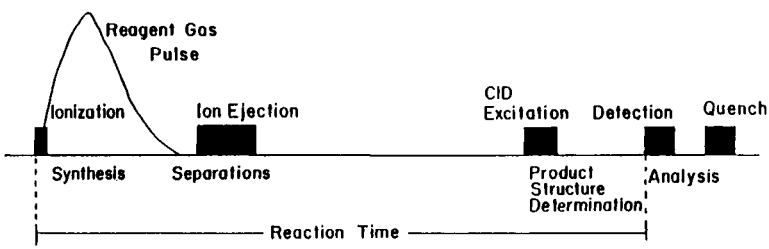

Fig. 10. Sequence of events for pulsed-valve addition of reagent gas for the F.t.m.s. experiment.

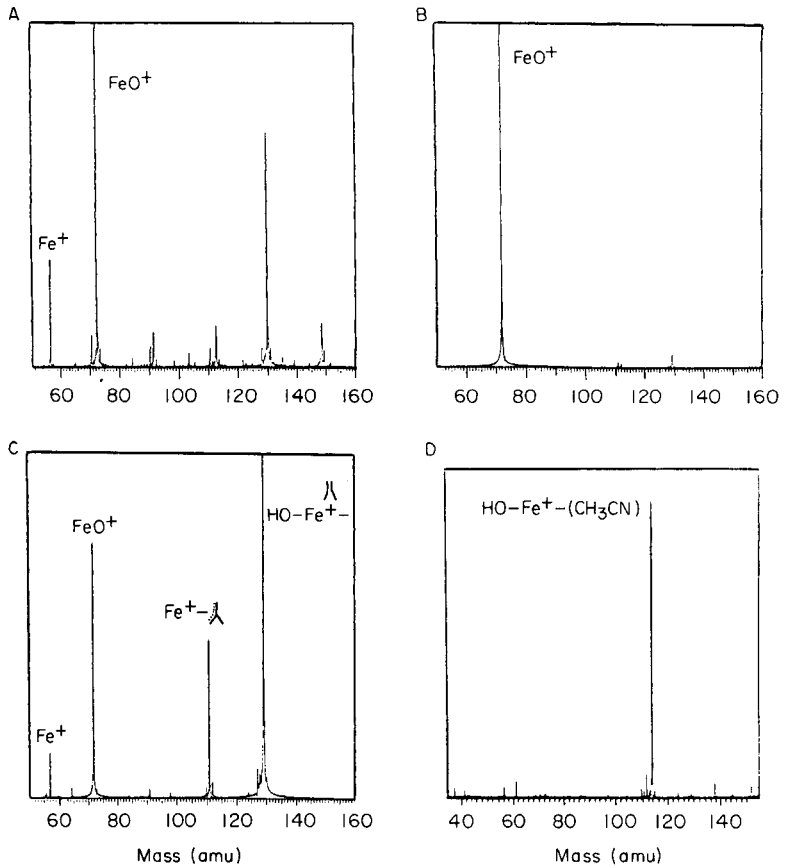

Fig. 11. (A) Spectrum obtained of Fe^+ in a mixture of N_2O and neopentane. (B) Isolation of FeO^+. (C) Same as B but allowing FeO^+ to react with neopentane. (D) Same as C, but isolating HO-Fe^+-⅄ and allowing it to react with CH_3CN (see text).

efficiently and detected at higher resolution, and also eliminates further reactions with nitrous oxide. The FeO^+ generated by the reaction

$$Fe^+ + N_2O \rightarrow FeO^+ + N_2$$

is then isolated by ejecting all of the other ions present. The FeO^+ is then permitted to react with neopentane:

$$FeO^+ + \rightarrow \begin{cases} FeC_4H_9O^+ + CH_3 \\ FeC_4H_7^+ + H_2O + CH_3 \\ Fe^+ + (C_5H_{12}O) \end{cases}$$

Based on our knowledge of reaction mechanisms, the product of the first of these reactions could be postulated as having either structure I or II:

H_2O- Fe^+-

I

HO- Fe^+-

II

A chemical reaction was used to distinguish these structures. Acetonitrile, a good Lewis base and ligand, was added to the system which would be expected to displace water in structure I or isobutene in structure II. As can be seen in Fig. 11D, acetonitrile very clearly displaces isobutene providing strong evidence for structure II and, hence, important mechanistic information. Alternatively, collision-induced dissociation can be applied to this problem. Figure 12 plots c.i.d. product ion intensities vs. kinetic energy for the $FeC_4H_9O^+$ ion generated in the above reaction. These data support the proposed structure II, showing a loss of water via a rearrangement at low energy to give the iron-methylallyl complex; at higher energy the alkene ligand is lost, and at yet higher energies the bare metal ion is regenerated. It should be noted that selecting a structure on the basis of one c.i.d. spectrum at low energy alone would have led to an incorrect conclusion. Again, it is the chemistry (ligand displacement by acetonitrile) that provides the most concrete evidence.

This work has been expanding rapidly and to date a variety of metal/ligand species has been investigated, including: MH^+ (M = Fe, Co, Ni) [45], MCH_2^+ (M = Fe, Co, Rh) [46], MCH_3^+ (M = Fe, Co) [47], Fe(olefin)$^+$ [48], $CoC_5H_5^+$ [49], MO^+ (M = Fe, V) [44], MOH^+ (M = Fe, Co, Ni) [50],

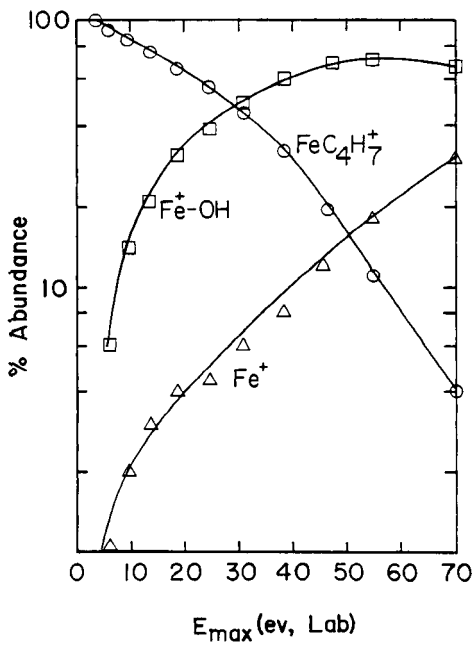

Fig. 12. The c.i.d. product ion intensities vs. kinetic energy for HO—Fe^+-⅄ generated in the reaction of FeO^+ with neopentane. Reprinted with permission [44].

and MS^+ (M = Fe, Co, Ni, V) [19]. It is probably fair to say that at this stage, virtually any small ligand can be prepared from suitable precursors. Underlying our excitement about this area is the fact that the transition metal-organic fragment chemical bond may be the key to linking the three disciplines of surface chemistry, catalysis, and organometallic chemistry [51].

PHOTODISSOCIATION STUDIES

An alternative method for obtaining structural information on ions is by examining their absorption spectra. Unfortunately, because the concentrations of the ions in the trapping cell are on the order of 10^{-20} M, a direct absorption spectrum obviously cannot be obtained. By monitoring the disappearance of AB^+ or the appearance of A^+ in the reaction

$$AB^+ + h\nu \rightarrow A^+ + B$$

as a function of wavelength, however, the photodissociation [52] spectrum of AB^+ can be derived [53]. In order to see the connection between the true absorption spectrum of the ion and its photodissociation spectrum, it is important to realize that band intensities in photodissociation spectra depend not only on the intrinsic transition probability or gas-phase absorption coefficient, $\epsilon_g(\lambda)$, but also on the photodissociation quantum yield, $\phi_d(\lambda)$. The relative photodissociation cross-section, $\sigma_d(\lambda)$ is the actual quantity measured and is proportional to the product of these two variables: $\sigma_d(\lambda) \propto \epsilon_g(\lambda)\ \phi_d(\lambda)$. If the quantum yield for photodissociation is relatively constant over an absorption band (Fig. 13, band I), then the photodissociation spectrum will exactly mimic the intrinsic gas-phase absorption spectrum. If, however, ϕ_d varies significantly over an absorption band (Fig. 13, band II), then the photodissociation spectrum will be a distorted

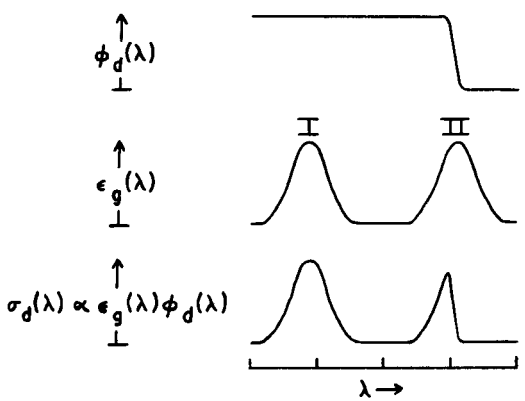

Fig. 13. Comparison of expected photodissociation cross-section $\sigma_d(\lambda)$ and absorption spectrum $\epsilon_g(\lambda)$ for cases where the photodissociation quantum yield $\phi_d(\lambda)$ is constant (I) and varying (II) over the absorption band.

representation of the actual absorption spectrum. In particular, below the thermodynamic threshold for the photodissociation process (i.e., at photon energies below the A^+—B bond dissociation energy), $\phi_d(\lambda) = 0$ and the ion is not observed to photodissociate even if it absorbs in the wavelength region, assuming a 1-photon process; multiphoton photodissociation of ions has been reported [54]. In summary, it is reasonable to assume to a first approximation that the photodissociation spectrum will mimic the direct absorption spectrum above the thermodynamic threshold [53], and that the photodissociation threshold can yield bond energy information.

Preliminary results from this laboratory suggest that a wide variety of metal ion complexes and clusters will in fact photodissociate in the visible and near ultraviolet regions [50]. Three representative examples are shown in Figs. 14 and 15. Figure 14 demonstrates that two isomeric ions can readily be distinguished not only by their different photodissociation spectra, but also by their different fragmentation products:

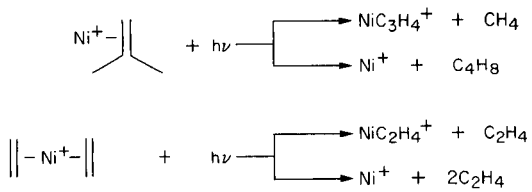

Also of interest is that the fragment produced in the first of these photoexcitation processes is not observed when the parent Ni(isobutene)$^+$ species is collisionally activated (see Table 1). We have observed several examples of this to date and attribute it to the difference in the way that the energy is put into the ion as opposed to a difference in the amount of energy. It is conceivable, for example, that photoexcitation permits the access of isolated

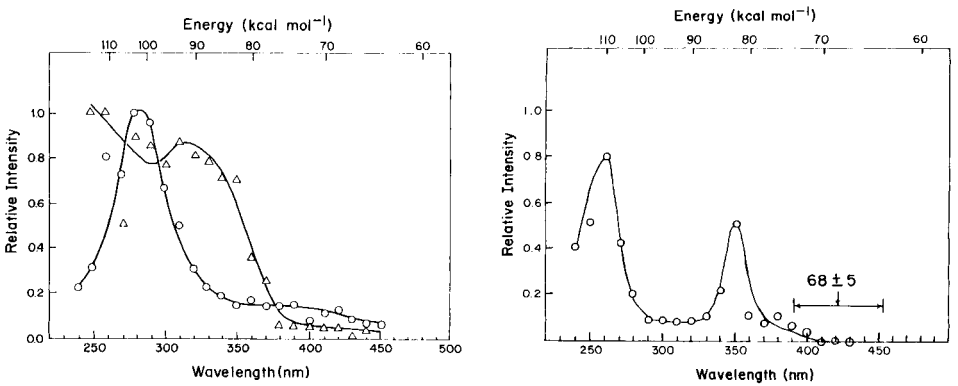

Fig. 14. Photodissociation spectra of two isomeric $NiC_4H_8^+$ ions. (○) Ni(isobutene)$^+$ (×10); (△) $Ni(C_2H_4)_2^+$. See text for elucidation.

Fig. 15. Photodissociation spectrum of FeO^+: $FeO^+ + h\nu \rightarrow Fe^+ + O$.

electronic states, but this awaits further study. Figure 15 shows the photodissociation spectrum of FeO^+ obtained by monitoring the process

$$FeO^+ + h\nu \rightarrow Fe^+ + O$$

The threshold observed at 410 ± 10 nm corresponds to 70 ± 5 kcal mol^{-1} in excellent agreement with an earlier ion beam result of $D^0(Fe^+—O)$ = 68 ±5 kcal mol^{-1} [40]. We have recently used photodissociation for the first time to determine the metal-metal bond energy of the heteronuclear diatomic metal cluster VFe^+. These results indicate the potential of what could become a very fruitful area of investigation.

SYNTHESIS OF MIXED METAL CLUSTER IONS BY m.s./m.s./m.s./m.s.

One of the most exciting areas in metal chemistry today is the study of small metal clusters, because of their relevance to catalysis. Despite this intense interest, relatively few studies have appeared on small metal cluster ions because of the difficulty in generating and studying these species. Perhaps no other example, therefore, best highlights the potential of F.t.m.s. than its application to the in situ synthesis and study of mixed metal clusters which was recently reported [55, 56]. Metal ions undergo a clustering reaction with $Fe(CO)_5$ in the gas phase:

$$M^+ + Fe(CO)_5 \rightarrow MFe(CO)_{5-x}^+ + xCO$$

eliminating one or more carbonyls [57, 58]. Subsequent c.i.d. on the product ions strips off the remaining carbonyls to produce MFe^+:

$$MFe(CO)_{5-x}^+ \xrightarrow[-CO]{\text{c.i.d.}} MFe(CO)_{4-x}^+ \left(\xrightarrow[-CO]{\text{c.i.d.}} \cdots \xrightarrow[-CO]{\text{c.i.d.}}\right) MFe^+$$

This process undoubtedly generates bare cluster ions with a distribution of internal and translational energies. The c.i.d. collision gas pressure is kept high (ca. 5×10^{-6} Torr) relative to the reagent gas pressure ($1—3 \times 10^{-7}$ Torr), therefore, in order to allow the excess energy to be dissipated by thermalizing collisions with argon prior to reaction.

This method has been used to generate $CoFe^+$ [55, 56], VFe^+, $CuFe^+$, $NiFe^+$, $RhFe^+$, YFe^+, $ScFe^+$, $LaFe^+$, and $NbFe^+$. A similar reaction with $Co_2(CO)_8$ yields the bare trimer ion [55]. Figure 16 provides an interesting example. Spectrum (a) shows the reaction of Co^+ with a mixture of 1-pentene and $Fe(CO)_5$. The $CoFe(CO)_3^+$ (generated as indicated above) is isolated (spectrum b) and then its subsequent c.i.d. (see above) and isolation of the product $CoFe^+$ result in spectrum (c). The $CoFe^+$ then reacts with

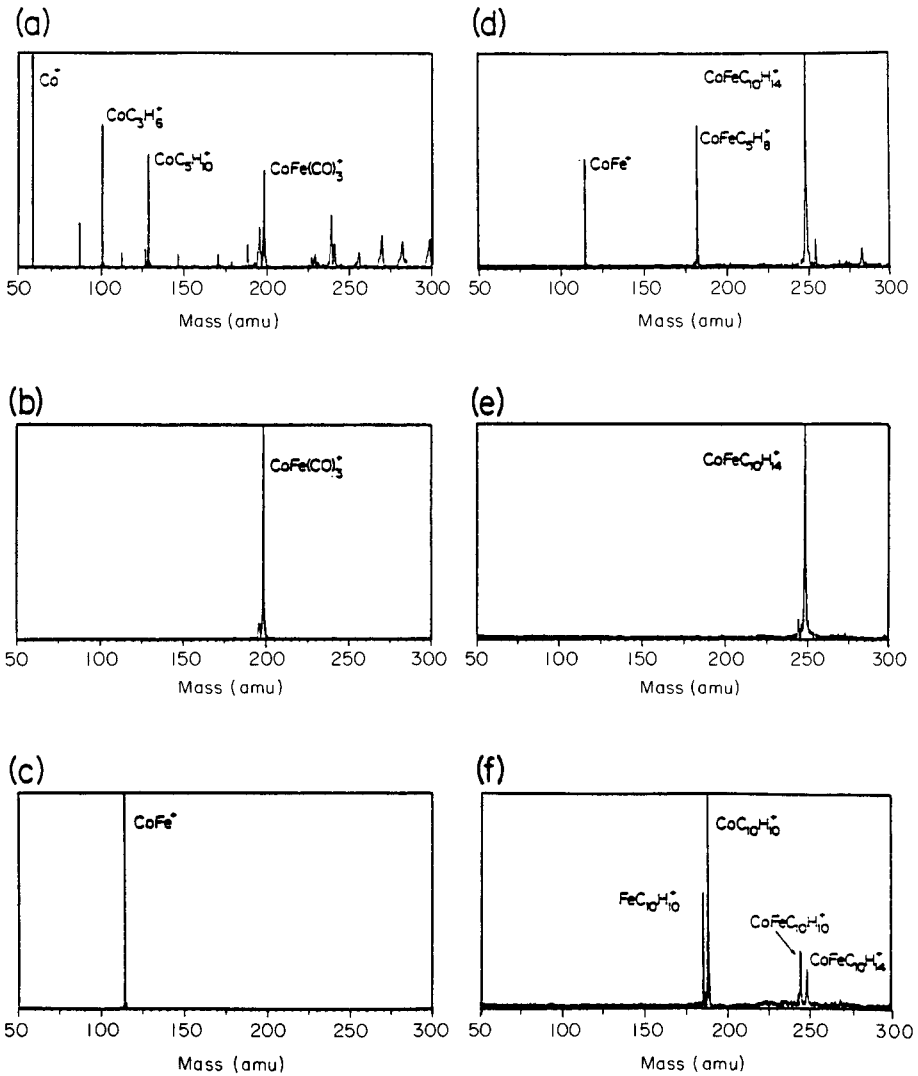

Fig. 16. Multistep synthesis and reaction of $CoFe^+$ (see text). Reprinted with permission [56].

the neutral gas mixture, but it is evident in spectrum (d) that it reacts more readily with 1-pentene than with $Fe(CO)_5$:

$$CoFe^+ + \text{1-pentene} \rightarrow CoFeC_5H_8^+ + H_2$$

$$CoFeC_5H_8^+ + \text{1-pentene} \rightarrow CoFeC_{10}H_{14}^+ + 2H_2$$

One of the products, $CoFeC_{10}H_{14}^+$, is isolated (spectrum e) and then colli-

sionally activated (spectrum f). The products observed in the following reactions correspond to metallocenes:

$$CoFe(C_{10}H_{14})^+ \xrightarrow[Ar]{\text{c.i.d.}} \begin{cases} \rightarrow CoFeC_{10}H_{10}^+ + 2H_2 \\ \rightarrow CoC_{10}H_{10}^+ + 2H_2 + Fe \\ \rightarrow FeC_{10}H_{10}^+ + 2H_2 + Co \end{cases}$$

Interestingly, the process of taking linear pentenes to cyclic products, termed dehydrocyclization, is analogous to what is observed on surfaces [34]. It is instructive to compare this F.t.m.s. experiment with the equipment needed to run the equivalent experiment using a generalized tandem instrument. It is clear from Fig. 17 that the final metallocene products are the result of $(m.s.)^4$ or m.s./m.s./m.s./m.s.

Initial testing of some new target geometries designed to promote cluster formation has recently started. In particular, it has been found that by focussing the beam of a pulsed Nd:YAG laser down the center of a small-diameter hole drilled into an iron metal rod, the tetrameric species Fe_4^+ could be generated (Fig. 18), although not routinely. Apparently by confining the plasma generated by the laser to a small volume, as compared to the flat plate, condensation can occur. These techniques, together with the very promising supersonic beam expansion techniques [59], will permit continuing progress in this important area.

Conclusion

Fourier-transform mass spectrometry is an emerging technology which holds great potential for the future. Its unusual ability to store ions on the order of seconds, together with the ease in which both ionic and neutral populations can be manipulated under computer control, make F.t.m.s. a highly versatile instrument and a method of choice for studying fundamental ion/molecule reaction chemistry. In addition, the Fourier advantage of speed, signal averaging and high resolution, all bode well for the instrument as an analytical mass spectrometer.

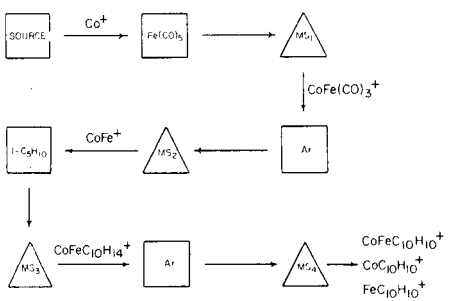

Fig. 17. Generalized tandem mass spectrometer for m.s./m.s./m.s./m.s. required to run an experiment equivalent to that shown in Fig. 16. The squares indicate collision regions and the triangles indicate sector or quadrupole mass selectors.

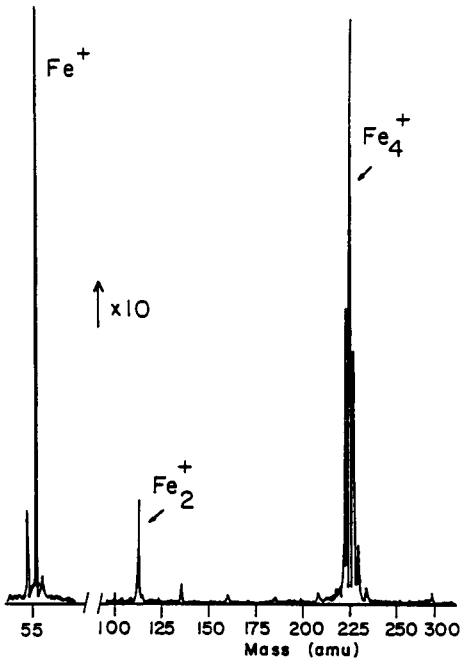

Fig. 18. Direct generation of Fe_4^+ by focussing the laser down the center of a small hole (3-mm deep, 1-mm diameter) drilled in an iron rod.

The combination of laser ionization and F.t.m s. provides a convenient and powerful method of generating and studying metal ions in the gas phase. With this technique, thermodynamic, kinetic and mechanistic information on atomic metal cations and anions, metal-ion complexes and metal-ion clusters can readily be obtained. It is hoped that ultimately these studies will provide a better understanding of the fundamental controlling factors in organotransition metal chemistry and catalysis. Finally, returning to the theme outlined in the introduction, the growing data base available on fundamental ion/molecule chemistry should find increasing use by the analytical mass spectroscopist.

Acknowledgement is made to the Division of Chemical Sciences in the Office of Basic Energy Sciences in the United States Department of Energy (DE-AC02-80ER10689) and to the National Science Foundation (CHE-8310039) for supporting the advancement of F.t.m.s. methodology.

REFERENCES

1 M. S. B. Munson and F. H. Field, J. Am. Chem. Soc., 88 (1966) 2621.
2 R. B. Cody, R. C. Burnier, W. D. Reents, Jr., T. J. Carlin, D. A. McCrery, R. K. Lengel and B. S. Freiser, Int. J. Mass Spectrom. Ion Phys., 33 (1980) 37.

3 J. R. Ready, Effects of High-Power Laser Radiation, Academic Press, New York, 1971.
4 K. R. Thomas, Anal. Chem., 48 (1976) 696.
5 M. A. Posthumus, P. G. Kistemaker, H. L. C. Meuzelaar and M. C. Ten Noever de Brauw, Anal. Chem., 50 (1978) 985.
6 M. S. Foster and J. L. Beauchamp, J. Am. Chem. Soc., 93 (1971) 4924.
7 J. Allison and D. P. Ridge, J. Am. Chem. Soc., 101 (1979) 4998.
8 P. B. Armentrout, L. F. Halle and J. L. Beauchamp, J. Am. Chem. Soc., 103 (1981) 6624.
9 P. B. Armentrout and J. L. Beauchamp, J. Am. Chem. Soc., 103 (1982) 6628.
10 N. Aristov and P. B. Armentrout, J. Am. Chem. Soc., 106 (1984) 4065.
11 A. Harrison, Chemical Ionization, Wiley-Interscience, New York, 1984.
12 R. L. Hunter and R. T. McIver, Jr., Anal. Chem., 51 (1979) 699.
13 S. Ghaderi, M. L. Gross, P. S. Kulkarni, E. B. Ledford and C. L. Wilkins, Anal. Chem., 58 (1981) 428.
14 R. C. Burnier, G. D. Byrd and B. S. Freiser, Anal. Chem., 52 (1980) 1641.
15 R. C. Burnier, G. D. Byrd and B. S. Freiser, J. Am. Chem. Soc., 103 (1981) 4360.
16 G. D. Byrd, R. C. Burnier and B. S. Freiser, J. Am. Chem. Soc., 104 (1982) 3565.
17 G. D. Byrd and B. S. Freiser, J. Am. Chem. Soc., 104 (1982) 5944.
18 M. B. Wise, Ph.D. Thesis, Purdue University, 1984.
19 T. J. Carlin, Ph.D. Thesis, Purdue University, 1983.
20 G. D. Byrd, Ph.D. Thesis, Purdue University, 1982.
21 F. W. McLafferty, Interpretation of Mass Spectra, W. A. Benjamin, Reading, Massachusetts, 3rd Edition.
22 F. H. Field, M. S. B. Munson and D. A. Becker, in R. F. Gould (Ed.), Ion Molecule Reactions in the Gas Phase, ACS Publications, Washington, 1966.
23 D. B. Jacobson and B. S. Freiser, J. Am. Chem. Soc., 105 (1983) 5197.
24 M. Lombarski and J. Allison, Int. J. Mass Spectrom. Ion Phys., 49 (1983) 281.
25 R. V. Hodges and J. L. Beauchamp, Anal. Chem., 48 (1976) 825.
26 D. A. Peake and M. L. Gross, Anal. Chem., 57 (1985) 115.
27 R. G. Cooks, in R. G. Cooks (Ed.), Collision Spectroscopy, Plenum Press, New York, 1978.
28 F. W. McLafferty and F. M. Bockhoff, Anal. Chem., 50 (1978) 69.
29 R. A. Yost and C. G. Enke, J. Am. Chem. Soc., 100 (1978) 2274.
30 L. R. Anders, J. L. Beauchamp, R. C. Dunbar and J. D. Baldeschwieler, J. Chem. Phys., 45 (1966) 1062.
31 M. B. Comisarow, V. Grassi and G. Parisod, Chem. Phys. Lett., 57 (1978) 413.
32 K. L. Busch, S. E. Unger and R. G. Cooks, 29th Annual Conference on Mass Spectrometry and Allied Topics, May, 1981, Minneapolis.
33 G. Webb, in C. Kemball (Ed.), Catalysis (Specialist Periodical Report), The Chemical Society of London, (1977) Vol. 1, p. 1.
34 O. V. Bragin and S. A. Krasavin, Russ. Chem. Rev. (Eng. Transl.), 52 (1983) 625.
35 R. B. Cody and B. S. Freiser, Int. J. Mass Spectrom. Ion Phys., 41 (1982) 199.
36 R. B. Cody, R. C. Burnier and B. S. Freiser, Anal. Chem., 54 (1982) 96.
37 D. B. Jacobson and B. S. Freiser, J. Am. Chem. Soc., 105 (1983) 736.
38 L. F. Halle, R. Houriet, M. Kappes, R. Staley and J. L. Beauchamp, J. Am. Chem. Soc., 104 (1982) 6293.
39 (a) L. Sallans, K. Lane, R. R. Squires and B. S. Freiser, J. Am. Chem. Soc., 105 (1983) 6352.
(b) L. Sallans, K. Lane, R. R. Squires and B. S. Freiser, J. Am. Chem. Soc., 107 (1985) 4379. Copyright (1985) American Chemical Society.
40 L. F. Halle, P. B. Armentrout and J. L. Beauchamp, Organometallics, 1 (1982) 963.
41 E. Murad, J. Chem. Phys., 73 (1980) 1381.
42 D. L. Hildebrand, Chem. Phys. Lett., 34 (1975) 352.

43 T. J. Carlin and B. S. Freiser, Anal. Chem., 55 (1983) 571.
44 T. C. Jackson, D. B. Jacobson and B. S. Freiser, J. Am. Chem. Soc., 106 (1984) 1252. Copyright (1984) American Chemical Society.
45 T. J. Carlin, L. Sallans, C. J. Cassady, D. B. Jacobson and B. S. Freiser, J. Am. Chem. Soc., 105 (1983) 6320.
46 D. B. Jacobson and B. S. Freiser, J. Am. Chem. Soc., 107 (1985) 67, 2605, 4373.
47 D. B. Jacobson and B. S. Freiser, J. Am. Chem. Soc., 106 (1984) 3891, 3900.
48 D. B. Jacobson and B. S. Freiser, J. Am. Chem. Soc., 105 (1983) 7484.
49 D. B. Jacobson and B. S. Freiser, J. Am. Chem. Soc., 107 (1985) in press.
50 C. J. Cassady and B. S. Freiser, J. Am. Chem. Soc., 106 (1984) 6176.
51 H. F. Schaefer III, Acc. Chem. Res., 10 (1977) 287.
52 R. C. Dunbar, in M. T. Bowers (Ed.), Gas Phase Ion Chemistry, Academic Press, New York, 1979, Vol. 2, Chap. 14.
53 B. S. Freiser and J. L. Beauchamp, J. Am. Chem. Soc., 98 (1975) 6893.
54 See e.g., B. S. Freiser and J. L. Beauchamp, Chem. Phys., 16 (1976) 439.
55 D. B. Jacobson and B. S. Freiser, J. Am. Chem. Soc., 106 (1984) 4623, 5351.
56 D. B. Jacobson and B. S. Freiser, J. Am. Chem. Soc., 107 (1985) 1581. Copyright (1985) American Chemical Society.
57 R. C. Burnier, G. D. Byrd, T. J. Carlin, M. B. Wise, R. B. Cody and B. S. Freiser, in K.-P. Wanczek (Ed.), Lecture Notes in Chemistry, Springer-Verlag, West Germany, 1982.
58 R. H. Staley, J. Phys. Chem., 86 (1982) 1332.
59 M. D. Morse, G. P. Hansen, P. R. R. Langridge-Smith, L. S. Zheng, M. E. Gensic, D. L. Michalopoulos and R. E. Smalley, J. Chem. Phys., 80 (1984) 5400.

0003-2670/85/$03.30

Printed in The Netherlands

VOL. 178 No. 1 ANALYTICA CHIMICA ACTA DECEMBER 1, 1985

CONTENTS

(Abstracted, Indexed in: Anal. Abstr.; Biol. Abstr.; Chem. Abstr.; Curr. Contents Phys. Chem. Earth Sci.; Life Sci.; Index Med.; Mass Spectrom. Bull.; Sci. Citation Index; Excerpta Med.)